Title
Electrocatalytic reduction of carbon dioxide to carbon monoxide by rhenium and manganese polypyridyl catalysts

Author
Smieja, Jonathan Mark

Publication Date
2012

Peer reviewed|Thesis/dissertation

UNIVERSITY OF CALIFORNIA, SAN DIEGO

Electrocatalytic reduction of carbon dioxide to carbon monoxide by rhenium and manganese polypyridyl catalysts

A dissertation submitted in partial satisfaction of the requirements for the degree of

Doctor of Philosophy

in

Chemistry

by

Jonathan Mark Smieja

Committee in charge:

Professor Clifford P. Kubiak, Chair
Professor Andrew G. Dickson
Professor Joshua S. Figueroa
Professor William C. Trogler
Professor Jerry Yang

2012

This dissertation of Jonathan Mark Smieja is approved, and it is acceptable in quality and form for publication on microfilm and electronically:

Chair

University of California, San Diego

2012

DEDICATION

This dissertation is dedicated to my Dad who loved and supported me always and worked harder than anyone I have ever known to support his family.

EPIGRAPH

Oh I'm a lucky man, to count on both hands

the ones I love.

Some folks just have one,

yeah, others, they've got none, huh-uh

Eddie Vedder

TABLE OF CONTENTS

LIST OF FIGURES

LIST OF TABLES

ACKNOWLEDGEMENTS

Simply put, a PhD in chemistry is unattainable without help. If I were to thank everyone who helped me along the way this dissertation would be 600 pages long. Additionally, it is impossible to properly thank some of those people in words on a page. I will try to be thorough in my acknowledgements here, but I must apologize before I start to those that I have missed.

First of all I have to thank my wife and my best friend. *Lacey*, without you there is no way I would have made it through living in San Diego for nearly six years and there is no way I would be writing this document. As cliché as it may sound, you are the first person I want to see in the morning and the last person I want to talk to before falling asleep. I am grateful every day that you are in my life and I am constantly in awe of your intelligence, your sense of humor, and your ability to brighten my day. This degree is as much yours as it is mine, and I hope you never forget that.

I need to thank my family. *Dad*, there are no words to express how much I miss you. I have you to thank for the man I am today, and I strive to match your work ethic and your quiet strength in everything I do. I wish you were here to see me close this chapter of my life and move on to the next. I know you are looking over me and I will always remember everything you did to get me where I am today. *Mommy*, I thank my lucky stars every day that you are my Mother. You have taught me more than you could ever know about how to treat people, how to present myself, and how to live. You are one of the strongest people I have ever met and I only hope to be half

as strong as you some day. *Christina*, I have always looked up to you and the chances you have taken in life, the independence you have shown, and the way you love your family. I will never forget everything you and Chris did for the family during our hardest time. *Denise*, it is no secret how much we have in common. You are the reason I love camping and hiking, you are the reason I have spent half the money I've ever made at REI, and you are one of my greatest role models. I've never told you how proud I am to have a sister like you who cares so much for those less fortunate than us, but I should have a long time ago and I look up to you every day because of it. *Maddie*, *Abby*, and *Brooks*, I love you all so much and I am so excited to watch you grow up and become the great people I know you will be.

I also owe a million thanks to my friends. *Mikey*, together we have made up words, lost countless hours of sleep to quoting movies, and seen everyone from Van Morrison to Marilyn Manson in concert. Moving in to your dorm room was the best decision I've ever made and I'm lucky to have you as a friend. *Christopher*, we are so different and yet so alike, and that is what I have always loved about our friendship. I look forward to our many more rounds of golf, trips to Vegas, and Twins games in the future. *Baines*, *Joey*, *Heitz*, *Danny*, *Justin*, and *Mad Dog*, thank you for the many beers of our past and the many more we have to look forward to. *Annie*, you are one of my oldest and best friends and one of my role models for how to treat people. Don't ever change. To *Gavin*, *Kristi*, *Jenna*, *Erin*, *Ryan*, *Brooke*, *Leylla*, *Khalisa*, *Jay*, and everyone else that has made San Diego a livable place… thank you.

It would not be possible to get a PhD in chemistry without an advisor, and I am lucky to have one who allowed me to make mistakes, explore the chemistry I was interested in, and grow as not only a researcher, but as a person. *Cliff*, I appreciate everything you have done for me, and I will never forget the opportunity you gave me to succeed as a scientist.

Behind every good research laboratory is a good group of people. I have been lucky to work with some amazing people at UCSD, and I need to thank a few of them by name. *Benson*, I don't know that I could have got through this without you, and I am forever grateful that we were able to work side by side. *Goeltz*, you are not only one of the smartest people I've ever met, but also one of my best friends. Thank you for your patience with my questions and ineptitude while you were my desk neighbor. *Starla*, we have a textbook love/hate relationship, but I think in the end the love half prevailed and I am very lucky to know you. *Candace*, I will never forget your poise and your very soft-spoken confidence. I strive every day to be a little more like you. *Gabe*, I will always appreciate your European-ness and your great sense of humor. Thanks for teaching me so much about how to live. *Bhupi*, what can I do but thank you for teaching me what it means to work hard in the lab and accomplish things that seem impossible from the outset. To everyone else in the Kubiak lab current, future, and past, you make this lab a great place to be a graduate student. Don't let me down.

The following thanks are in no particular order and I wish I had more time and space to give everyone a proper acknowledgement, but I do want to finish this dissertation and graduate someday. Thank you *Linda*, *Gale*, *Nicole*, *Ben*, *Mark*, *Judi*,

Bud, the faculty at *UST* (especially *Dr. O*), my *high school teachers, Tony's Jacal*, *Bronx Pizza*, *Small Bar*, *Hamilton's*, *Art of Espresso*, *Olivetto*, *Wit's End* (R.I.P.), *REI*, the *outdoors*, all the kids at the *Kroc Center*, *Torrey Pines Golf Course*, and everyone/everything that I forgot to thank.

CHAPTER SPECIFIC ACKNOWLEDGEMENTS

Chapter 1. Much of the material for this chapter comes directly from a manuscript entitled "Electrocatalytic and homogeneous approaches to conversion of CO_2 to liquid fuels" by Eric E. Benson, Clifford P. Kubiak, Aaron J. Sathrum, and Jonathan M. Smieja, which has been published in *Chemical Society Reviews*, **2009**, *38*, 89-99. http://dx.doi.org/10.1039/B804323J. The dissertation author is an equal contributor to this manuscript.

Chapter 2. Much of the material for this chapter comes directly from a manuscript entitled "Re(bipy-*t*Bu)$(CO)_3$Cl – improved catalytic activity for reduction of carbon dioxide. IR-Spectroelectrochemical and mechanistic studies." by Jonathan M. Smieja and Clifford P. Kubiak, which has been published in *Inorganic Chemistry*, **2010**, *49* (20), 9283-9289. http://dx.doi.org/10.1021/ic1008363. The dissertation author is the primary author of this manuscript.

Chapter 3. Much of the material for this chapter comes directly from a manuscript entitled "Artificial photosynthesis of CO: Kinetic and structural studies, origins of selectivity and the importance of interfacial charge transfer." by Jonathan M. Smieja, Eric E. Benson, Bhupendra Kumar, Kyle A. Grice, Candace S. Seu, Alexander A. J. Miller, James M. Mayer, and Clifford P. Kubiak, which has been published in

Proceedings of the National Academy of Sciences, **2012**, *In Press*. The dissertation author is the primary author of this manuscript.

Chapter 4. The material in this chapter is unpublished work and was performed in collaboration with Eric E. Benson, Ian D. Sharp, and Heinz Frei at the JCAP Laboratory facilities in Berkeley, CA.

Chapter 5. The material in this chapter is unpublished work and was performed in collaboration with Eric E. Benson and Matthew D. Sampson.

Chapter 6. The material in this chapter is unpublished work and was performed in collaboration with Mr. Timo Schotzko and Dr. Bhupendra Kumar.

VITA

2005 Bachelor of Science, University of Saint Thomas

2008 Master of Science, University of California, San Diego

2012 Doctor of Philosophy, University of California, San Diego

PUBLICATIONS

Smieja, J. M.; Benson, E. E.; Kumar, B.; Grice, K. A.; Seu, C. S.; Miller, A. J. M.; Mayer, J. M.; Kubiak, C. P. "Artificial photosynthesis of CO: Kinetic and structural studies, origins of selectivity, and importance of interfacial charge transfer," *PNAS*, **2012**, *In Press.*

Kumar, B.; Smieja, J. M.; Kubiak, C. P. "Tunable photo-assisted co-generation of CO and H_2 from CO_2 and H_2O using Re(bipy-*t*Bu)$(CO)_3$Cl and p-Si in non-aqueous media," *Chem. Commun.*, **2012**, *48*, 272-274.

Smieja, J. M.; Kubiak, C. P. "Re(bipy-*t*Bu)$(CO)_3$Cl – improved catalytic activity for reduction of carbon dioxide. IR-Spectroelectrochemical and mechanistic studies," *Inorg. Chem.*, **2010**, *49*, 9283-9289.

Kumar, B.; Smieja, J. M.; Kubiak, C. P. "Photoreduction of CO_2 on p-type Silicon Using Re(bipy-*t*Bu)$(CO)_3$Cl: Photovoltages Exceeding 600 mV for the Selective Reduction of CO_2 to CO," *J. Phys. Chem. C*, **2010**, *114*, 14220-14223.

Benson, E. E.; Kubiak, C. P.; Sathrum, A. J.; Smieja, J. M. **"**Electrocatalytic and homogeneous approaches to conversion of CO_2 to liquid fuels," *Chem. Soc. Rev.***,** **2009**, *38*, 89-99.

Ojala, W. H.; Smieja, J. M.; Spude, J. M.; Arola, T. M.; Kuspa, M. K.; Herrera, N.; Ojala, C. R. "Isostructuralism among 'bridge-flipped' isomeric benzylideneanilines and phenylhydrazones," *Acta Cryst. B*, **2007**, *B63*, 485-496.

ABSTRACT OF THE DISSERTATION

Electrocatalytic reduction of carbon dioxide to carbon monoxide by rhenium and manganese polypyridyl catalysts

by

Jonathan Mark Smieja

Doctor of Philosophy in Chemistry

University of California, San Diego, 2012

Professor Clifford P. Kubiak, Chair

The electrocatalytic reduction of carbon dioxide (CO_2) to carbon monoxide (CO) is explored for both rhenium and manganese complexes. Electrochemistry, X-ray crystallography, Infrared spectroelectrochemistry, and stopped-flow kinetics are employed in order to identify catalysts and probe their mechanism and selectivity.

Two catalysts in particular, Re(bipy-*t*Bu)$(CO)_3$(L) and Mn(bipy-*t*Bu)$(CO)_3$L (where bipy-*t*Bu = 4,4'-di-*tert*-butyl-2,2'-bipyridine and L = Cl^-, Br^- or $(MeCN)(OTf)^-$), were studied extensively and displayed high activity, Faradaic efficiency, and selectivity for the reduction of CO_2 to CO. The Re-Cl catalyst exhibits a turnover frequency of >200 s^{-1}, one of the fastest reported rates for a catalyst with

appreciable turnover number. The Mn catalysts, when Brönsted acid sources are added to the electrochemical solution, exhibit current densities rivaling those of the Re-Cl catalyst. Amazingly, these catalysts showed high selectivity for CO_2 in both dry solvents and those with significant amounts of Brönsted acid added. Stopped-flow UV-Vis kinetics experiments showed that the reaction of the active form of the catalysts, $[M(bipy\text{-}t\text{Bu})(CO)]^{-1}$, is *ca.* 50 times faster with CO_2 than they do with protons. Stopped-flow IR kinetics experiments comparing the reactions $[Re(bipy\text{-}t\text{Bu})(CO)_3]^{-1}$ with CO_2 and $[Re(bipy)(CO)_3]^{-1}$ with CO_2 shows, that at equal CO_2 concentrations, the bipy-*t*Bu analog reacts ten times faster than the bipy analog. CO_2 also appears to react with both complexes via a concerted, two-electron oxidative addition of CO_2 to the metal center.

The heterogenization of these catalysts was also explored with limited success. Intercalation, covalent bonds to gold, and covalent bonds to p-Si were all demonstrated, but none displayed activity towards the reduction of CO_2. Future experiments are suggested to solve this issue.

Chapter 1

Without fossil fuels: a look at the challenges ahead and solutions for future generations.

1.1 The Problem

The world has gone through wholesale changes in its energy system in the past. The key to survival is to recognize the issues at hand and adapt before a collapse occurs. Before 1900, humans relied heavily on wood to heat homes, cook food, and supply the energy for life's activities. The population grew as a direct result of the energy wood provided, and eventually the constraints of nature took over. Wood became scarce, populations suffered, and a new energy source had to be discovered to sustain civilization (Figure 1-1).[1] Humans were able to survive and thrive through the discovery and wide implementation of coal and petroleum as new energy sources.

The problem we face today with our energy system may seem similar at face value. The burning of fossil fuels such as coal, oil, and natural gas has been a boon to society for more than 100 years and has propelled the human population to both size

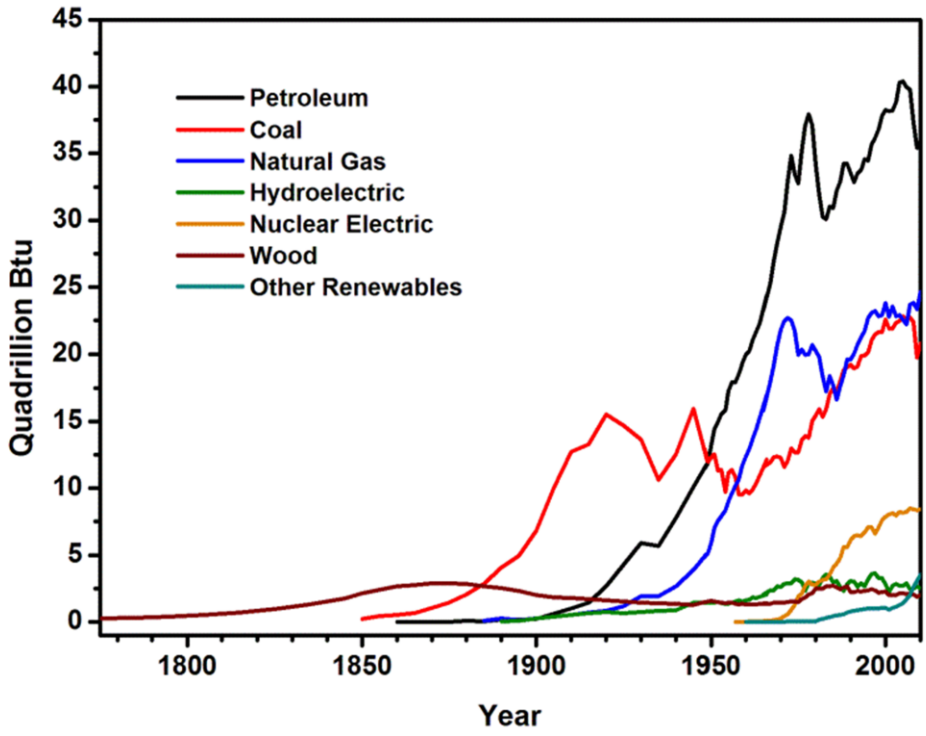

Figure 1-1. Energy resource use from 1775–2010.[1] This graph displays not only the shift in energy from wood to fossil fuels, but also shows that total energy usage has increased substantially since 1900 due to the industrial revolution and the large increase in world population over that time.

and wealth that was unimaginable in the wood-based energy economy that preceded it. The problem today, though, is being played out on a much larger scale. Fossil fuel resources are finite, and humans are using those resources at alarming rates. The world consumption of oil, for instance, currently stands at *ca.* 84 million barrels per day.[1] Many countries, the United States included, that were once among the largest producers of crude oil are on the decline of the peak oil production curve, and the world as a whole may be at or past the peak (Figure 1-2).[2] The combination of growing demand and shrinking supply is working to increase the price of oil and is likely to make access to energy a challenge in emerging markets. The same issues that

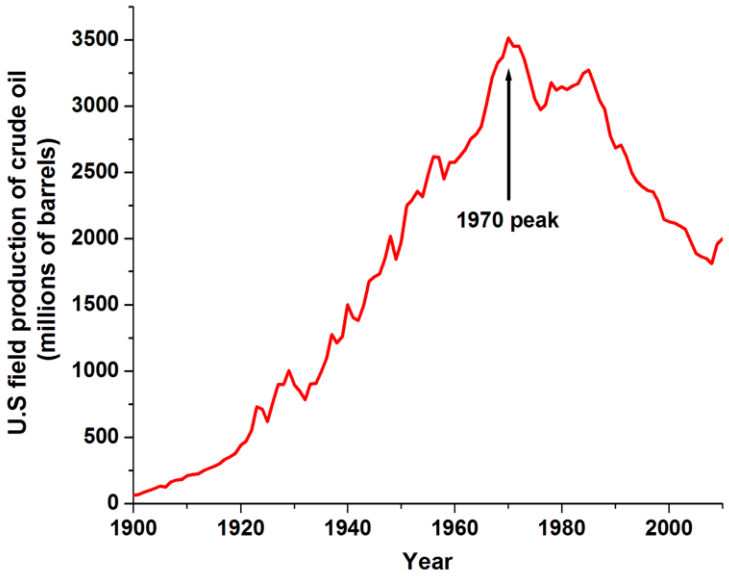

Figure 1-2. United States oil production from 1900-2010. The shape of this curve is similar to other oil production curves for those countries that have passed peak production and is projected to mirror the shape of the World's oil production. Source: United States Energy Information Administration.[2]

affect oil supply and price are likely to affect coal and natural gas in the not-so-distant future, as they are also subject to a peak followed by a decline.

Unlike the pre-1900 problem of wood scarcity that was largely regional and recoverable over time, the problem of fossil fuel scarcity we face today is worldwide and permanent. To add to the problem, the human population was 1.7 billion at the time of the discovery of oil only 100 years ago,[3] but is currently approaching 7 billion.[4] The growth in population made possible by the energy derived from coal and oil not only puts a strain on energy resources, but it also puts a strain on fresh water sources, food supplies, raw industrial products, and the world's forests. All this strain makes the current human situation look very much like we are heading for what ecologists refer to as an "overshoot-and-collapse." In this scenario, the demand for energy and resources exceeds the sustainable yield of natural systems, and if

significant changes are not made, a societal collapse can occur. To avoid collapse, the human population must adapt quickly to either drastically decrease overall energy use through efficiency and rationing or transition to a new form of energy, or more likely, a combination of the two.

A scarcity of energy resources (amongst other commodities) often results in international conflict, widening of the gap between rich and poor, and regional inequalities. To avoid these issues, new technology must be implemented. Some implementation of new energy resources has already begun, as can be seen in Figure 1-1, but the overwhelming majority of the World's energy still comes from fossil fuel resources. One solution to this problem is to roll out solar and wind power en masse. These energy sources have more than enough capability/capacity to supply the world's energy needs, but suffer from intermittency and high cost. It is easy to see that solar photovoltaics cannot supply energy at night and wind turbines cannot supply energy when the wind doesn't blow (i.e., intermittency). In addition, some areas in the U.S. receive over 80% of the possible sun irradiation (Yuma, AZ, Las Vegas, NV, etc.), while others get less than 40% (Juneau, AK, Mount Washington, NH, etc.).[5] The issue of high cost can be overcome through research, technical advancement, economies of scale,[6] and through the proper pricing of the externalities of dirty fuels such as coal and oil. Solar photovoltaic electricity generation, for example, has decreased in price significantly since systems hit the commercial market in 1978.[7] The key to overcoming these issues, then, is to develop ways to store the large amounts of energy that solar and wind can provide.

Another problem we face today comes from climate change. Climate change is an accepted phenomenon among most scientists of the 21st century but is currently a hot topic dividing citizens and political parties worldwide. We will not debate the reality of climate change caused by human activity here. It is instructive, nonetheless, to discuss the possible planetary changes in store for the Earth as greenhouse gas concentrations increase, polar ice caps melt, and the globe warms. Initial changes in temperature can follow three different manifolds, as shown in Figure 1-3.[8] Any of these climate change regimes will disrupt ecosystems, affect global economies, and change the Earth's landscape forever. A large majority of climate scientists agree that atmospheric CO_2 concentrations must be held at a level much lower than our current trajectory to avoid disruptive changes in climate, and that action must be quickly taken to do so.

CO_2 emissions are everywhere in life (Figure 1-4). The two largest emitters by far are the electricity generation and transportation sectors. One way to think about the emission of CO_2 in to the atmosphere is with some algebra introduced by Bill Gates in

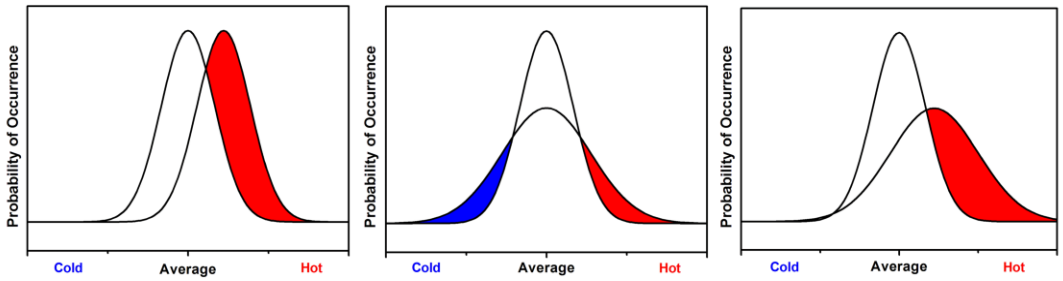

Figure 1-3. Possible temperature anomalies in a future with climate change.[8] The first possibility (left) is that the distribution of temperature will not change, but the average will shift to become hotter. The second possibility (center) is that the average will not change, but the distribution will change so as to make colder and hotter temperatures more likely. The third, and most probable, possibility (right) is that the average temperature will shift hotter and the distribution will become wider so that extreme heat events and erratic weather both become more likely.

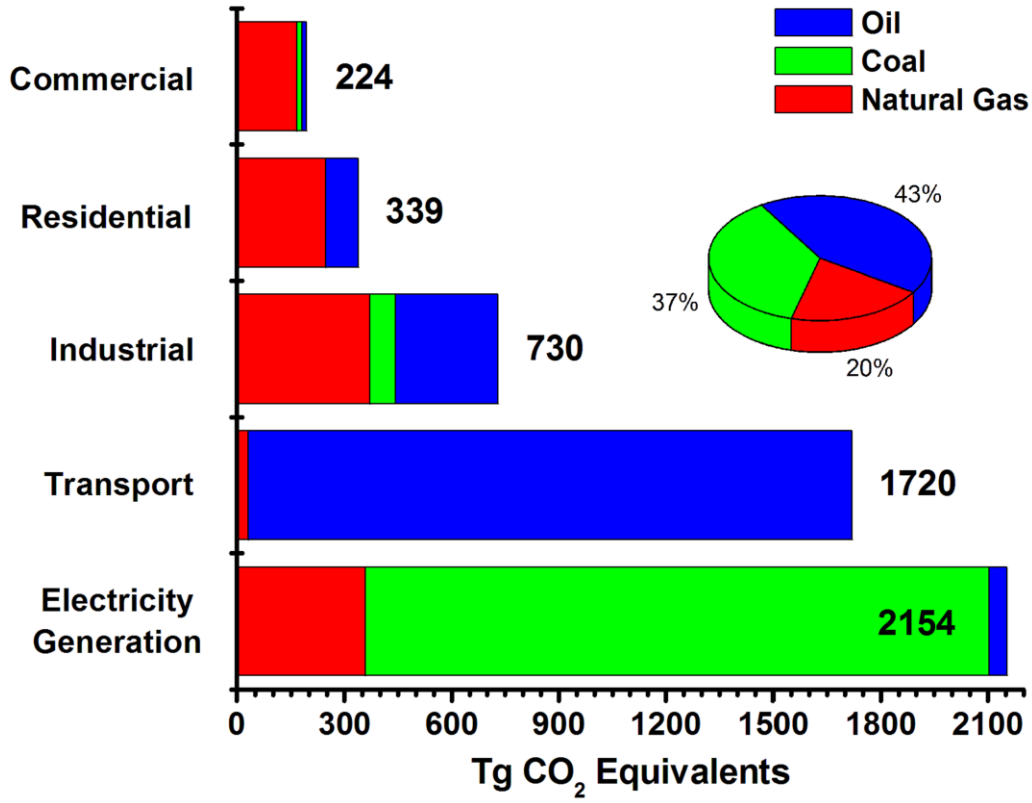

Figure 1-4. CO_2 equivalent (CO_2e) emissions for sectors with large emissions in the United States. Transportation and electricity generation account for more than 70% of the total CO_2e emissions and could be substantially decreased or eliminated by reducing CO_2 from the atmosphere to liquid fuels for renewable energy storage as well as for transportation fuel.

his 2010 TED talk.[9] Equation 1-1 below summarizes the emissions of CO_2 and provides a logical way to think about limiting those emissions.

$$CO_2e = P \times S \times E \times (CO_2/E) \qquad \textbf{E1-1}$$

In this equation, CO_2e represents emissions of CO_2 equivalents in to the atmosphere, P is the number of people on Earth, S is the services those people use for everyday life, E is the energy needed for those services, and (CO_2/E) is the quantity of

CO_2 per unit of energy. To get a handle on climate change and stabilize greenhouse gas concentrations, we must move the CO_2 quantity on the left side of the equation as close to zero as possible. How do we accomplish this goal?

It is clear that population is still growing and that this presents its own set of problems and strains on the environment. The population is estimated to rise until 2050 to a maximum of *ca.* nine billion before stabilizing and possibly decreasing after that.[10] In an ideal situation, all nine billion of those people will have access to basic services including health care, housing, fresh water, food, etc. Those services all use energy. In addition, new individuals and populations are climbing out of poverty every day and using more and more services, including a service with substantial associated emissions: the personal automobile. This phenomenon means that we will not see the *S* in the equation drop towards zero any time in the foreseeable future. *E* is tied directly to services. Increases in efficiency have, can, and will continue to lower the amount of energy per service, but it is unlikely that those increases in efficiency will be able to extend far below one-half of the energy per service that we currently observe. Therefore, the only variable in the equation that can possibly go to zero in the future is the CO_2/E term. According to the U.S. Energy Information Administration, 86% of the world's energy comes from the burning of fossil fuels.[11] Because all burning of fossil fuels contributes to greenhouse gas emissions, it is imperative that the world shift its energy uses to carbon free or carbon neutral energy resources so that the CO_2/E term in the equation drops and the overall product trends towards zero.

The wide deployment of renewable and clean energy systems can accomplish a large part of this goal if a suitable energy storage medium can be found. There is still, however, the issue of transportation fuel. There will be a need for high energy density liquid transportation fuels for the foreseeable future even if the majority of everyday commuting and regular driving is electrified. Uses for liquid fuels in the near (and not so near future) include air travel, long distance transport of goods, and powering large machinery for industrial and agricultural purposes.

One technology that has the potential to meet both the energy storage and transportation needs is the reverse combustion of CO_2 and H_2O to liquid fuels. Significant research must be done to make this option a reality. However, the benefits of accomplishing this goal would be enormous, as the fuels created would fit well into the existing infrastructure and would effectively recycle atmospheric carbon dioxide. In the next section I will discuss our approach for accomplishing this transformation.

1.2 The Electrocatalytic Approach

While universal transportation electrification remains an important societal goal, many transportation applications will continue to require the high mass and volumetric energy storage density of liquid hydrocarbon fuels. The catalytic conversion of CO_2 and H_2O to liquid fuels is a process that would positively impact the global carbon balance by recycling CO_2 from the atmosphere. The challenges presented here are great, but the potential rewards are enormous. CO_2 is a stable molecule generally produced by fossil fuel combustion and respiration. Returning CO_2

to a useful state by activation/reduction is a scientifically challenging problem, requiring appropriate catalysts and energy input. This poses several fundamental challenges in chemical catalysis, electrochemistry, photochemistry, semiconductor physics and engineering. In addition, substantial research must be done to advance atmospheric CO_2 collection strategies to be both cost and energy efficient, but that is a topic for a different day and a different author.

With respect to CO_2 reduction to liquid fuels or fuel precursors, proton-coupled multi-electron steps are more favorable than single electron reductions, as thermodynamically more stable molecules are produced. This condition is summarized in Equations 1-2 to 1-6 (with potentials given for pH 7 in aqueous solution versus NHE, 25 °C, 1 atmosphere gas pressures, and 1 M for the other solutes).[12, 13] In contrast, the single electron reduction of CO_2 to $CO_2^{\bullet-}$ occurs at E° = –1.90 V (Equation 1-7) due to a large reorganizational barrier between the linear molecule and bent radical anion.

$CO_2 + 2H^+ + 2e^- \rightarrow CO + H_2O$	E° = – 0.53 V	**E1-2**
$CO_2 + 2H^+ + 2e^- \rightarrow HCO_2H$	E° = – 0.61 V	**E1-3**
$CO_2 + 4H^+ + 4e^- \rightarrow HCHO + H_2O$	E° = – 0.48 V	**E1-4**
$CO_2 + 6H^+ + 6e^- \rightarrow CH_3OH + H_2O$	E° = – 0.38 V	**E1-5**
$CO_2 + 8H^+ + 8e^- \rightarrow CH_4 + 2H_2O$	E° = – 0.24 V	**E1-6**
$CO_2 + e^- \rightarrow CO_2^{\bullet -}$	E° = – 1.90 V	**E1-7**

One key problem in the conversion of CO_2 to liquid fuels is the assembly of the nuclei and chemical bonds to convert a relatively simple molecule into a more energetic one. Strategically, there are two primary ways to conceptualize this problem.

The first is to convert CO_2 and H_2O into CO and H_2 (synthesis gas), and then to use well-proven (but expensive) Fischer-Tröpsch technologies to convert the synthesis gas to liquid fuels, including diesel fuel and gasoline.[14] The advantage here is that it is considerably easier to convert CO_2 to CO and H_2O to H_2 than it is to make even a simple liquid fuel such as methanol by electrocatalytic processes. The second primary option is to convert CO_2 directly to liquid fuels by an electrocatalytic process. Here, the kinetic challenges are great. One possibility is to identify a single catalyst that can direct the complete sequence of steps necessary for converting CO_2 to formic acid (HCOOH), then to formaldehyde (H_2CO), then to hydrocarbons or alcohols, *all* with low kinetic barriers. Catalysts that bring the required functionalities into the proper position at the proper time will be required. A second possibility is to identify catalyst "panels," where each panel contains optimal catalysts for each of the steps in the overall transformation of CO_2 to liquid fuel (Figure 1-5). Here we envision three catalysts (each optimized for a particular reaction) that could produce first formic acid, then formaldehyde, and finally release methanol. An advantage of the parallel approach is that the catalysts for each step can be optimized independently using combinatorial or traditional ligand tuning methods, and then the catalyst panel can be assembled from the proven catalyst components. Literature precedent for such an approach does exist, as recently reported by Huff and Sanford.[15] In their system, however, the panel consisted of a catalyst for the reduction of CO_2 to formic acid, followed by a catalyst for the esterification of formic acid to a formate ester, and finally a catalyst for the hydrogenation of the ester to release methanol. One challenge

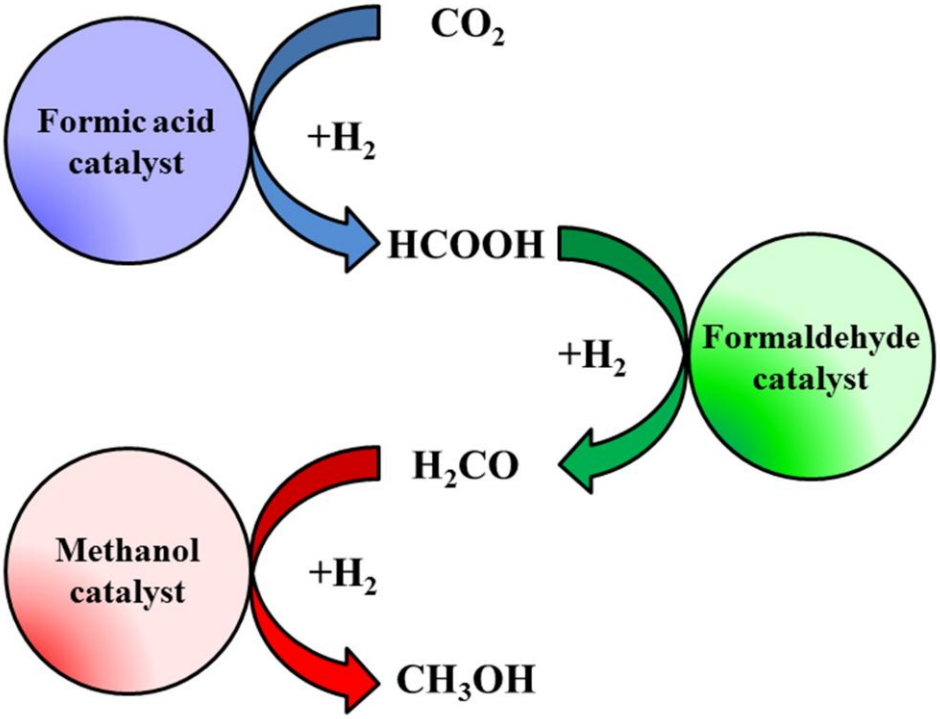

Figure 1-5. Proposed pathway for the tandem catalytic reduction of CO_2 to methanol. A series of catalysts that each contributes to the overall reduction of CO_2 to methanol in optimized single steps.

to this approach, however, is that of avoiding catalyst poisoning issues, and will require by careful transport of products from reaction vessel to reaction vessel or making several catalysts compatible with each other.

This dissertation will focus largely on the conversion of CO_2 to CO for later use as a component in synthesis gas, but research is ongoing in many laboratories, including our own, to identify methods for the transformation of CO_2 directly to liquid fuels using single catalysts,[16] algae[17, 18] or catalyst panels.[15]

1.3 Electrocatalysis Tutorial

If the reduction of carbon dioxide to liquid fuels is to be accomplished through photovoltaic or other electrochemical means, the deployment of efficient *electrocatalysts* will be necessary. An electrocatalyst participates in both an electron transfer reaction (at an electrode) and facilitates acceleration of a chemical reaction. The electron transfer and chemical kinetics must both be optimized for an efficient electrocatalyst. Additionally, an *optimal* electrocatalyst must display a good thermodynamic match between the redox potential (E°) for the electron transfer reaction and the chemical reaction that is being catalyzed (*e.g.*, the reduction of CO_2 to CO). These factors can be optimized through the chemical tuning of the electrocatalyst metal centers via appropriate ligand design. Electrocatalysts are typically screened for their redox potentials, current efficiencies, electron transfer rate constants and chemical kinetics in order to identify the best overall catalysts.

In general, electrocatalysts are electron transfer agents that ideally operate near the thermodynamic potential of the reaction to be driven, E°(products/substrates) (Figure 1-6). The direct electrochemical reduction of carbon dioxide on most electrode surfaces requires a large overvoltage and consequently the overall system conversion efficiency suffers. The overvoltage can be considered to be the difference between the applied electrode potential, $V_{applied}$, and the thermodynamic potential for the desired reaction, E°(products/substrates). Both thermodynamic and kinetic considerations are important here. Clearly, in order to minimize overvoltages while maintaining appreciable current densities, catalysts need to be developed that have formal

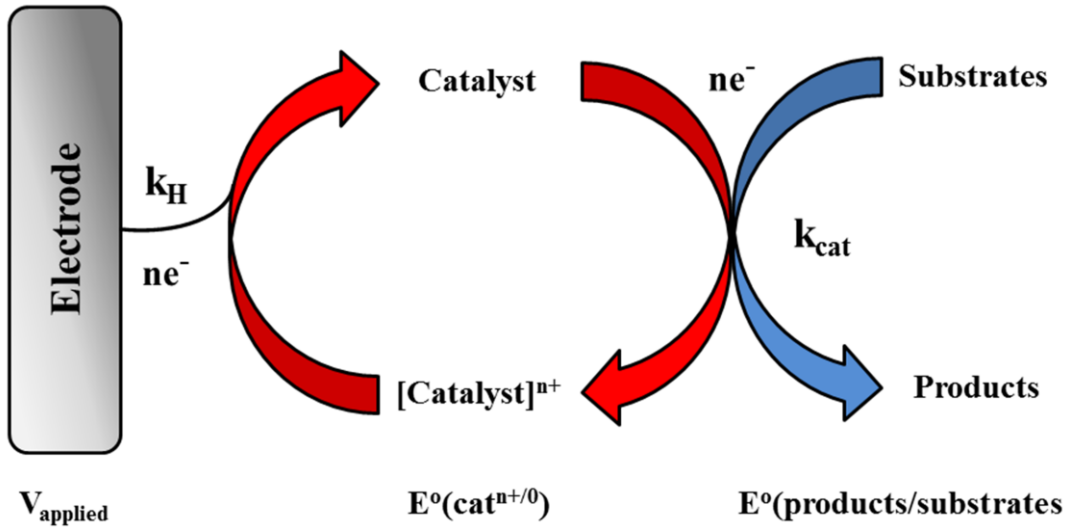

Figure 1-6. A general scheme for the electrocatalytic reduction of a substrate by a homogeneous electrocatalyst includes the heterogeneous electron transfer from the electrode to the catalyst (k_H), the rate of homogeneous catalysis (k_{cat}), and various potentials including the voltage applied by the electrode ($V_{applied}$), the E° for the catalyst, and the E° for the products being made in the reaction.

potentials, $E^\circ(Cat^{n+/0})$, well matched to the E°(products/substrates), and appreciable rate constants, k_{cat}, for the chemical reduction of substrates to products at this potential. In addition, the heterogeneous rate constant, k_H, for the electronic reduction of the electrocatalyst must be high for $V_{applied}$ near $E^\circ(Cat^{n+/0})$.

Reaction rates for these processes can be estimated from the steady-state limiting current in cyclic voltammetry or by rotating disk voltammetry studies of the heterogeneous electron transfer kinetics. Homogeneous electrocatalytic activity can be identified easily in a cyclic voltammogram (CV) (Figure 1-7). In a CV under a dry and inert atmosphere, an electrocatalyst should show a reversible or quasi-reversible redox couple. Upon addition of CO_2, however, the diffusion limited current increases, the potential shifts anodically, and the reversibility in the return oxidation wave is lost due to the chemical reaction between CO_2 and the electrocatalyst. The conversion of CO_2

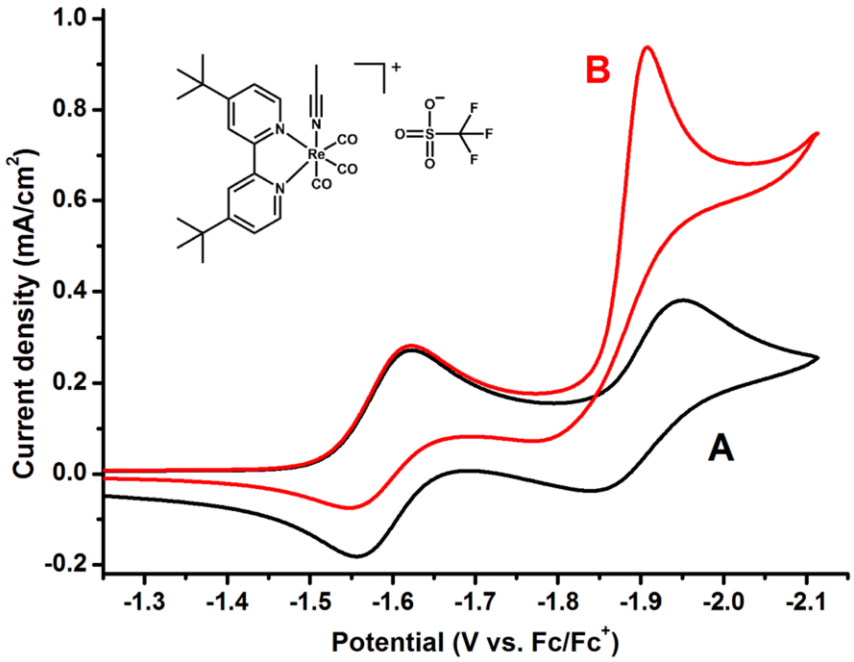

Figure 1-7. Example cyclic voltammogram (CV) under (a) Ar and (b) CO_2. Under a CO_2 environment we observe an anodic potential shift, an increase in current, and a non-reversible waveform.

to CO requires two electrons. In the case of the rhenium system in Figure 1-7 the electrons enter the catalyst sequentially, with the first electron transferred to the bipyridine and the second to the metal center (discussed in Chapter 2 of this dissertation). The two electrons can then be transferred to CO_2 simultaneously through the rhenium center. Electrocatalysts can offer lower overpotentials for chemical reactions, improve selectivity, and increase the reaction kinetics of carbon dioxide conversion.

The field of transition metal-catalyzed reduction of CO_2 is relatively new, with its origins tracing back to the 1970's, but the field has gained in breadth and intensity over the last 30 years. Before reviewing the important studies in the electrocatalytic reduction of CO_2, though, we must consider several molecular studies of the reactivity

of CO_2 toward transition metal complexes. Aresta and Nobile published the first crystal structure of CO_2 bound to a transition metal complex in 1975: an η^2-bidentate binding mode involving the carbon atom and one oxygen atom, with significant bending in the CO_2 structure.[19] Another important study came in 1981, when Darensbourg and co-workers reported that anionic group 6B metal hydrides would react readily with CO_2 to form metal formate complexes.[20] This reaction proceeds according to Equation 1-8 and is believed to be essential in the water-gas shift reaction catalyzed by metal carbonyl complexes in basic solutions.

$$HM(CO)_5^- + CO_2 \leftrightarrow HC(O)OM(CO)_5^- \qquad \textbf{E1-8}$$

Transition metal-catalyzed reductions of CO_2 were preceded by work focused on the reduction of CO_2 at various types of electrode materials. The most successful electrode for the reduction of CO_2 to formic acid was found to be a mercury drop electrode. Although groups had studied this reaction previously, Eyring and co-workers reported an in-depth study of the mechanism and kinetics of the reaction in 1969. They were able to obtain current efficiencies of 100% in pH 6.7 solutions with a lithium bicarbonate electrolyte.[21] Since then many more studies reporting the electrocatalytic reduction of CO_2 to value-added products at electrode surfaces have been published, including a study by Hori et al. reporting the Faradaic efficiencies for many products of CO_2 reduction at many metal electrodes.[22] To better visualize the wide variety of products produced at these surfaces I have adapted the data from the

Hori paper to Figure 1-8 below. These studies have helped direct the development of molecular catalysts and have been very important for the advancement of the field.

In the years following these first examples of carbon dioxide activation, many reports appeared in the literature that can be divided into three major categories: (1) metal catalysts with macrocyclic ligands, (2) metal catalysts with phosphine ligands, and (3) metal catalysts with bipyridine ligands. These seminal studies are summarized

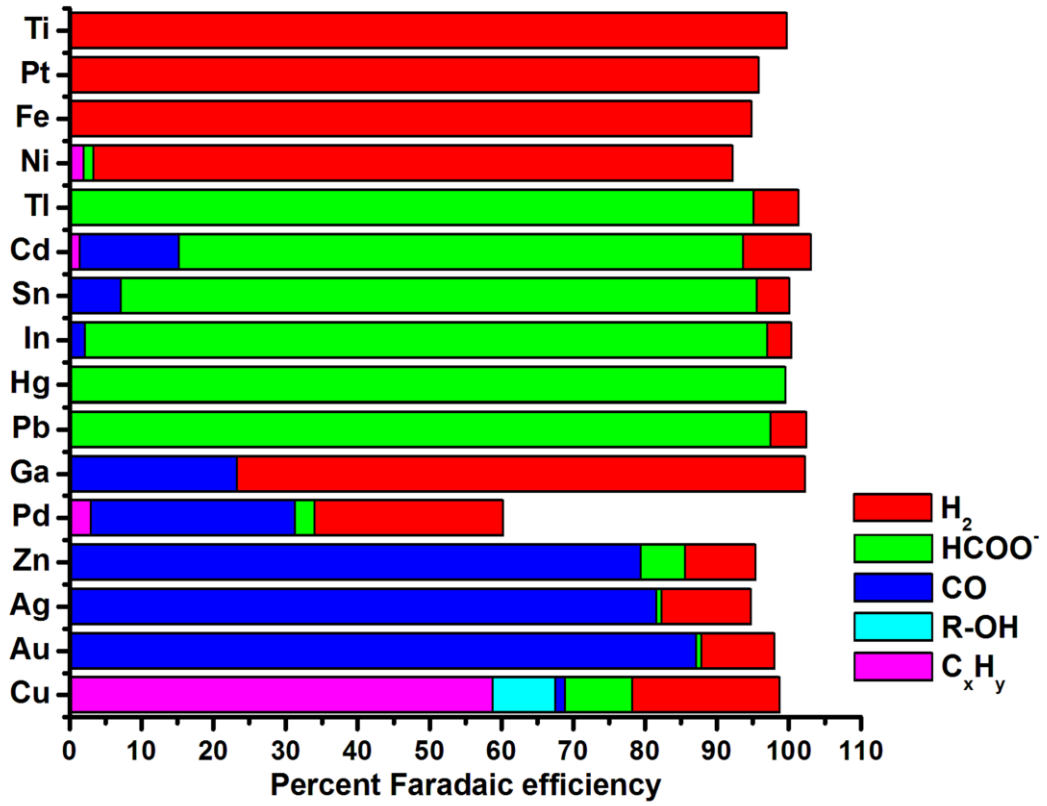

Figure 1-8. Product distribution for the electrocatalytic reduction of CO_2 to value-added products at various metal electrodes. Important points about this graph are, 1) the high percentage of H_2 made at many metal electrodes in aqueous solution, 2) the tendency of metal electrodes to make high percentages of two electron reduced species, and 3) the wide distribution of products made at electrodes that are able to reduce CO_2 by more than two electrons to products such as alkanes, alkenes, and alcohols.

in a 2009 review by our group.[23]

1.4 The Re(bipy)(CO)$_3$(L) System

The first report of catalysis by the Re(bipy)(CO)$_3$X came in 1983 by Hawecker, Lehn, and Ziessel.[25] In that study, the Re complex was used as both a photosensitizer and a photocatalyst that acted to perform the two electron reduction of CO_2 to CO. The source of CO was confirmed using $^{13}CO_2$ and the catalyst displayed higher turnover numbers than even the best-case scenario with $Ru(bipy)_3^{2+}/Co^{II}$.

In 1984 the Lehn group reported the electrocatalytic reduction of CO_2 using Re(bipy)(CO)$_3$Cl (bipy = 2,2'-bipyridine).[26] Using this rhenium bipyridine complex they were able to show the selective reduction of CO_2 to CO at a potential of -1.49 V vs. SCE using a 9:1 DMF/H_2O solution. It was also noted that as the percentage of water was increased the selectivity for CO was diminished, and when the reduction was run under an atmosphere of argon, only molecular hydrogen was produced. While this system had high current efficiencies (98%), and excellent selectivity for carbon monoxide over hydrogen production, the limiting factor was the low TOF of 21 hour^{-1} calculated using bulk electrolysis experimental yields. The communications described in this and the previous paragraph, were expanded in a follow-up full paper in 1986 that further described the studies as well as mechanistic experiments and changes in the catalytic conditions.[27]

The system has been studied extensively since those seminal studies by experimentalists and theorists, electrocatalytic and photocatalytic groups, and by

several who were not even interested in the catalytic properties of the complex. We find it informative to reflect on these studies before delving in to the current research. We will discuss here the "non-catalysis" studies, photocatalytic studies, and electrocatalytic studies for complexes of the type Re(α-diimine)$(CO)_3$L.

Very early reports on the Re(bipy) system from Sullivan and Meyer looked at CO_2 insertion into the Re-H bond of Re(bipy)$(CO)_3$H. It was observed that the complex underwent both photo-induced [27] and thermally activated [28] reactions with CO_2. The photo-induced reaction was reported first in a very short communication. The thermally activated reaction, though, was later reported to form a stable formate complex in THF, acetone, CH_3CN, and other solvents. In this in-depth report, the authors were able to establish a first-order dependence of k_{obs} on [CO_2] and dramatic solvent effects for the CO_2 insertion. Based on this study it is reasonable to hypothesize that electrochemical catalysis in the presence of protons could lead to the production of formate instead of CO. This was addressed in the research and will be discussed in depth in Chapter 3.

A number of groups have studied the photophysical properties of the Re(bipy)$(CO)_3$X system. One such study by Meyer and co-workers found that, amongst other things, the energetic separation between the dπ(Re) and π^*(4,4'-X_2-bipy) (where X = NH_2, NEt_2, $NHCOCH_3$, OCH_3, CH_3, H, Ph, Cl, CO_2Et or NO_2) orbitals is high.[28] This leads to enhanced excited-ground state energy gaps, decreased π-π^* mixing, and decreased oscillator strengths. They also found that the extent of the

distortion in the 4,4'-X_2-bipy ligand in the excited state increases linearly with the energy gap between the excited and ground states.

Another important set of experiments was conducted by Hartl and co-workers and published in 1995.[29] It was not only the first published IR and UV-Vis spectroelectrochemistry published for the system, but it also showed that the stability of the Re-L' bond (L' = halide, OTf^-, THF, MeCN, *n*-PrCN, PPh_3, or $P(OMe)_3$) is altered drastically in the reduced state by the nature of the α-diimine ligand (bipy, *i*-Pr-PyCa, dapa, dpp, or abpy) and its ability to accommodate the unpaired electron in its π^* LUMO. That sixth coordination spot is very important for catalysis as the position for substrate binding, as we will see throughout this dissertation.

The star of this dissertation is Re(bipy-*t*Bu)$(CO)_3$(L) (where bipy-*t*Bu = 4,4'-di-*tert*-butyl-2,2'-bipyridine and L = halide, MeCN, or pyridine). The first report of that specific complex was a photophysical report by Yam and co-workers in 1995.[30] The X-ray crystal structure of Re(bipy-*t*Bu)$(CO)_3$Cl was reported at room temperature and showed a slightly distorted octahedron with the three carbonyl ligands arranged in a facial fashion. The other main findings of that paper are not important for the current discussion.

Some efforts have been made to heterogenize CO_2 photo- and electrocatalysts. One such strategy involved zeolite-entrapped molecules. In that scenario, the steric and electrostatic constraints in the zeolite altered the photochemical and photophysical properties of the guest complex.[31] Re(bipy)$(CO)_3$Cl and $[Re(bipy)(CO)_3(py)]^+$ have been encapsulated in NaY and A1MCM-41 molecular sieves respectively, and their

photocatalytic properties have been studied.[32] In each case, the photoirradiation of the heterogenized complex under 100 Torr CO_2 led to the production of CO (measured by GC) and carbonate (measured by IR) species. The authors concluded that, in both systems, the molecular sieve acted as an electron donor to afford $[Re(bipy)(CO)_3L]^-$ that can go on to react with CO_2. Another study by Cosnier, Deronzier and Moutet showed the electrocatalytic reduction of CO_2 on electrodes modified by $Re(bipy)(CO)_3Cl$ bound to polypyrrole films.[33] The system described in that report operates with high Faradaic efficiency and catalytic efficiency corresponding to an optimum film thickness.

A thorough study of the photocatalytic properties of many different Re^I complexes was reported in 2006 by Alberto and co-workers.[34] A head-to-head comparison of catalysts that varied in diimine ligand, anion X ligand, and metal center was completed. The nature of the diimine ligand affected the yield of CO in those experiments, but the nature of the anionic X ligand also played a major role. Studies like this were one major motivation for modifications of $Re(bipy)(CO)_3Cl$ as an electrocatalyst for the reduction of CO_2 to CO in this dissertation.

Several attempts have been made to elucidate the electrocatalytic reduction mechanism for the system. Meyer *et al.* identified both one- and two-electron pathways for the reduction of CO_2 to CO by rhenium complexes.[35] The one-electron pathway leads to the disproportionation reaction yielding CO and CO_3^{2-}, while the two-electron pathway leads to the formation of CO with no detectable amount of CO_3^{2-}. They also established that, after the first reduction of the complex, reversible

dimer formation occurs. Pre-catalytic species were further studied by Hartl, Turner, and co-workers using infrared spectroelectrochemistry (IR-SEC).[36] IR-SEC experiments revealed the pre-catalytic reduction species in detail, including the bipy-based first reduction, the dimer formation, and the metal-based second reduction.

Another important study came from Wong, Chung and Lau in 1998. They probed both rate enhancement and mechanism of CO_2 reduction to CO by the addition of weak Brönsted acids to Re(bipy)$(CO)_3$L(OTf) where L is either acetonitrile or pyridine.[37] Two major findings came from their experiments that are relevant to this dissertation. The first is that the addition of Brönsted acids leads to a large increase in catalytic current, pointing to a synergistic effect of proton sources as "co-catalysts" or "co-substrates." The second is that the rate of catalysis displayed a second-order dependence on $[H^+]$. This is important when exploring possible mechanistic pathways because it points to the double protonation of one of the oxygen atoms on CO_2 to be released as H_2O.

With this rich history of research on rhenium complexes in mind, we set out to improve the catalytic activity of these complexes. We also hoped to gain valuable insight for the future development of catalysts based on earth-abundant metals that display high turnover rates, high turnover numbers, high Faradaic efficiencies, and low overpotentials.

Note: Much of the material for this chapter comes directly from a manuscript entitled "Electrocatalytic and homogeneous approaches to conversion of CO_2 to liquid fuels" by Eric E. Benson, Clifford P. Kubiak, Aaron J. Sathrum, and Jonathan M. Smieja, which has been published in *Chemical Society Reviews*, **2009**, *38*, 89-99. http://dx.doi.org/10.1039/B804323J. The dissertation author is an equal contributor to this manuscript.

1.5 References

1. United States Energy Information Administration (2011) *Energy Perspectives 1949-2010*.

2. United States Energy Information Administration (2011) *Petroleum & Other Liquids* (Accessed 01/09/2012) http://www.eia.gov/dnav/pet/hist/LeafHandler.ashx?n=PET&s=MCRFPUS1&f=A.

3. United Nations Population Division (1999) *World Population Prospects: The 1998 Revision* (New York).

4. United States Census Bureau (2011) *U.S. & World Population Clocks* (Accessed 12/15/2011) http://www.census.gov/main/www/popclock.html.

5. National Oceanographic and Atmospheric Association (2004) *Ranking of Cities Based on % Annual Possible Sunshine* (Accessed 01/09/2012) http://www.ncdc.noaa.gov/oa/climate/online/ccd/pctposrank.txt.

6. Christensen LR, Greene WH (1976) Economies of Scale in U.S. Electric Power Generation. *JPE* 84(4):655-676.

7. Lacey S (2011) *Anatomy of a Solar PV System: How to Continue "Ferocious Cost Reductions" for Solar Electricity* (Accessed 01/09/2012) http://thinkprogress.org/romm/2011/07/06/261550/solar-pv-system-cost-reductions/.

8. Gershunov A (2011) Expected Changes in Key Weather-related Extreme Events in California. *Vulnerability and Adaptation to Extreme Events in California in the Context of a Changing Climate: New Scientific Findings*.

9. TED Conferences, LLC (2010) *Bill Gates on energy: Innovating to zero!* (Accessed 02/01/2012) www.ted.com.

10. United Nations Department of Economic and Social Affairs (2004) *World Population to 2300* (New York).

11. International Energy Agency (2010) *Key World Energy Statistics* (Paris).

12. Halmann MM, Steinberg M (1999) *Greenhouse Gas Carbon Dioxide Mitigation Science and Technology* (Lewis Publishers, Boca Raton, FL).

13. Sutin N, Creutz C, Fujita E (1997) Photo-induced generation of dihydrogen and reduction of carbon dioxide using transition metal complexes. *Comments Inorg. Chem.* 19(2):67-92.

14. Underwood AJV (1940) Industrial synthesis of hydrocarbons from hydrogen and carbon monoxide. *Ind. Eng. Chem. Res.* 32:449-454.

15. Huff CA, Sanford MS (2011) Cascade Catalysis for the Homogeneous Hydrogenation of CO_2 to Methanol. *J. Am. Chem. Soc.* 133(45):18122-18125.

16. Barton EE, Rampulla DM, Bocarsly AB (2008) Selective Solar-Driven Reduction of CO_2 to Methanol Using a Catalyzed p-GaP Based Photoelectrochemical Cell. *J. Am. Chem. Soc.* 130(20):6342-6344.

17. Amaro HM, Guedes AC, Malcata FX (2011) Advances and perspectives in using microalgae to produce biodiesel. *Applied Energy* 88(10):3402-3410.

18. Dragone G, Fernandes B, Vicente AA, Teixeira JA (2010) Third generation biofuels from microalgae. *Current Research, Technology and Education Topics in Applied Microbiology and Microbial Biotechnology*, ed A. Mendez-Vilas (Formatex, Badajoz, Spain), Vol 1, pp 1355-1366.

19. Aresta M, Nobile CF, Albano VG, Forni E, Manassero M (1975) New Nickel-Carbon Dioxide Complex - Synthesis, Properties, and Crystallographic Characterization of (CO_2)-Bis(Tricyclohexylphosphine)Nickel. *J. Chem. Soc., Chem. Commun.* (15):636-637.

20. Darensbourg DJ, Rokicki A, Darensbourg MY (1981) Facile reduction of carbon dioxide by anionic Group 6b metal hydrides. Chemistry relevant to catalysis of the water-gas shift reaction. *J. Am. Chem. Soc.* 103(11):3223-3224.

21. Paik W, Andersen TN, Eyring H (1969) Kinetic Studies of Electrolytic Reduction of Carbon Dioxide on a Mercury Electrode. *Electrochim. Acta* 14(12):1217-&.

22. Hori Y, Wakebe H, Tsukamoto T, Koga O (1994) Electrocatalytic process of CO selectivity in electrochemical reduction of CO_2 at metal electrodes in aqueous media. *Electrochim. Acta* 39(11–12):1833-1839.

23. Benson EE, Kubiak CP, Sathrum AJ, Smieja JM (2009) Electrocatalytic and homogeneous approaches to conversion of CO_2 to liquid fuels. *Chem. Soc. Rev.* 38(1):89-99.

24. Wilson AD, *et al.* (2005) Hydrogen Oxidation and Production Using Nickel-Based Molecular Catalysts with Positioned Proton Relays. *J. Am. Chem. Soc.* 128(1):358-366.

25. Hawecker J, Lehn J-M, Ziessel R (1983) Efficient photochemical reduction of CO_2 to CO by visible light irradiation of systems containing Re(bipy)$(CO)_3$X or $[Ru(bipy)_3]^{2+}$-Co^{2+} combinations as homogeneous catalysts. *J. Chem. Soc., Chem. Commun.* (9):536-538.

26. Hawecker J, Lehn JM, Ziessel R (1984) Electrocatalytic reduction of carbon dioxide mediated by Re(bipy)$(CO)_3$Cl (bipy = 2,2'-bipyridine). *J. Chem. Soc., Chem. Commun.* (6):328-330.

27. Hawecker J, Lehn JM, Ziessel R (1986) Photochemical and Electrochemical Reduction of Carbon Dioxide to Carbon Monoxide Mediated by (2,2'-Bipyridine)Tricarbonylchlororhenium(I) and Related Complexes as Homogeneous Catalysts. *HeIv. Chim. Acta* 69(8):1990-2012.

28. Worl LA, Duesing R, Chen P, Ciana LD, Meyer TJ (1991) Photophysical properties of polypyridyl carbonyl complexes of rhenium(I). *J. Chem. Soc., Dalton Trans.* (S):849-858.

29. Stor GJ, Hartl F, van Outersterp JWM, Stufkens DJ (1995) Spectroelectrochemical (IR, UV/Vis) Determination of the Reduction Pathways for a Series of $[Re(CO)_3$(alpha-diimine)$L']^{0/+}$ (L' = Halide, OTf^-, THF, MeCN, n-PrCN, PPh_3, $P(OMe)_3$) Complexes. *Organometallics* 14(3):1115-1131.

30. Yam VWW, Lau VCY, Cheung KK (1995) Synthesis and Photophysics of Luminescent Rhenium(I) Acetylides-Precursors for Organometallic Rigid-Rod Materials - X-Ray Crystal-Structures of $[Re(^tBu_2$-Bpy$)(CO)_3(^tBuC{\equiv}C)]$ and $[Re(^tBu_2$-Bpy$)(CO)_3Cl]$. *Organometallics* 14(6):2749-2753.

31. Yoon KB (1993) Electron- and charge-transfer reactions within zeolites. *Chem. Rev.* 93(1):321-339.

32. Sung-Suh HM, Kim DS, Lee CW, Park S-E (2000) Photoinduced activation of CO_2 by rhenium complexes encapsulated in molecular sieves. *Appl. Organomet. Chem.* 14(12):826-830.

33. Cosnier S, Deronzier A, Moutet J-C (1988) Electrocatalytic reduction of CO_2 on electrodes modified by *fac*-Re(2,2'-bipyridine)$(CO)_3$Cl complexes bonded to polypyrrole films. *J. Mol. Catal.* 45(3):381-391.

34. Kurz P, Probst B, Spingler B, Alberto R (2006) Ligand Variations in [ReX(diimine)$(CO)_3$] Complexes: Effects on Photocatalytic CO_2 Reduction. *Eur. J. Inorg. Chem.* 2006(15):2966-2974.

35. Sullivan BP, Bolinger CM, Conrad D, Vining WJ, Meyer TJ (1985) One- and two-electron pathways in the electrocatalytic reduction of CO_2 by *fac*-Re(bpy)$(CO)_3$Cl (bpy = 2,2'-bipyridine). *J. Chem. Soc., Chem. Commun.* (20):1414-1416.

36. Johnson FPA, George MW, Hartl F, Turner JJ (1996) Electrocatalytic Reduction of CO_2 Using the Complexes [Re(bpy)$(CO)_3$L]n (n = +1, L = $P(OEt)_3$, CH_3CN; n = 0, L = Cl^-, OTf^-; bpy = 2,2‘-Bipyridine; OTf^- = CF_3SO_3) as Catalyst Precursors: Infrared Spectroelectrochemical Investigation. *Organometallics* 15(15):3374-3387.

37. Wong K-Y, Chung W-H, Lau C-P (1998) The effect of weak Brönsted acids on the electrocatalytic reduction of carbon dioxide by a rhenium tricarbonyl bipyridyl complex. *J. Electroanal. Chem.* 453(1–2):161-169.

Chapter 2

Re(bipy-*t*Bu)$(CO)_3$Cl – improved catalytic activity for reduction of carbon dioxide. IR-Spectroelectrochemical and mechanistic studies.

2.1 Introduction

In general, there are three main classes of synthetic carbon dioxide (CO_2) reduction catalysts. These are: 1) metal complexes with macrocyclic ligands, 2) metal complexes with phosphine ligands, and 3) metal complexes with bipyridine ligands.[1] Of these classes of catalysts, metal bipyridine complexes have shown both reasonable activities and lifetimes. In particular, the complex Re(bipy)$(CO)_3$Cl (where bipy = 2,2'-bipyridine) [**2**], reported by Lehn and co-workers in 1984, was reported to catalyze the reduction of CO_2 to carbon monoxide (CO) on a glassy carbon electrode in a 9:1 DMF:H_2O solution during a 14 hour experiment with 98% Faradaic efficiency and no significant decrease in performance from catalyst degradation.[2, 3]

Photoreduction of CO_2 to CO has also been reported using Re(bipy)$(CO)_3$X complexes (where X is an anionic ligand).[3-8] In these experiments, monochromatic light and a sacrificial donor (triethylamine, nitroethanol, or triethanolamine) were used to effect photocatalysis.

In the time since Lehn's original report of the Re(bipy)$(CO)_3$Cl catalyst many other synthetic CO_2 reduction catalysts have been reported as summarized in reference 1. The best of these catalysts in terms of rate constant (1000 $M^{-1}s^{-1}$) is the bimetallic Pd-phosphine developed by Dubois and co-workers, but this catalyst has a turnover number of only eight.[9] [Pd(tridentate)(solvent)]$(BF_4)_2$] catalysts with more reasonable turnover numbers in the hundreds or more have also been developed, but in that case the rate constant drops to only ~150 $M^{-1}s^{-1}$.[9, 10]

Other complexes with modified bipyridine ligands have been reported, including Re(bipy-COOH)$(CO)_3$Cl (bipy-COOH = 4,4'-dicarboxyl-2,2'-bipyridine) [**1**],[11] Re(dmb)$(CO)_3$Cl (dmb = 4,4'-dimethyl-2,2'-bipyridine) [**3**],[12-14] Re(bipy-*t*Bu)$(CO)_3$Cl (bipy-*t*Bu = 4,4'-di-*tert*-butyl-2,2'-bipyridine) [**4**],[15] and Re(bipy-OMe)$(CO)_3$Cl (bipy-OMe = 4,4'-dimethoxy-2,2'-bipyridine) [**5**],[8] but none of those complexes were studied for electrocatalytic reduction of CO_2.

In this study, all of the above complexes were studied by cyclic voltammetry to determine their relative reactivity in the catalytic reduction of carbon dioxide. In the end, we determined that complex [**4**] is the best catalyst in the group with a second order rate constant of 1000 $M^{-1}s^{-1}$ and a Faradaic efficiency of 99 ± 2 %; a marked improvement in rate of catalysis over the original Lehn catalyst, [**2**]. The catalyst also

showed long term stability, displaying no significant loss in activity over the course of a five hour bulk electrolysis experiment. IR-spectroelectrochemical studies of this catalyst revealed several mechanistic details which suggest important considerations for future improvement of CO_2 reduction catalysts.

2.2 Results and Discussion

Electrochemical studies. Electrochemical studies of a series of Re(bipyridyl)$(CO)_3$Cl complexes showed that the bipyridine ligand substituents affect the first and second reduction potentials. A series of five complexes with varying electron donating/withdrawing substituents in the 4,4' positions of the bipyridine ligand were studied: COOH [**1**] < H [**2**] < Me [**3**] < *t*Bu [**4**] < OCH_3 [**5**] (Figure 2-1). It is convenient to consider the complexes in the above order because of increasing pK_a of the pyridine ligand (4-carboxylpyridine pK_a = 3.10, pyridine pK_a = 5.17, 4-methylpyridine pK_a = 5.94, 4-*tert*-butylpyridine pK_a = 5.99, 4-methoxypyridine pK_a = 6.62).[16] This trend is reflected in the increasingly negative reduction potentials for the

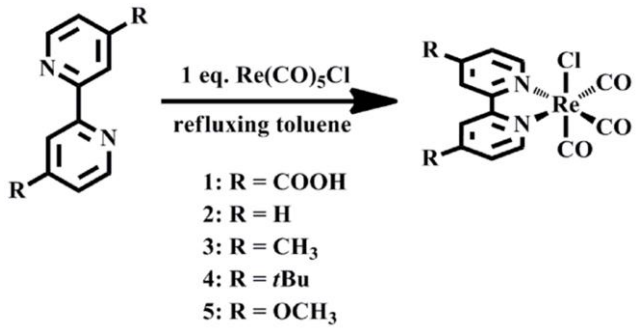

Figure 2-1. Synthetic scheme for complexes [1]–[5] in this chapter. Further synthetic detail is found in the experimental section.

Table 2-1. Measured reduction potentials and ν(CO) stretches for complexes [**1**]–[**5**] in this chapter. First reduction potential is the $E_{1/2}$ and the second reduction potential is measured at the peak maximum for the irreversible reduction. All ν(CO) stretches were recorded in acetonitrile.

Complex	**1st reduction (V *vs.* Fc/Fc$^+$)**	**2nd reduction (V *vs.* Fc/Fc$^+$)**	**ν(CO) stretches (cm^{-1})**
Re(bipy-COOH)(CO)$_3$Cl [**1**]	–1.34	–2.13	2037, 1935, 1911
Re(bipy)(CO)$_3$Cl [**2**]	–1.74	–2.13	2025, 1918, 1902
Re(dmb)(CO)$_3$Cl [**3**]	–1.83	–2.17	2025, 1918, 1902
Re(bipy-*t*Bu)(CO)$_3$Cl [**4**]	–1.85	–2.23	2023, 1916, 1898
Re(bipy-OMe)(CO)$_3$Cl [**5**]	–1.89	–2.26	2022, 1914, 1896

series, and it is also reflected in the ν(CO) values observed in the IR spectra (Table 2-1). All cyclic voltammograms (CVs) of these complexes displayed similar features under an atmosphere of argon, namely a one electron quasi-reversible reduction wave followed by a one electron irreversible reduction wave at more negative potential. At slower scan rates it was also possible to see a small wave in the CV of complex [**2**] between the first and second reductions, corresponding to the production of the [*fac*-Re(bipyridyl)(CO)$_3$]$_2$ dimer that has been reported previously.[17]

When acetonitrile solutions were saturated with CO_2, vast differences were observed in the second reduction wave from complex to complex. In order of increasing e$^-$ donating ability, complex [**1**] showed little to no current enhancement under CO_2 at the second reduction wave. Complex [**2**] showed a 3.4-fold current increase in peak current at 100 mV/s between the complex under argon and the complex under CO_2 at –2.13 V (*vs.* Fc/Fc$^+$). Complex [**3**] showed a current enhancement under CO_2 that was slightly larger than [**2**]. Complex [**4**] showed the largest catalytic current with an 18-fold increase in peak current at a scan rate of 100

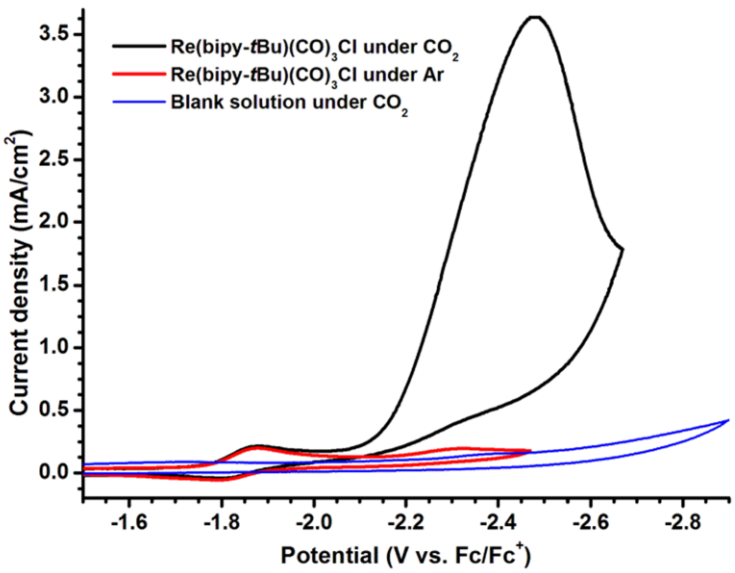

Figure 2-2. CVs of Complex [**4**] under argon (red) and CO_2 (black) showing significant current increase representing catalysis. The blue scan is a solution under the same CO_2 conditions, but without catalyst present. 1 mM catalyst, 0.1 M TBAH supporting electrolyte, 3 mM diameter glassy carbon working electrode, Pt counter electrode, Ag wire pseudo-reference with ferrocene added as an internal reference, acetonitrile as solvent under an atmosphere of CO_2 (~0.25 M in solution).

mV/s under CO_2 at –2.23 V (*vs.* Fc/Fc^+) (Figure 2-2). Complex [**5**] showed almost no current enhancement under CO_2. Complexes [**4**] and [**2**] were compared directly at equal concentrations of Re and CO_2. Complex [**4**] performed significantly better, showing more than 3.5 times more catalytic current at 100 mV/s than [**2**] at 100 mV more negative potential (Figure 2-3).

At the outset, these data make it clear that catalytic activity for CO_2 reduction depends on factors other than the electrocatalyst reduction potentials. We note, for example, that although complex [**5**] has the most negative reduction potential and should have a more nucleophilic Re center for CO_2 reduction, it shows essentially no catalytic current, pointing to a possible π-donor vs. σ-donor effect. Experiments are

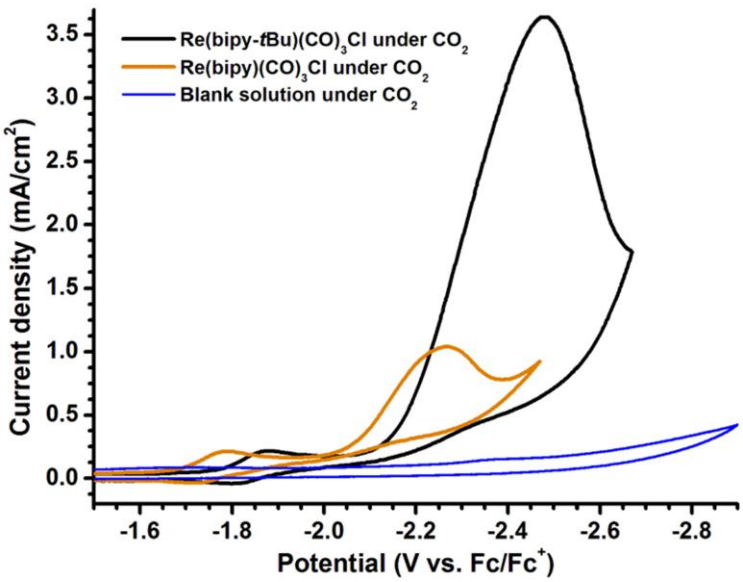

Figure 2-3. CVs of complex [**4**] (black) and complex [**2**] (orange) under the same conditions. 1 mM catalyst, 0.1 M TBAH supporting electrolyte, 3 mM diameter glassy carbon working electrode, Pt wire counter electrode, Ag wire pseudo-reference with ferrocene added as an internal reference, acetonitrile as solvent under an atmosphere of CO_2 (~0.25 M in solution).

ongoing in our laboratory to further examine this phenomenon by designing and testing new bipyridine ligands with a variety of substituents in the 4,4' positions.

Although the catalytic activity of [**4**] is 3.5-fold greater than [**2**] at the same catalyst concentration and only 100 mV more negative reduction potential, it was also noted that [**4**] shows a 1.4 fold increase in catalytic current over [**2**] at identical potentials (–2.13 V *vs.* Fc/Fc^+ at [**2**]'s maximum catalytic current).

Rotating disc electrode (RDE) experiments were carried out on complex [**4**] in order to determine the diffusion coefficients of the complex. The data obtained from these experiments display Levich-Koutecky behavior with linear fits having R^2 values of greater than 0.99 for both the first and second reductions, indicating that the complex behaves well under the conditions of the experiment (Figure 2-4). The

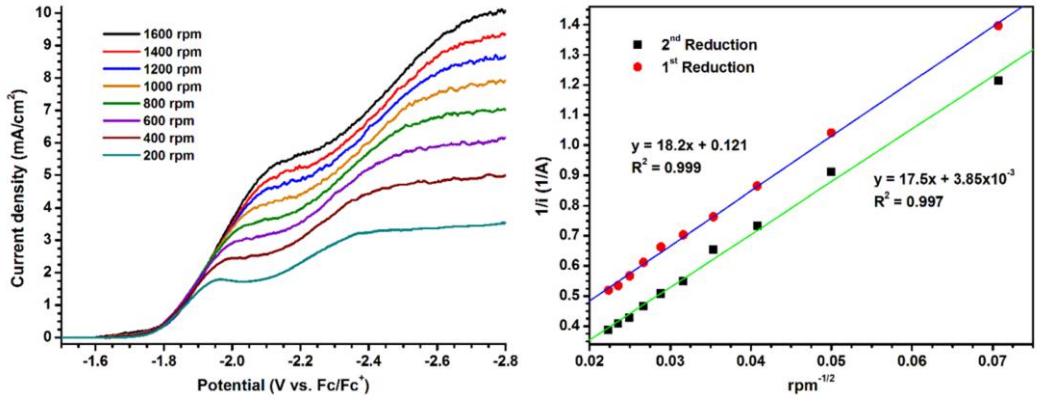

Figure 2-4. Rotating disk electrode data for Re(bipy-*t*Bu)$(CO)_3$Cl [**4**] in acetonitrile with mM Re, 0.1 M TBAH, glassy carbon working electrode, platinum wire counter electrode, and silver wire pseudo-reference with ferrocene added as an internal reference. Levich-Koutecky plot on the right shows linear fit for both first (R^2 = 0.999) and second (R^2 = 0.997) reductions.

Levich-Koutecky equation was used to obtain diffusion coefficients from that data (E2-1).[18]

$$i_L = (0.620)nFAD^{2/3}\omega^{1/2}\upsilon^{-1/6}C \qquad \textbf{E2-1}$$

In the above equation, i_L is the Levich current from the rotating disc experiment, *n* is the number of electrons (1 in this case), F is Faraday's constant, A is the electrode area, D is the diffusion coefficient, ω is the rotation rate, υ is the kinematic viscosity of the solution, and *C* is the concentration of the analyte in solution. These data yielded diffusion coefficients of $1.1\text{x}10^{-5}$ cm^2/s for Re(bipy-*t*Bu)$(CO)_3$Cl and $8.1\text{x}10^{-6}$ cm^2/s for the singly reduced species. These values are reasonable when compared to diffusion coefficients for other complexes in the literature.[19] From the diffusion coefficient of the complex, along with additional data from the experiment it was possible to calculate the second order rate constant for the CO_2 reduction using equation E2-2.[10, 20]

$$i_c = nFA[\text{cat}](Dk[\text{Q}]^y)^{1/2} \qquad \textbf{E2-2}$$

In the equation above, i_c is the catalytic current observed in the CV, *n* is the number of electrons (2 for this reaction reflecting the reduction of CO_2 to CO), F is Faraday's constant, A is the area of the electrode surface, *D* is the diffusion coefficient of the active catalytic species, *k* is the rate constant (the variable of interest in this case), Q is the concentration of substrate, and *y* is the order of the substrate in the reaction in question. Equation 2-2 can be applied when either a plateau current is established for catalysis *or* when catalytic current is scan rate independent. In this case the equation was applied based on the second condition of scan rate independence. A second order rate constant of 650 $M^{-1}s^{-1}$ is obtained using this equation, and a similar value of 1000 $M^{-1}s^{-1}$ was obtained using the electrochemical simulation software DigiSim. The DigiSim fit and the assumed mechanism for the voltammograms can be found in Figure 2-5. When equations E2-1 and E2-2 were applied to rotating disk data and CVs of [**2**], a second order rate constant of 50 $M^{-1}s^{-1}$ was obtained.

Controlled potential electrolysis (CPE). Additional catalytic experiments have been done involving complex [**4**] in order to draw comparisons with complex [**2**]. Controlled potential electrolysis of both complexes were performed in an acetonitrile solution in a sealed cell developed in our laboratory with a carbon working electrode, platinum counter electrode, and Ag/AgCl pseudo reference (with internal ferrocene reference added). In the acetonitrile solution, [**4**] performed significantly better than [**2**] producing 2.2 times the CO in the first 15 minutes of CPE as measured by gas chromatography when held at –2.25 V (*vs.* Fc/Fc^+). It is also noteworthy that [**4**]

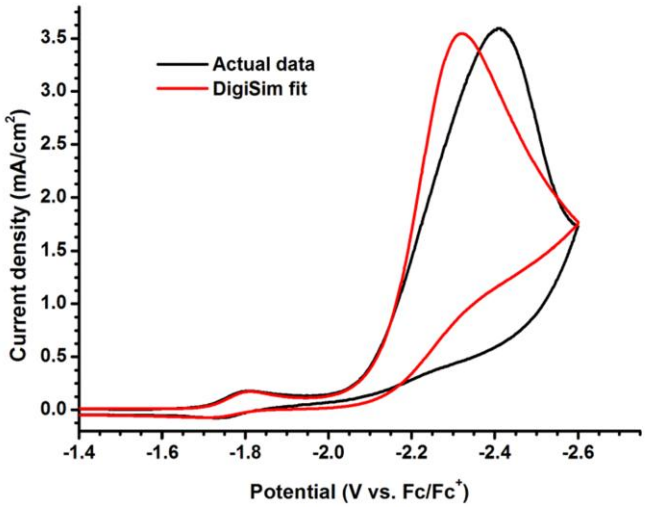

A + e = B	first reduction of the complex
B + e = C	second reduction of the complex
C + D = A + F	reaction of the reduced complex with CO_2
A + C = B + B	disproportionation reaction of the complex
B = G	small degradation of the singly reduced species
C = H	small degradation of the doubly reduced species
I + e = J	reduction of acetonitrile beyond experimental window

Figure 2-5. Digital simulation of catalytic CV for Re(bipy-*t*Bu)$(CO)_3$Cl [**4**] under CO_2 at 100 mV/s with 1 mM catalyst, 0.1 M TBAH, a glassy carbon working electrode, a platinum wire counter electrode, a silver wire pseudo-reference with ferrocene added as an internal reference, and ~0.25 M CO_2 in solution. The assumed mechanism for the digital simulation is also displayed below.

retained high electrocatalytic activity for upwards of five hours in acetonitrile, again outperforming [**2**], which loses some catalytic activity in acetonitrile over the same time period.

Further CPE experiments were carried out to determine the Faradaic efficiency of [**4**] in acetonitrile. A solution of [**4**] in acetonitrile was held at a constant potential of –2.40 V (*vs.* Fc/Fc$^+$) for two hours and GC samples were taken every 30 minutes. The output from the GC was plotted and gave a linear plot for mmol of electrons

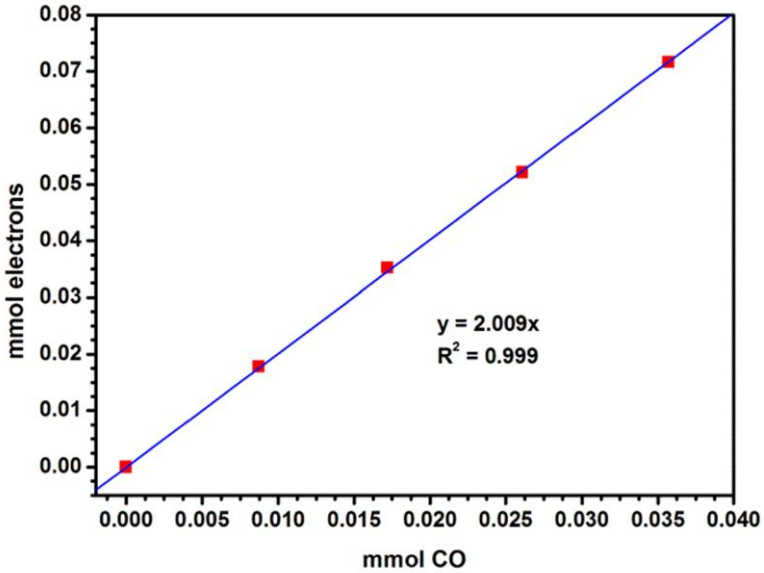

Figure 2-6. Faradaic efficiency study for complex [**4**] in dry acetonitrile with CO_2. The slope of 2.009 corresponds to 99±2 % Faradaic efficiency for the conversion of CO_2 to CO.

passed vs. mmol CO produced with a slope of 2.009. The data correspond to a Faradaic efficiency of 99 ± 5 % in acetonitrile (Figure 2-6).

Infrared spectroelectrochemistry (IR-SEC). IR-SEC was performed on [**2**] and [**4**] to compare the two species at various stages of reduction. Both complexes showed three carbonyl peaks at rest potential as expected from previous data on similar complexes.[21] The ν(CO) peaks for complex [**4**] appear at 2023 cm^{-1}, 1916 cm^{-1}, and 1898 cm^{-1}. These ν(CO) bands are typical of facial tricarbonyl systems with pseudo C_{3V} symmetry: one higher energy stretch (A_1) is separated from the two lower energy stretches (split E) , which overlap slightly.

When a voltage is applied to the solutions at the potential of the first reduction, for both [**4**] and [**2**], each carbonyl peak in the spectrum shifts approximately 20 cm^{-1} to lower energy to create new species [**4a**] and [**2a**] (for [**4a**], ν(CO) at 2005 cm^{-1},

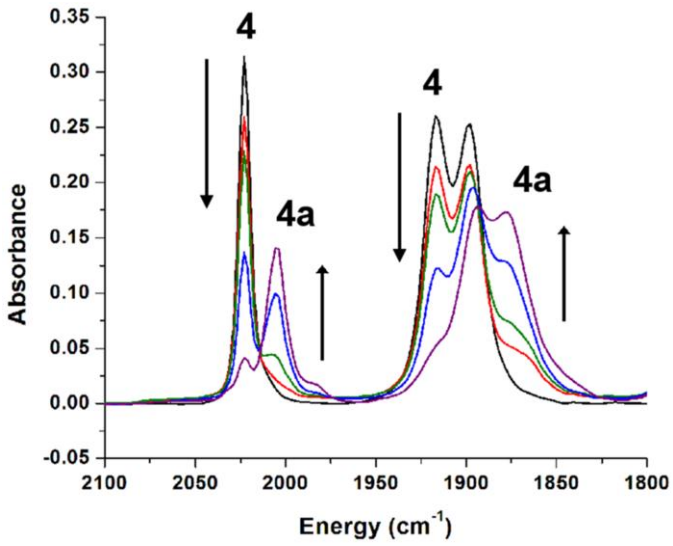

Figure 2-7. First reduction of [**4**] in IR-SEC experiment in acetonitrile. 20–30 cm^{-1} shifts indicative of a mostly bipyridine-based reduction of the complex. Initial reduction of [**4**] leads to a 19 electron, six-coordinate, negatively charged complex.

1894 cm^{-1}, and 1878 cm^{-1}) (Figure 2-7). This shift is indicative of a primarily bipyridine-based reduction of the complex as was concluded in previous studies.[17, 21]

When all unreduced complex was singly reduced, another species was produced from [**4a**] at potentials positive of that for the second reduction wave. This intermediate species shows ν(CO) modes that were again shifted 20-30 cm^{-1} lower in energy (ν(CO): 1983 cm^{-1}, 1865 cm^{-1}, and 1850 cm^{-1} [**4b**]) (Figure 2-8). The new species has been assigned as the neutral five coordinate $bipy^0Re^0$ complex with no bound Cl^-. Evidence for this species exists in a crystal structure of [Re(trip-bipy)$(CO)_3$] (trip-bipy = 6,6'-(2,4,6-triisopropylphenyl)-2,2'-bipyridine) that has a corollary infrared spectrum to be published in a future manuscript and in the dissertation of Eric E. Benson.[22]

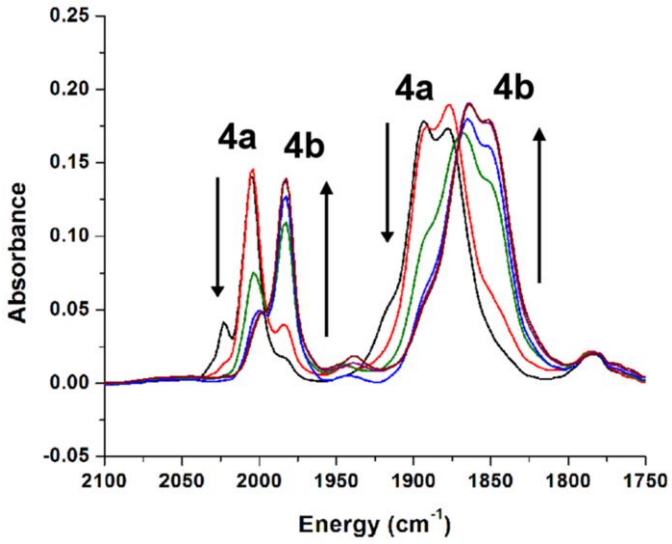

Figure 2-8. Second transition from [**4a**] to [**4b**] in the IR-SEC experiment in acetonitrile. This 20 cm^{-1} shift is due to a ligand to metal charge transfer and subsequent loss of Cl^-. This electron transfer is facilitated by the electron donating nature of the *tert*-butyl groups on the bipyridine ligand that destabilizes the bipy radical.

At this potential $Re(bipy)(CO)_3Cl^{\bullet-}$ [**2a**] formed a significant amount of Re-Re dimer[21] upon loss of Cl^- while [**4a**] does not form measurable quantities of dimer in these experiments. Fujita et al. reported that with $Re(dmb)(CO)_3(OTf)$ (OTf = trifluoromethanesulfonate) the formation of dimer happens very slowly in UV-Vis experiments at lower concentrations.[12] When performing IR-SEC on [**3**] we noted a small amount of dimer formation, most likely due to the intermediate bulk of the methyl group when compared to the bulk in [**2**] and [**4**]. We also independently synthesized the dimer $[Re(bipy\text{-}t\text{Bu})(CO)_3]_2$ [**6**] via reflux of $Re_2(CO)_{10}$ with two equivalents of 4,4'-di-*tert*-butyl-2,2'-bipyridine and obtained a liquid FTIR of the product in xylenes. This IR spectrum had a very similar ν(CO) signature to the reported $[Re(bipy)(CO)_3]_2$ IR by Turner *et al.*[21] This spectrum, however, does not match any of the major species observed in the IR-SEC of [**4**], which provides

additional evidence that a significant amount of dimer is not formed in the SEC or bulk electrolysis studies.

We assign the next species, formed at potentials equal to (and negative of) the second reduction, in the IR-SEC of complex [**4**] as the two electron reduced Re(bipy-*t*Bu)$(CO)_3^{-1}$ with two ν(CO) modes at 1938 cm^{-1} and 1834 cm^{-1} (broad) [**4c**] (Figure 2-9). The loss of one low energy stretch is expected due to rearrangement of the ligands around the Re center upon loss of Cl^- and the second reduction to a trigonal bipyrimidal geometry (see below) that is expected to have only two IR active vibrations. The larger ν(CO) shift for the higher energy stretch is indicative of a mostly metal-based reduction of the complex as is expected for the second reduction. The "family photo" of the four species observed in the IR-SEC experiments of [**4**] is displayed in Figure 2-10 and all relevant IR stretching frequencies are reported in

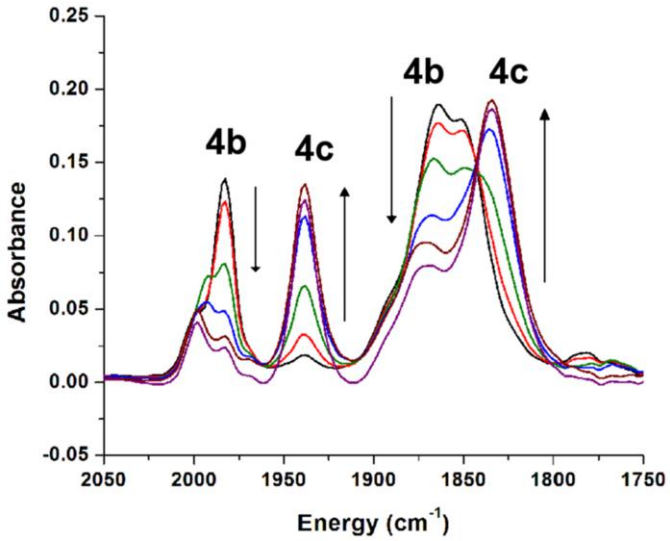

Figure 2-9. Second reduction of [**4**] in the IR-SEC experiment. 40 cm^{-1} shift for the second reduction is indicative of a mostly metal-based reduction of the complex forming the five-coordinate Re^{-1} complex [**4c**].

Table 2-2.

It is worthwhile here to note the difference between the IR-SEC reported here for [**4**] and that observed by Turner *et al.* for [**2**]. The main difference between Turner's study and ours is the assignment of the third species formed ([**4b**] in our study). We see no indication that [**4b**] is a result of a second reduction. Instead we invoke a ligand to metal charge transfer from the bipy to the Re center to explain the further shift in the ν(CO) in the singly reduced complex. This electron transfer is promoted by the donating nature of the *tert*-butyl groups on the bipy, which destabilize the bipy radical and allow electron occupancy of the d_z^2 orbital after loss of Cl^-.

IR-SEC of [**4**] was also performed in CO_2-saturated CH_3CN demonstrating the production of CO at catalytic potentials. This CO production could be seen via the

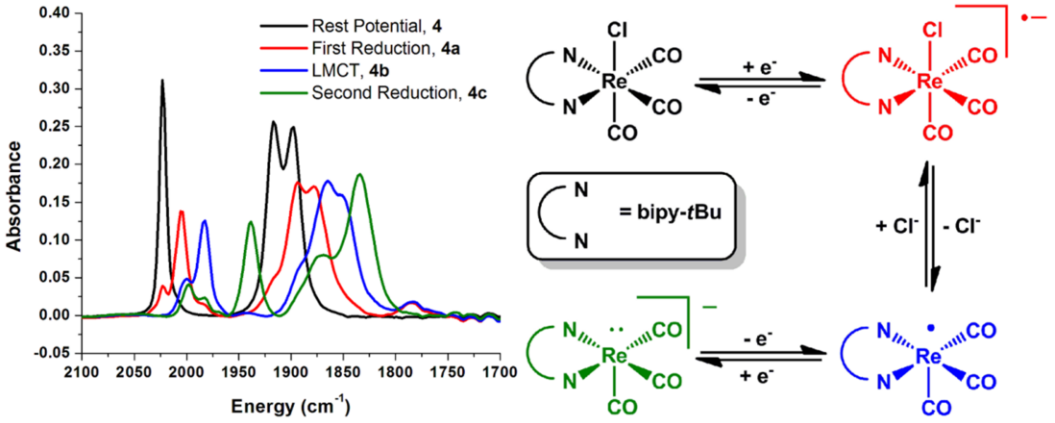

Figure 2-10. IR-SEC "family photo" for complex [**4**] in acetonitrile with TBAH supporting electrolyte. [**4a**] is formed by the first reduction of the complex to form a radical anion with added electron density mostly centered on the bipyridine ligand. [**4b**] follows through a ligand to metal charge transfer facilitated by the electron donating nature of the *tert*-butyl groups on the bipyridine. [**4c**] represents the second reduction of the complex to the five-coordinate anion that then goes on the reduce CO_2 to CO.

stretch at 2120 cm^{-1} indicative of dissolved CO in the acetonitrile solution (Figure 2-11).

Table 2-2. IR-SEC relevant stretching frequencies for various Re complexes studied in this work[a] as well as in work by Turner *et al.*[21]

Complex	υ(CO)/cm^{-1}	Solvent	Ref.
[Re(bipy-tBu)$(CO)_3$Cl] (**4**)	2023, 1916, 1898	MeCN	a
[Re(bipy-tBu)$(CO)_3$Cl]$^{\bullet-}$ (**4a**)	2005, 1895, 1878	MeCN	a
[Re(bipy-tBu)$(CO)_3$]$^{\bullet}$ (**4b**)	1983, 1865, 1850	MeCN	a
[Re(bipy-tBu)$(CO)_3$]$^{-1}$ (**4c**)	1938, 1834 (br)	MeCN	a
[Re(bipy)$(CO)_3$Cl] (**2**)	2025, 1918, 1902	MeCN	a
[Re(bipy)$(CO)_3$Cl]$^{\bullet-}$ (**2a**)	1998, 1885, 1867	MeCN	21
[Re(bipy)$(CO)_3$]$^{-1}$ (**2c**)	1947, 1843 (br)	MeCN	21
[Re(bipy-COOH)$(CO)_3$Cl] (**1**)	2037, 1935, 1911	MeCN	a
[Re(dmb)$(CO)_3$Cl] (**3**)	2023, 1916, 1899	MeCN	a
[Re(bipy-OMe)$(CO)_3$Cl] (**5**)	2022, 1914, 1896	MeCN	a
[Re(bipy-tBu)$(CO)_3$Cl] (**4**)	2020, 1916, 1893	THF	a
[Re(bipy-tBu)$(CO)_3$Cl]$^{\bullet-}$ (**4a**)	1995, 1882, 1867	THF	a
[Re(bipy-tBu)$(CO)_3$]$^{-1}$ (**4c**)	1943, 1839	THF	a

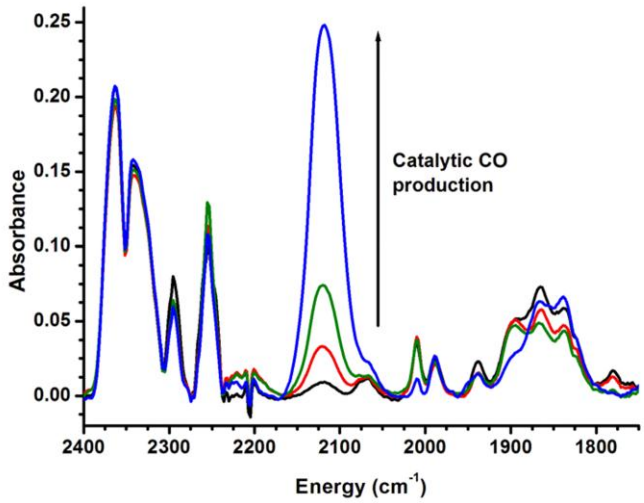

Figure 2-11. Band for free CO growing in at second reduction potential for [**4**] in IR-SEC experiment with CO_2-saturated acetonitrile.

2.3 Conclusions

We have reported here an improved catalyst for the reduction of CO_2 to CO with high turnover number and frequency. This catalyst was identified in a systematic study of a series of Re(bipyridyl)$(CO)_3$Cl complexes with varying degrees of electron donating/withdrawing substituents in the 4, 4' positions of the bipyridine. We have seen by IR-SEC studies that the Re(bipy-*t*Bu)$(CO)_3$Cl complex forms a stable Re(0) radical, and significantly less dimer during electrolysis than does its Re(bipy)$(CO)_3$Cl counterpart. This may also help explain the enhanced catalytic activity of [**4**]. Studies are ongoing in our laboratory to investigate the bulk electrocatalytic properties of the Re(bipy-*t*Bu)$(CO)_3$Cl complex in acetonitrile/water mixtures and also to study and compare its mechanism of catalysis with other complexes that appear to follow a similar mechanism.

2.4 Experimental

General Experimental Procedures. NMR spectra were recorded on a Jeol 500 MHz spectrometer at 298 K and data was manipulated using Jeol Delta software. ^{1}H chemical shifts are reported relative to solvent residual peaks. Mass spectrometry data was collected on a Finnigan LCQDECA in ESI positive ion mode. Infrared spectra were collected on a Bruker Equinox 55 spectrometer. Microanalyses were performed by Midwest Microlab, LLC, Indianapolis, IN for C, H, and N content and all analyses were performed in duplicate.

Syntheses. Manipulations were performed open to air and solvents were not dried before use. Reagents were used as received. Chemicals were received from the following: $Re(CO)_5Cl$ (Strem), 2,2'-bipyridine (Aldrich), 4,4'-di-*tert*-butyl-2,2'-bipyridine (Aldrich), 4,4'-dicarboxy-2,2'-bipyridine (Strem), 4,4'-dimethoxy-2,2'-bipyridine (Aldrich), 4,4'-dimethyl-2,2'-bipyridine (Acros), and $Re_2(CO)_{10}$ (Acros).

[Re(4,4'-dicarboxyl-2,2'-bipyridine)$(CO)_3$Cl] [1]. This complex was prepared with slight modifications to literature methods.[11] $Re(CO)_5Cl$ (0.200 g, 0.55 mmol) was dissolved in 50 mL of hot toluene and 20 ml methanol. An equimolar amount of 4,4'-dicarboxy-2,2'-bipyridine (0.130 g, 0.55 mmol) was added to the solution and the reaction mixture was stirred under reflux for one hour with initial color change from clear to orange occurring in the first 15 minutes. The reaction mixture was removed from heat after the one hour reflux and the unreacted starting material was precipitated

from solution in the freezer over a one hour period. After that time, the white starting material was filtered and the bright orange filtrate was rotary evaporated to dryness. ^{1}H NMR (acetonitrile-d_3): δ 6.80 (d, 2H, 5 and 5' H's), δ 7.68 (s, 2H, 3 and 3' H's), δ 7.84 (d, 2H, 6 and 6' H's). IR (CH_3CN) ν(CO): 2037 cm^{-1}, 1935 cm^{-1}, 1911 cm^{-1}.

[Re(2,2'-bipyridine)(CO)$_3$Cl] [2]. This complex was prepared with slight modifications to literature methods.[23] $Re(CO)_5Cl$ (0.3020 g, 0.83 mmol) was dissolved in 50 mL hot toluene. An equimolar amount of 2,2'-bipyridine (0.130 g, 0.83 mmol) was then added to the hot solution and the reaction mixture was stirred with reflux for one hour. Within the first five minutes of applying heat the solution began to turn yellow and the intensity of the color increased with time during reflux. After one hour of reflux the mixture was removed from heat and put in a freezer for one hour where all product precipitated from solution. After removing from the freezer, the bright yellow powder product was filtered from the slurry. The product was then put in the vacuum oven at 90 °C overnight to eliminate any residual solvent and water. Spectroscopically pure product was isolated from this reaction for an overall yield of 84%. ^{1}H NMR (acetonitrile-d_3): δ 7.44 (t, 2H, 5 and 5' H's), δ 8.00 (t, 2H, 4 and 4' H's), δ 8.23 (d, 2H, 6 and 6' H's), δ 8.82 (d, 2H, 3 and 3' H's). IR (CH_3CN) ν(CO): 2025 cm^{-1}, 1918 cm^{-1}, 1902 cm^{-1}. ESI-MS (*m/z*): 444.65 (100, $[M\text{-}Cl^- + H_2O]^+$), 484.90 (29, $[M+Na^+]^+$).

[Re(4,4'-dimethyl-2,2'-bipyridine)(CO)$_3$Cl] [3]. Re(CO)$_5$Cl (0.984 g, 2.72 mmol) was dissolved in 150 mL hot toluene in a 250 ml round bottom flask. An equimolar amount of 2,2'-dimethyl-2,2'-bipyridine (0.501 g, 2.72 mmol) was added and the reaction was refluxed for 90 minutes. The solution turned yellow after 15 minutes of reflux, orange after that, and product precipitated after only 30 minutes of reflux. After removing from heat, the reaction mixture was placed in a freezer overnight to force all products from solution. The product was filtered and dried in a vacuum oven at 90 °C. Spectroscopically pure product was obtained from the reaction for a total yield of 94%. ^{1}H NMR (acetonitrile-d_3): δ 2.33 (s, 6H, CH$_3$), δ 7.22 (d, 2H, 5 and 5' H's), δ 8.05 (s, 2H, 6 and 6' H's), δ 8.60 (d, 2H, 3 and 3' H's). IR (CH$_3$CN) ν(CO): 2025 cm^{-1}, 1918 cm^{-1}, 1902 cm^{-1}. ESI-MS (*m/z*): 472.62 (100, [M-Cl$^-$+H$_2$O]$^+$), 507.77 (60, [M+NH$_4^+$]$^+$), 455.10 (21, [M-Cl$^-$]$^+$. Anal. Calcd for **2**, C$_{15}$H$_{12}$ClN$_2$O$_3$Re: C, 36.77; H,

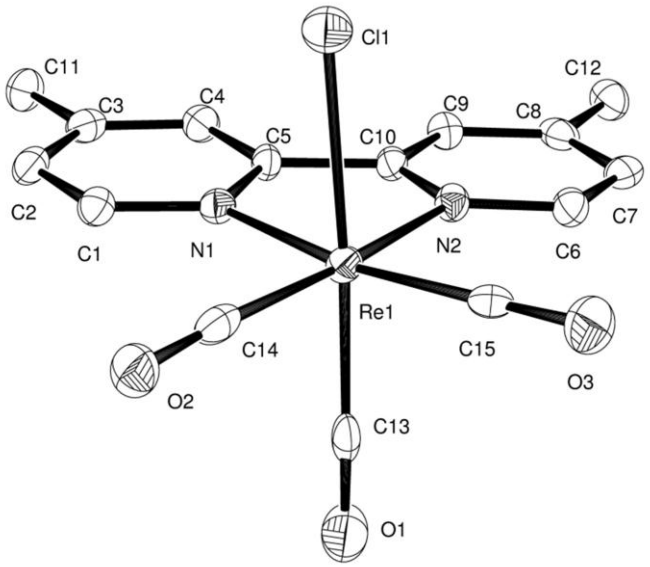

Figure 2-12. ORTEP drawing of Re(dmb)(CO)$_3$Cl [**3**]. Structure refined to R value of 3.4% in the monoclinic space group P$_{21/n}$. Hydrogens and solvent (chloroform) have been omitted for clarity.

2.47; N, 5.72. Found: C, 36.72; H, 2.41; N, 5.75. X-ray quality crystals were grown from the vapor diffusion of pentane into a chloroform solution of **3** (Figure 2-12, Tables 2-3 and 2-4).

[Re(4,4'-di-*tert*-butyl-2,2'-bipyridine)(CO)$_3$Cl] [4]. Re(CO)$_5$Cl (0.1075 g, 0.30 mmol) was dissolved in 50 mL of hot toluene. An equimolar amount of 4,4'-di-*tert*-butyl-2,2'-bipyridine (0.0800 g, 0.30 mmol) was added to the hot solution and the reaction mixture was stirred with reflux for one hour. Once the solution reached reflux the mixture began to change color from clear, to yellow, and finally to orange. After one hour of reflux the reaction mixture was removed from heat and cooled in a freezer. Solid did not precipitate from cold toluene in this reaction so the solvent was removed in *vacuo* leaving a gold solid. This solid was then dissolved in acetone and an equal amount of heptane was added. The acetone was removed by vacuum, leaving only heptane. The product immediately precipitated from heptane and was isolated by filtration. The yellow solid was dried overnight in a vacuum oven at 90 °C. Spectroscopically pure product was obtained from the reaction with an overall yield of 95%. ^{1}H NMR (acetonitrile-d_3): δ 1.45 (s, 18H, *t*Bu), δ 7.64 (dd, 2H, 5 and 5' H's), δ 8.41 (d, 2H, 6 and 6' H's), δ 8.88 (d, 2H, 3 and 3' H's). IR (CH$_3$CN) ν(CO): 2023 cm^{-1}, 1916 cm^{-1}, 1898 cm^{-1}. ESI-MS (*m/z*): 556.69 (100, [M-Cl$^-$+H$_2$O]$^+$), 596.96 (54, [M+Na$^+$]$^+$). Anal. Calcd for **2**, $C_{21}H_{24}ClN_2O_3Re$: C, 43.93; H, 4.21; N, 4.88. Found: C, 43.91; H, 4.21; N, 4.89.

[Re(4,4'-dimethoxy-2,2'-bipyridine)(CO)$_3$Cl] [5]. This complex was prepared by with slight modifications to literature methods.[23] Re(CO)$_5$Cl (0.101 g, 0.28 mmol) was dissolved in 50 mL of hot toluene. An equimolar amount of 4,4'-dimethoxy-2,2'-bipyridine (0.060 g, 0.28 mmol) was added and a reflux condenser was attached. After five minutes of stirring with heat the reaction mixture started to turn yellow. Reflux was continued for two hours and the reaction mixture was allowed to cool. The solution was put in a freezer for one hour to precipitate the product. The yellow solid was filtered and washed with pentane before being dried overnight at 90 °C under vacuum. The spectroscopically pure product was weighed (0.126g) and a yield of 85% was obtained for the reaction. ^{1}H NMR (acetonitrile-d_3): δ 4.01 (s, 6H, CH$_3$), δ 7.10 (dd, 2H, 5 and 5' H's), δ 7.86 (d, 2H, 3 and 3' H's), δ 8.74 (d, 2H, 6 and 6' H's). IR (CH$_3$CN) ν(CO): 2022 cm^{-1}, 1914 cm^{-1}, 1896 cm^{-1}. ESI-MS (*m/z*): 504.48 (100, [M-Cl$^-$+H$_2$O]$^+$), 544.84 (18, [M+Na$^+$]$^+$). X-ray quality crystals were grown from the vapor diffusion of diethyl ether into an acetonitrile solution of **5** (Figure 2-13, Tables 2-5 and 2-6).

[*fac*-Re(4,4'-di-*tert*-butyl-2,2'-bipyridine)(CO)$_3$]$_2$ [6]. Re$_2$(CO)$_{10}$ (0.081 g, 0.124 mmol) was dissolved in 100 mL of hot xylenes with stirring. To the hot solution, 2 equivalents of 4,4'-di-*tert*-butyl-2,2'-bipyridine (0.066 g, 0.248 mmol) was added and the solution was refluxed for 72 hours. Over the course of the reflux the solution turned from clear to dark purple. After 72 hours, the reaction mixture was removed from heat and an aliquot was taken for FTIR analysis. Solid product was obtained

from the reaction mixture by recrystallization with copious amounts of diethyl ether. IR (xylenes) ν(CO): 1990 cm^{-1}, 1952 cm^{-1}, 1890 cm^{-1}, 1862 cm^{-1}.

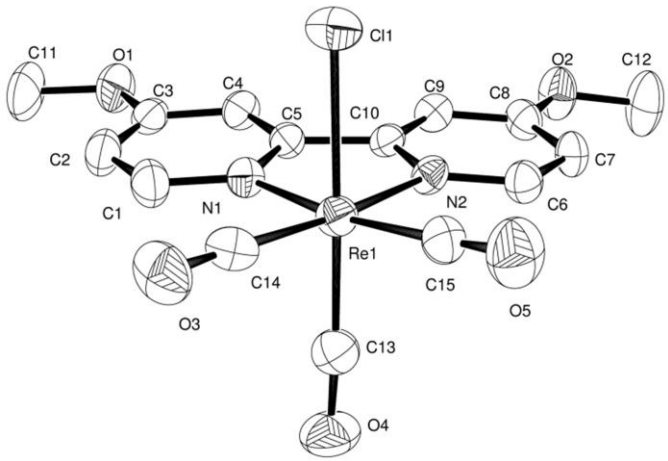

Figure 2-13. ORTEP drawing of Re(bipy-OMe)$(CO)_3$Cl [**5**]. Structure refined to an R-value of 3.0% in the monoclinic space group $C_{2/c}$. Hydrogens omitted for clarity and disordered acetonitrile molecules squeezed from structure using Platon.

Electrochemistry. Electrochemical experiments were performed using either a BAS CV-50 or BAS Epsilon potentiostat. A one compartment cell was used for all cyclic voltammetry experiments with a glassy carbon electrode (3 mm in diameter from BASi), a Pt wire counter electrode, and a Ag/AgCl reference with added Fc/Fc^+ as an internal reference. All electrochemical experiments were performed with 0.1 M tetrabutylammonium hexafluorophosphate (TBAH) as supporting electrolyte and all solutions were purged with argon or CO_2 before CVs were taken. Re complex concentrations ranged from 0.5–1.5 mM and experiments with CO_2 were performed at gas saturation (~ 0.25 M) in acetonitrile.[24, 25]

A Teflon-shrouded glassy carbon rotating disc electrode was employed to determine the diffusion coefficient of Re(bipy-*t*Bu)$(CO)_3$Cl [**4**], along with a Pt counter electrode and Ag/AgCl reference. A Pine Instruments, Inc., Model ASR2 electrode rotator was employed for all rotating disc experiments. In these experiments, a 70–75 ml, 5 mM solution of the rhenium complex with 0.1 M tetrabutylammonium hexafluorophosphate (TBAH) was used in a 100 ml round bottom flask. CVs were taken from 0–2000 rpm rotation rates at potentials from 0 to –2.90 V (*vs.* Fc/Fc^+) at 100 mV/s. In these scans, both reductions of the rhenium complex were seen. The absolute current heights for each reduction were tabulated for every scan rate in order to construct a Levich-Koutecky plot for the data. Data from both reduction peaks fit a linear plot of inverse current vs. the negative square root of the rotation rate. A good linear fit for the data in this plot represents usable data for the calculation of diffusion coefficient. Data points from the line were then inserted in the Levich-Koutecky equation in order to calculate the diffusion coefficient for each species in the reduction pathway.

Bulk electrolysis. Bulk electrolysis experiments were carried out in a single compartment cell with a carbon disc working electrode, a platinum cage counter electrode, and an Ag/AgCl reference electrode on the BAS Epsilon potentiostat. The bulk reductions were carried out in a 0.1 M TBAH/CH_3CN solution. The bulk electrolysis solution was purged with CO_2 for 20 minutes prior to electrolysis. Gas analysis for bulk electrolysis experiments were performed using 1 mL sample

injection volume on a Hewlett Packard 7890A Series gas chromatograph with a molsieve column (30m x 0.53 mm ID x 25 μm film).

Cyclic voltammetry simulation. Cyclic voltammograms were simulated using Digisim software.[26] All simulations were done on cyclic voltammograms for the first reduction only, and then extended to the second reduction on full voltammograms. Catalyst and substrate concentrations were held constant in the simulations based on experimental details and the diffusion coefficients of Re(bipyridyl) complexes were determined as described above using rotating disc electrode experiments.

Infrared Spectroelectrochemistry (FTIR-SEC). The design of the IR spectroelectrochemical cell used for the rhenium catalyst studies has been reported previously by our laboratory [27] and is based on a cell used by Mann and co-workers.[28-32] IR spectral changes accompanying thin-layer bulk electrolyses were measured using a flow-through spectroelectrochemical cell. All spectroelectrochemical experiments were carried out in a 0.1 M TBAH solution using acetonitrile and all solutions were prepared under an atmosphere of dry nitrogen in a dry box. Blank acetonitrile solutions with 0.1 M TBAH were used for the FTIR solvent subtractions. A Pine Instrument Company Model AFCBP1 bipotentiostat was used to affect and monitor thin layer bulk electrolysis. The IR spectra were acquired using the Bruker Equinox 55 spectrometer mentioned above. For the $CO_{2(g)}$ experiments, CO_2 was bubbled through the catalyst solution for 10 minutes prior to injection into the SEC cell.

Note: Much of the material for this chapter comes directly from a manuscript entitled "Re(bipy-*t*Bu)$(CO)_3$Cl – improved catalytic activity for reduction of carbon dioxide. IR-Spectroelectrochemical and mechanistic studies." by Jonathan M. Smieja and Clifford P. Kubiak, which has been published in *Inorganic Chemistry*, **2010**, *49* (20), 9283-9289. http://dx.doi.org/10.1021/ic1008363. The dissertation author is the primary author of this manuscript.

2.5 References

1. Benson EE, Kubiak CP, Sathrum AJ, Smieja JM (2009) Electrocatalytic and homogeneous approaches to conversion of CO_2 to liquid fuels. *Chem. Soc. Rev.* 38(1):89-99.

2. Hawecker J, Lehn JM, Ziessel R (1984) Electrocatalytic reduction of carbon dioxide mediated by Re(bipy)$(CO)_3$Cl (bipy = 2,2'-bipyridine). *J. Chem. Soc., Chem. Commun.* (6):328-330.

3. Hawecker J, Lehn JM, Ziessel R (1986) Photochemical and Electrochemical Reduction of Carbon Dioxide to Carbon Monoxide Mediated by (2,2'-Bipyridine)Tricarbonylchlororhenium(I) and Related Complexes as Homogeneous Catalysts. *HeIv. Chim. Acta* 69(8):1990-2012.

4. Hori H, Johnson FPA, Koike K, Ishitani O, Ibusuki T (1996) Efficient photocatalytic CO_2 reduction using Re(bpy)$(CO)_3\{P(OEt)_3\}^+$. *J. Photochem. Photobiol. A* 96(1-3):171-174.

5. Sung-Suh HM, Kim DS, Lee CW, Park S-E (2000) Photoinduced activation of CO_2 by rhenium complexes encapsulated in molecular sieves. *Appl. Organomet. Chem.* 14(12):826-830.

6. Hori H, Takano Y, Koike K, Sasaki Y (2003) Efficient rhenium-catalyzed photochemical carbon dioxide reduction under high pressure. *Inorg. Chem. Commun.* 6(3):300-303.

7. Kurz P, Probst B, Spingler B, Alberto R (2006) Ligand Variations in [ReX(diimine)$(CO)_3$] Complexes: Effects on Photocatalytic CO_2 Reduction. *Eur. J. Inorg. Chem.* 2006(15):2966-2974.

8. Takeda H, Koike K, Inoue H, Ishitani O (2008) Development of an efficient photocatalytic system for CO_2 reduction using rhenium(l) complexes based on mechanistic studies. *J. Am. Chem. Soc.* 130(6):2023-2031.

9. Raebiger JW, *et al.* (2006) Electrochemical Reduction of CO_2 to CO Catalyzed by a Bimetallic Palladium Complex. *Organometallics* 25(14):3345-3351.

10. DuBois DL, Miedaner A, Haltiwanger RC (1991) Electrochemical reduction of carbon dioxide catalyzed by [Pd(triphosphine)(solvent)]$(BF_4)_2$ complexes: synthetic and mechanistic studies. *J. Am. Chem. Soc.* 113(23):8753-8764.

11. Juris A, Campagna S, Bidd I, Lehn JM, Ziessel R (1988) Synthesis and photophysical and electrochemical properties of new halotricarbonyl(polypyridine)rhenium(I) complexes. (Translated from English) *Inorg. Chem.* 27(22):4007-4011 (in English).

12. Hayashi Y, Kita S, Brunschwig BS, Fujita E (2003) Involvement of a binuclear species with the Re-C(O)O-Re moiety in CO_2 reduction catalyzed by tricarbonyl rhenium(I) complexes with diimine ligands: Strikingly slow formation of the Re-Re and Re-C(O)O-Re species from $Re(dmb)(CO)_3S$ (dmb=4,4 '-dimethyl-2,2 '-bipyridine, S = solvent). *J. Am. Chem. Soc.* 125(39):11976-11987.

13. Fujita E, Hayashi Y, Kita S, Brunschwig BS (2004) *Carbon Dioxide Utilization for Global Sustainability* (Elsevier, Maryland Heights, MO) pp 271-276.

14. Fujita E, Muckerman JT (2004) Why is Re-Re bond formation/cleavage in $[Re(bpy)(CO)_3]_2$ different from that in $[Re(CO)_5]_2$? Experimental and theoretical studies on the dimers and fragments. *Inorg. Chem.* 43(24):7636-7647.

15. Yam VWW, Lau VCY, Cheung KK (1995) Synthesis and Photophysics of Luminescent Rhenium(I) Acetylides-Precursors for Organometallic Rigid-Rod Materials - X-Ray Crystal-Structures of $[Re(^tBu_2\text{-}Bpy)(CO)_3(^tBuC{\equiv}C)]$ and $[Re(^tBu_2\text{-}Bpy)(CO)_3Cl]$. *Organometallics* 14(6):2749-2753.

16. Brown HC, Braude EA, Nachod FC (1955) *Determination of Organic Structures by Physical Methods* (Academic Press, New York).

17. Sullivan BP, Bolinger CM, Conrad D, Vining WJ, Meyer TJ (1985) One- and two-electron pathways in the electrocatalytic reduction of CO_2 by *fac*-$Re(bpy)(CO)_3Cl$ (bpy = 2,2'-bipyridine). *J. Chem. Soc., Chem. Commun.* (20):1414-1416.

18. Bard AJ, Faulkner LR (2001) *Electrochemical Methods: Fundamentals and applications* (Wiley) 2nd Ed p 833.

19. Haines RJ, Wittrig RE, Kubiak CP (1994) Electrocatalytic Reduction of Carbon-Dioxide by the Binuclear Copper Complex $[Cu_2(6\text{-}(Diphenylphosphino)\text{-}2,2'\text{-}Bipyridyl)_2(MeCN)_2](PF_6)_2$. *Inorg. Chem.* 33(21):4723-4728.

20. Savéant JM, Vianello E (1962) Potential-sweep chronoamperometry theory of kinetic currents in the case of a first order chemical reaction preceding the electron-transfer process. *Electrochim. Acta* 8(12):905-923.

21. Johnson FPA, George MW, Hartl F, Turner JJ (1996) Electrocatalytic Reduction of CO_2 Using the Complexes $[Re(bpy)(CO)_3L]n$ (n = +1, L = $P(OEt)_3$, CH_3CN; n = 0, L = Cl^-, OTf^-; bpy = 2,2‘-Bipyridine; OTf^- = CF_3SO_3) as Catalyst Precursors: Infrared Spectroelectrochemical Investigation. *Organometallics* 15(15):3374-3387.

22. Benson, E. E. Structural, electronic, and mechanistic studies of transition metal complexes for the electrocatalytic reduction of carbon dioxide. University of California – San Diego, La Jolla, CA, 2012.

23. Worl LA, Duesing R, Chen P, Ciana LD, Meyer TJ (1991) Photophysical properties of polypyridyl carbonyl complexes of rhenium(I). *J. Chem. Soc., Dalton Trans.* (S):849-858.

24. Fujita E, Szalda DJ, Creutz C, Sutin N (1988) Carbon dioxdie activation - thermodynamics of CO_2 binding and the involvement of two cobalt centers in the reduction of CO_2 by a cobalt(I) macrocycle *J. Am. Chem. Soc.* 110(14):4870-4871.

25. Gennaro A, Isse AA, Vianello E (1990) Solubility and electrochemical determination of CO_2 in some dipolar aprotic solvents *J. Electroanal. Chem.* 289(1-2):203-215.

26. Rudolph M (1991) A fast implicit finite-difference algorithm for the digital-simulation of electrochemical processes. *J. Electroanal. Chem.* 314(1-2):13-22.

27. Zavarine IS, Kubiak CP (2001) A versatile variable temperature thin layer reflectance spectroelectrochemical cell. *J. Electroanal. Chem.* 495(2):106-109.

28. Bullock JP, Mann KR (1989) Uv-Vis-Ir Thin-Layer Spectroelectrochemical Studies of Hexakis(Aryl Isocyanide)Chromium Complexes - In situ Generation and Characterization of 4 Oxidation States. *Inorg. Chem.* 28(21):4006-4011.

29. Bullock JP, Palazzotto MC, Mann KR (1990) Electrochemistry and infrared spectroelectrochemistry of $MnSnPh_{4-n}$ (M = $CpMo(CO)_3$, $Mn(CO)_5$, $CpFe(CO)_2$; n = 1, 2). *Inorg. Chem.* 29(22):4413-4421.

30. Bullock JP, Palazotto MC, Mann KR (1991) Electrochemistry and Infrared Spectroelectrochemistry of $[(h^5\text{-}C_5R_5)Fe(CO_2)_2]$ (R = H, Me): Generation and Characterization of $[(h^5\text{-}C_5R_5)Fe(CO)_2]_2(PF_6)$ complexes. *Inorg. Chem.* 30(6):1284-1293.

31. Hill MG, Mann KR (1991) Thermodynamics of Multielectron Transfer - Variable-Temperature Uv-Vis and Ir Spectroelectrochemical Studies of the Disproportionation of D7-D8 Binuclear Rhodium Complexes. *Inorg. Chem.* 30(7):1429-1431.

32. Ito T, *et al.* (1997) Effects of rapid intramolecular electron transfer on vibrational spectra. *Science* 277(5326):660-663.

2.6 Appendix

Table 2-3. Crystal data and structure refinement for Re(dmb)$(CO)_3$Cl [**3**].

Identification code	js_375_0m	
Empirical formula	C15 H12 Cl N2 O5 Re	
Formula weight	521.92	
Temperature	100(2) K	
Wavelength	0.71073 Å	
Crystal system	Monoclinic	
Space group	$P_{21/n}$	
Unit cell dimensions	a = 19.05(2) Å	α = 90°.
	b = 17.878(20) Å	β = 119.765(13)°.
	c = 12.197(13) Å	γ = 90°.
Volume	3606(7) $Å^3$	
Z	8	
Density (calculated)	1.923 Mg/m^3	
Absorption coefficient	6.913 mm^{-1}	
F(000)	1984	
Crystal size	0.10 x 0.10 x 0.10 mm^3	
Theta range for data collection	1.68 to 25.34°.	
Index ranges	-22<=h<=22, -21<=k<=21, -12<=l<=14	
Reflections collected	16286	
Independent reflections	3276 [R(int) = 0.0757]	
Completeness to theta = 25.34°	99.3 %	
Max. and min. transmission	0.5448 and 0.5448	
Refinement method	Full-matrix least-squares on F^2	
Data / restraints / parameters	3276 / 0 / 220	
Goodness-of-fit on F^2	1.062	
Final R indices [I>2sigma(I)]	R1 = 0.0472, wR2 = 0.1339	
R indices (all data)	R1 = 0.0593, wR2 = 0.1424	
Extinction coefficient	0.00052(9)	
Largest diff. peak and hole	5.572 and -0.714 e. $Å^{-3}$	

Table 2-4. Bond lengths [Å] and angles [°] Re(dmb)$(CO)_3$Cl [**3**].

C(1)-N(1)	1.328(12)	C(12)-H(13A)	0.9800
C(1)-C(2)	1.376(14)	C(12)-H(13B)	0.9800
C(1)-H(3)	0.9500	C(12)-H(13C)	0.9800
C(2)-C(3)	1.394(15)	C(13)-O(3)	1.166(13)
C(2)-H(4)	0.9500	C(13)-Re(1)	1.891(12)
C(3)-O(1)	1.351(12)	C(14)-O(4)	1.151(13)
C(3)-C(4)	1.403(14)	C(14)-Re(1)	1.907(10)
C(4)-C(5)	1.370(14)	C(15)-O(5)	1.170(13)
C(4)-H(6)	0.9500	C(15)-Re(1)	1.899(11)
C(5)-N(1)	1.366(13)	N(1)-Re(1)	2.178(8)
C(5)-C(10)	1.481(13)	N(2)-Re(1)	2.172(8)
C(6)-N(2)	1.363(13)	Cl(1)-Re(1)	2.494(3)
C(6)-C(7)	1.383(16)		
C(6)-H(12)	0.9500	N(1)-C(1)-C(2)	125.1(9)
C(7)-C(8)	1.368(16)	N(1)-C(1)-H(3)	117.5
C(7)-H(11)	0.9500	C(2)-C(1)-H(3)	117.5
C(8)-O(2)	1.336(13)	C(1)-C(2)-C(3)	117.3(9)
C(8)-C(9)	1.421(14)	C(1)-C(2)-H(4)	121.4
C(9)-C(10)	1.378(14)	C(3)-C(2)-H(4)	121.4
C(9)-H(9)	0.9500	O(1)-C(3)-C(2)	125.2(9)
C(10)-N(2)	1.367(12)	O(1)-C(3)-C(4)	115.8(9)
C(11)-O(1)	1.422(13)	C(2)-C(3)-C(4)	119.1(9)
C(11)-H(14A)	0.9800	C(5)-C(4)-C(3)	119.0(9)
C(11)-H(14B)	0.9800	C(5)-C(4)-H(6)	120.5
C(11)-H(14C)	0.9800	C(3)-C(4)-H(6)	120.5
C(12)-O(2)	1.426(13)	N(1)-C(5)-C(4)	122.5(9)

Table 2-4 (Cont.)

N(1)-C(5)-C(10)	114.8(8)	H(13A)-C(12)-H(13C)	109.5
C(4)-C(5)-C(10)	122.7(9)	H(13B)-C(12)-H(13C)	109.5
N(2)-C(6)-C(7)	121.9(10)	O(3)-C(13)-Re(1)	176.6(10)
N(2)-C(6)-H(12)	119.1	O(4)-C(14)-Re(1)	177.9(9)
C(7)-C(6)-H(12)	119.1	O(5)-C(15)-Re(1)	177.5(9)
C(8)-C(7)-C(6)	120.2(10)	C(1)-N(1)-C(5)	117.1(8)
C(8)-C(7)-H(11)	119.9	C(1)-N(1)-Re(1)	125.6(6)
C(6)-C(7)-H(11)	119.9	C(5)-N(1)-Re(1)	117.3(6)
O(2)-C(8)-C(7)	125.4(10)	C(6)-N(2)-C(10)	118.5(9)
O(2)-C(8)-C(9)	116.2(10)	C(6)-N(2)-Re(1)	124.3(7)
C(7)-C(8)-C(9)	118.5(10)	C(10)-N(2)-Re(1)	117.1(6)
C(10)-C(9)-C(8)	119.2(10)	C(3)-O(1)-C(11)	118.1(9)
C(10)-C(9)-H(9)	120.4	C(8)-O(2)-C(12)	118.0(10)
C(8)-C(9)-H(9)	120.4	C(13)-Re(1)-C(15)	87.7(4)
N(2)-C(10)-C(9)	121.7(9)	C(13)-Re(1)-C(14)	91.5(5)
N(2)-C(10)-C(5)	115.3(8)	C(15)-Re(1)-C(14)	87.5(5)
C(9)-C(10)-C(5)	123.0(9)	C(13)-Re(1)-N(2)	93.9(4)
O(1)-C(11)-H(14A)	109.5	C(15)-Re(1)-N(2)	99.3(4)
O(1)-C(11)-H(14B)	109.5	C(14)-Re(1)-N(2)	171.5(4)
H(14A)-C(11)-H(14B)	109.5	C(13)-Re(1)-N(1)	94.9(4)
O(1)-C(11)-H(14C)	109.5	C(15)-Re(1)-N(1)	173.6(4)
H(14A)-C(11)-H(14C)	109.5	C(14)-Re(1)-N(1)	98.3(4)
H(14B)-C(11)-H(14C)	109.5	N(2)-Re(1)-N(1)	74.7(3)
O(2)-C(12)-H(13A)	109.5	C(13)-Re(1)-Cl(1)	177.2(3)
O(2)-C(12)-H(13B)	109.5	C(15)-Re(1)-Cl(1)	93.2(3)
H(13A)-C(12)-H(13B)	109.5	C(14)-Re(1)-Cl(1)	91.2(3)
O(2)-C(12)-H(13C)	109.5	N(2)-Re(1)-Cl(1)	83.3(2)

Table 2-4 (Cont.)

N(1)-Re(1)-Cl(1)	83.9(2)

Table 2-5. Crystal data and structure refinement for Re(bipy-OMe)$(CO)_3$Cl [**5**].

Identification code	jms475	
Empirical formula	C16 H13 Cl4 N2 O3 Re	
Formula weight	609.31	
Temperature	100(2) K	
Wavelength	0.71073 Å	
Crystal system	Monoclinic	
Space group	$C_{2/c}$	
Unit cell dimensions	a = 6.4460(15) Å	α = 90°
	b = 14.022(3) Å	β = 93.886(3)°
	c = 21.399(5) Å	γ = 90°
Volume	1929.7(8) $Å^3$	
Z	4	
Density (calculated)	2.097 Mg/m^3	
Absorption coefficient	6.870 mm^{-1}	
F(000)	1160	
Crystal size	0.10 x 0.10 x 0.05 mm^3	
Theta range for data collection	1.74 to 28.66°.	
Index ranges	-8<=h<=7, -13<=k<=18, -28<=l<=21	
Reflections collected	22911	
Independent reflections	4648 [R(int) = 0.0472]	
Completeness to theta = 25.00°	100.0 %	
Absorption correction	Semi-empirical from equivalents	
Max. and min. transmission	0.7251 and 0.5466	
Refinement method	Full-matrix least-squares on F^2	
Data / restraints / parameters	4648 / 0 / 238	
Goodness-of-fit on F^2	1.037	
Final R indices [I>2sigma(I)]	R1 = 0.0337, wR2 = 0.0693	
R indices (all data)	R1 = 0.0442, wR2 = 0.0740	
Extinction coefficient	0.00031(10)	
Largest diff. peak and hole	2.293 and -1.132 e. $Å^{-3}$	

Table 2-6. Bond lengths [Å] and angles [°] Re(bipy-OMe)$(CO)_3$Cl [**5**].

C(1)-N(1)	1.350(6)	C(12)-H(12C)	0.9800
C(1)-C(2)	1.382(7)	C(13)-O(1)	1.069(7)
C(1)-H(1)	0.9500	C(13)-Re(1)	1.959(6)
C(2)-C(3)	1.392(7)	C(14)-O(2)	1.141(6)
C(2)-H(2)	0.9500	C(14)-Re(1)	1.936(5)
C(3)-C(4)	1.390(7)	C(15)-O(3)	1.151(6)
C(3)-C(11)	1.492(7)	C(15)-Re(1)	1.918(5)
C(4)-C(5)	1.390(7)	C(16)-Cl(4)	1.747(6)
C(4)-H(4)	0.9500	C(16)-Cl(3)	1.756(6)
C(5)-N(1)	1.360(6)	C(16)-Cl(2)	1.777(6)
C(5)-C(10)	1.476(6)	C(16)-H(16)	1.0000
C(6)-N(2)	1.338(6)	N(1)-Re(1)	2.163(4)
C(6)-C(7)	1.382(7)	N(2)-Re(1)	2.172(4)
C(6)-H(6)	0.9500	Cl(1)-Re(1)	2.4890(13)
C(7)-C(8)	1.390(7)		
C(7)-H(7)	0.9500	N(1)-C(1)-C(2)	122.7(5)
C(8)-C(9)	1.403(7)	N(1)-C(1)-H(1)	118.7
C(8)-C(12)	1.493(7)	C(2)-C(1)-H(1)	118.7
C(9)-C(10)	1.387(7)	C(1)-C(2)-C(3)	120.0(5)
C(9)-H(9)	0.9500	C(1)-C(2)-H(2)	120.0
C(10)-N(2)	1.355(6)	C(3)-C(2)-H(2)	120.0
C(11)-H(11A)	0.9800	C(4)-C(3)-C(2)	117.1(5)
C(11)-H(11B)	0.9800	C(4)-C(3)-C(11)	121.0(5)
C(11)-H(11C)	0.9800	C(2)-C(3)-C(11)	121.9(5)
C(12)-H(12A)	0.9800	C(3)-C(4)-C(5)	120.8(5)
C(12)-H(12B)	0.9800	C(3)-C(4)-H(4)	119.6

Table 2-6 (Cont.)

C(5)-C(4)-H(4)	119.6	H(12A)-C(12)-H(12B)	109.5
N(1)-C(5)-C(4)	121.3(4)	C(8)-C(12)-H(12C)	109.5
N(1)-C(5)-C(10)	115.2(4)	H(12A)-C(12)-H(12C)	109.5
C(4)-C(5)-C(10)	123.5(4)	H(12B)-C(12)-H(12C)	109.5
N(2)-C(6)-C(7)	123.0(5)	O(1)-C(13)-Re(1)	175.5(5)
N(2)-C(6)-H(6)	118.5	O(2)-C(14)-Re(1)	176.1(4)
C(7)-C(6)-H(6)	118.5	O(3)-C(15)-Re(1)	177.5(5)
C(6)-C(7)-C(8)	119.8(5)	Cl(4)-C(16)-Cl(3)	110.6(3)
C(6)-C(7)-H(7)	120.1	Cl(4)-C(16)-Cl(2)	110.1(3)
C(8)-C(7)-H(7)	120.1	Cl(3)-C(16)-Cl(2)	109.8(3)
C(7)-C(8)-C(9)	117.1(5)	Cl(4)-C(16)-H(16)	108.8
C(7)-C(8)-C(12)	121.5(5)	Cl(3)-C(16)-H(16)	108.8
C(9)-C(8)-C(12)	121.4(5)	Cl(2)-C(16)-H(16)	108.8
C(10)-C(9)-C(8)	120.2(5)	C(1)-N(1)-C(5)	118.1(4)
C(10)-C(9)-H(9)	119.9	C(1)-N(1)-Re(1)	124.5(3)
C(8)-C(9)-H(9)	119.9	C(5)-N(1)-Re(1)	117.2(3)
N(2)-C(10)-C(9)	121.6(4)	C(6)-N(2)-C(10)	118.3(4)
N(2)-C(10)-C(5)	115.3(4)	C(6)-N(2)-Re(1)	124.5(3)
C(9)-C(10)-C(5)	123.0(4)	C(10)-N(2)-Re(1)	117.1(3)
C(3)-C(11)-H(11A)	109.5	C(15)-Re(1)-C(14)	89.6(2)
C(3)-C(11)-H(11B)	109.5	C(15)-Re(1)-C(13)	90.4(2)
H(11A)-C(11)-H(11B)	109.5	C(14)-Re(1)-C(13)	86.3(2)
C(3)-C(11)-H(11C)	109.5	C(15)-Re(1)-N(1)	170.52(17)
H(11A)-C(11)-H(11C)	109.5	C(14)-Re(1)-N(1)	98.87(18)
H(11B)-C(11)-H(11C)	109.5	C(13)-Re(1)-N(1)	94.47(18)
C(8)-C(12)-H(12A)	109.5	C(15)-Re(1)-N(2)	96.66(18)
C(8)-C(12)-H(12B)	109.5	C(14)-Re(1)-N(2)	173.78(18)

Table 2-6 (Cont.)

C(13)-Re(1)-N(2)	93.57(18)	C(13)-Re(1)-Cl(1)	175.99(15)
N(1)-Re(1)-N(2)	74.93(15)	N(1)-Re(1)-Cl(1)	81.74(11)
C(15)-Re(1)-Cl(1)	93.58(15)	N(2)-Re(1)-Cl(1)	86.74(11)
C(14)-Re(1)-Cl(1)	92.99(15)		

Chapter 3

Artificial photosynthesis of CO: Kinetic studies, structural determination and origins of selectivity.

3.1 Introduction

The development and deployment of artificial photosynthetic systems is of immediate concern in view of the world's continued dependence on fossil fuels and the increasing emissions of CO_2 due to their use. Rapid industrial growth in developing nations will significantly increase the global energy demand in coming years, and while known reserves of fuels such as natural gas and coal are sufficient for the near future, they are becoming increasingly costly to obtain. As the use of fossil fuels is fundamentally unsustainable and generates greenhouse gases and other pollutants, the development of environmentally benign energy sources is important. Solar energy is an abundant alternative, but it suffers from being a diffuse energy source, and its availability varies by location and time of day. If we can capture solar energy and use CO_2 as a C_1 feedstock for liquid fuels, we can envision converting our global energy economy into a nearly carbon-neutral system.[1]

Photosynthesis is one of the great triumphs of nature, and is the cornerstone for advanced life on the planet. While solar energy is already being harvested on a commercial scale via photovoltaics and solar thermal power, mankind has yet to master nature's ability to store sunlight as chemical energy by splitting CO_2 and H_2O to form C–C, C–H and O–O bonds. The energy-dense liquid fuels formed by this process would have the advantage of conforming to the existing infrastructure. Photosynthesis can be divided into two parts: water oxidation and reduction of carbon dioxide. The first half of the photosynthetic equation, water oxidation, has been reviewed extensively by others.[2-4]

Our laboratory has recently focused on the second half and we are currently exploring the development of CO_2 reduction catalysts with the goal of implementing a directly photo-driven system. A few systems for the direct conversion of solar energy into chemical energy using a CO_2 reduction catalyst at a semiconductor photoelectrode have been reported previously,[5-9] and further development of this concept will require optimization of both the catalyst and the semiconductor components.

One key aspect of catalyst optimization deals with selectivity of the catalyst towards the desired substrates. The reduction of CO_2 to useful products is inherently proton-dependent. This is true not only for the production of carbohydrates by natural photosynthesis, but also for the synthetic production of other value-added products from the reduction of CO_2. The protons required are susceptible to competitive, direct reduction to H_2, a process that occurs at a more positive (i.e., more favorable) thermodynamic potential. A functional artificial photosynthetic system therefore

requires a catalyst that is kinetically *selective* for CO_2 reduction over H^+ reduction.

Recently, we have explored complexes of the type Re(bipy-R)$(CO)_3$(L) (where bipy-R = 4,4'-disubstituted-2,2'-bipyridine and L = an anionic ligand, or a neutral ligand with $^-$OTf as the counter ion) and reported that Re(bipy-*t*Bu)$(CO)_3$Cl [**1**] is a pre-catalyst for the electrochemical reduction of CO_2 to CO at high turnover frequency (>200 s^{-1}) compared with the previous reports on Re(bipy)$(CO)_3$Cl.[10-12] Complex [**1**] has one of the highest turnover frequencies reported for the reduction of CO_2 to CO, and exhibits nearly 100% Faradaic efficiency with very high turnover numbers (less than 5% degradation over a period of more than 24 hours). We have also successfully coupled the catalyst to a semiconductor electrode, p-type silicon (p-Si), which enables us to provide part of the thermodynamic energy for catalysis using illumination with light in the solar spectrum.[9]

A fully operational photoelectrochemical device will require the coordination of photovoltaics, semiconductor electrodes, catalysts, and substrates. We believe that understanding the individual components of the system will accelerate research towards a functional device. Herein, we report detailed studies of two of the key components in an artificial photosynthetic system based on the Re(bipy-*t*Bu)$(CO)_3$(L) catalyst that are widely applicable to homogeneous electrochemical catalysis. The first is the interaction between the catalyst and the two potential substrates, CO_2 and H^+. We show by stopped-flow UV-Vis spectroscopy that the active catalyst displays remarkable selectivity for CO_2 over H^+. The origins of this desirable activity were further investigated through crystallographic and DFT characterization of the reduced

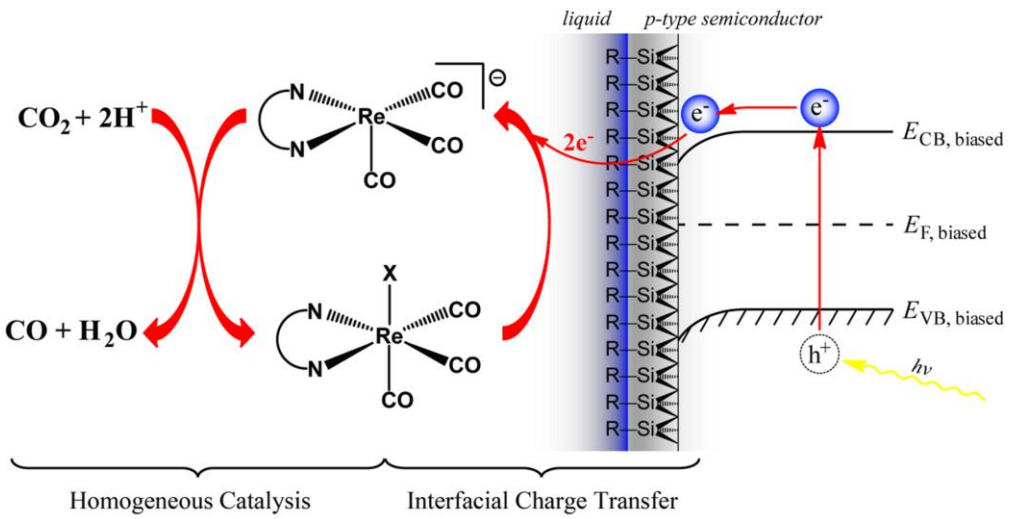

Figure 3-1. Schematic for a device using a p-Si/Re(bipy-*t*Bu)$(CO)_3$Cl semiconductor/molecular catalyst junction to reduce CO_2 photoelectrochemically. An applied potential bias thermodynamically favors the movement of photogenerated electrons to the semiconductor/catalyst interface. The semiconductor surface may be modified by functional groups to affect the heterogeneous charge transfer rate.

catalytic intermediate. We also show here that CO_2 reduction is enhanced by the addition of Brönsted acids, and exhibits a primary H/D kinetic isotope effect (KIE). Another key component of the system would be the integration of the catalyst into a photoelectrochemical device. This step is not discussed here, but is represented schematically in Figure 3-1 above.

3.2 Results and Discussion

Synthesis and IR of [Re(bipy-*t*Bu)$(CO)_3]^{-1}$. Previously published results suggested that the doubly-reduced [Re(bipy-*t*Bu)$(CO)_3]^{-1}$ anion is the species that actively binds CO_2, rendering it the most immediately relevant intermediate in studies of CO_2/H^+ selectivity.[12] We discovered that solutions of this species could be generated by

reduction of Re(bipy-*t*Bu)$(CO)_3$Cl [**1**] with KC_8, and that by careful handling, they could be maintained and characterized by a variety of techniques. The IR spectrum of the reduced compound in THF shows a shift of the high energy band from 2018 cm^{-1} to 1940 cm^{-1}, suggesting significant back donation to the carbonyls. These stretches are in good agreement with the frequencies reported in previous spectroelectrochemical studies.[12, 13] This KC_8 method was thus used to generate the samples used in the experiments reported below.

UV-Vis Stopped-Flow Spectroscopy: Probing the Selectivity of the Re Catalyst. Recently published results demonstrated the remarkable selectivity of the [Re(bipy-*t*Bu)$(CO)_3]^{-1}$ anion towards CO_2 over H^+ reduction.[14] We investigated the CO_2/H^+ selectivity in detail using stopped-flow UV-Vis experiments to quantify their relative rates of reaction with the Re catalyst anion. While the exact products are not well-defined in these stoichiometric reactions, the relative rates of the reactions are still informative. This UV-Vis spectrum of the reduced Re anion contains a strong, richly featured absorption at 570 nm (14,000 $M^{-1}cm^{-1}$) that presumably arises from a bipyridine-based radical. The persistence of the anion was thus monitored at this absorption. This is in contrast to [**1**], which has a λ_{max} at 384 nm (3900 $M^{-1}cm^{-1}$).[15] Solutions of the reduced complex were mixed in the stopped-flow apparatus with either CO_2-saturated THF (0.20 M)[16] or with 0.20 M solutions of H_2O, CH_3OH, or TFE (CF_3CH_2OH) in THF.

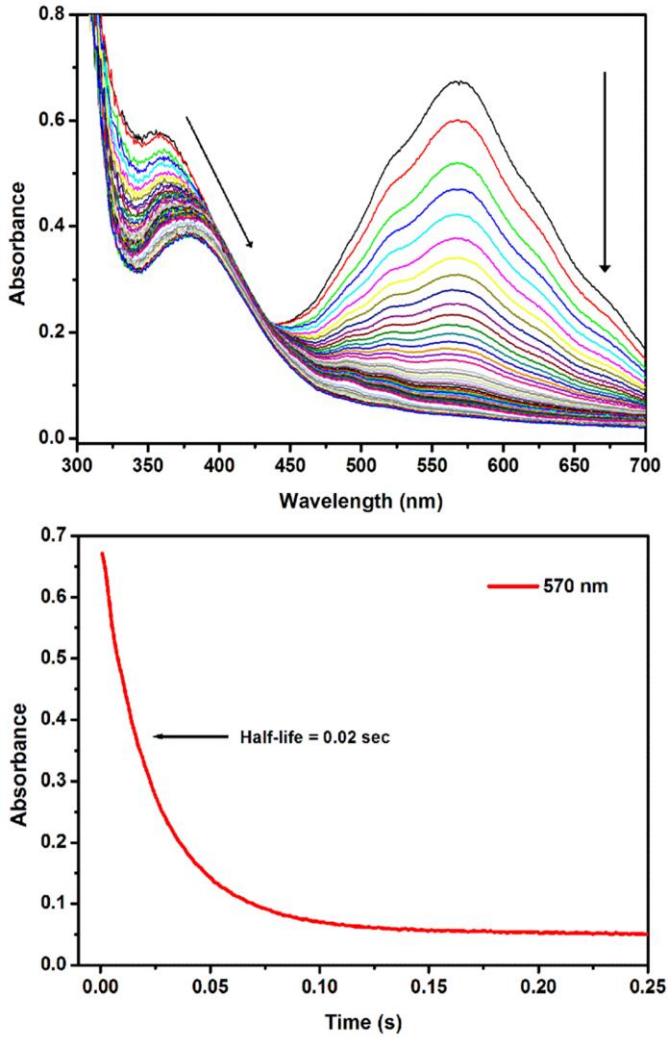

Figure 3-2. Reaction of $[Re(bipy\text{-}tBu)(CO)_3]^{-1}$ in THF with a solution of 200 mM CO_2 in THF over 0.75 sec in a stopped-flow UV-Vis experiment. Scans were taken every 1.5 ms over the course of the experiment and the degradation of the peak at 570 nm was followed for the half-life and pseudo-first order rate constant determination.

The spectral changes for the CO_2 reaction show rapid and complete decay of Re anion (Figure 3-2). The absorbance at 570 nm follows simple first-order kinetics over three half-lives, with $t_{1/2}$ = 20 ms and a pseudo first order rate constant of 35 s^{-1} (Table 3-1). The reactions with water, MeOH, and TFE were much slower, requiring multiple seconds to proceed to completion. Control reactions mixing the Re anion with

pure THF (no CO_2 or proton source) showed background degradation on this longer timescale. Remarkably, TFE did not appear to react with the Re complex on the time scale of the experiments (up to 150 s), beyond the background degradation. These results mirror the electrochemical conclusion that CO_2 is more readily reduced than H^+ by the Re anion, and suggest that this selectivity may have its origin in the initial reaction of the substrate with the doubly-reduced Re species.

The H_2O and methanol reactions were more complicated than simple first-order decay of the Re anion. The absorbance at 570 nm did not fully bleach, and new absorbances are observed at ~520 and 370 nm (Figures 3-3 and 3-4), due to as yet unidentified species. Until more detailed kinetic analyses can be completed, we have estimated half-lives for these reactions to provide a comparison with the well-behaved CO_2 reaction: ~0.5 s for H_2O, ~1 s MeOH and ≥100 s for TFE. These values imply that the reaction with CO_2 is *ca.* 25 times faster than that with H_2O, and 50 times faster than that with methanol. The slower reaction with TFE than with H_2O or MeOH is

Table 3-1. Results from UV-Vis stopped-flow experiments of $[Re(bipy\text{-}tBu)(CO)_3]^{-1}$

Reactant	**Half-life ($t_{1/2}$)**	**pseudo-first order rate constant**
CO_2	0.02 s	35 s^{-1}
H_2O	[0.5 s]	[~1 s^{-1}]
CH_3OH	[1 s]	[~1 s^{-1}]

The first three half-lives for the CO_2 reaction fit well to pseudo-first order kinetics. The H_2O and CH_3OH reactions, however, as described in the text, are more complex. The values given above in square brackets are rough estimates of the time for the first half life of reaction, estimated from the spectral changes in Figures 3 and 4.

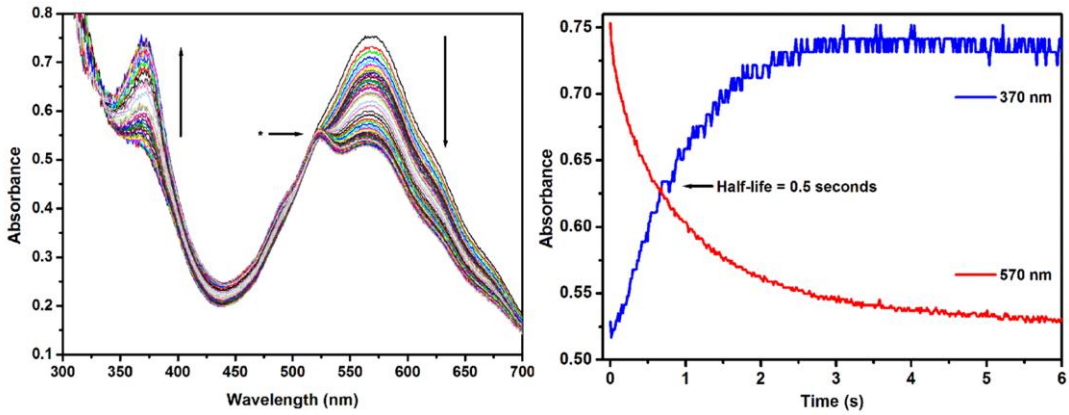

Figure 3-4. Reaction of activated $[Re(bipy\text{-}t Bu)(CO)_3]^{-1}$ in THF with a 200 mM water solution in THF over 7.5 sec in a stopped-flow UV-Vis experiment. Scans were taken every 15.0 ms over the course of the experiment and either the degradation of the peak at 570 nm or the growth of the peak at 370 nm could be followed to obtain half-lives and estimates for the rate of the reaction. It is notable that the products of this reaction are different than those in the CO_2 reaction and that the peak at 570 nm does not bleach to 0 abs. *In addition, note the growth of the peak at 520 nm that is not present in the CO_2 reaction.

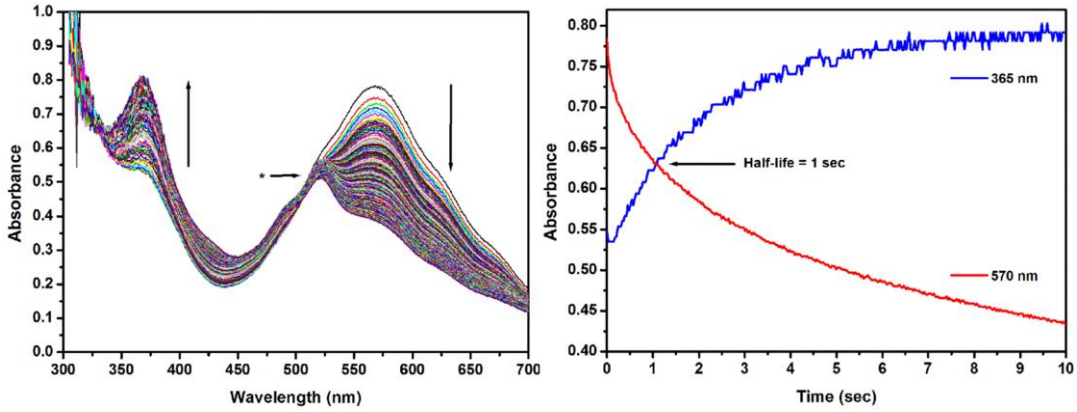

Figure 3-3. Reaction of activated $[Re(bipy\text{-}t Bu)(CO)_3]^{-1}$ in THF with a 200 mM methanol solution in THF over 15.0 sec in a stopped-flow UV-Vis experiment. Scans were taken every 30.0 ms over the course of the experiment and either the degradation of the peak at 570 nm or the growth of the peak at 370 nm could be followed to obtain half-lives and estimates for the rate of the reaction. It is notable that the products of this reaction are different than those in the CO_2 reaction and that the peak at 570 nm does not bleach to 0 abs. *In addition, note the growth of the peak at 520 nm that is not present in the CO_2 reaction.

surprising given the higher acidity of TFE than of H_2O or MeOH, and suggests that these reactions may be more complicated than simple protonation of the Re anion. Still, the conclusion is very clear that the rhenium anion reacts much more quickly with CO_2 than with sources of H^+.

Crystallography and DFT of the Re Anion: Origins of Selectivity. With stable solutions of the $[Re(bipy\text{-}t\text{Bu})(CO)_3]^{-1}$ species in hand, the source of CO_2 selectivity could be investigated through structural studies. Single crystals suitable for X-ray diffraction were grown from the vapor diffusion of pentane into a THF solution of the anion containing 18-crown-6 as a stabilizing agent. Upon reduction, the pre-catalyst

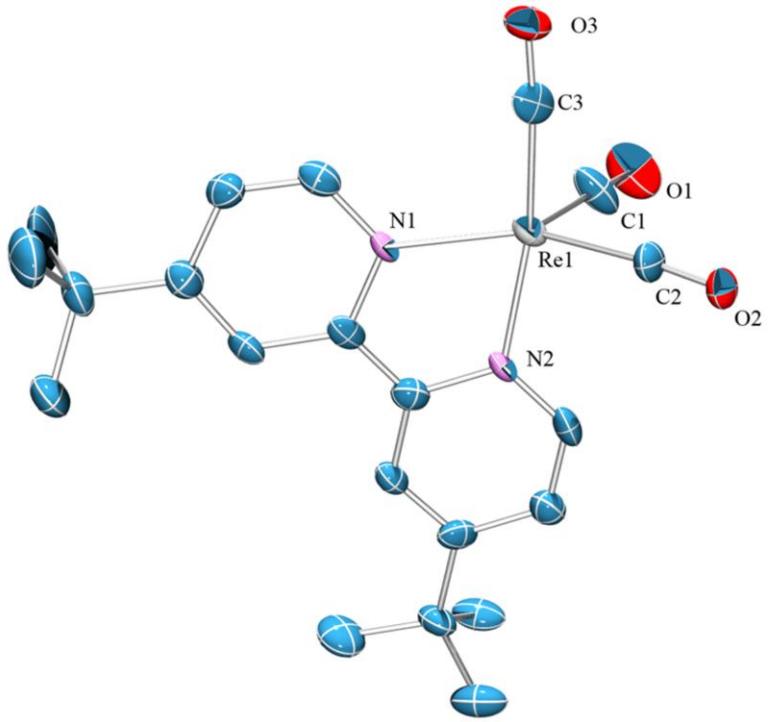

Figure 3-5. Molecular structure of the $[Re(bipy\text{-}t\text{Bu})(CO)_3]^{-1}$ anion. Hydrogen atoms, counter-ion and solvent molecules are omitted for clarity. Ellipsoids are shown at 50% probability.

[**1**] loses chloride and adopts a distorted trigonal bipyramidal structure (τ_5 = 0.46) in the solid state with the Re coordinated by three facial carbonyl ligands and a chelating bipyridine (Figure 3-5).[17] A table of selected bond lengths and angles can be found in Table 3-3 (appendix) and a full structure including the numbering scheme can be found in Figure 3-12 (appendix). The potassium cation is encapsulated by the crown ether and has one bound THF molecule. It is also associated with the axial carbonyl (O3–K1, 2.945(7) Å) (Figure 3-13, appendix). The Re–N distance contracts and the bite angle of the bipyridine increases slightly compared with the unreduced starting material [**1**] (Figure 3-14, appendix). This behavior is indicative of an improved orbital overlap between the ligand and metal center in the anion.

To obtain a better understanding of the electronics of this reduced state, we employed DFT calculations using ADF 2007.1. The calculated HOMO is a hybrid involving both the ligand and the metal center, containing substantial π* character (Figure 3-6, *xyz* coordinates in Table 3-4 in the appendix). This is consistent with the

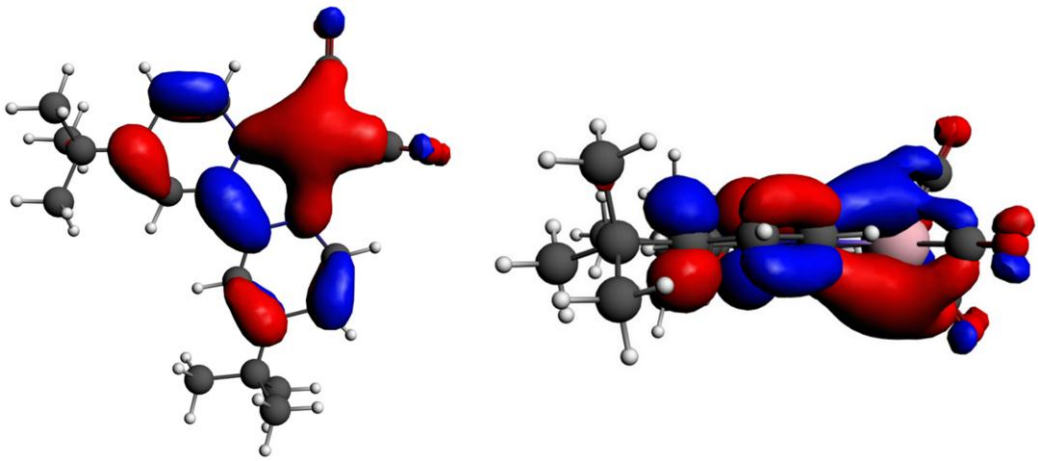

Figure 3-6. HOMO of Re(bipy-*t*Bu)$(CO)_3^{-1}$ anion calculated using ADF 2007.1.

bond length alternation observed in the bipyridine rings of the Re anion crystal structure. The bond alternation in the bipy is similar to what is seen in crystal structures of reduced 2,2'-bipyridine and suggests significant electron density on the ligand.[18] The geometry of the HOMO diffuses the directional basicity of the Re anion, and thus, other factors such as π interactions become important. We expect that the mixed character of the HOMO ($bipy^{-}$ + Re^{0}) relative to a pure doubly occupied d_z^2 "lone-pair" is sufficient to cause CO_2 binding to be more favorable than H^+ binding. Similarly, a HOMO that is delocalized over bipy (π*) and Re *d*-orbitals disfavors direct protonation of the Re d_z^2 orbital to produce a hydride.

The nature of the binding of CO_2 to the anion can also be better understood through DFT. The geometry optimized electronic structure of a Re(bipy-*t*Bu)$(CO)_3(CO_2)$K complex was calculated. The structure did not converge without the

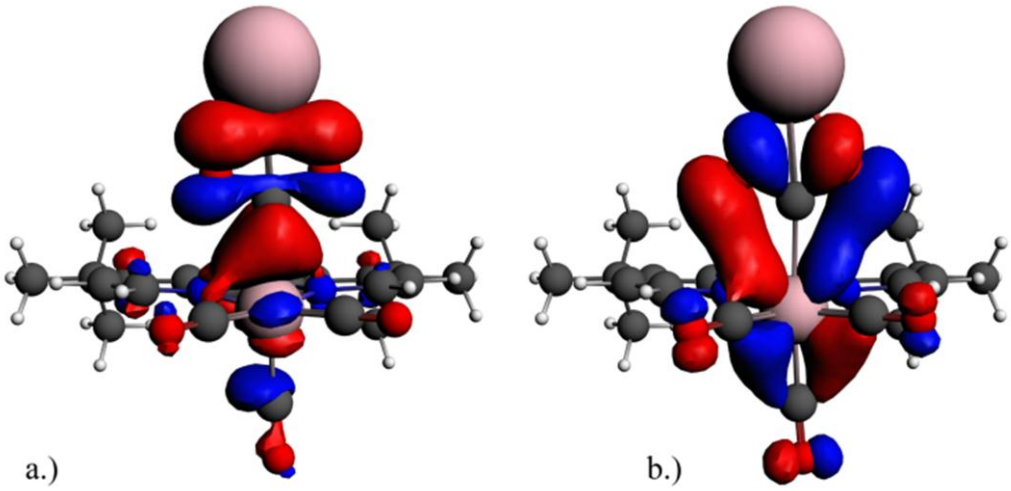

Figure 3-7. Calculated orbitals of Re(bipy-*t*Bu)$(CO)_3(CO_2)$K using ADF 2007.1 showing a.) the d_z^2 orbital that forms a σ bond to CO_2 and b.) the π interactions with CO_2.

addition of a cation (H, Li, Na, or K) to support the highly electronegative oxygen atoms. We observed that the d_z^2 orbital can form a σ bond to the carbon atom of CO_2 (HOMO) and the interaction with CO_2 can be further stabilized by a π interaction of the metal d_{xz} and d_{yz} orbitals with *p* orbitals on the CO_2 oxygen atoms (HOMO-4) (Figure 3-7, *xyz* coordinates in Table 3-5 in the appendix). This stabilizing interaction is clearly not available for the interaction with H^+. This interaction is somewhat similar to that calculated by Fujita and co-workers in the $[Co(macrocycle)(CO_2)(CH_3CN)]^+$ binding, but the Re complex forms an extended bonding interaction with the CO_2 oxygen atoms rather than just with the carbon center as in the Co example.[19]

Brönsted acid rate enhancement and Kinetic Isotope Effects. Having established a marked selectivity for CO_2 over H^+, we then investigated the catalytic system in the presence of added proton sources. The previously reported parent catalyst system, [**1**], has a very negative catalytic potential of –2.23 V (vs. Fc/Fc^+) relative to the thermodynamic potential of the reduction of CO_2 to CO (*ca.* –1.2 V vs. Fc/Fc^+ in water at pH 7). The high overpotential creates a situation where catalysis can occur without an added proton source. Previous reports have suggested that the second oxygen from CO_2 is transferred to an unknown oxide acceptor.[20] In similar systems, the necessary proton can be extracted from acetonitrile[21] or even from the electrolyte via Hoffman degradation.[22] More recently, evidence pointing to protons as the oxide acceptor was reported by Wong and co-workers. They showed that the catalytic

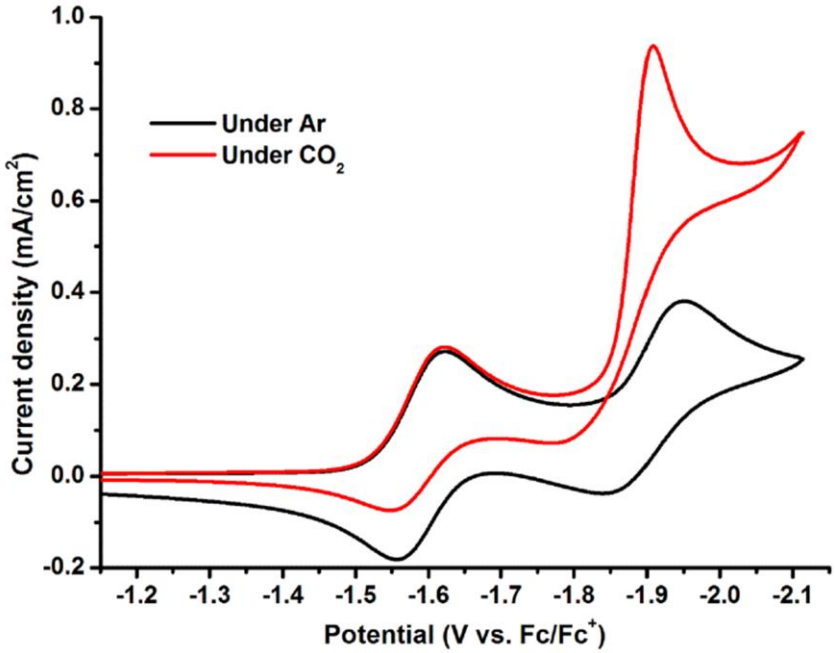

Figure 3-8. Re(bipy-*t*Bu)$(CO)_3$(MeCN)(OTf) [**2**] under argon (black) and CO_2 (red). The solution is 1 mM in catalyst with 0.1 M tetrabutylammonium hexafluorophosphate (TBAH) as the supporting electrolyte. A 1 mm diameter glassy carbon electrode, a Pt wire counter electrode, and an Ag wire pseudo-reference were used with ferrocene added as an internal reference.

current increased for the reduction of Re(bipy)$(CO)_3$(py)(OTf) under CO_2 in the presence of increasing concentrations of weak Brönsted acids.[23] In their study, the rate of electrocatalytic CO_2 reduction increased for the series: water (H_2O) < methanol (CH_3OH) < phenol < trifluoroethanol (TFE). In all cases, the Faradaic efficiency for the production of CO remained > 95%.

As a follow up to that work, the CO_2 reduction behavior of the improved catalysts Re(bipy-*t*Bu)$(CO)_3$(MeCN)(OTf) [**2**] and Re(bipy-*t*Bu)$(CO)_3$(py)(OTf) [**3**] were studied in the presence of H_2O, D_2O, CH_3OH, CD_3OD, TFE, and TFE-d_3 under an atmosphere of CO_2. Under argon and before the addition of protons, complex [**2**] exhibits one reversible reduction at –1.71 V followed by a quasi-reversible reduction at –1.94 V (*vs.* Fc/Fc^+). Complex [**3**] exhibits one reversible reduction at –1.64 V and

Table 3-2. Summary of results for addition of Brönsted acids.

Pre-catalyst	**Brönsted acid**	**Highest i_{cat} / i_p** [b]	**CO_2 solubility at highest i_{cat} / i_p**
Re(bipy-tBu)$(CO)_3$(MeCN)(OTf) [**2**]	TFE	54.0 (1.6 M)	0.19 M
Re(bipy-tBu)$(CO)_3$(MeCN)(OTf) [**2**]	Methanol	41.9 (9.9 M)	0.22 M
Re(bipy-tBu)$(CO)_3$(MeCN)(OTf) [**2**]	Water	9.0 (10.0 M)	0.18 M
Re(bipy-tBu)$(CO)_3$(py)(OTf) [**3**]	TFE	62.0 (1.5 M)	0.27 M
Re(bipy-tBu)$(CO)_3$(py)(OTf) [**3**]	Methanol	28.9 (8.0 M)	0.23 M
Re(bipy-tBu)$(CO)_3$(py)(OTf) [**3**]	Water	8.2 (7.3 M)	0.19 M
Re(bipy)$(CO)_3$(py)(OTf) [a]	TFE	47.1 (0.77 M)	0.27 M
Re(bipy)$(CO)_3$(py)(OTf) [a]	Phenol	39.5 (0.57 M)	0.30 M
Re(bipy)$(CO)_3$(py)(OTf) [a]	Methanol	31.1 (7.20 M)	0.24 M
Re(bipy)$(CO)_3$(py)(OTf) [a]	Water	11.4 (10.4 M)	0.17 M

[a] From Wong et al. (27)
[b] Acid concentration in parenthesis.

one quasi-reversible reduction at –1.95 V (*vs.* Fc/Fc^+) (Figure 3-8). The first reduction of the complex represents reduction of the bipyridine ligand and the second reduction is mostly metal-based.[12, 13] It was observed that the addition of 0.5 M pyridine to the solution of [**3**] increases the reversibility of the second reduction.

Given that [**1**] showed a substantial increase in the rate of catalysis over the original Re(bipy)$(CO)_3$Cl catalyst,[12] we expected to see even higher current densities upon the addition of protons to [**2**] and [**3**] in the presence of CO_2 in MeCN. Upon addition of TFE or methanol, an increased i_{cat}/i_p was observed compared with the results of Wong and co-workers, whereas for water a similar i_{cat}/i_p was observed (Table 3-2).

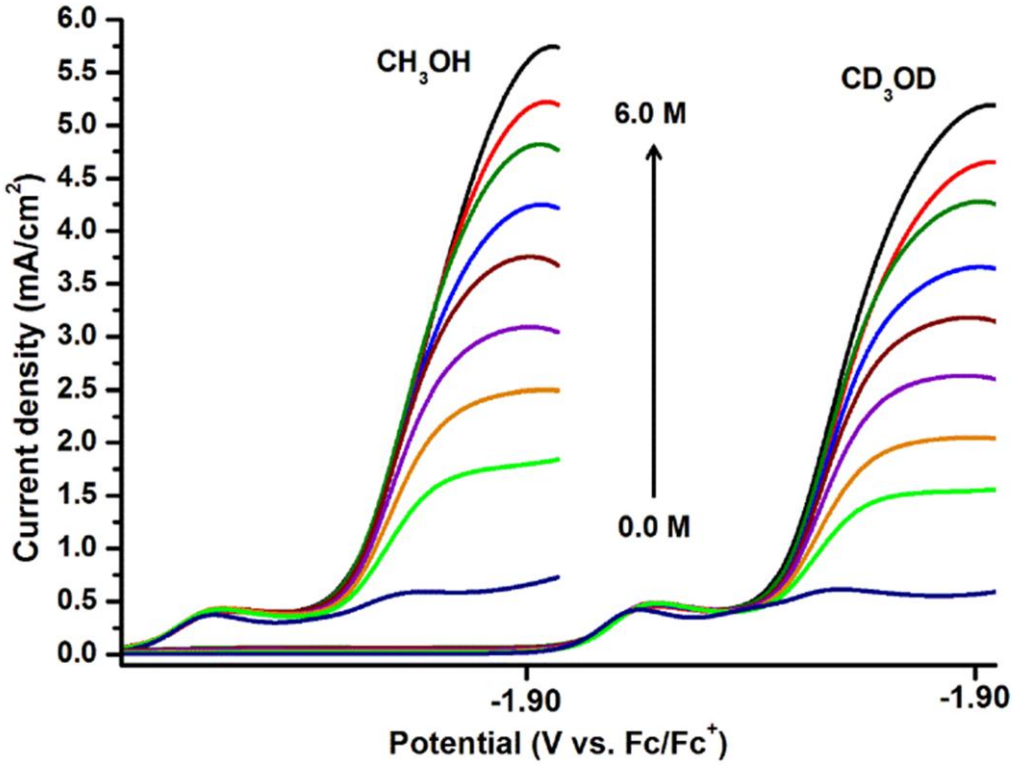

Figure 3-9. KIE study for methanol and methanol-d_4 addition to the catalytic reaction of $[Re(bipy\text{-}tBu)(CO)_3]^{-1}$ with CO_2. In each case we see a significant increase in the catalytic current upon addition of the Brönsted acid. This data is representative of the results for H_2O/D_2O and TFE/TFE-d_3.

A normal primary H/D kinetic isotope effect was observed in these experiments (see the data for CH_3OH *vs.* CD_3OD in Figure 3-9). For complex [**2**], the KIE for H_2O/D_2O is 1.8(±0.1), the KIE for CH_3OH/CD_3OD is 1.8(±0.1), and the KIE for TFE/TFE-d_3 is 1.2(±0.1). The decreased KIE for TFE is attributed to an increased mismatch between the pK_a of the metal-bound CO_2 and the pK_a of the acid.[24] The observation of a KIE suggests that proton transfer to the Re-CO_2 adduct is likely involved in the rate limiting step in this reaction.

The Brönsted acid experiments also suggest that the catalytic reaction is second order in acid. A linear region can be observed in a plot of the ratio of catalytic

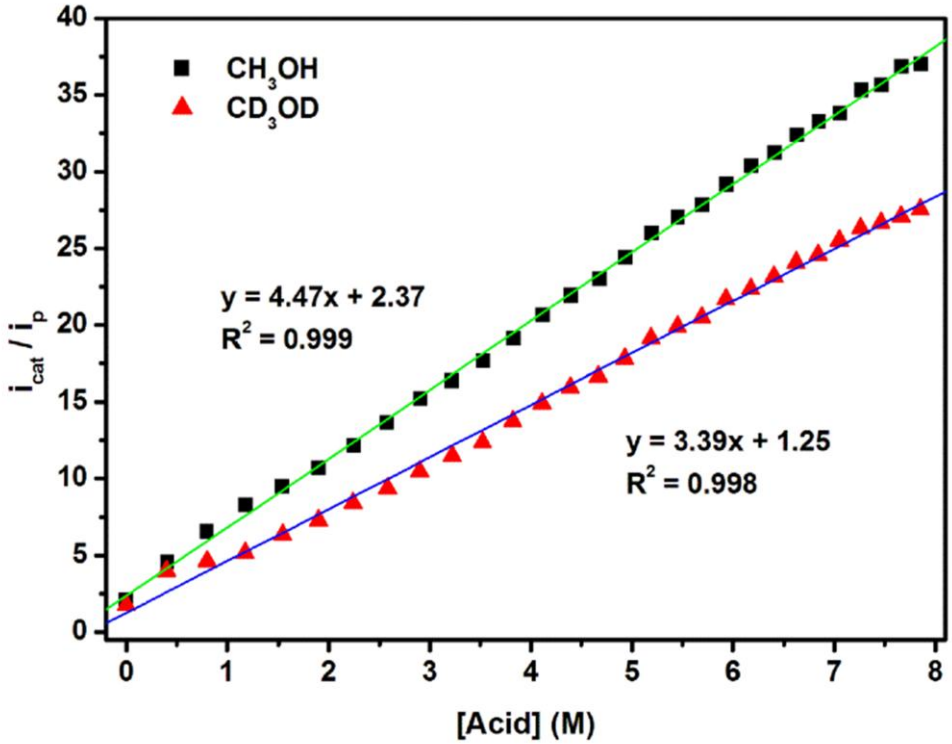

Figure 3-10. Kinetics of the catalytic reduction of CO_2 by 1.0 mM $[Re(bipy\text{-}t\text{Bu})(CO_3)(MeCN)]^+$ in CH_3CN + 0.1 M TBAH with added CH_3OH or CD_3OD. The variation of i_{cat} / i_p is analogous to plotting $k'^{1/2}$ and leads to a second order dependence on $[H^+]$ in the rate equation.

current (i_{cat}) to non-catalytic current (i_p) versus substrate concentration (Figure 3-10). This behavior is expected for an EC' catalytic mechanism, in which the relationship between substrate concentration and current ratio can be described by (E3-1).[25, 26]

$$TOF = k[sub]^x = \frac{F\vartheta n_p}{RT}\left(\frac{0.4463}{n_{cat}}\right)^2\left(\frac{i_{cat}}{i_p}\right)^2 \qquad \textbf{E3-1}$$

The molar range of the linear region changes for each acid in the series. All of the acids exhibit this behavior before tapering and establishing a steady catalytic i_{cat}/i_p.

Catalytic currents do not plateau in the cyclic voltammograms under CO_2 (even at high H^+ concentrations), but E3-1 applies because the catalytic current is scan rate independent. Additional experiments have established that the reaction is first order in $[CO_2]$,[23] leading to the rate equation:

$$k_{obs} = k[CO_2][H^+]^2 \qquad \textbf{E3-2}$$

For all Brönsted acids, the production of CO was nearly quantitative (>95% current efficiency) even at acid concentrations where i_{cat}/i_p was at its maximum, consistent with other data indicating that the catalyst remains very selective for CO_2 even in the presence of a large excess of H^+. Together, the KIE and second-order $[H^+]$ dependence of this catalytic reaction provide strong evidence for H_2O formation from the second oxygen atom of the CO_2 substrate. The H^+ dependence is ideal for an artificial photosynthesis system because the oxygen-evolving half reaction produces protons.

3.3 Concluding Remarks

We have shown that the Re(bipy-*t*Bu)$(CO)_3$(L) electrocatalytic system is very selective for the reduction of CO_2, and that the rate of catalysis can be enhanced by the addition of a proton source. Stopped-flow UV-Vis experimental data indicate that CO_2 reacts ca. 25 times faster than water and ca. 50 times faster than methanol with $[Re(bipy\text{-}tBu)(CO)_3]^{-1}$. The reduced form presumed to be the active catalyst was

studied by X-ray crystallography for the first time. The structural data, combined with DFT studies of the reduced complex, suggest that the HOMO contains mixed metal-ligand character. Kinetic isotope effect and kinetic studies indicate that protons are involved in the rate determining step for the reduction of CO_2 to CO by Re(bipy-*t*Bu)$(CO)_3$(L).

3.4 Experimental

General considerations. Complex [**1**] was synthesized by previously reported methods.[12] X-ray quality crystals of **1** were grown from the vapor diffusion of pentane into THF. THF, CH_3CN, and Pentane were sparged with argon and dried over basic alumina with a custom dry solvent system, THF and pentane were then stored over activated molecular sieves. KC_8 was prepared by literature methods.[27] 18-crown-6 was recrystallized from acetonitrile, tetrabutylammonium hexafluorophosphate (TBAH) was recrystallized twice from methanol, and both were dried *in vacuo*. All other chemicals were purchased from commercial sources and used as received.

Synthesis of Re(bipy-*t*Bu)$(CO)_3$(MeCN)(OTf) [2]. Re(bipy-*t*Bu)$(CO)_3$Cl (0.540 g, 0.94 mmol) was added to ~80 mL acetonitrile under nitrogen. Silver triflate (0.243 g, 0.95 mmol) was added to the flask with stirring and covered with foil to protect from light. The reaction mixture was refluxed for 24 hours followed by rotary evaporation yielding a yellow powder. A basic alumina column was run first with CH_2Cl_2 to elute any remaining Cl^- complex followed by CH_3CN to elute complex [**2**]. ^{1}H NMR (400

MHz, methylene chloride-d_2, 20 °C): δ 1.48 (s, 18H), δ 2.23 (s, 3H), δ 7.65 (dd, 2H, *J* = 6 Hz, 2 Hz), δ 8.34 (d, 2H, *J* = 2 Hz), δ 8.85 (d, 2H, *J* = 6 Hz). IR(CH_3CN) ν(CO): 2038 cm^{-1}, 1934 cm^{-1} (broad). Anal. Calcd for **2**, $C_{24}H_{27}F_3N_3O_6ReS$: C, 39.55; H, 3.73; N, 5.77. Found: C, 39.49; H, 3.69; N, 5.66.

Synthesis of Re(bipy-*t*Bu)(CO)$_3$(py)(OTf) [3]. $Re(CO)_5Cl$ (0.500 g, 1.4 mmol) was added to ~50 mL CH_2Cl_2 under a nitrogen atmosphere. Silver triflate (0.3760 g, 1.46 mmol) was added to the flask with stirring and covered with foil to protect from light. After 24 hours of stirring the reaction mixture was filtered to remove AgCl. 4,4'-di-*tert*-butyl-2,2'-bipyridine (0.364 g, 1.35 mmol) was added to the clear, colorless solution and heat was applied to reflux. After 23 hours of reflux vacuum was applied to the yellow solution with gentle warming to remove the solvent. A yellow solid was obtained and argon-sparged pyridine (20 mL) was added. The yellow solid dissolved in the pyridine and heat was applied to reflux. After four hours of reflux the pyridine was removed under a stream of argon with gentle warming. The resulting yellow-green solid was purified by column chromatography on basic alumina with CH_2Cl_2 to elute any Cl^- complex followed by CH_3CN to elute complex [**3**]. The product was rotary evaporated and dried in a vacuum oven at 90 °C overnight. Spectroscopically pure [**3**] was obtained from the reaction with a total yield of 90%. ^{1}H NMR (400 MHz, Methylene Chloride-d_2, 20 °C): δ 1.46 (s, 18H), δ 7.37 (t. 2H, *J* = 7 Hz), δ 7.73 (dd, 2H, *J* = 6 Hz, 2 Hz), δ 7.86 (t, 1H, *J* = 8 Hz), δ 8.22 (d, 2H, *J* = 4 Hz), δ 8.26 (d, 2H, *J* = 1.5 Hz) δ 9.02 (d, 2H, *J* = 5.5 Hz). IR(CH_3CN) ν(CO): 2033 cm^{-1}, 1927 cm^{-1}

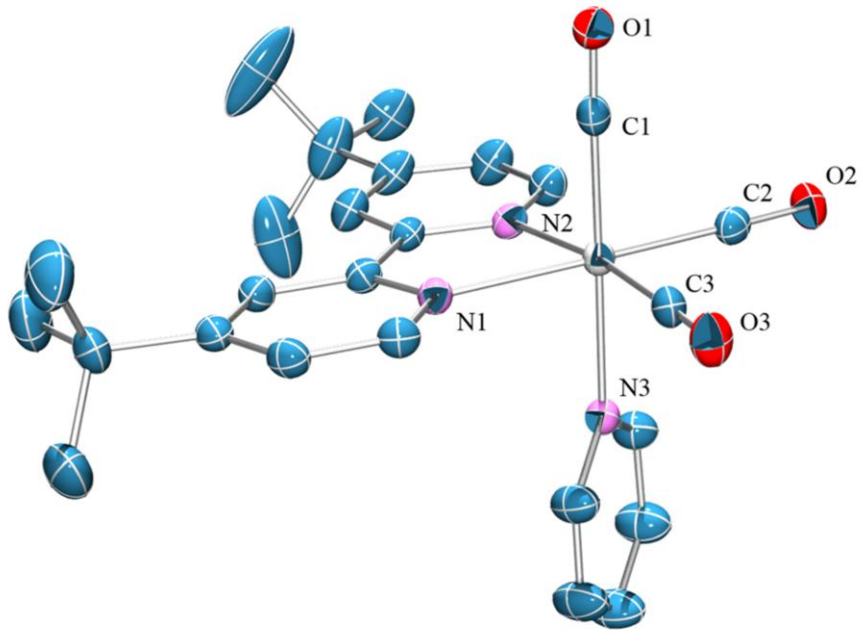

Figure 3-11. Molecular structure of Re(bipy-*t*Bu)$(CO)_3$(py)(CF_3SO_3). Hydrogen atoms and a disordered triflate are omitted for clarity. Ellipsoids are shown at 50% probability.

(broad). Anal. Calcd for **3**, $C_{27}H_{29}F_3N_3O_6ReS$: C, 42.29; H, 3.81; N, 5.48. Found: C, 42.39; H, 3.79; N, 5.21. X-ray quality crystals were grown from vapor diffusion of diethyl ether into acetonitrile. Crystal structure details can be found in Figure 3-11 and Table 3-2.

Reduction of Re(bipy-*t*Bu)$(CO)_3$Cl with KC_8. 1–10 mM solutions of Re(bipy-*t*Bu)$(CO)_3$Cl were prepared in THF in an inert atmosphere and cooled to –35 °C. Either 18-crown-6 (2.5 eq. for X-ray and FTIR) or tetrabutylammonium hexafluorophosphate (0.1 M for stopped-flow) were added as stabilizing agents. 2.1 equivalents of KC_8 were added to the cooled solution and allowed to warm to room temperature over a period of 30 minutes. The solution was then filtered, affording a

deep purple solution of the anion. The solution was concentrated from 20 mL to approximately 3 mL and 15 mL of pentane was added. That solution was stored in the freezer for two hours, was then decanted, and the purple solid was dried under vacuum. X-ray quality crystals were grown by the vapor diffusion of pentane in to a THF solution of the complex. A typical yield of 66% was observed. FTIR(THF) ν(CO): 1940 cm^{-1} and 1835 cm^{-1}. ^1H NMR (500 MHz, TFH-d_8, 20 °C): δ 1.21 (s, 18H), δ 3.54 (s(br), 24H), δ 3.59 (d, 2H, *J* = 6 Hz), δ 7.13 (s, 2H), δ 8.86 (d, 2H, *J* = 7 Hz). Anal. Calcd, $C_{33}H_{48}KN_2O_9Re$: C, 47.07; H, 5.75; N, 3.33. Found: C, 47.02; H, 5.72; N, 3.35.

Stopped-Flow Measurements. Stopped-flow measurements were performed using a Hi-Tech/TgK Scientific SF-61DX2 Cryo Stopped-Flow system. A xenon-lamp illuminated the mixing chamber (1 cm path length, fused UV silica) in conjunction with a diode array detector. Reactions were run at ~295 K with time scale ranging from 0.75 to 150 seconds (first data point at 0.75 ms). All samples were prepared under a nitrogen atmosphere in a dry box and were transported to the stopped-flow apparatus in gas-tight syringes. The apparatus was flushed with dry, degassed THF thoroughly before loading the samples into the drive syringes. Samples were relatively stable over a few hours (<10% decomposition). The concentration of $[Re(bipy\text{-}tBu)(CO)_3]^{-1}$ before mixing was 0.12 mM, CO_2 was at saturation (~ 200 mM) in THF, H_2O, methanol and TFE were all prepared at 200 mM in THF. Control reactions mixing $[Re(bipy\text{-}tBu)(CO)_3]^-$ with THF alone showed a background degradation

reaction, with 75% decomposition over 150 s. Data was analyzed using Kinetic Studio 2.23 (Hi-Tech Scientific).

X-ray structure determination. The single crystal X-ray diffraction studies were carried out on a Bruker Kappa APEX-II CCD diffractometer equipped with Mo Kα radiation (λ = 0.71073 Å) or a Bruker Kappa APEX CCD diffractometer equipped with Cu Kα radiation (λ = 1.54184 Å). The crystals were mounted on a Cryoloop with Paratone oil and data was collected under a nitrogen gas stream at 100(2) K using ω and ϕ scans. Data was integrated using the Bruker SAINT software program and scaled using the SADABS software program. Solution by direct methods (SHELXS) produced a complete phasing model consistent with the proposed structure. All non-hydrogen atoms were refined anisotropically by full-matrix least-squares (SHELXL-97).[28] All hydrogen atoms were placed using a riding model. Their positions were constrained relative to their parent atom using the appropriate HFIX command in SHELXL-97. Crystallographic data are summarized in Table 3-2.

Computational methods. The DFT calculations were performed with the Amsterdam Density Functional (ADF) program suite,[29, 30] version 2007.1 using the triple-ζ Slater-type orbital basis set. Zero-order regular approximation (ZORA)[31, 32] was included for relativistic effects in conjunction with the local density approximation of Vosko *et al.* (VWN).[33] Generalized gradient approximations for electron exchange and

correlation were used as described by Becke[34] and Perdew.[35, 36] Molecular orbitals and final geometries were visualized with ADF-GUI.

Electrochemistry. All electrochemical experiments were performed using a BASi Epsilon potentiostat and an air-tight one compartment electrochemical cell. Either glassy carbon (BASi 1 mm diameter) or p-Si were used as the working electrode, a Pt wire was used as the counter, and an Ag wire separated from the solution by a Vycor tip was used as a pseudo reference (Ferrocene added as an additional reference). All electrochemical experiments were performed in acetonitrile with 0.1 M tetrabutylammonium hexafluorophosphate (TBAH) as the supporting electrolyte except where otherwise noted, and were purged with either argon or CO_2 before CVs were taken. Re concentrations started at 1 mM in all cases and decreased with addition of Brönsted acid. CO_2 experiments were performed at gas saturation (~ 0.25 M).

Note: Much of the material for this chapter comes directly from a manuscript entitled "Artificial photosynthesis of CO: Kinetic and structural studies, origins of selectivity and the importance of interfacial charge transfer." by Jonathan M. Smieja, Eric E. Benson, Bhupendra Kumar, Kyle A. Grice, Candace S. Seu, Alexander A. J. Miller, James M. Mayer, and Clifford P. Kubiak, which has been published in *Proceedings of the National Academy of Sciences*, **2012**, *In Press*. The dissertation author is the primary author of this manuscript.

3.5 References

1. Olah GA, Prakash GKS, Goeppert A (2011) Anthropogenic Chemical Carbon Cycle for a Sustainable Future. *J. Am. Chem. Soc.* 133(33):12881-12898.

2. Rüttinger W, Dismukes GC (1997) Synthetic Water-Oxidation Catalysts for Artificial Photosynthetic Water Oxidation. *Chem. Rev.* 97(1):1-24.

3. Yagi M, Kaneko M (2000) Molecular Catalysts for Water Oxidation. *Chem. Rev.* 101(1):21-36.

4. Dau H, *et al.* (2010) The Mechanism of Water Oxidation: From Electrolysis via Homogeneous to Biological Catalysis. *ChemCatChem* 2(7):724-761.

5. Bradley MG, Tysak T, Graves DJ, Viachiopoulos NA (1983) Electrocatalytic reduction of carbon dioxide at illuminated p-type silicon semiconduccting electrodes. *J. Chem. Soc., Chem. Commun.* (7):349-350.

6. Beley M, Collin J-P, Sauvage J-P, Petit J-P, Chartier P (1986) Photoassisted electro-reduction of CO_2 on p-GaAs in the presence of $[Ni(cyclam)]^{2+}$. *J. Electroanal. Chem.* 206(1-2):333-339.

7. J.-P. Petit PC, M. Beley, and J.-P. Sauvage, (1987) Selective Photoelectrochemical reduction of CO_2 to CO in an aqueous medium on p-GaP mediated by $[Ni(cyclam)]^{2+}$. *N. J. Chim.* 11:751.

8. Barton EE, Rampulla DM, Bocarsly AB (2008) Selective Solar-Driven Reduction of CO_2 to Methanol Using a Catalyzed p-GaP Based Photoelectrochemical Cell. *J. Am. Chem. Soc.* 130(20):6342-6344.

9. Kumar B, Smieja JM, Kubiak CP (2010) Photoreduction of CO_2 on p-type Silicon Using Re(bipy-*t*Bu)$(CO)_3$Cl: Photovoltages Exceeding 600 mV for the Selective Reduction of CO_2 to CO. *J Phys. Chem. C* 114(33):14220-14223.

10. Hawecker J, Lehn JM, Ziessel R (1984) Electrocatalytic reduction of carbon dioxide mediated by Re(bipy)$(CO)_3$Cl (bipy = 2,2'-bipyridine). *J. Chem. Soc., Chem. Commun.* (6):328-330.

11. Hawecker J, Lehn JM, Ziessel R (1986) Photochemical and Electrochemical Reduction of Carbon Dioxide to Carbon Monoxide Mediated by (2,2'-Bipyridine)Tricarbonylchlororhenium(I) and Related Complexes as Homogeneous Catalysts. *HeIv. Chim. Acta* 69(8):1990-2012.

12. Smieja JM, Kubiak CP (2010) Re(bipy-*t*Bu)$(CO)_3$Cl−improved Catalytic Activity for Reduction of Carbon Dioxide: IR-Spectroelectrochemical and Mechanistic Studies. *Inorg. Chem.* 49(20):9283-9289.

13. Johnson FPA, George MW, Hartl F, Turner JJ (1996) Electrocatalytic Reduction of CO_2 Using the Complexes [Re(bpy)$(CO)_3$L]n (n = +1, L = $P(OEt)_3$, CH_3CN; n = 0, L = Cl^-, OTf^-; bpy = 2,2‘-Bipyridine; OTf^- = CF_3SO_3) as Catalyst Precursors: Infrared Spectroelectrochemical Investigation. *Organometallics* 15(15):3374-3387.

14. Kumar B, Smieja JM, Sasayama AF, Kubiak CP (2012) Tunable, light-assisted co-generation of CO and H_2 from CO_2 and H_2O by Re(bipy-*t*Bu)$(CO)_3$Cl and p-Si in non-aqueous medium. *Chem. Commun.* 48(2):272-274.

15. Yam VWW, Lau VCY, Cheung KK (1995) Synthesis and Photophysics of Luminescent Rhenium(I) Acetylides-Precursors for Organometallic Rigid-Rod Materials - X-Ray Crystal Structures of [Re($^tBu_2$-Bpy)$(CO)_3$($^tBuC{\equiv}C$)] and [Re($^tBu_2$-Bpy)$(CO)_3$Cl]. *Organometallics* 14(6):2749-2753.

16. Gennaro A, Isse AA, Vianello E (1990) Solubility and electrochemical determination of CO_2 in some dipolar aprotic solvents. *J. Electroanal. Chem.* 289(1–2):203-215.

17. Addison AW, Rao TN, Reedijk J, van Rijn J, Verschoor GC (1984) Synthesis, structure, and spectroscopic properties of copper(II) compounds containing nitrogen-sulphur donor ligands; the crystal and molecular structure of aqua[1,7-bis(N-methylbenzimidazol-2[prime or minute]-yl)-2,6-dithiaheptane]copper(II) perchlorate. *J. Chem. Soc., Dalton Trans.* (7):1349-1356.

18. Gore-Randall E, Irwin M, Denning MS, Goicoechea JM (2009) Synthesis and Characterization of Alkali-Metal Salts of 2,2′- and 2,4′-Bipyridyl Radicals and Dianions. *Inorg. Chem.* 48(17):8304-8316.

19. Schneider J, Jia H, Muckerman JT, Fujita E (2012) Thermodynamics and kinetics of CO_2, CO, and H^+ binding to the metal centre of CO_2 reduction catalysts. *Chem. Soc. Rev.* 41(6).

20. Sullivan BP, Bolinger CM, Conrad D, Vining WJ, Meyer TJ (1985) One- and two-electron pathways in the electrocatalytic reduction of CO_2 by *fac*-Re(bpy)$(CO)_3$Cl (bpy = 2,2'-bipyridine). *J. Chem. Soc., Chem. Commun.* (20):1414-1416.

21. Slater S, Wagenknecht JH (1984) Electrochemical reduction of carbon dioxide catalyzed by Rh$(diphos)_2$Cl. *J. Am. Chem. Soc.* 106(18):5367-5368.

22. Bolinger CM, *et al.* (1985) Electrocatalytic reduction of CO_2 based on polypyridyl complexes of rhodium and ruthenium. *J. Chem. Soc., Chem. Commun.* (12):796-797.

23. Wong K-Y, Chung W-H, Lau C-P (1998) The effect of weak Brönsted acids on the electrocatalytic reduction of carbon dioxide by a rhenium tricarbonyl bipyridyl complex. *J. Electroanal. Chem.* 453(1–2):161-169.

24. Dixon JE, Bruice TC (1970) Dependence of the primary isotope effect (kH/kD) on base strength for the primary amine catalyzed ionization of nitroethane. *J. Am. Chem. Soc.* 92(4):905-909.

25. Savéant JM, Vianello E (1962) Potential-sweep chronoamperometry theory of kinetic currents in the case of a first order chemical reaction preceding the electron-transfer process. *Electrochim. Acta* 8(12):905-923.

26. DuBois DL, Miedaner A, Haltiwanger RC (1991) Electrochemical reduction of carbon dioxide catalyzed by [Pd(triphosphine)(solvent)]$(BF_4)_2$ complexes: synthetic and mechanistic studies. *J. Am. Chem. Soc.* 113(23):8753-8764.

27. Schwindt MA, Lejon T, Hegedus LS (1990) Improved synthesis of (aminocarbene)chromium(0) complexes with use of C_8K-generated $[Cr(CO)_5]^{2-}$. Multivariant optimization of an organometallic reaction. *Organometallics* 9(10):2814-2819.

28. Sheldrick G (2008) A short history of SHELX. *Acta Crystallogr. Sect. A* 64(1):112-122.

29. Fonseca Guerra C, Snijders JG, te Velde G, Baerends EJ (1998) Towards an order-N DFT method. *Theor. Chem. Acc.* 99(6):391-403.

30. te Velde G, *et al.* (2001) Chemistry with ADF. *J. Comput. Chem.* 22(9):931-967.

31. van Lenthe E, Baerends EJ, Snijders JG (1993) Relativistic regular two-component Hamiltonians. *J. Chem. Phys.* 99(6):4597-4610.

32. van Lenthe E, Snijders JG, Baerends EJ (1996) The zero-order regular approximation for relativistic effects: The effect of spin-orbit coupling in closed shell molecules. *J. Chem. Phys.* 105(15):6505-6516.

33. Vosko SH, Wilk L, Nusair M (1980) Accurate spin-dependent electron liquid correlation energies for local spin density calculations: a critical analysis. *Can. J. Phys.* 58(8):1200-1211.

34. Becke AD (1988) Density-functional exchange-energy approximation with correct asymptotic behavior. *Phys. Rev. A* 38(6):3098-3100.

35. Perdew JP (1986) Density-functional approximation for the correlation energy of the inhomogeneous electron gas. *Phys. Rev. B* 33(12):8822-8824.

36. Perdew JP (1986) Erratum: Density-functional approximation for the correlation energy of the inhomogeneous electron gas. *Phys. Rev. B* 34(10):7406-7406.

3.6 Appendix

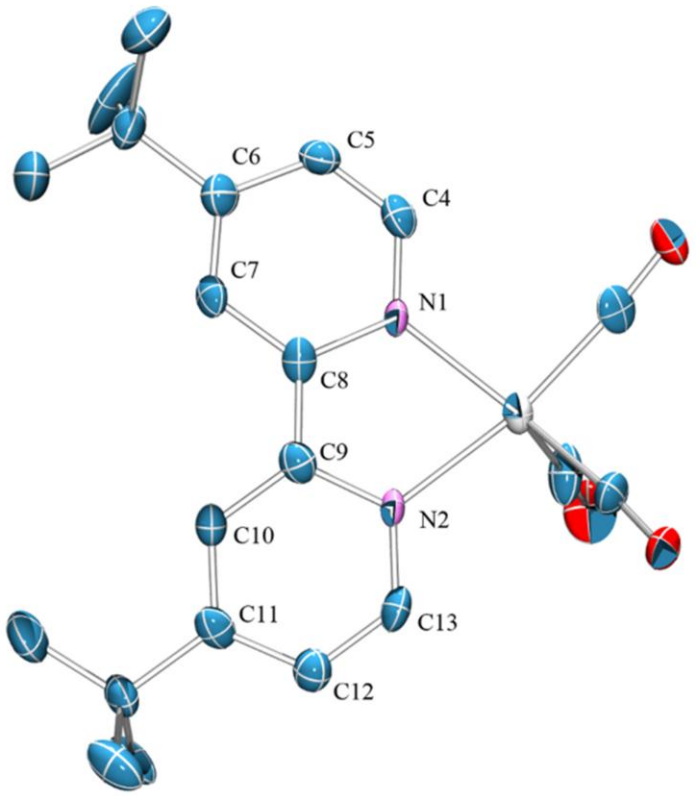

Figure 3-12. Moleculuar structure of $[Re(bipy\text{-}tBu)(CO)_3]^{-1}$ and labeling scheme.

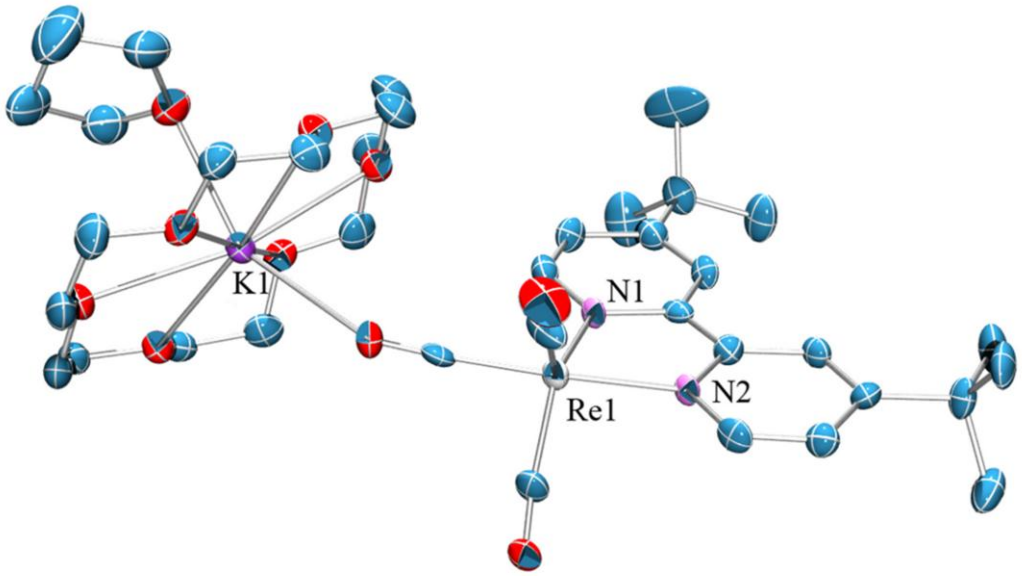

Figure 3-13. Full structure of [Re(bipy-*t*Bu)$(CO)_3$][K(18-crown-6)•THF]. Hydrogen atoms are omitted for clarity and ellipsoids are shown at 50% probability.

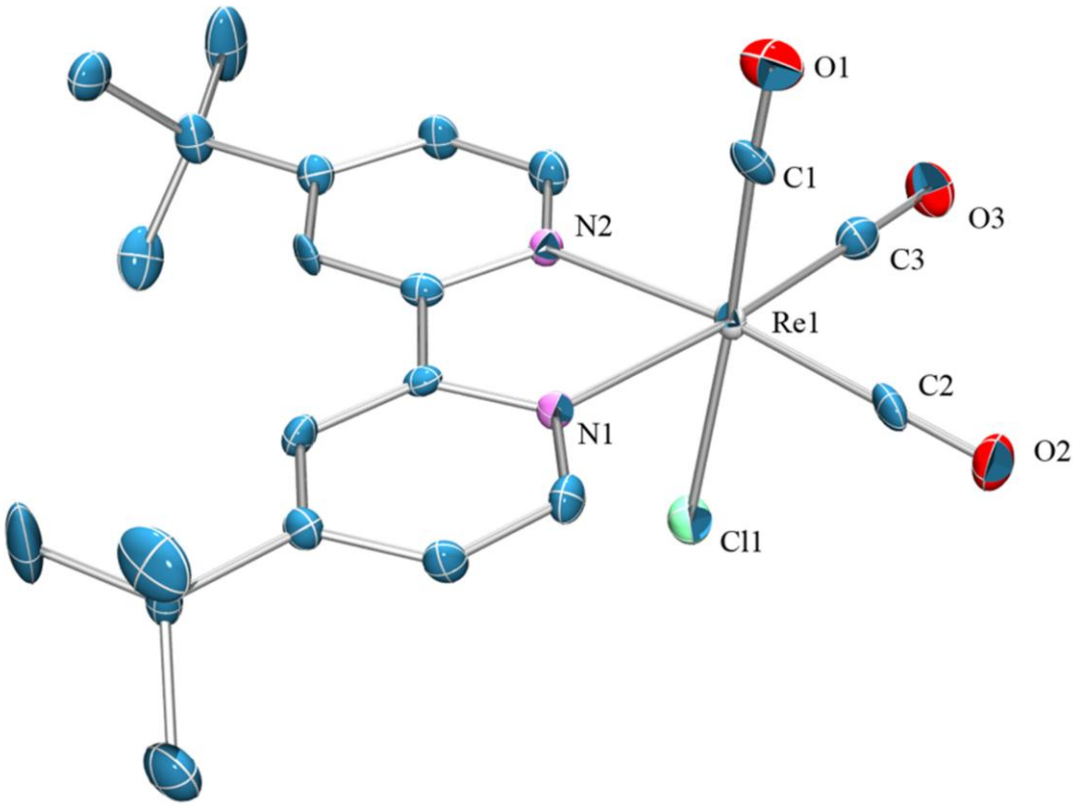

Figure 3-14. Molecular structure of one of the molecules of Re(bipy-*t*Bu)$(CO)_3$Cl in the asymmetric unit, Z' = 2. Hydrogen atoms are omitted for clarity and ellipsoids are shown at 50% probability.

Table 3-3. Selected bond lengths and angles for Re(bipy-*t*Bu)$(CO)_3$Cl, [Re(bipy-*t*Bu)$(CO)_3]^{-1}$ and Re(bipy-*t*Bu)$(CO)_3$(py)(OTf).

	Re(bipy-*t*Bu)$(CO)_3$Cl	Re(bipy-*t*Bu)$(CO)_3^-$	Re(bipy-*t*Bu) $(CO)_3$(py)(OTf)
Re - N1	2.174(3)	2.070(7)	2.165(2)
Re - N2	2.178(3)	2.115(7)	2.167(2)
Re - C1	1.909(4)	1.903(11)	1.922(3)
Re - C2	1.909(4)	1.919(8)	1.922(3)
Re - C3	1.914(4)	1.926(11)	1.927(3)
C1 - O1	1.148(5)	1.145(15)	1.153(3)
C2 - O2	1.172(5)	1.144(12)	1.151(3)
C3 - O3	1.161(5)	1.166(13)	1.151(3)
N1 - Re1 - N2	74.36(11)	75.1(3)	74.93(8)
N1 - Re1 - C1	92.73(14)	127.2(5)	94.2(1)
N1 - Re1 - C2	100.45(14)	142.4(3)	171.2(1)
N1 - Re1 - C3	171.97(14)	95.3(4)	97.9(1)
N2 - Re1 - C1	96.05(14)	97.3(4)	95.1(1)
N2 - Re1 - C2	173.67(14)	95.1(3)	96.6(1)
N2 - Re1 - C3	97.72(14)	170.0(4)	172.2(1)
N1 - C4	1.337(5)	1.372(14)	1.349(3)
C4 - C5	1.379(5)	1.324(15)	1.373(4)
C5 - C6	1.396(5)	1.442(13)	1.397(4)
C6 - C7	1.393(5)	1.364(14)	1.389(4)
C7 - C8	1.385(5)	1.439(14)	1.390(4)
C8 - N1	1.360(5)	1.422(12)	1.355(4)
C8 - C9	1.487(5)	1.373(15)	1.476(3)
C9 - N2	1.361(5)	1.402(12)	1.360(3)
C9 - C10	1.386(5)	1.424(13)	1.387(4)
C10 - C11	1.404(5)	1.370(16)	1.401(3)
C11 - C12	1.385(5)	1.407(16)	1.380(4)
C12 - C13	1.378(5)	1.375(14)	1.379(4)
C13 - N2	1.345(5)	1.346(13)	1.343(3)
Re1 - N3	N/A	N/A	2.209(2)
N2 - Re1 - N3	N/A	N/A	85.23(8)
N3 - Re1 - C1	N/A	N/A	179.0(1)
N3 - Re1 - C2	N/A	N/A	91.9(1)
N3 - Re1 - C3	N/A	N/A	91.2(1)

Table 3-4. Geometry optimized *xyz* coordinates for $[Re(bipy\text{-}t Bu)(CO)_3]^{-1}$ from DFT calculations.

Atom	X	Y	Z
Re1	0.536714	1.381065	-0.833598
C1	1.13192	3.214844	-0.768546
C2	-1.093185	1.912348	-1.64912
C3	1.37484	1.178334	-2.555934
C4	0.401052	-1.676506	-1.46259
H4	0.524419	-1.306904	-2.477681
C5	0.271962	-3.019266	-1.222763
H5	0.303856	-3.694769	-2.074695
C6	0.098872	-3.50264	0.11749
C7	0.077756	-2.539753	1.105094
H7	-0.051004	-2.834852	2.147055
C8	0.22211	-1.156056	0.833505
C9	0.238145	-0.130762	1.798988
C10	0.117953	-0.32202	3.197314
H10	-0.015705	-1.344652	3.551552
C11	0.167304	0.715712	4.104612
C12	0.347367	2.025323	3.541019
H12	0.399406	2.913565	4.167289
C13	0.454233	2.190824	2.186593
H13	0.581222	3.183538	1.762001
C14	-0.044013	-4.995009	0.456281
C15	-0.032561	-5.871241	-0.809085
H15a	-0.85427	-5.606527	-1.488719
H15b	0.912093	-5.767909	-1.36051
H15c	-0.147772	-6.930275	-0.533054
C16	1.127316	-5.443314	1.361034
H16a	1.14728	-4.866999	2.295266
H16b	1.035774	-6.511398	1.618364
H16c	2.090208	-5.288419	0.854475
C17	-1.374341	-5.244274	1.202986
H17a	-1.427189	-4.657602	2.129144
H17b	-2.230273	-4.955092	0.5775
H17c	-1.479156	-6.309208	1.46693
C18	0.04751	0.459715	5.615171
C19	1.228821	-0.415173	6.096603
H19a	1.154162	-0.612541	7.178887
H19b	1.244004	-1.380296	5.573281
H19c	2.187151	0.084946	5.89937
C20	-1.275507	-0.277341	5.925667
H20a	-2.138519	0.325585	5.610274
H20b	-1.330205	-1.237441	5.396129
H20c	-1.365918	-0.478618	7.005784
C21	0.065813	1.770884	6.421235
H21a	-0.035667	1.551812	7.494927
H21b	1.007829	2.317721	6.277283
H21c	-0.76077	2.43383	6.130744
N1	0.387006	-0.706788	-0.492001
N2	0.411623	1.167047	1.266153
O1	1.511642	4.329432	-0.70028
O2	-2.098259	2.253439	-2.164843
O3	1.901737	1.006333	-3.596916

Table 3-5. Geometry optimized *xyz* coordinates for [Re(bipy-*t*Bu)$(CO)_3(CO_2)$(K)] from DFT.

Atom	X	Y	Z
Re1	-0.770017	0.812243	-0.525125
C1	-0.215189	0.393285	1.305915
C2	-0.760067	-1.071318	-0.961721
C3	1.068274	0.93293	-1.096108
C4	-3.750073	-0.027131	0.037431
H4	-3.382341	-0.970276	-0.356338
C5	-5.041344	0.088645	0.525417
H5	-5.675972	-0.794397	0.508073
C6	-5.50508	1.314911	1.035163
C7	-4.605151	2.380633	0.965222
H7	-4.906157	3.364895	1.318921
C8	-3.313391	2.218027	0.454889
C9	-2.340146	3.297151	0.337055
C10	-2.596415	4.622215	0.70273
H10	-3.568995	4.865816	1.125458
C11	-1.637769	5.625482	0.545193
C12	-0.421466	5.220989	-0.037713
H12	0.38055	5.931232	-0.225499
C13	-0.210384	3.896331	-0.381947
H13	0.723443	3.575634	-0.833593
C14	-6.903421	1.504609	1.641305
C15	-7.694845	2.540761	0.811281
H15a	-7.819239	2.203244	-0.227077
H15b	-8.693925	2.687828	1.2477
H15c	-7.189135	3.515676	0.793259
C16	-6.768266	2.02001	3.092941
H16a	-6.210101	1.306492	3.714579
H16b	-6.245488	2.984864	3.13489
H16c	-7.764434	2.159045	3.538304
C17	-7.697362	0.187437	1.665234
H17a	-8.682575	0.358586	2.120625
H17b	-7.86277	-0.207397	0.653392
H17c	-7.184896	-0.583076	2.25736
C18	-1.92514	7.064964	0.994337
C19	-3.136897	7.624505	0.214803
H19a	-2.937677	7.643878	-0.865677
H19b	-4.039743	7.021684	0.382778
H19c	-3.353154	8.651874	0.543379
C20	-2.252162	7.074979	2.505815
H20a	-1.411699	6.681817	3.093974
H20b	-2.456506	8.102751	2.840335
H20c	-3.137453	6.465832	2.733121
C21	-0.720246	7.99031	0.752647
H21a	-0.960317	9.004652	1.099154
H21b	0.168297	7.651582	1.302513
H21c	-0.463563	8.054242	-0.313574
C22	-1.408784	1.129889	-2.690726
N1	-2.866848	0.995755	0.025125
N2	-1.126782	2.920552	-0.180207
O1	0.110322	0.088974	2.385489
O2	-0.782213	-2.213096	-1.204893
O3	2.189237	1.030124	-1.411852
O4	-2.347448	0.430007	-3.189785
O5	-0.785641	2.04654	-3.322452
K1	-2.489982	2.037527	-5.149897

Table 3-6. Crystal data and structure refinement for Re(bipy-*t*Bu)$(CO)_3$-K(18-crown-6).

Identification code	cc	
Empirical formula	C37 H56 K N2 O10 Re	
Formula weight	914.14	
Temperature	100(2) K	
Wavelength	1.54184 Å	
Crystal system	Monoclinic	
Space group	Cc	
Unit cell dimensions	a = 20.856(2) Å	α = 90°.
	b = 10.2525(8) Å	β = 112.170(11)°
	c = 20.295(2) Å	γ = 90°.
Volume	4018.9(6) $Å^3$	
Z	4	
Density (calculated)	1.511 Mg/m^3	
Absorption coefficient	7.300 mm^{-1}	
F(000)	1864	
Crystal size	0.10 x 0.10 x 0.01 mm^3	
Theta range for data collection	4.58 to 68.43°.	
Index ranges	-24<=h<=23, -11<=k<=12, -24<=l<=23	
Reflections collected	15825	
Independent reflections	5770 [R(int) = 0.0501]	
Completeness to theta = 60.00°	99.0 %	
Absorption correction	Semi-empirical from equivalents	
Max. and min. transmission	0.9306 and 0.5289	
Refinement method	Full-matrix least-squares on F^2	
Data / restraints / parameters	5770 / 2 / 454	
Goodness-of-fit on F^2	1.035	
Final R indices [I>2sigma(I)]	R1 = 0.0495, wR2 = 0.1241	
R indices (all data)	R1 = 0.0535, wR2 = 0.1278	
Absolute structure parameter	-0.056(15)	
Largest diff. peak and hole	2.875 and -1.004 $e.Å^{-3}$	

Table 3-7. Bond lengths [Å] and angles [°] for Re(bipy-*t*Bu)$(CO)_3$-K(18-crown-6).

Re(1)-C(1)	1.902(12)	O(8)-C(30)	1.431(12)
Re(1)-C(2)	1.922(9)	O(9)-C(33)	1.412(15)
Re(1)-C(3)	1.927(11)	O(9)-C(32)	1.416(14)
Re(1)-N(1)	2.070(7)	O(10)-C(35)	1.407(18)
Re(1)-N(2)	2.115(7)	O(10)-C(38)	1.422(19)
K(1)-O(5)	2.761(8)	N(1)-C(4)	1.373(14)
K(1)-O(10)	2.773(9)	N(1)-C(8)	1.419(12)
K(1)-O(6)	2.774(8)	N(2)-C(13)	1.348(13)
K(1)-O(8)	2.779(8)	N(2)-C(9)	1.401(12)
K(1)-O(4)	2.806(7)	C(4)-C(5)	1.323(15)
K(1)-O(7)	2.836(9)	C(4)-H(4)	0.9500
K(1)-O(9)	2.868(8)	C(5)-C(6)	1.442(13)
K(1)-O(3)	2.945(7)	C(5)-H(5)	0.9500
K(1)-C(24)	3.513(11)	C(6)-C(7)	1.362(14)
K(1)-C(35)	3.537(14)	C(6)-C(14)	1.517(13)
O(1)-C(1)	1.147(15)	C(7)-C(8)	1.444(14)
O(2)-C(2)	1.146(12)	C(7)-H(7)	0.9500
O(3)-C(3)	1.164(12)	C(8)-C(9)	1.370(15)
O(4)-C(34)	1.373(16)	C(9)-C(10)	1.424(13)
O(4)-C(22)	1.426(14)	C(10)-C(11)	1.368(16)
O(5)-C(23)	1.404(14)	C(10)-H(10)	0.9500
O(5)-C(24)	1.407(15)	C(11)-C(12)	1.408(16)
O(6)-C(25)	1.412(14)	C(11)-C(18)	1.539(15)
O(6)-C(27)	1.425(14)	C(12)-C(13)	1.375(14)
O(7)-C(28)	1.393(17)	C(12)-H(12)	0.9500
O(7)-C(29)	1.411(15)	C(13)-H(13)	0.9500
O(8)-C(31)	1.423(14)	C(14)-C(17)	1.518(14)

Table 3-7 (Cont.)

C(14)-C(15)	1.530(18)	C(23)-H(23B)	0.9900
C(14)-C(16)	1.539(19)	C(24)-C(25)	1.501(16)
C(15)-H(15A)	0.9800	C(24)-H(24A)	0.9900
C(15)-H(15B)	0.9800	C(24)-H(24B)	0.9900
C(15)-H(15C)	0.9800	C(25)-H(25A)	0.9900
C(16)-H(16A)	0.9800	C(25)-H(25B)	0.9900
C(16)-H(16B)	0.9800	C(27)-C(28)	1.51(2)
C(16)-H(16C)	0.9800	C(27)-H(27A)	0.9900
C(17)-H(17A)	0.9800	C(27)-H(27B)	0.9900
C(17)-H(17B)	0.9800	C(28)-H(28A)	0.9900
C(17)-H(17C)	0.9800	C(28)-H(28B)	0.9900
C(18)-C(19)	1.482(17)	C(29)-C(30)	1.477(18)
C(18)-C(20)	1.521(18)	C(29)-H(29A)	0.9900
C(18)-C(21)	1.544(16)	C(29)-H(29B)	0.9900
C(19)-H(19A)	0.9800	C(30)-H(30A)	0.9900
C(19)-H(19B)	0.9800	C(30)-H(30B)	0.9900
C(19)-H(19C)	0.9800	C(31)-C(32)	1.492(16)
C(20)-H(20A)	0.9800	C(31)-H(31A)	0.9900
C(20)-H(20B)	0.9800	C(31)-H(31B)	0.9900
C(20)-H(20C)	0.9800	C(32)-H(32A)	0.9900
C(21)-H(21A)	0.9800	C(32)-H(32B)	0.9900
C(21)-H(21B)	0.9800	C(33)-C(34)	1.541(19)
C(21)-H(21C)	0.9800	C(33)-H(33A)	0.9900
C(22)-C(23)	1.46(2)	C(33)-H(33B)	0.9900
C(22)-H(22A)	0.9900	C(34)-H(34A)	0.9900
C(22)-H(22B)	0.9900	C(34)-H(34B)	0.9900
C(23)-H(23A)	0.9900	C(35)-C(36)	1.55(2)

Table 3-7 (Cont.)

C(35)-H(35A)	0.9900	O(5)-K(1)-O(4)	61.1(2)
C(35)-H(35B)	0.9900	O(10)-K(1)-O(4)	79.0(3)
C(36)-C(37)	1.52(3)	O(6)-K(1)-O(4)	121.9(2)
C(36)-H(36A)	0.9900	O(8)-K(1)-O(4)	119.2(2)
C(36)-H(36B)	0.9900	O(5)-K(1)-O(7)	117.7(3)
C(37)-C(38)	1.47(2)	O(10)-K(1)-O(7)	87.6(3)
C(37)-H(37A)	0.9900	O(6)-K(1)-O(7)	60.0(3)
C(37)-H(37B)	0.9900	O(8)-K(1)-O(7)	60.4(3)
C(38)-H(38A)	0.9900	O(4)-K(1)-O(7)	166.5(2)
C(38)-H(38B)	0.9900	O(5)-K(1)-O(9)	120.2(2)
		O(10)-K(1)-O(9)	79.0(3)
C(1)-Re(1)-C(2)	89.7(5)	O(6)-K(1)-O(9)	172.7(2)
C(1)-Re(1)-C(3)	90.8(5)	O(8)-K(1)-O(9)	59.1(2)
C(2)-Re(1)-C(3)	90.8(4)	O(4)-K(1)-O(9)	60.4(2)
C(1)-Re(1)-N(1)	127.2(5)	O(7)-K(1)-O(9)	116.0(3)
C(2)-Re(1)-N(1)	142.4(4)	O(5)-K(1)-O(3)	74.6(2)
C(3)-Re(1)-N(1)	95.3(4)	O(10)-K(1)-O(3)	152.3(3)
C(1)-Re(1)-N(2)	97.3(4)	O(6)-K(1)-O(3)	79.9(2)
C(2)-Re(1)-N(2)	95.2(4)	O(8)-K(1)-O(3)	111.4(2)
C(3)-Re(1)-N(2)	169.9(4)	O(4)-K(1)-O(3)	81.2(2)
N(1)-Re(1)-N(2)	75.1(3)	O(7)-K(1)-O(3)	111.8(2)
O(5)-K(1)-O(10)	78.9(3)	O(9)-K(1)-O(3)	107.4(2)
O(5)-K(1)-O(6)	61.0(2)	O(5)-K(1)-C(24)	22.0(3)
O(10)-K(1)-O(6)	94.5(3)	O(10)-K(1)-C(24)	93.2(3)
O(5)-K(1)-O(8)	174.0(2)	O(6)-K(1)-C(24)	42.3(3)
O(10)-K(1)-O(8)	95.2(3)	O(8)-K(1)-C(24)	160.1(3)
O(6)-K(1)-O(8)	118.9(2)	O(4)-K(1)-C(24)	80.1(3)

Table 3-7 (Cont.)

O(7)-K(1)-C(24)	102.1(3)	C(30)-O(8)-K(1)	117.2(6)
O(9)-K(1)-C(24)	140.5(3)	C(33)-O(9)-C(32)	114.0(9)
O(3)-K(1)-C(24)	64.4(2)	C(33)-O(9)-K(1)	112.0(7)
O(5)-K(1)-C(35)	100.0(3)	C(32)-O(9)-K(1)	109.4(6)
O(10)-K(1)-C(35)	21.7(3)	C(35)-O(10)-C(38)	108.7(11)
O(6)-K(1)-C(35)	100.1(3)	C(35)-O(10)-K(1)	111.4(7)
O(8)-K(1)-C(35)	74.0(3)	C(38)-O(10)-K(1)	114.3(10)
O(4)-K(1)-C(35)	93.8(3)	C(4)-N(1)-C(8)	115.5(8)
O(7)-K(1)-C(35)	72.9(3)	C(4)-N(1)-Re(1)	126.3(6)
O(9)-K(1)-C(35)	72.7(3)	C(8)-N(1)-Re(1)	118.2(7)
O(3)-K(1)-C(35)	174.0(3)	C(13)-N(2)-C(9)	117.4(7)
C(24)-K(1)-C(35)	111.5(3)	C(13)-N(2)-Re(1)	125.4(5)
C(3)-O(3)-K(1)	155.4(7)	C(9)-N(2)-Re(1)	117.2(6)
C(34)-O(4)-C(22)	111.4(9)	O(1)-C(1)-Re(1)	177.4(11)
C(34)-O(4)-K(1)	113.7(7)	O(2)-C(2)-Re(1)	174.8(9)
C(22)-O(4)-K(1)	111.0(7)	O(3)-C(3)-Re(1)	175.0(9)
C(23)-O(5)-C(24)	114.5(9)	C(5)-C(4)-N(1)	125.0(9)
C(23)-O(5)-K(1)	114.2(7)	C(5)-C(4)-H(4)	117.5
C(24)-O(5)-K(1)	110.6(6)	N(1)-C(4)-H(4)	117.5
C(25)-O(6)-C(27)	112.1(9)	C(4)-C(5)-C(6)	121.6(9)
C(25)-O(6)-K(1)	117.1(7)	C(4)-C(5)-H(5)	119.2
C(27)-O(6)-K(1)	118.5(8)	C(6)-C(5)-H(5)	119.2
C(28)-O(7)-C(29)	112.1(9)	C(7)-C(6)-C(5)	116.2(9)
C(28)-O(7)-K(1)	114.9(7)	C(7)-C(6)-C(14)	122.3(8)
C(29)-O(7)-K(1)	112.0(7)	C(5)-C(6)-C(14)	121.5(9)
C(31)-O(8)-C(30)	113.0(8)	C(6)-C(7)-C(8)	121.3(8)
C(31)-O(8)-K(1)	120.0(6)	C(6)-C(7)-H(7)	119.4

Table 3-7 (Cont.)

C(8)-C(7)-H(7)	119.4	H(15A)-C(15)-H(15B)	109.5
C(9)-C(8)-N(1)	114.6(9)	C(14)-C(15)-H(15C)	109.5
C(9)-C(8)-C(7)	125.1(9)	H(15A)-C(15)-H(15C)	109.5
N(1)-C(8)-C(7)	120.3(9)	H(15B)-C(15)-H(15C)	109.5
C(8)-C(9)-N(2)	114.8(8)	C(14)-C(16)-H(16A)	109.5
C(8)-C(9)-C(10)	126.8(9)	C(14)-C(16)-H(16B)	109.5
N(2)-C(9)-C(10)	118.4(9)	H(16A)-C(16)-H(16B)	109.5
C(11)-C(10)-C(9)	123.5(9)	C(14)-C(16)-H(16C)	109.5
C(11)-C(10)-H(10)	118.3	H(16A)-C(16)-H(16C)	109.5
C(9)-C(10)-H(10)	118.3	H(16B)-C(16)-H(16C)	109.5
C(10)-C(11)-C(12)	116.0(10)	C(14)-C(17)-H(17A)	109.5
C(10)-C(11)-C(18)	123.5(10)	C(14)-C(17)-H(17B)	109.5
C(12)-C(11)-C(18)	120.6(10)	H(17A)-C(17)-H(17B)	109.5
C(13)-C(12)-C(11)	120.2(10)	C(14)-C(17)-H(17C)	109.5
C(13)-C(12)-H(12)	119.9	H(17A)-C(17)-H(17C)	109.5
C(11)-C(12)-H(12)	119.9	H(17B)-C(17)-H(17C)	109.5
N(2)-C(13)-C(12)	124.4(8)	C(19)-C(18)-C(20)	109.7(11)
N(2)-C(13)-H(13)	117.8	C(19)-C(18)-C(11)	112.2(9)
C(12)-C(13)-H(13)	117.8	C(20)-C(18)-C(11)	109.8(9)
C(6)-C(14)-C(17)	113.1(9)	C(19)-C(18)-C(21)	108.8(10)
C(6)-C(14)-C(15)	109.6(9)	C(20)-C(18)-C(21)	109.3(9)
C(17)-C(14)-C(15)	107.2(10)	C(11)-C(18)-C(21)	107.0(9)
C(6)-C(14)-C(16)	108.6(9)	C(18)-C(19)-H(19A)	109.5
C(17)-C(14)-C(16)	108.3(11)	C(18)-C(19)-H(19B)	109.5
C(15)-C(14)-C(16)	110.1(12)	H(19A)-C(19)-H(19B)	109.5
C(14)-C(15)-H(15A)	109.5	C(18)-C(19)-H(19C)	109.5
C(14)-C(15)-H(15B)	109.5	H(19A)-C(19)-H(19C)	109.5

Table 3-7 (Cont.)

H(19B)-C(19)-H(19C)	109.5	C(25)-C(24)-K(1)	82.7(7)
C(18)-C(20)-H(20A)	109.5	O(5)-C(24)-H(24A)	109.7
C(18)-C(20)-H(20B)	109.5	C(25)-C(24)-H(24A)	109.7
H(20A)-C(20)-H(20B)	109.5	K(1)-C(24)-H(24A)	157.0
C(18)-C(20)-H(20C)	109.5	O(5)-C(24)-H(24B)	109.7
H(20A)-C(20)-H(20C)	109.5	C(25)-C(24)-H(24B)	109.7
H(20B)-C(20)-H(20C)	109.5	K(1)-C(24)-H(24B)	84.3
C(18)-C(21)-H(21A)	109.5	H(24A)-C(24)-H(24B)	108.2
C(18)-C(21)-H(21B)	109.5	O(6)-C(25)-C(24)	108.9(9)
H(21A)-C(21)-H(21B)	109.5	O(6)-C(25)-H(25A)	109.9
C(18)-C(21)-H(21C)	109.5	C(24)-C(25)-H(25A)	109.9
H(21A)-C(21)-H(21C)	109.5	O(6)-C(25)-H(25B)	109.9
H(21B)-C(21)-H(21C)	109.5	C(24)-C(25)-H(25B)	109.9
O(4)-C(22)-C(23)	109.5(10)	H(25A)-C(25)-H(25B)	108.3
O(4)-C(22)-H(22A)	109.8	O(6)-C(27)-C(28)	108.7(10)
C(23)-C(22)-H(22A)	109.8	O(6)-C(27)-H(27A)	109.9
O(4)-C(22)-H(22B)	109.8	C(28)-C(27)-H(27A)	109.9
C(23)-C(22)-H(22B)	109.8	O(6)-C(27)-H(27B)	109.9
H(22A)-C(22)-H(22B)	108.2	C(28)-C(27)-H(27B)	109.9
O(5)-C(23)-C(22)	109.1(11)	H(27A)-C(27)-H(27B)	108.3
O(5)-C(23)-H(23A)	109.9	O(7)-C(28)-C(27)	112.1(11)
C(22)-C(23)-H(23A)	109.9	O(7)-C(28)-H(28A)	109.2
O(5)-C(23)-H(23B)	109.9	C(27)-C(28)-H(28A)	109.2
C(22)-C(23)-H(23B)	109.9	O(7)-C(28)-H(28B)	109.2
H(23A)-C(23)-H(23B)	108.3	C(27)-C(28)-H(28B)	109.2
O(5)-C(24)-C(25)	109.9(9)	H(28A)-C(28)-H(28B)	107.9
O(5)-C(24)-K(1)	47.4(5)	O(7)-C(29)-C(30)	111.5(10)

Table 3-7 (Cont.)

O(7)-C(29)-H(29A)	109.3	C(34)-C(33)-H(33B)	110.0
C(30)-C(29)-H(29A)	109.3	H(33A)-C(33)-H(33B)	108.4
O(7)-C(29)-H(29B)	109.3	O(4)-C(34)-C(33)	107.9(9)
C(30)-C(29)-H(29B)	109.3	O(4)-C(34)-H(34A)	110.1
H(29A)-C(29)-H(29B)	108.0	C(33)-C(34)-H(34A)	110.1
O(8)-C(30)-C(29)	108.6(9)	O(4)-C(34)-H(34B)	110.1
O(8)-C(30)-H(30A)	110.0	C(33)-C(34)-H(34B)	110.1
C(29)-C(30)-H(30A)	110.0	H(34A)-C(34)-H(34B)	108.4
O(8)-C(30)-H(30B)	110.0	O(10)-C(35)-C(36)	105.8(12)
C(29)-C(30)-H(30B)	110.0	O(10)-C(35)-K(1)	46.9(6)
H(30A)-C(30)-H(30B)	108.4	C(36)-C(35)-K(1)	110.4(10)
O(8)-C(31)-C(32)	108.9(9)	O(10)-C(35)-H(35A)	110.6
O(8)-C(31)-H(31A)	109.9	C(36)-C(35)-H(35A)	110.6
C(32)-C(31)-H(31A)	109.9	K(1)-C(35)-H(35A)	65.4
O(8)-C(31)-H(31B)	109.9	O(10)-C(35)-H(35B)	110.6
C(32)-C(31)-H(31B)	109.9	C(36)-C(35)-H(35B)	110.6
H(31A)-C(31)-H(31B)	108.3	K(1)-C(35)-H(35B)	137.7
O(9)-C(32)-C(31)	108.7(9)	H(35A)-C(35)-H(35B)	108.7
O(9)-C(32)-H(32A)	109.9	C(37)-C(36)-C(35)	101.8(15)
C(31)-C(32)-H(32A)	109.9	C(37)-C(36)-H(36A)	111.4
O(9)-C(32)-H(32B)	109.9	C(35)-C(36)-H(36A)	111.4
C(31)-C(32)-H(32B)	109.9	C(37)-C(36)-H(36B)	111.4
H(32A)-C(32)-H(32B)	108.3	C(35)-C(36)-H(36B)	111.4
O(9)-C(33)-C(34)	108.4(10)	H(36A)-C(36)-H(36B)	109.3
O(9)-C(33)-H(33A)	110.0	C(38)-C(37)-C(36)	104.2(14)
C(34)-C(33)-H(33A)	110.0	C(38)-C(37)-H(37A)	110.9
O(9)-C(33)-H(33B)	110.0	C(36)-C(37)-H(37A)	110.9

Table 3-7 (Cont.)

C(38)-C(37)-H(37B)	110.9	C(37)-C(38)-H(38A)	109.7
C(36)-C(37)-H(37B)	110.9	O(10)-C(38)-H(38B)	109.7
H(37A)-C(37)-H(37B)	108.9	C(37)-C(38)-H(38B)	109.7
O(10)-C(38)-C(37)	109.9(14)	H(38A)-C(38)-H(38B)	108
O(10)-C(38)-H(38A)	109.7		

Table 3-8. Crystal data and structure refinement for Re(bipy-*t*Bu)$(CO)_3$Cl.

Identification code	eb_111110mo_0m	
Empirical formula	C21 H24 Cl N2 O3 Re	
Formula weight	574.07	
Temperature	100(2) K	
Wavelength	0.71073 Å	
Crystal system	Monoclinic	
Space group	P2(1)/n	
Unit cell dimensions	a = 15.9538(6) Å	α= 90°.
	b = 12.8056(5) Å	β= 104.2910(10)°
	c = 22.6304(10) Å	γ = 90°.
Volume	4480.3(3) $Å^3$	
Z	8	
Density (calculated)	1.702 Mg/m^3	
Absorption coefficient	5.566 mm^{-1}	
F(000)	2240	
Crystal size	0.10 x 0.07 x 0.04 mm^3	
Theta range for data collection	1.79 to 25.44°.	
Index ranges	-19<=h<=17, -13<=k<=15, -27<=l<=27	
Reflections collected	28704	
Independent reflections	8253 [R(int) = 0.0415]	
Completeness to theta = 25.00°	100.0 %	
Absorption correction	Semi-empirical from equivalents	
Max. and min. transmission	0.8080 and 0.6060	
Refinement method	Full-matrix least-squares on F^2	
Data / restraints / parameters	8253 / 0 / 527	
Goodness-of-fit on F^2	1.144	
Final R indices [I>2sigma(I)]	R1 = 0.0239, wR2 = 0.0551	
R indices (all data)	R1 = 0.0283, wR2 = 0.0564	
Largest diff. peak and hole	0.957 and -1.105 $e.Å^{-3}$	

Table 3-9. Bond lengths [Å] and angles [°] for Re(bipy-*t*Bu)$(CO)_3$Cl.

Re(1)-C(1)	1.909(4)	N(4)-C(34)	1.340(5)
Re(1)-C(2)	1.909(4)	N(4)-C(30)	1.361(5)
Re(1)-C(3)	1.914(4)	C(4)-C(5)	1.379(5)
Re(1)-N(1)	2.174(3)	C(4)-H(4)	0.9500
Re(1)-N(2)	2.178(3)	C(5)-C(6)	1.396(5)
Re(1)-Cl(1)	2.4626(10)	C(5)-H(5)	0.9500
Re(2)-C(22B)	1.82(4)	C(6)-C(7)	1.393(5)
Re(2)-C(22A)	1.892(6)	C(6)-C(14)	1.521(5)
Re(2)-C(24)	1.925(4)	C(7)-C(8)	1.385(5)
Re(2)-C(23)	1.938(4)	C(7)-H(7)	0.9500
Re(2)-N(4)	2.164(3)	C(8)-C(9)	1.487(5)
Re(2)-N(3)	2.175(3)	C(9)-C(10)	1.386(5)
Re(2)-Cl(2B)	2.453(11)	C(10)-C(11)	1.404(5)
Re(2)-Cl(2A)	2.4749(14)	C(10)-H(10)	0.9500
O(1)-C(1)	1.148(5)	C(11)-C(12)	1.385(5)
O(2)-C(2)	1.172(5)	C(11)-C(18)	1.535(5)
O(3)-C(3)	1.161(5)	C(12)-C(13)	1.378(5)
O(4A)-C(22A)	1.174(8)	C(12)-H(12)	0.9500
O(4B)-C(22B)	1.14(5)	C(13)-H(13)	0.9500
O(5)-C(23)	1.145(4)	C(14)-C(17)	1.532(6)
O(6)-C(24)	1.157(4)	C(14)-C(16)	1.533(6)
N(1)-C(4)	1.337(5)	C(14)-C(15)	1.536(6)
N(1)-C(8)	1.360(5)	C(15)-H(15A)	0.9800
N(2)-C(13)	1.345(5)	C(15)-H(15B)	0.9800
N(2)-C(9)	1.361(5)	C(15)-H(15C)	0.9800
N(3)-C(25)	1.343(5)	C(16)-H(16A)	0.9800
N(3)-C(29)	1.360(5)	C(16)-H(16B)	0.9800

Table 3-9 (Cont.)

C(16)-H(16C)	0.9800	C(31)-H(31)	0.9500
C(17)-H(17A)	0.9800	C(32)-C(33)	1.388(5)
C(17)-H(17B)	0.9800	C(32)-C(39)	1.528(5)
C(17)-H(17C)	0.9800	C(33)-C(34)	1.377(5)
C(18)-C(21)	1.531(6)	C(33)-H(33)	0.9500
C(18)-C(19)	1.531(6)	C(34)-H(34)	0.9500
C(18)-C(20)	1.539(6)	C(35)-C(36)	1.532(5)
C(19)-H(19A)	0.9800	C(35)-C(37)	1.536(6)
C(19)-H(19B)	0.9800	C(35)-C(38)	1.547(6)
C(19)-H(19C)	0.9800	C(36)-H(36A)	0.9800
C(20)-H(20A)	0.9800	C(36)-H(36B)	0.9800
C(20)-H(20B)	0.9800	C(36)-H(36C)	0.9800
C(20)-H(20C)	0.9800	C(37)-H(37A)	0.9800
C(21)-H(21A)	0.9800	C(37)-H(37B)	0.9800
C(21)-H(21B)	0.9800	C(37)-H(37C)	0.9800
C(21)-H(21C)	0.9800	C(38)-H(38A)	0.9800
C(25)-C(26)	1.381(5)	C(38)-H(38B)	0.9800
C(25)-H(25)	0.9500	C(38)-H(38C)	0.9800
C(26)-C(27)	1.388(5)	C(39)-C(41)	1.529(5)
C(26)-H(26)	0.9500	C(39)-C(40)	1.532(6)
C(27)-C(28)	1.404(5)	C(39)-C(42)	1.535(5)
C(27)-C(35)	1.515(5)	C(40)-H(40A)	0.9800
C(28)-C(29)	1.396(5)	C(40)-H(40B)	0.9800
C(28)-H(28)	0.9500	C(40)-H(40C)	0.9800
C(29)-C(30)	1.475(5)	C(41)-H(41A)	0.9800
C(30)-C(31)	1.388(5)	C(41)-H(41B)	0.9800
C(31)-C(32)	1.404(5)	C(41)-H(41C)	0.9800

Table 3-9 (Cont.)

C(42)-H(42A)	0.9800	C(24)-Re(2)-N(4)	96.52(14)
C(42)-H(42B)	0.9800	C(23)-Re(2)-N(4)	171.62(14)
C(42)-H(42C)	0.9800	C(22B)-Re(2)-N(3)	87.5(11)
		C(22A)-Re(2)-N(3)	98.1(2)
C(1)-Re(1)-C(2)	87.74(17)	C(24)-Re(2)-N(3)	169.30(14)
C(1)-Re(1)-C(3)	89.37(17)	C(23)-Re(2)-N(3)	97.52(14)
C(2)-Re(1)-C(3)	87.37(17)	N(4)-Re(2)-N(3)	74.37(12)
C(1)-Re(1)-N(1)	92.73(14)	C(22B)-Re(2)-Cl(2B)	171.5(11)
C(2)-Re(1)-N(1)	100.45(14)	C(22A)-Re(2)-Cl(2B)	13.0(3)
C(3)-Re(1)-N(1)	171.97(14)	C(24)-Re(2)-Cl(2B)	100.9(3)
C(1)-Re(1)-N(2)	96.05(15)	C(23)-Re(2)-Cl(2B)	90.2(2)
C(2)-Re(1)-N(2)	173.67(14)	N(4)-Re(2)-Cl(2B)	91.2(2)
C(3)-Re(1)-N(2)	97.72(14)	N(3)-Re(2)-Cl(2B)	85.1(3)
N(1)-Re(1)-N(2)	74.36(11)	C(22B)-Re(2)-Cl(2A)	9.2(11)
C(1)-Re(1)-Cl(1)	174.82(12)	C(22A)-Re(2)-Cl(2A)	176.42(18)
C(2)-Re(1)-Cl(1)	92.40(12)	C(24)-Re(2)-Cl(2A)	91.43(12)
C(3)-Re(1)-Cl(1)	95.80(13)	C(23)-Re(2)-Cl(2A)	94.62(12)
N(1)-Re(1)-Cl(1)	82.15(9)	N(4)-Re(2)-Cl(2A)	82.29(9)
N(2)-Re(1)-Cl(1)	83.36(9)	N(3)-Re(2)-Cl(2A)	81.91(9)
C(22B)-Re(2)-C(22A)	173.3(11)	Cl(2B)-Re(2)-Cl(2A)	166.7(3)
C(22B)-Re(2)-C(24)	87.0(11)	C(4)-N(1)-C(8)	117.4(3)
C(22A)-Re(2)-C(24)	88.0(2)	C(4)-N(1)-Re(1)	124.3(3)
C(22B)-Re(2)-C(23)	86.6(11)	C(8)-N(1)-Re(1)	118.2(2)
C(22A)-Re(2)-C(23)	88.9(2)	C(13)-N(2)-C(9)	117.8(3)
C(24)-Re(2)-C(23)	91.33(16)	C(13)-N(2)-Re(1)	124.4(3)
C(22B)-Re(2)-N(4)	90.8(11)	C(9)-N(2)-Re(1)	117.7(2)
C(22A)-Re(2)-N(4)	94.3(2)	C(25)-N(3)-C(29)	117.7(3)

Table 3-9 (Cont.)

C(25)-N(3)-Re(2)	125.1(3)	C(9)-C(10)-H(10)	119.4
C(29)-N(3)-Re(2)	116.5(3)	C(11)-C(10)-H(10)	119.4
C(34)-N(4)-C(30)	117.6(3)	C(12)-C(11)-C(10)	116.4(3)
C(34)-N(4)-Re(2)	124.7(3)	C(12)-C(11)-C(18)	123.1(4)
C(30)-N(4)-Re(2)	117.6(2)	C(10)-C(11)-C(18)	120.5(3)
O(1)-C(1)-Re(1)	177.0(4)	C(13)-C(12)-C(11)	120.2(4)
O(2)-C(2)-Re(1)	179.2(4)	C(13)-C(12)-H(12)	119.9
O(3)-C(3)-Re(1)	179.3(4)	C(11)-C(12)-H(12)	119.9
N(1)-C(4)-C(5)	123.2(4)	N(2)-C(13)-C(12)	123.3(4)
N(1)-C(4)-H(4)	118.4	N(2)-C(13)-H(13)	118.3
C(5)-C(4)-H(4)	118.4	C(12)-C(13)-H(13)	118.3
C(4)-C(5)-C(6)	120.5(4)	C(6)-C(14)-C(17)	111.1(3)
C(4)-C(5)-H(5)	119.7	C(6)-C(14)-C(16)	108.9(3)
C(6)-C(5)-H(5)	119.7	C(17)-C(14)-C(16)	109.4(4)
C(7)-C(6)-C(5)	116.0(4)	C(6)-C(14)-C(15)	109.2(3)
C(7)-C(6)-C(14)	124.2(3)	C(17)-C(14)-C(15)	108.6(4)
C(5)-C(6)-C(14)	119.8(3)	C(16)-C(14)-C(15)	109.6(4)
C(8)-C(7)-C(6)	121.0(3)	C(14)-C(15)-H(15A)	109.5
C(8)-C(7)-H(7)	119.5	C(14)-C(15)-H(15B)	109.5
C(6)-C(7)-H(7)	119.5	H(15A)-C(15)-H(15B)	109.5
N(1)-C(8)-C(7)	121.8(3)	C(14)-C(15)-H(15C)	109.5
N(1)-C(8)-C(9)	114.5(3)	H(15A)-C(15)-H(15C)	109.5
C(7)-C(8)-C(9)	123.6(3)	H(15B)-C(15)-H(15C)	109.5
N(2)-C(9)-C(10)	121.1(3)	C(14)-C(16)-H(16A)	109.5
N(2)-C(9)-C(8)	115.1(3)	C(14)-C(16)-H(16B)	109.5
C(10)-C(9)-C(8)	123.8(4)	H(16A)-C(16)-H(16B)	109.5
C(9)-C(10)-C(11)	121.2(4)	C(14)-C(16)-H(16C)	109.5

Table 3-9 (Cont.)

H(16A)-C(16)-H(16C)	109.5	C(18)-C(21)-H(21B)	109.5
H(16B)-C(16)-H(16C)	109.5	H(21A)-C(21)-H(21B)	109.5
C(14)-C(17)-H(17A)	109.5	C(18)-C(21)-H(21C)	109.5
C(14)-C(17)-H(17B)	109.5	H(21A)-C(21)-H(21C)	109.5
H(17A)-C(17)-H(17B)	109.5	H(21B)-C(21)-H(21C)	109.5
C(14)-C(17)-H(17C)	109.5	O(4A)-C(22A)-Re(2)	177.9(6)
H(17A)-C(17)-H(17C)	109.5	O(4B)-C(22B)-Re(2)	174(3)
H(17B)-C(17)-H(17C)	109.5	O(5)-C(23)-Re(2)	178.2(3)
C(21)-C(18)-C(19)	109.6(4)	O(6)-C(24)-Re(2)	175.7(3)
C(21)-C(18)-C(11)	111.4(4)	N(3)-C(25)-C(26)	123.9(4)
C(19)-C(18)-C(11)	108.9(3)	N(3)-C(25)-H(25)	118.1
C(21)-C(18)-C(20)	107.9(4)	C(26)-C(25)-H(25)	118.1
C(19)-C(18)-C(20)	109.4(3)	C(25)-C(26)-C(27)	120.1(4)
C(11)-C(18)-C(20)	109.6(3)	C(25)-C(26)-H(26)	119.9
C(18)-C(19)-H(19A)	109.5	C(27)-C(26)-H(26)	119.9
C(18)-C(19)-H(19B)	109.5	C(26)-C(27)-C(28)	115.9(4)
H(19A)-C(19)-H(19B)	109.5	C(26)-C(27)-C(35)	123.3(4)
C(18)-C(19)-H(19C)	109.5	C(28)-C(27)-C(35)	120.8(4)
H(19A)-C(19)-H(19C)	109.5	C(29)-C(28)-C(27)	121.7(4)
H(19B)-C(19)-H(19C)	109.5	C(29)-C(28)-H(28)	119.1
C(18)-C(20)-H(20A)	109.5	C(27)-C(28)-H(28)	119.1
C(18)-C(20)-H(20B)	109.5	N(3)-C(29)-C(28)	120.7(4)
H(20A)-C(20)-H(20B)	109.5	N(3)-C(29)-C(30)	115.3(3)
C(18)-C(20)-H(20C)	109.5	C(28)-C(29)-C(30)	124.0(3)
H(20A)-C(20)-H(20C)	109.5	N(4)-C(30)-C(31)	121.5(3)
H(20B)-C(20)-H(20C)	109.5	N(4)-C(30)-C(29)	114.5(3)
C(18)-C(21)-H(21A)	109.5	C(31)-C(30)-C(29)	124.0(3)

Table 3-9 (Cont.)

C(30)-C(31)-C(32)	121.0(4)	C(35)-C(37)-H(37C)	109.5
C(30)-C(31)-H(31)	119.5	H(37A)-C(37)-H(37C)	109.5
C(32)-C(31)-H(31)	119.5	H(37B)-C(37)-H(37C)	109.5
C(33)-C(32)-C(31)	115.9(4)	C(35)-C(38)-H(38A)	109.5
C(33)-C(32)-C(39)	123.1(3)	C(35)-C(38)-H(38B)	109.5
C(31)-C(32)-C(39)	121.0(3)	H(38A)-C(38)-H(38B)	109.5
C(34)-C(33)-C(32)	120.8(4)	C(35)-C(38)-H(38C)	109.5
C(34)-C(33)-H(33)	119.6	H(38A)-C(38)-H(38C)	109.5
C(32)-C(33)-H(33)	119.6	H(38B)-C(38)-H(38C)	109.5
N(4)-C(34)-C(33)	123.2(4)	C(32)-C(39)-C(41)	108.4(3)
N(4)-C(34)-H(34)	118.4	C(32)-C(39)-C(40)	109.4(3)
C(33)-C(34)-H(34)	118.4	C(41)-C(39)-C(40)	109.9(3)
C(27)-C(35)-C(36)	111.8(3)	C(32)-C(39)-C(42)	111.3(3)
C(27)-C(35)-C(37)	108.9(3)	C(41)-C(39)-C(42)	109.5(3)
C(36)-C(35)-C(37)	108.9(4)	C(40)-C(39)-C(42)	108.3(3)
C(27)-C(35)-C(38)	110.0(3)	C(39)-C(40)-H(40A)	109.5
C(36)-C(35)-C(38)	107.4(3)	C(39)-C(40)-H(40B)	109.5
C(37)-C(35)-C(38)	109.8(4)	H(40A)-C(40)-H(40B)	109.5
C(35)-C(36)-H(36A)	109.5	C(39)-C(40)-H(40C)	109.5
C(35)-C(36)-H(36B)	109.5	H(40A)-C(40)-H(40C)	109.5
H(36A)-C(36)-H(36B)	109.5	H(40B)-C(40)-H(40C)	109.5
C(35)-C(36)-H(36C)	109.5	C(39)-C(41)-H(41A)	109.5
H(36A)-C(36)-H(36C)	109.5	C(39)-C(41)-H(41B)	109.5
H(36B)-C(36)-H(36C)	109.5	H(41A)-C(41)-H(41B)	109.5
C(35)-C(37)-H(37A)	109.5	C(39)-C(41)-H(41C)	109.5
C(35)-C(37)-H(37B)	109.5	H(41A)-C(41)-H(41C)	109.5
H(37A)-C(37)-H(37B)	109.5	H(41B)-C(41)-H(41C)	109.5

Table 3-9 (Cont.)

C(39)-C(42)-H(42A)	109.5	C(39)-C(42)-H(42C)	109.5
C(39)-C(42)-H(42B)	109.5	H(42A)-C(42)-H(42C)	109.5
H(42A)-C(42)-H(42B)	109.5	H(42B)-C(42)-H(42C)	109.5

Table 3-10. Crystal data and structure refinement for Re(bipy-*t*Bu)$(CO)_3$(py)(CF_3SO_3).

Identification code	eb_110615b_0m	
Empirical formula	C27 H29 F3 N3 O6 Re S	
Formula weight	766.79	
Temperature	100(2) K	
Wavelength	0.71073 Å	
Crystal system	Monoclinic	
Space group	P2(1)/n	
Unit cell dimensions	a = 12.1032(4) Å	α= 90°.
	b = 10.2197(4) Å	β= 96.5900(10)°.
	c = 25.5513(9) Å	γ = 90°.
Volume	3139.6(2) $Å^3$	
Z	4	
Density (calculated)	1.622 Mg/m^3	
Absorption coefficient	3.997 mm^{-1}	
F(000)	1512	
Crystal size	0.20 x 0.10 x 0.05 mm^3	
Theta range for data collection	1.60 to 25.35°.	
Index ranges	-14<=h<=14, -12<=k<=12, -30<=l<=30	
Reflections collected	50114	
Independent reflections	5757 [R(int) = 0.0316]	
Completeness to theta = 25.00°	100.0 %	
Absorption correction	Semi-empirical from equivalents	
Max. and min. transmission	0.8252 and 0.5020	
Refinement method	Full-matrix least-squares on F^2	
Data / restraints / parameters	5757 / 0 / 304	
Goodness-of-fit on F^2	1.069	
Final R indices [I>2sigma(I)]	R1 = 0.0191, wR2 = 0.0453	
R indices (all data)	R1 = 0.0202, wR2 = 0.0459	
Largest diff. peak and hole	0.777 and -0.424 $e.Å^{-3}$	

Table 3-11. Bond lengths [Å] and angles [°] for Re(bipy-*t*Bu)$(CO)_3$(py)(CF_3SO_3).

Re(1)-C(1)	1.922(3)	C(11)-C(12)	1.380(4)
Re(1)-C(2)	1.923(3)	C(11)-C(18)	1.537(4)
Re(1)-C(3)	1.927(3)	C(12)-C(13)	1.379(4)
Re(1)-N(1)	2.164(2)	C(12)-H(12)	0.9500
Re(1)-N(2)	2.167(2)	C(13)-H(13)	0.9500
Re(1)-N(3)	2.209(2)	C(14)-C(16)	1.508(5)
O(1)-C(1)	1.153(3)	C(14)-C(15)	1.532(4)
O(2)-C(2)	1.150(3)	C(14)-C(17)	1.549(5)
O(3)-C(3)	1.151(3)	C(15)-H(15A)	0.9800
N(1)-C(4)	1.349(3)	C(15)-H(15B)	0.9800
N(1)-C(8)	1.355(3)	C(15)-H(15C)	0.9800
N(2)-C(13)	1.343(3)	C(16)-H(16A)	0.9800
N(2)-C(9)	1.360(3)	C(16)-H(16B)	0.9800
N(3)-C(22)	1.340(4)	C(16)-H(16C)	0.9800
N(3)-C(26)	1.348(3)	C(17)-H(17A)	0.9800
C(4)-C(5)	1.374(4)	C(17)-H(17B)	0.9800
C(4)-H(4)	0.9500	C(17)-H(17C)	0.9800
C(5)-C(6)	1.397(4)	C(18)-C(19)	1.524(5)
C(5)-H(5)	0.9500	C(18)-C(20)	1.528(5)
C(6)-C(7)	1.389(4)	C(18)-C(21)	1.548(6)
C(6)-C(14)	1.527(4)	C(19)-H(19A)	0.9800
C(7)-C(8)	1.389(4)	C(19)-H(19B)	0.9800
C(7)-H(7)	0.9500	C(19)-H(19C)	0.9800
C(8)-C(9)	1.477(4)	C(20)-H(20A)	0.9800
C(9)-C(10)	1.387(4)	C(20)-H(20B)	0.9800
C(10)-C(11)	1.401(4)	C(20)-H(20C)	0.9800
C(10)-H(10)	0.9500	C(21)-H(21A)	0.9800

Table 3-11 (Cont.)

C(21)-H(21B)	0.9800	C(4)-N(1)-C(8)	118.0(2)
C(21)-H(21C)	0.9800	C(4)-N(1)-Re(1)	124.59(18)
C(22)-C(23)	1.376(4)	C(8)-N(1)-Re(1)	117.35(17)
C(22)-H(22)	0.9500	C(13)-N(2)-C(9)	117.4(2)
C(23)-C(24)	1.377(4)	C(13)-N(2)-Re(1)	125.42(19)
C(23)-H(23)	0.9500	C(9)-N(2)-Re(1)	117.15(17)
C(24)-C(25)	1.368(5)	C(22)-N(3)-C(26)	116.8(2)
C(24)-H(24)	0.9500	C(22)-N(3)-Re(1)	121.52(18)
C(25)-C(26)	1.371(4)	C(26)-N(3)-Re(1)	121.65(18)
C(25)-H(25)	0.9500	O(1)-C(1)-Re(1)	177.6(2)
C(26)-H(26)	0.9500	O(2)-C(2)-Re(1)	177.0(2)
		O(3)-C(3)-Re(1)	178.5(2)
C(1)-Re(1)-C(2)	89.04(11)	N(1)-C(4)-C(5)	122.7(3)
C(1)-Re(1)-C(3)	88.34(11)	N(1)-C(4)-H(4)	118.7
C(2)-Re(1)-C(3)	90.42(11)	C(5)-C(4)-H(4)	118.7
C(1)-Re(1)-N(1)	94.25(9)	C(4)-C(5)-C(6)	120.2(3)
C(2)-Re(1)-N(1)	171.16(9)	C(4)-C(5)-H(5)	119.9
C(3)-Re(1)-N(1)	97.87(10)	C(6)-C(5)-H(5)	119.9
C(1)-Re(1)-N(2)	95.10(9)	C(7)-C(6)-C(5)	116.9(2)
C(2)-Re(1)-N(2)	96.61(10)	C(7)-C(6)-C(14)	122.7(3)
C(3)-Re(1)-N(2)	172.21(10)	C(5)-C(6)-C(14)	120.3(3)
N(1)-Re(1)-N(2)	74.94(8)	C(8)-C(7)-C(6)	120.5(3)
C(1)-Re(1)-N(3)	179.00(9)	C(8)-C(7)-H(7)	119.7
C(2)-Re(1)-N(3)	91.85(10)	C(6)-C(7)-H(7)	119.7
C(3)-Re(1)-N(3)	91.21(10)	N(1)-C(8)-C(7)	121.6(2)
N(1)-Re(1)-N(3)	84.93(8)	N(1)-C(8)-C(9)	115.3(2)
N(2)-Re(1)-N(3)	85.24(8)	C(7)-C(8)-C(9)	123.0(2)

Table 3-11 (Cont.)

N(2)-C(9)-C(10)	121.3(2)	C(14)-C(16)-H(16A)	109.5
N(2)-C(9)-C(8)	115.2(2)	C(14)-C(16)-H(16B)	109.5
C(10)-C(9)-C(8)	123.5(2)	H(16A)-C(16)-H(16B)	109.5
C(9)-C(10)-C(11)	121.2(3)	C(14)-C(16)-H(16C)	109.5
C(9)-C(10)-H(10)	119.4	H(16A)-C(16)-H(16C)	109.5
C(11)-C(10)-H(10)	119.4	H(16B)-C(16)-H(16C)	109.5
C(12)-C(11)-C(10)	116.3(3)	C(14)-C(17)-H(17A)	109.5
C(12)-C(11)-C(18)	124.1(3)	C(14)-C(17)-H(17B)	109.5
C(10)-C(11)-C(18)	119.7(3)	H(17A)-C(17)-H(17B)	109.5
C(13)-C(12)-C(11)	120.3(3)	C(14)-C(17)-H(17C)	109.5
C(13)-C(12)-H(12)	119.8	H(17A)-C(17)-H(17C)	109.5
C(11)-C(12)-H(12)	119.8	H(17B)-C(17)-H(17C)	109.5
N(2)-C(13)-C(12)	123.5(3)	C(19)-C(18)-C(20)	110.1(3)
N(2)-C(13)-H(13)	118.2	C(19)-C(18)-C(11)	108.3(3)
C(12)-C(13)-H(13)	118.2	C(20)-C(18)-C(11)	111.4(3)
C(16)-C(14)-C(6)	108.5(3)	C(19)-C(18)-C(21)	109.5(4)
C(16)-C(14)-C(15)	111.2(3)	C(20)-C(18)-C(21)	109.0(3)
C(6)-C(14)-C(15)	109.3(3)	C(11)-C(18)-C(21)	108.5(3)
C(16)-C(14)-C(17)	107.9(3)	C(18)-C(19)-H(19A)	109.5
C(6)-C(14)-C(17)	112.2(3)	C(18)-C(19)-H(19B)	109.5
C(15)-C(14)-C(17)	107.7(3)	H(19A)-C(19)-H(19B)	109.5
C(14)-C(15)-H(15A)	109.5	C(18)-C(19)-H(19C)	109.5
C(14)-C(15)-H(15B)	109.5	H(19A)-C(19)-H(19C)	109.5
H(15A)-C(15)-H(15B)	109.5	H(19B)-C(19)-H(19C)	109.5
C(14)-C(15)-H(15C)	109.5	C(18)-C(20)-H(20A)	109.5
H(15A)-C(15)-H(15C)	109.5	C(18)-C(20)-H(20B)	109.5
H(15B)-C(15)-H(15C)	109.5	H(20A)-C(20)-H(20B)	109.5

Table 3-11 (Cont.)

C(18)-C(20)-H(20C)	109.5	C(22)-C(23)-C(24)	118.9(3)
H(20A)-C(20)-H(20C)	109.5	C(22)-C(23)-H(23)	120.6
H(20B)-C(20)-H(20C)	109.5	C(24)-C(23)-H(23)	120.6
C(18)-C(21)-H(21A)	109.5	C(25)-C(24)-C(23)	118.6(3)
C(18)-C(21)-H(21B)	109.5	C(25)-C(24)-H(24)	120.7
H(21A)-C(21)-H(21B)	109.5	C(23)-C(24)-H(24)	120.7
C(18)-C(21)-H(21C)	109.5	C(24)-C(25)-C(26)	119.6(3)
H(21A)-C(21)-H(21C)	109.5	C(24)-C(25)-H(25)	120.2
H(21B)-C(21)-H(21C)	109.5	C(26)-C(25)-H(25)	120.2
N(3)-C(22)-C(23)	123.3(3)	N(3)-C(26)-C(25)	122.9(3)
N(3)-C(22)-H(22)	118.3	N(3)-C(26)-H(26)	118.6
C(23)-C(22)-H(22)	118.3	C(25)-C(26)-H(26)	118.6

Chapter 4

Probing the kinetics of the reaction of CO_2 with $[Re(bipy\text{-}tBu)(CO)_3]^{-1}$ and $[Re(bipy)(CO)_3]^{-1}$ by stopped-flow infrared spectroscopy.

4.1 Introduction

Electrocatalysts for the reduction of carbon dioxide (CO_2) are of interest due to the impending peak in oil production and the threat of climate change associated with greenhouse gas accumulation in the Earth's atmosphere. Many important contributions to this field have been published in the last 30 years, but gaps in understanding still exist. In order to optimize catalysts for scale up and use in industrial processes, efforts must be made to understand the mechanism of CO_2 reduction.

Stopped-flow is a spectroscopic technique used for studying fast reaction mechanisms in solution over timescales from 1 ms up to 100's of seconds. In general, two reagents are rapidly mixed together and then 'stopped' in an observation cell. The change in reagents and formation of products are then recorded as a function of time,

usually as a fluorescence signal[1] or the absorbance at a specific wavelength.[2-6] Analysis of the resulting kinetic data can determine reaction rates, complexity of the reaction mechanism, information on short-lived reaction intermediates, etc. In addition, a series of stopped-flow experiments can be used to show the effect of parameters such as temperature,[7] pH,[8] and reagent concentration[9] on the kinetics of the reaction.

Stopped-flow is not a new technique, but its application in studying the reaction kinetics of active catalyst species and their substrates in not well-developed. The Re(polypyridyl)$(CO)_3$X framework is ideal for stopped-flow because the active form of the catalyst, [Re(polypyridyl)$(CO)_3]^{-1}$, is accessible through chemical reduction by potassium graphite (KC_8) and is soluble in a variety of solvents (MeCN and THF). A catalyst of particular interest in our laboratory is Re(bipy-*t*Bu)$(CO)_3$X (where bipy-*t*Bu = 4,4'-di-*tert*-butyl-2,2'-bipyridine and X = Cl^- or MeCN with a triflate counterion). We have compared this catalyst to Re(bipy)$(CO)_3$Cl and others that vary only in the substitution in the 4,4' positions of 2,2'-bipyridine by electrochemical means and have found that it outperforms them in both turnover frequency and turnover number.[10] We also performed the infrared spectroelectrochemistry (IR-SEC) of the catalyst and identified the important species in the sequential reduction leading up to the active catalyst, [Re(bipy-*t*Bu)$(CO)_3]^{-1}$ [**1**] (see Chapter 2 of this dissertation).

Recently we reported the stopped-flow kinetics of [**1**] with CO_2 and Brönsted acids (CF_3CH_2OH, CH_3OH and H_2O) by UV-Vis in order to gain a better

understanding of its astonishing selectivity for CO_2 over protons (H^+).[11] While we were able to study the reacion kinetics between substrates, we were unable to shed light on one of the most important mysteries surrounding this catalyst: what are the intermediates in the catalytic mechanism? The presence of strong infrared-absorbing CO ligands and the previous detailed IR-SEC data make stopped-flow IR a perfect method for elucidation of mechanistic intermediates and comparison of reaction rates between catalysts.

Here we discuss a stopped-flow IR investigation of the kinetics of the reaction between CO_2 and two active catalyst species, $[Re(bipy\text{-}tBu)(CO)_3]^{-1}$ and $[Re(bipy)(CO)_3]^{-1}$. A kinetic comparison between the two catalysts, as well as a CO_2 concentration study are reported.

4.2 Results and discussion

Two active catalyst species, $[Re(bipy\text{-}tBu)(CO)_3]^{-1}$ [**1**] and $[Re(bipy)(CO)_3]^{-1}$ [**2**], were prepared in solution (THF, 5 mM) in a dry box under an inert atmosphere using previously reported methods.[11] In a typical experiment, a solution of [**1**] or [**2**], a solution of *ca*. 0.1 M CO_2 in THF, and blank THF were loaded into three syringes of a stopped-flow instrument with multiple mixing capabilities (mixing schematic shown in Figure 4-1). In order to control the final concentration of CO_2 in the infrared (IR) observation head, the CO_2/THF solution was mixed with pure THF before final mixing with the Re anion solutions. This pre-mixing of the CO_2 solution allowed for control of the final CO_2 concentration from 5-100 mM. Because the original concentration of CO_2 was not known precisely, the absorbance of the CO_2 peak at

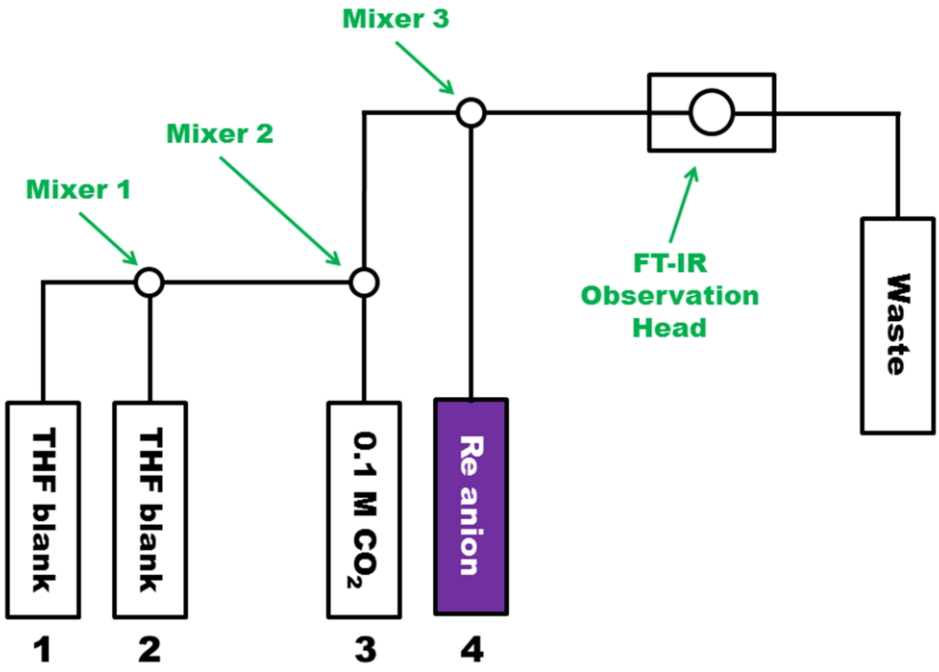

Figure 4-1. Mixing schematic for a typical stopped flow IR experiment in this work.

each mixing shot of the stopped-flow, along with the extinction coefficient for CO_2 in the IR,[12] was used to calculate the concentration of CO_2 present for reaction with the active Re complexes. We also independently verified the extinction coefficient using the stopped-flow mixing technique and obtained a number that was in good agreement with the previous report.

The IR spectrum of [**1**] has two strong ν(CO) stretches at 1940 and 1832 cm^{-1} and [**2**] has a very similar IR spectrum, with ν(CO) stretches at 1940 and 1840 cm^{-1}. These active species can react with CO_2, yielding an IR spectrum that resembles those of the starting materials, Re(bipy-*t*Bu)$(CO)_3$Cl or Re(bipy)$(CO)_3$Cl. Those spectra have one high energy ν(CO) stretch (A1) at *ca*. 2020 cm^{-1} and two overlapping stretches (split E) at *ca*. 1915 and 1900 cm^{-1}. In the previous IR-SEC studies of the

two chloro compounds they displayed two singly-reduced species, one with the chloride still present in the sixth coordination position (2005, 1895 and 1880 cm^{-1}), and one where the chloride had been liberated, yielding the five-coordinate, neutral complex (1980, 1865 and 1850 cm^{-1}). We are interested not only in the reaction kinetics of [**1**] and [**2**] with CO_2, but also with the method of reaction. For example, does the reaction with CO_2 go through a process involving two, one-electron steps? Or, is the reaction a concerted oxidative addition to the rhenium center?

In the reactions of [**1**] and [**2**] with CO_2 we observed only the fully reduced and fully oxidized species, with no appreciable formation of singly oxidized intermediates. This could be a result of two-electron oxidative addition to the metal center, but it could also be due to inadequate time resolution in the rapid scan IR experiment. Step scan experiments[13-15] may be able to answer this question, but until they can be completed to gain time resolution, we are classifying the reaction of CO_2 with [**1**] and [**2**] as a concerted oxidative addition yielding Re^{+1}–CO_2^{-2}.

Kinetic analysis was performed for both complexes at various CO_2 concentrations in order to compare the reaction rates against each other as well as to establish a reaction order in CO_2. At equal concentrations of both Re-anion and CO_2, [**1**] reacts ten times faster than [**2**]. This difference is slightly smaller than calculated between the two catalysts by cyclic voltammetry under an atmosphere of CO_2 in acetonitrile (13 times faster for [**1**] than for [**2**]), but is should be noted that this rate only represents the initial reaction with CO_2 and not the full catalytic cycle as the electrochemical studies do. We have established in a previous report that proton

$$Re^{-1} + CO_2 \xrightarrow{k} Re\text{-}CO_2^{-1} \qquad k_{obs} = k[Re^{-1}][CO_2]$$

Figure 4-2. Second-order reaction of Re^{-1} with CO_2 and rate law for the reaction.

transfer to the activated CO_2 molecule is likely part of the rate limiting step.[11] That observation leads to the hypothesis that, besides being ten times faster in initial reaction with CO_2, the bipy-*t*Bu analog is also superior in its ability to draw advantageous protons from solution to complete the catalytic transformation.

Further kinetic analysis shows that the disappearance of the low energy ν(CO) stretch fits second order exponential decay and scales with CO_2 concentration. The second order decay is reasonable for these reactions because the $[CO_2]$ ranges from 5-25 times that of the Re complex (Figure 4-2). In the previous study using stopped flow UV-Vis, pseudo first order kinetics were assumed because the CO_2 concentration was >1500 times that of the Re anion (100 mM *vs*. 0.06 mM). For complex [**1**], the rate is 1400 $M^{-1}s^{-1}$ at 30 mM CO_2 ($t_{1/2}$ ~ 20 ms), and for [**2**], the rate is 140 $M^{-1}s^{-1}$ at 30 mM CO_2 ($t_{1/2}$ ~ 200 ms). Figure 4-3 shows a side-by-side comparison between [**1**] and [**2**]. The increase in reaction rates for both [**1**] and [**2**] can be seen qualitatively in Figures 4-4 and 4-5, respectively (see Appendix). The second-order reaction rates and half-lives for all the concentrations of CO_2 studied can be found in Tables 4-1 and 4-2, for [**1**] and [**2**] respectively (see Appendix).

It is clear by visual inspection that the reaction of [**1**] with CO_2 is much faster than the reaction of [**2**] at similar CO_2 concentration. We can also visualize the dependence of the reaction rate on $[CO_2]$ by plotting the decay of the ν(CO) band at

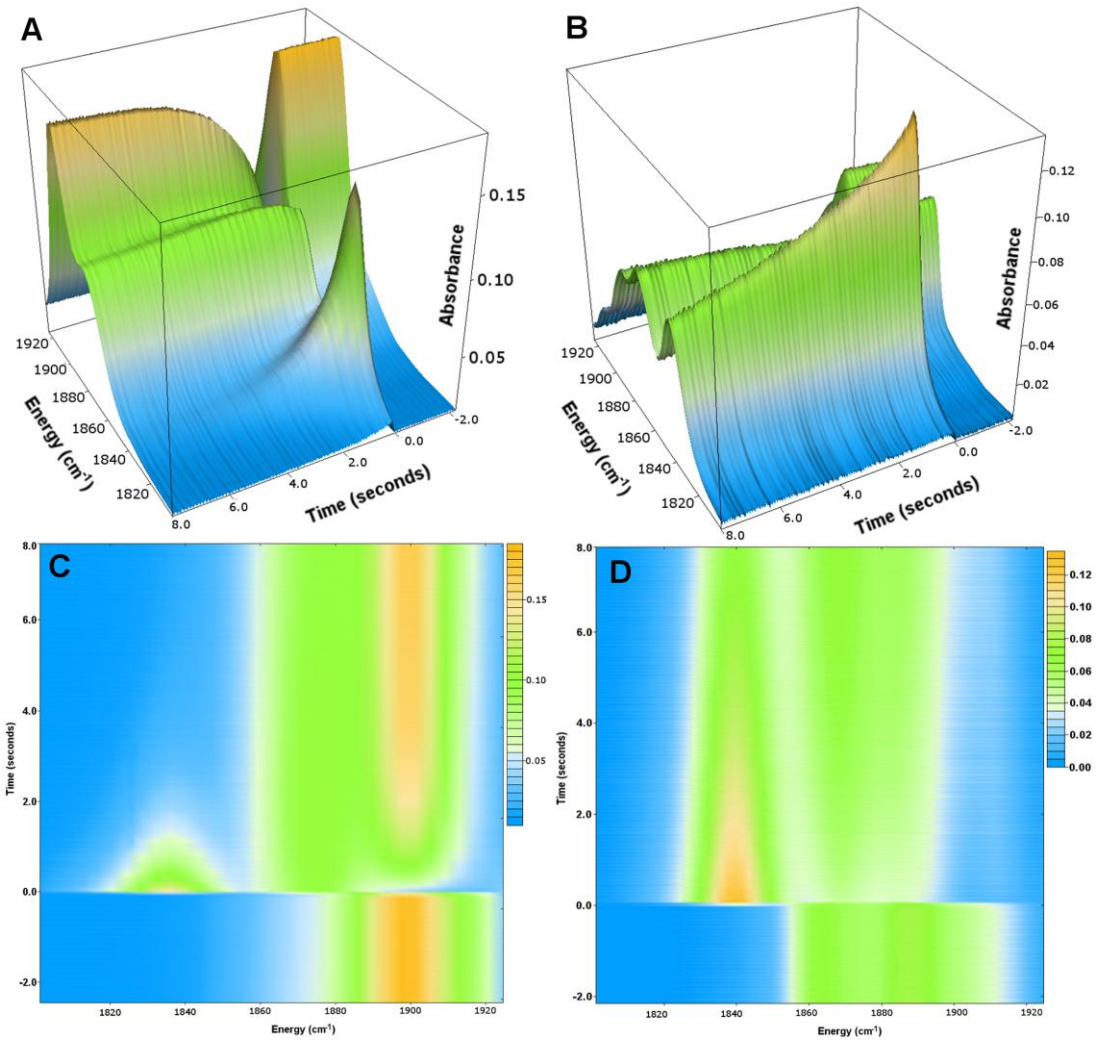

Figure 4-3. A.) Reaction of 2.5 mM [Re(bipy-*t*Bu)$(CO)_3]^{-1}$ [1] with 30 mM CO_2 showing the decay of the lowest energy ν(CO) band at 1832 cm^{-1}. B.) Reaction of 2.5 mM [Re(bipy)$(CO)_3]^{-1}$ [2] with 30 mM CO_2 showing the decay of the lowest energy ν(CO) band at 1840 cm^{-1}. C.) Topographical view of the reaction of [1] with 30 mM CO_2. D.) Topographical view of the reaction of [2] with 30 mM CO_2.

1832 cm^{-1} for [**1**] at various CO_2 concentrations. This enables a qualitative comparison of the rate and half-life of the reaction (Figure 4-6 in Appendix).

4.3 Conclusions

Through the use of rapid scan FT-IR and stopped flow mixing we were able to further elucidate the kinetics and mechanism of the reaction between two Re^{-1} complexes and CO_2. $[Re(bipy\text{-}t\text{Bu})(CO)_3]^{-1}$ reacts considerably faster than $[Re(bipy)(CO)_3]^{-1}$ (~10 fold) at similar CO_2 concentrations, but both reactions yield an IR spectrum that looks very much like a $Re^{+1}bipy^0$ complex, similar to the starting $Re(bipy\text{-}R)(CO)_3Cl$ complexes. We were not able to observe any intermediates on this timescale during the reaction, leading us to believe that the reaction proceeds by a concerted, two-electron oxidative addition of CO_2 to the metal center. The growth of a peak at *ca.* 1620 cm^{-1} as the reaction proceeds could be a CO_2 adduct, but further experimentation is necessary to confirm this assignment.

4.4 Experimental

General Considerations. $[Re(bipy\text{-}t\text{Bu})(CO)_3]^{-1}$ [**1**] and $[Re(bipy)(CO)_3]^{-1}$ [**2**] were prepared by previously reported methods.[10, 11] Anhydrous THF (>99 %, inhibitor-free) was stored over activated 3 Å molecular sieves and was used as the solvent for all experiments. CO_2 solutions of THF were prepared by sparging the solvent with dry CO_2 for 15 minutes, followed by 1:1 dilution of the saturated solution (*ca.* 0.2 M) with pure THF.

Stopped-flow Infrared Spectroscopy. A Biologic SFM-400 stopped-flow apparatus with four syringes and multiple mixing capabilities was used for rapid mixing with a

custom-made Biologic IR observation head (Mixing schematic in Figure 4-1 above). In a typical experiment, syringe 4 was filled with 5 mM [**1**] or [**2**], syringe 3 with a THF solution with 0.1 M CO_2, and syringes 1 and 2 with pure THF.

The observation head and stopped flow apparatus were separated by an umbilical of approximately 18 inches that allowed for conformational flexibility. The observation head contains two capillary ports, an inlet and outlet, allowing for flow of substrates through the small-volume mixing chamber created by a 0.2 mm PTFE spacer between two calcium fluoride (CaF) windows. A schematic of the observation head can be found in Figure 4-7 (see Appendix). No "hard stop" was used in these experiments, but a 10 mL syringe was attached to the waste port on the observation head to provide some resistance for mixing.

Rapid scan infrared transmission spectra were collected using a Bruker Vertex 80v equipped with a liquid nitrogen cooled MCT detector and a 4000 cm^{-1} low-pass filter. During measurement, the interferometer compartment was evacuated and the sample compartment was purged with dry nitrogen. In order to obtain quantitative kinetic data, stopped flow mixing was synchronized to the forward motion of the traveling mirror of the interferometer. The output trigger of the Bruker spectrometer, which signals the start of the forward mirror motion, was input to a BNC Model 575 Pulsedelay Generator that was programmed to account for the delayed response of the Biologic Stopped Flow mixing unit, the total time of the pushing phase, and the period of oscillation of the traveling mirror of the interferometer. The shot-to-shot jitter was determined to be approximately ± 2 ms by monitoring all synchronization pulses with

a Tektronix DPO 4054 Digital Phosphor Oscilloscope. After splitting interferograms, this method provided a full spectrum approximately every 11.5 ms at 8 cm^{-1} resolution and every 17 ms at 4 cm^{-1} resolution. Data was collected and manipulated using OPUS 6.5, second-order kinetics were fit in Microsoft Excel, and the decay plots for specific energy stretches were constructed in Origin 6.0.

Kinetic analysis. Second-order kinetics were fit by plotting the decay of the lowest energy ν(CO) stretch at 1832 cm^{-1} for [**1**] and 1840 cm^{-1} for [**2**] versus time. The absorbance values at each time point were converted to Re concentration using the initial concentration and it's absorbance as a guidepost. Plotting 1/[Re] versus time gave linear plots through the first three half-lives of the reaction and the slope of the plots gave rates in units of $M^{-1}s^{-1}$ for each complex at each CO_2 concentration.[16]

Note: The material in this chapter is unpublished work and was performed in collaboration with Eric E. Benson, Ian D. Sharp, and Heinz Frei at the JCAP Laboratory facilities in Berkeley, CA.

4.5 References

1. Johnson JD, Charlton SC, Potter JD (1979) A fluorescence stopped flow analysis of Ca^{2+} exchange with troponin C. *J. Biol. Chem.* 254(9):3497-3502.

2. Christian GD, Růžička J (1992) Exploiting stopped-flow injection methods for quantitative chemical assays. *Analytica Chimica Acta* 261(1–2):11-21.

3. Corraine MS, Atwood JD (1989) Kinetics and mechanism of electron transfer from pentacarbonylrhenate to metal carbonyl dimers by infrared stopped-flow spectroscopy. *Inorg. Chem.* 28(20):3781-3782.

4. Fabian H, Naumann D (2004) Methods to study protein folding by stopped-flow FT-IR. *Methods* 34(1):28-40.

5. George SJ, Kurkin S, Thorneley RNF, Albracht SPJ (2004) Reactions of H_2, CO, and O_2 with Active [NiFe]-Hydrogenase from Allochromatium vinosum. A Stopped-Flow Infrared Study. *Biochemistry* 43(21):6808-6819.

6. Groves JT, Lee J, Marla SS (1997) Detection and Characterization of an Oxomanganese(V) Porphyrin Complex by Rapid-Mixing Stopped-Flow Spectrophotometry. *J. Am. Chem. Soc.* 119(27):6269-6273.

7. Nichols PJ, Ducommun Y, Merbach AE (1983) High-pressure stopped-flow study of the complexation of vanadium(II) with thiocyanate in water: further evidence for the associative character of substitution on this metal ion. *Inorg. Chem.* 22(26):3993-3995.

8. Janda KD, *et al.* (1994) Direct selection for a catalytic mechanism from combinatorial antibody libraries. *PNAS* 91(7):2532-2536.

9. Navas Diaz A, Garcia JAG (1994) Nonlinear Multicomponent Kinetic Analysis for the Simultaneous Stopped-Flow Determination of Chemiluminescence Enhancers. *Anal. Chem.* 66(7):988-993.

10. Smieja JM, Kubiak CP (2010) Re(bipy-*t*Bu)$(CO)_3$Cl−improved Catalytic Activity for Reduction of Carbon Dioxide: IR-Spectroelectrochemical and Mechanistic Studies. *Inorg. Chem.* 49(20):9283-9289.

11. Smieja JM, *et al.* (2012) Artificial photosynthesis of CO: Kinetic and structural studies, origins of selectivity, and importance of interfacial charge transfer. *PNAS* In Press.

12. Wittrig RE (1994) Electrochemical and spectroelectrochemical studies of nickel- and copper-based catalysts for the reduction of carbon dioxide. Ph.D. (Purdue University, West Lafayette, IN).

13. Braiman MS, Ahl PL, Rothschild KJ (1987) Millisecond Fourier-transform infrared difference spectra of bacteriorhodopsin's M412 photoproduct. *PNAS* 84(15):5221-5225.

14. Uhmann W, Becker A, Taran C, Siebert F (1991) Time-Resolved FT-IR Absorption Spectroscopy Using a Step-Scan Interferometer. *Appl. Spectrosc.* 45(3):390-397.

15. Palmer RA, Chao JL, Dittmar RM, Gregoriou VG, Plunkett SE (1993) Investigation of Time-Dependent Phenomena by Use of Step-Scan FT-IR. *Appl. Spectrosc.* 47(9):1297-1310.

16. Connors KA (1991) *Chemical kinetics, the study of reaction rates in solution* (Wiley-VCH Publishers, Weinheim, Germany).

4.6 Appendix

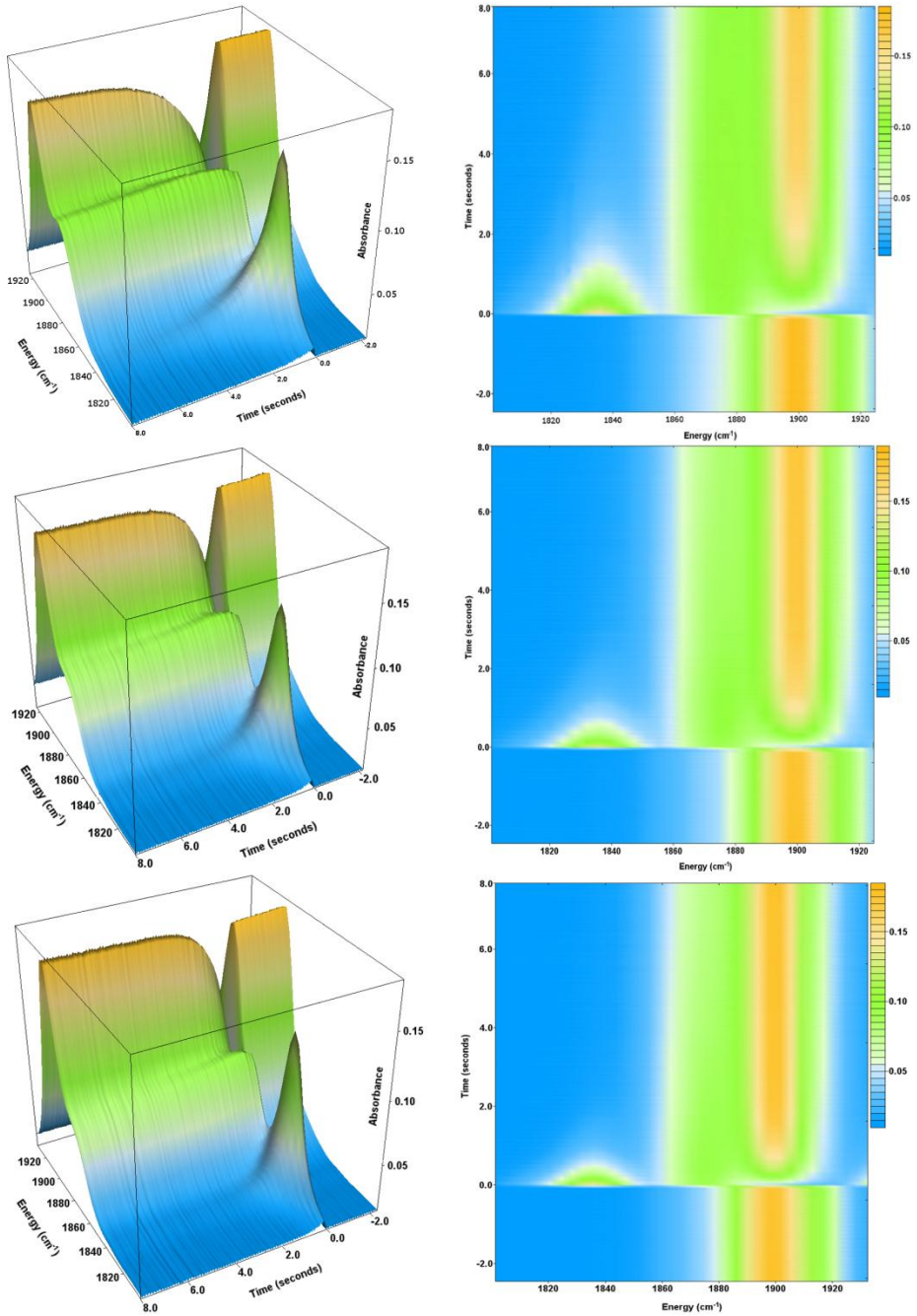

Figure 4-4. Stopped-flow IR traces for 2.5 mM Re(bipy-*t*Bu)$(CO)_3$Cl [**1**] at 15, 30 and 45 mM CO_2. All reactions are shown for 8 seconds after mixing for direct comparison and the decay of the lowest energy ν(CO) band at 1832 cm^{-1} is shown.

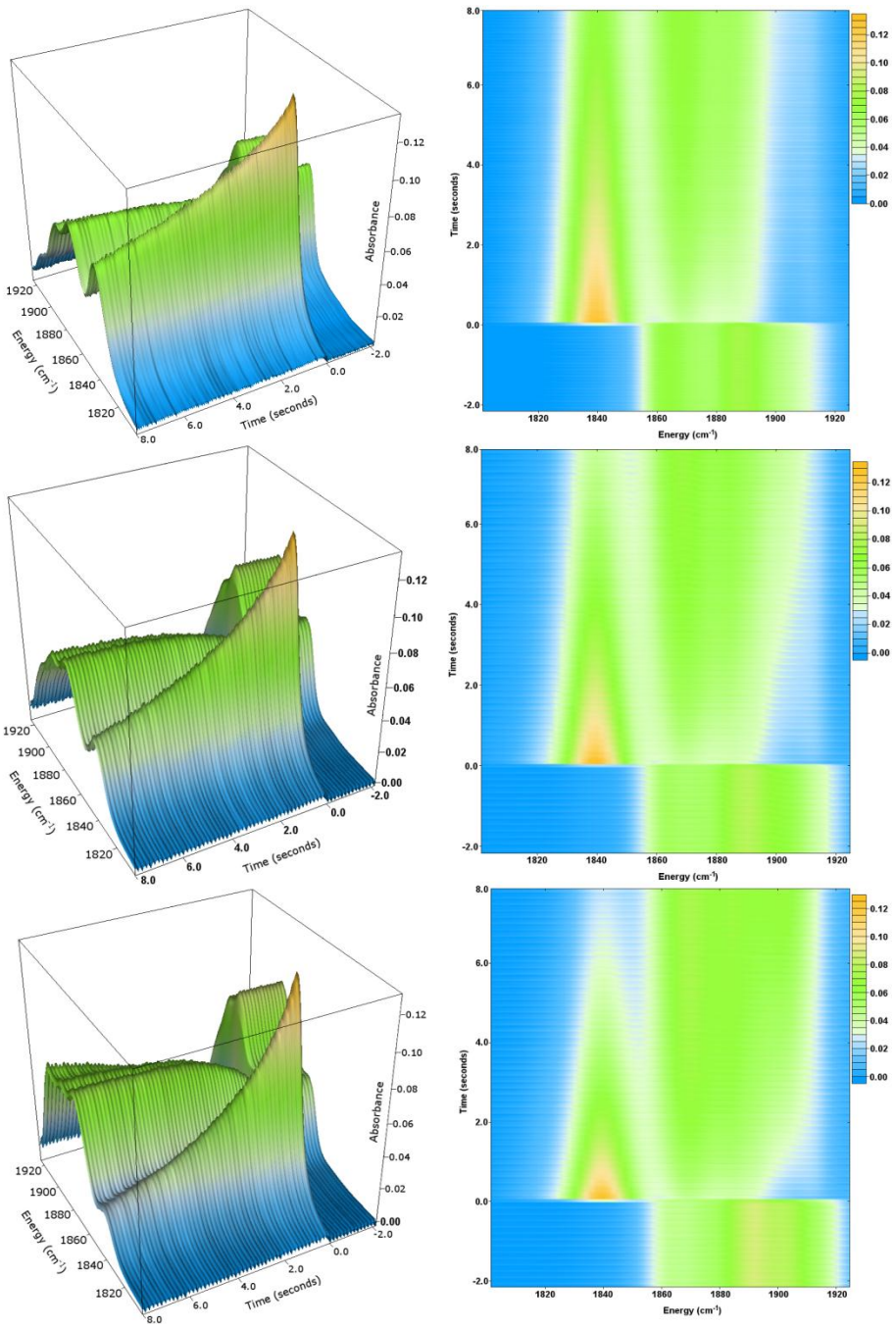

Figure 4-5. Stopped-flow IR traces for 2.5 mM Re(bipy)$(CO)_3$Cl [**2**] at 30, 50 and 60 mM CO_2. All reactions are shown for 8 seconds after mixing for direct comparison and the decay of the lowest energy ν(CO) band at 1840 cm^{-1} is shown.

Table 4-1. Second-order rates and half-lives for the reaction of [**1**] with various concentrations of CO_2 in the stopped-flow IR experiments as followed by the decay of the ν(CO) stretch at 1832 cm^{-1}.

[CO_2] (mM)	**Rate at 2.5 mM [Re(bipy-*t*Bu)(CO)$_3$]$^{-1}$ ($M^{-1}s^{-1}$)**
14	380
21	640
31	1400
43	2600
48	3350
52	4900

Table 4-2. Second-order rates and half-lives for the reaction of [**2**] with various concentrations of CO_2 in the stopped-flow IR experiments as followed by the decay of the ν(CO) stretch at 1840 cm^{-1}.

[CO_2] (mM)	**Rate at 2.5 mM [Re(bipy)(CO)$_3$]$^{-1}$ ($M^{-1}s^{-1}$)**
3	10
32	140
48	230
64	460

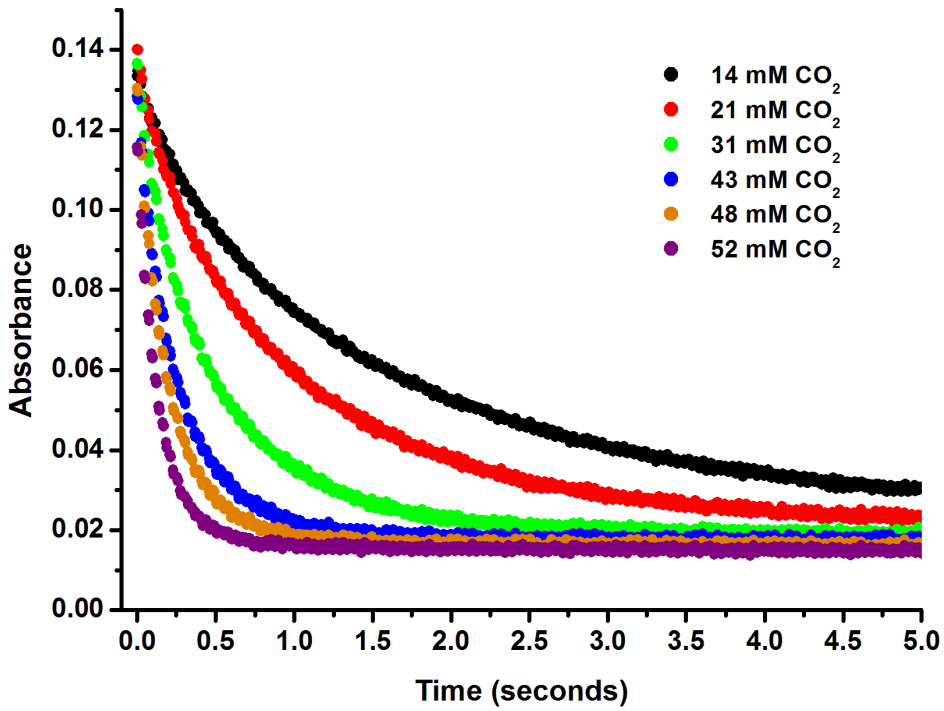

Figure 4-6. Decay of the lowest energy ν(CO) band at 1832 cm^{-1} over time for the reaction of 2.5 mM $[Re(bipy\text{-}tBu)(CO)_3]^{-1}$ with various concentrations of CO_2.

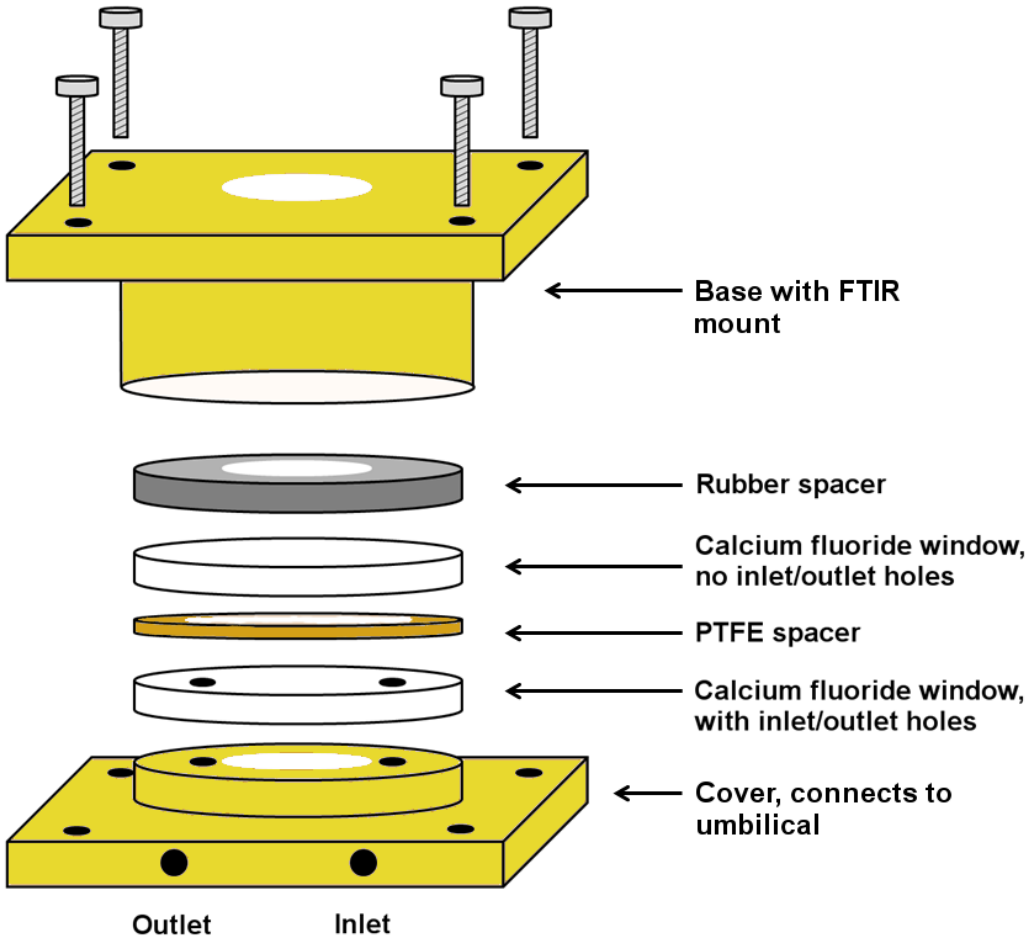

Figure 4-7. Schematic of flow through FTIR observation head for the Biologic SFM-400 stopped flow instrument.

Chapter 5

Mn(bipy-*t*Bu)$(CO)_3$Br as an earth-abundant alternative to rhenium. Electrocatalytic studies, X-ray crystallography and IR-SEC.

5.1 Introduction

One of the most challenging goals for current and future generations of chemists and engineers is the development of new technologies for the storage of electrical energy. Battery technology, pumped hydro, thermal storage, compressed air and hydrogen production are all frequently discussed as viable options for future energy storage.[1] Another option is the production of liquid fuels from carbon dioxide (CO_2) and water (H_2O). The production and burning of these energy-dense fuels could provide a route to carbon neutral energy that would not only fit into existing infrastructure, but would also enable convenient storage and transport. Achieving this goal, though, will require technological advances in carbon dioxide capture

(concentration) and catalysis (activation). Many groups are currently working on the issue of carbon dioxide capture from the atmosphere, and advances in that field can be found in several reviews and government reports.[2-7]

Second and third row transition metals have long been the gold standard for catalysis. Transition metals like platinum, palladium, rhodium, and iridium are, in many cases, far superior to their first row counterparts. This trend holds true for synthetic CO_2 reduction catalysts. Some of the best reported CO_2 electrocatalysts to date are based on Pd,[8-12] Ru,[13] Rh[14] and Re.[15-18] In the past, our group has studied catalysts based on the Re(bipy-R_2)$(CO)_3$(L) scaffold, where bipy-R_2 is a 4,4'-disubstituded-2,2'-bipyridine and L is either a halide (Cl^- or Br^-) or a solvent molecule accompanied by triflate as a non-coordinating counterion.[16, 17, 19, 20] Having learned much about the mechanism for the Re scaffold, we were interested in studying the effects of changing the metal center to its first row counterpart, manganese. Manganese is 1.3 million times more abundant in the Earth's crust than rhenium, at 950 mg Mn/kg crust versus only 7 x 10^{-4} mg Re/kg crust.[21] This fact becomes important when considering not only the cost of scale up, but also the environmental ramifications of mining large quantities of raw material.

In 2011, Deronzier and co-workers discovered that Mn(bipy)$(CO)_3$Br and Mn(dmb)$(CO)_3$Br (where bipy = 2,2'-bipyridine and dmb = 4,4'-dimethyl-2,2'-bipyridine) were able to reduce CO_2 to CO with excellent efficiencies, selectivities, and stabilities when water was present in the electrochemical solution.[22] The Mn complexes are, however, inactive towards CO_2 reduction without the addition of an

external proton source. Compared to their Re counterparts, the Mn catalysts had the advantages of being more Earth-abundant and running at lower overpotentials, but suffered from lower current densities and lower stabilities, as observed during bulk electrolysis.

Herein we describe the synthesis, electrocatalysis, infrared spectroelectrochemistry, and X-ray crystallography of modified manganese catalysts. Mn(bipy-*t*Bu)$(CO)_3$Br and Mn(bipy-*t*Bu)$(CO)_3$(MeCN)(OTf) (where bipy-*t*Bu = 4,4'-di-*tert*-butyl-2,2'-bipyridine and OTf = $CF_3SO_3^-$) were fully characterized and showed increased catalytic activity over both Mn(bipy)$(CO)_3$Br and Mn(dmb)$(CO)_3$Br. Notably, their catalytic activity also rivals that of their rhenium counterparts.

5.2 Results and discussion

Synthesis and characterization. Synthesis of Mn(bipy-*t*Bu)$(CO)_3$Br (**1**) was performed analogously to a previously reported procedure.[23] The product was characterized by ^{1}H NMR, FTIR, elemental analysis and X-ray crystallography (see Experimental section below). It was noted that the ^{1}H NMR spectrum of **1** displays broadening, and the usual aromatic splitting patterns are not resolved. This was in contrast to the related Re(bipy-*t*Bu)$(CO)_3$Cl complex where splitting was observed in the aromatic peaks. Mn(bipy-*t*Bu)$(CO)_3$(MeCN)(OTf) (**2**) was synthesized from **1** by reflux with AgOTf in acetonitrile and characterized by ^{1}H NMR, FTIR, elemental analysis and X-ray crystallography (see below).

Electrochemical experiments. Electrochemical experiments were undertaken to evaluate the electrocatalytic properties of **1** and **2**. The electrochemistry of **1** in dry acetonitrile under an atmosphere of argon is very similar to the previously reported electrochemistry of $Mn(bipy)(CO)_3Br$ and $Mn(dmb)(CO)_3Br$ and is displayed in Figure 5-1.[22] The cyclic voltammogram (CV) consists of two irreversible, one-electron reduction waves. The first wave, at –1.39 V vs. SCE, is bipyridine-based and the second reduction, at –1.57 V vs. SCE, is metal-based. The second reduction of the catalyst leads to the catalytically active $[Mn(bipy\text{-}t\text{Bu})(CO)_3]^-$ anion. A large oxidation wave is observed in the CV of this compound at –0.30 V vs. SCE. This wave is attributed to the oxidative breaking of the Mn–Mn dimer formed upon the first reduction of the complex.[22] The electrochemistry of **2** is nearly identical to that of **1**, but the first reduction is *ca.* 50 mV more positive. Both complexes **1** and **2** are freely

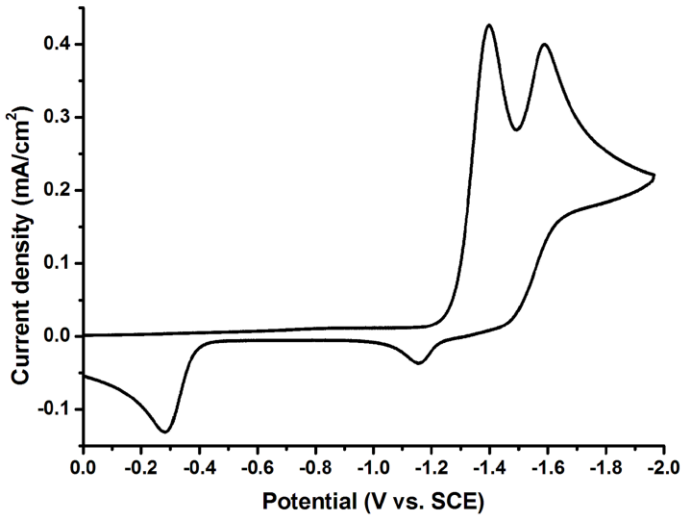

Figure 5-1. Cyclic voltammogram of 1 mM $Mn(bipy\text{-}t\text{Bu})(CO)_3Br$ in acetonitrile under an atmosphere of argon. Electrochemical conditions were 0.1 M TBAH as supporting electrolyte, 1 mm diameter glassy carbon working electrode, Pt wire counter electrode, and Ag wire reference electrode separated from the bulk solution by a Vycor thirsty glass tip.

diffusing in solution according to the Randles–Sevcik equation (Figure 5-2).[24]

It is useful to compare the electrochemistry of complex **1** to that of the closely related Re(bipy-*t*Bu)$(CO)_3$Cl that we have reported previously.[17] The Re complex also exhibits two single electron reductions. The first reduction of the Re complex is

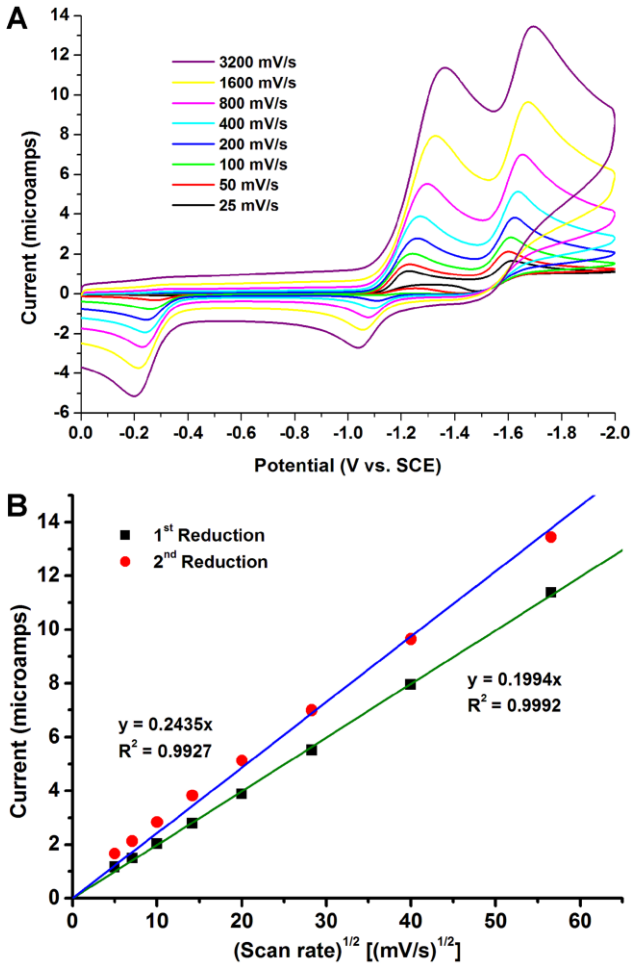

Figure 5-2. A.) Cyclic voltammogram scan rate dependence of 1 mM Mn(bipy-*t*Bu)$(CO)_3$Br under an atmosphere of argon in acetonitrile. Electrochemical conditions were 0.1 M TBAH as supporting electrolyte, 1 mm diameter glassy carbon working electrode, Pt wire counter electrode, and Ag wire reference electrode separated from the bulk solution by a Vycor thirsty glass tip. B.) Plot showing that the current is directly proportional to concentration and increases with the square root of the scan rate. This behavior is indicative of a freely diffusing species where the electrode reaction is controlled by mass transport.

reversible when the scan is stopped before reaching the second, but quasi-reversible when scanned to the second reduction. The first reduction of the Mn complex, however, is irreversible regardless of the switching potential or the scan rate up to 12 V/s, indicating that bromide loss upon first reduction is rapid. Another major difference is in the large oxidation peak at –0.30 V vs. SCE in the Mn complexes that is not present in either Re(bipy-R_2)$(CO)_3$X complexes or in Re(bipy-*t*Bu)$(CO)_3$(L)(OTf) (where L = MeCN or pyridine). This difference reflects the enhanced dimerization of Mn complexes upon single reduction when compared to Re complexes. The two reductions of complex **1** are closer in potential to each other than those of the Re analog. The two reductions of **1** are separated by only 180 mV, while the two reductions of Re(bipy-R_2)$(CO)_3$X complexes (where R = H, Me, *t*Bu, or OMe and X = Cl^- or Br^-) are separated by 300–400 mV, depending on bipyridine substitution. The other important difference between the Mn and Re complexes is the potential of the second reduction. The 260 mV anodic shift of the second reduction for the Mn complex compared to the Re complex represents a significant decrease in overpotential for the reduction of CO_2 to CO. This shift in potential may also be the reason why added proton sources are required for catalytic turnover to occur, a phenomenon not observed for Re complexes and one that will be discussed further in the conclusions.

The electrocatalytic properties of **1** were studied in a custom-made, two-compartment, air-tight cell with a glassy carbon working electrode, Pt counter electrode, and a Ag wire reference electrode separated from the main compartment by

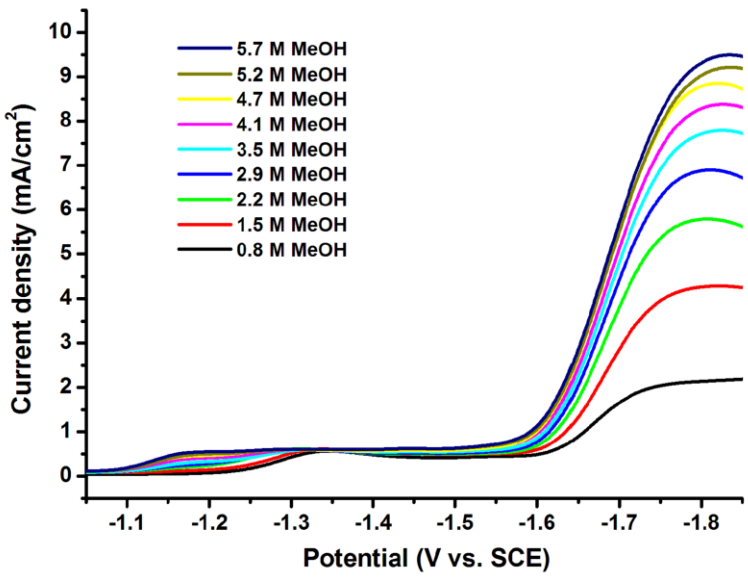

Figure 5-3. Linear scan voltammograms showing the electrocatalytic reduction of CO_2 to CO by 1 mM Mn(bipy-*t*Bu)$(CO)_3$Br in acetonitrile with addition of MeOH. Solution is under an atmosphere of, and saturated with (*ca.* 0.25 M) carbon dioxide. Electrochemical conditions were 0.1 M TBAH as supporting electrolyte, 1 mm diameter glassy carbon working electrode, Pt wire counter electrode, and Ag wire reference electrode separated from the bulk solution by a Vycor tip.

a Vycor tip. A 10 minute sparge of the acetonitrile solution with "bone dry" carbon dioxide yielded a gas-saturated solution (*ca.* 0.25 M). The electrochemistry of **1** did not change significantly under CO_2 in dry acetonitrile. Addition of weak Brönsted acids (water, methanol, or trifluoroethanol), however, results in an increase in the current at the second reduction potential, representing catalytic current for the reduction of CO_2 to CO. This increase in current can be seen in Figure 5-3 (methanol addition) and Figures 5-4 and 5-5 (addition of water and TFE, respectively).

Addition of water to a 1 mM solution of **1** under CO_2 results in a catalytic current of nearly 6 mA/cm^2 before plateauing and eventually dropping with addition of more H_2O. The maximum catalytic current is obtained at a water concentration of 2.65 M H_2O (*ca.* 5% by volume). The shape of the reduction waves before the

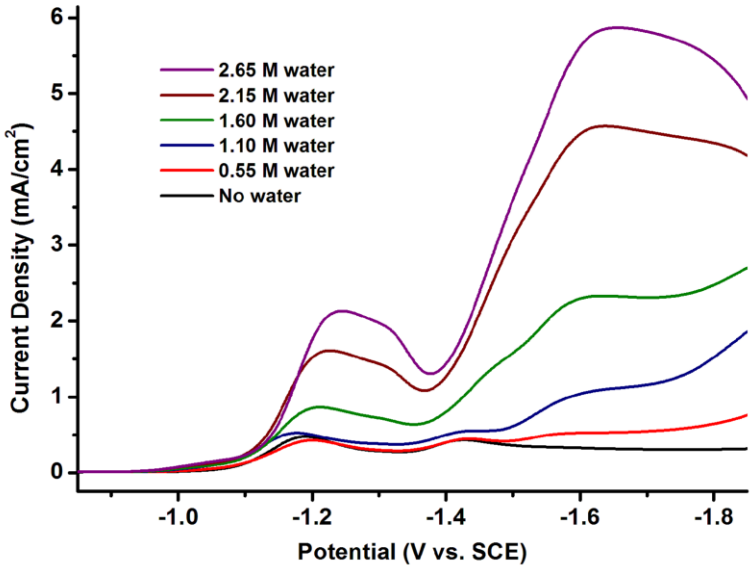

Figure 5-4. Linear scan voltammograms showing the electrocatalytic reduction of CO_2 to CO by 1 mM Mn(bipy-*t*Bu)$(CO)_3$Br in acetonitrile with addition of water. Solution is under an atmosphere of, and saturated with (*ca.* 0.25 M) carbon dioxide. Electrochemical conditions were 0.1 M TBAH as supporting electrolyte, 1 mm diameter glassy carbon working electrode, Pt wire counter electrode, and Ag wire reference electrode separated from the bulk solution by a Vycor tip.

catalytic wave change significantly upon water addition and increase in absolute current density, but this does not correspond to the production of H_2 (see below). The addition of stronger Brönsted acids leads to higher current densities in the CVs of **1** under CO_2. CVs with added methanol reach 9.5 mA/cm^2 at 5.7 M methanol and 1 mM catalyst. CVs with added trifluoroethanol (TFE) reach 16 mA/cm^2 at 1.25 M TFE and 1 mM catalyst, and 47 mA/cm^2 at 5 mM catalyst. Catalytic current scales linearly with catalyst concentration up to approximately 3 mM under an atmosphere of CO_2 with 0.86 M TFE added. The high current densities in the cyclic voltammograms of both **1** and **2** under CO_2 with added Brönsted acids rival those of Re complexes. This is an exciting finding given the increased abundance of Mn vs. Re and the decreased overpotential for the Mn catalysts.

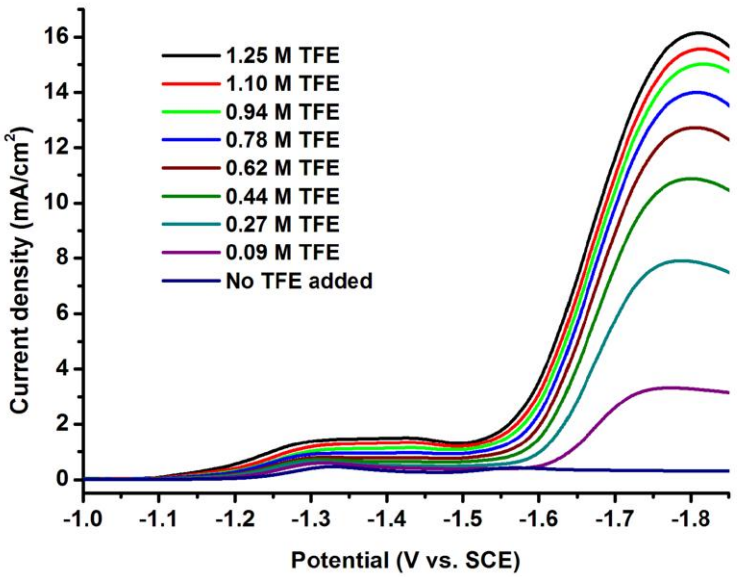

Figure 5-5. Linear scan voltammograms showing the electrocatalytic reduction of CO_2 to CO by 1 mM Mn(bipy-*t*Bu)$(CO)_3$Br in acetonitrile with addition of trifluoroethanol. Solution is under an atmosphere of, and saturated with (*ca.* 0.25 M) carbon dioxide. Electrochemical conditions were 0.1 M TBAH as supporting electrolyte, 1 mm diameter glassy carbon working electrode, Pt wire counter electrode, and Ag wire reference electrode separated from the bulk solution by a Vycor tip.

Bulk electrolysis monitored by gas chromatography indicates that no hydrogen is formed and a Faradaic efficiency of 100 ± 10 % is achieved for the formation of CO from CO_2 at 5 mM catalyst with water, methanol, or TFE (TFE example data in Figure 5-6). The catalyst is able to sustain current densities as high as 10 mA/cm^2 with added TFE for a period of more than three hours with very little loss of activity (*ca.* 15% over the first 10 minutes, followed by stable current over the next three hours). At lower catalyst concentration (1 mM), the catalyst was unable to sustain high current density during bulk electrolysis. The current density for bulk electrolysis in a stirred solution diminished to nearly zero in only 30-40 minutes. If bulk electrolysis is stopped, the solution is re-sparged and the electrode is cleaned, however, the catalytic current recovers to its starting point. This behavior was initially thought to be caused

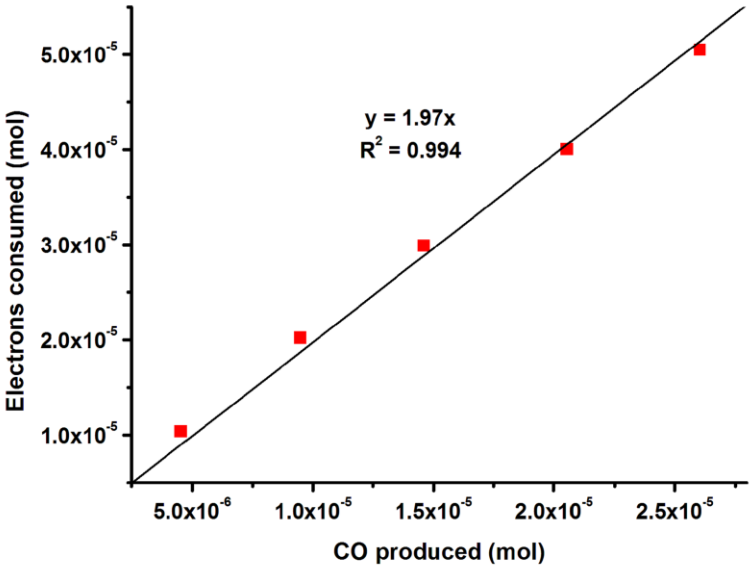

Figure 5-6. Production of CO from CO_2 by 5 mM Mn(bipy-*t*Bu)$(CO)_3$Br during bulk electrolysis with 0.8 M TFE. The slope of 2 represents a Faradaic efficiency of 100 ± 10 %. Bulk electrolysis of this solution showed 15 % current loss over the first 10 minutes as is usual to reach steady state, but no significant degradation over a period of more than three hours after that.

by the formation of stable dimers or some other chemical species on the surface of the electrode, but data for 5 mM solutions of catalyst is inconsistent with that hypothesis. Experiments are ongoing in our laboratory to determine the reason for low catalytic current stability in lower concentration bulk electrolysis runs.

X-ray crystallographic studies. Recently, we have had a great deal of success growing crystals of both the parent and anionic species of the Re complexes in our lab.[20] X-ray quality crystals of complex **1** were grown from the vapor diffusion of pentane into a tetrahydrofuran solution of the complex (Figure 5-7). The crystal structure of the active catalytic species, $[Mn(bipy\text{-}tBu)(CO)_3]^-[K(18\text{-crown-}6)]^+$ (**3**), was also obtained (Figures 5-8). Reduction of **1** by KC_8 (2.1 equivalents) in the presence of 18-crown-6 afforded pure **3**. 18-crown-6 was added as a stabilizing agent

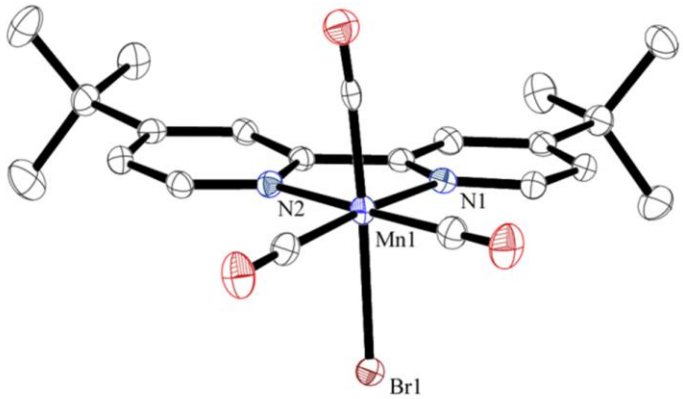

Figure 5-7. Molecular structure Mn(bipy-*t*Bu)$(CO)_3$Br, hydrogen atoms omitted for clarity. Showing one of two of the molecules in the asymmetric unit (Z=2), ellipsoids are set at the 50% probability level.

as well as a buffer to inhibit potassium coordination to the carbonyls of the Mn complex. Crystals of the anion were grown from the vapor diffusion of pentane into THF and crystallized in the space group P2(1)/n with two independent molecules in the unit cell. Reduction of the compound results in the loss of the bromide, forming the five coordinate unsaturated complex. The geometry of one of the anionic molecules in the asymmetric unit cell (Z' = 2) is somewhere between square pyramidal and trigonal bipyramidal with a τ_5 = 0.53. In this scale, a perfect square pyramid has a τ_5 = 0 and a perfect trigonal bipyramid has a τ_5 = 1.[25] This structure is very similar to the structure of $[Re(bipy\text{-}tBu)(CO)_3]^-[K(18\text{-crown-}6)]^+$, where the molecule is also five-coordinate and has a τ_5 = 0.46.[20] Of the two molecules in the asymmetric unit cell for **3**, one has a slight disorder in the rotation of the facial carbonyls, leading us to believe there is a shallow barrier for rotation between the square pyramid and the trigonal bipyramid.

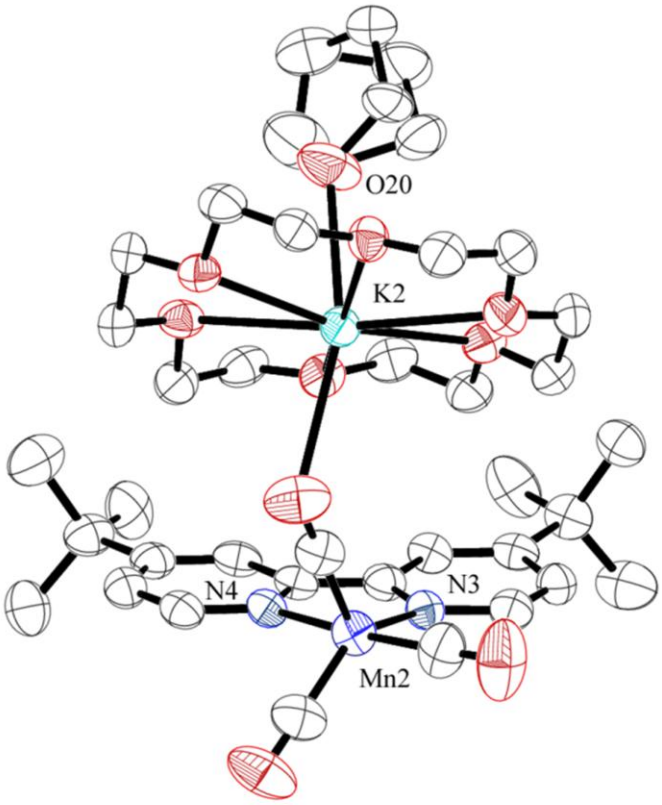

Figure 5-8. Molecular structure of [Mn(bipy-*t*Bu)(CO)$_3$][K(18-crown-6)(THF)], hydrogen atoms removed for clarity. Showing one of the two molecules in the asymmetric unit (Z=2). Ellipsoids are set at the 50% level.

Infrared Spectroelectrochemistry. Infrared spectroelectrochemistry (IR-SEC) of complex **1** under both N_2 and CO_2 was performed to gain insight into the precursors of the active catalyst. Three major species were observed in the progression through both reductions of complex **1** and are shown in Figure 5-9. In its resting state, Complex **1** has three characteristic ν(CO) stretches for facially coordinated tricarbonyl complexes at 2028, 1933 and 1923 cm^{-1}. Upon one-electron reduction of the parent complex, complete formation of the Mn-Mn dimer, [Mn(bipy-*t*Bu)(CO)$_3$]$_2$, is observed with no prior intermediates. This implies that loss of bromide, followed by dimerization,

occurs rapidly upon reduction. The ν(CO) for the dimer species are 1973, 1928, 1878 and 1850 cm^{-1}. These ν(CO) peaks match well with those previously reported for both $[Mn(bipy)(CO)_3]_2$ and $[Re(bipy)(CO)_3]_2$.[26, 27] Upon further reduction, a third species is formed with strong ν(CO) stretches at 1907 and 1807 cm^{-1}. This is indicative of the $[Mn(bipy\text{-}t\text{Bu})(CO)_3]^-$ anionic species that acts as the active catalyst for CO_2 reduction. The stretches also correlate well with the $[Mn(bipy\text{-}t\text{Bu})(CO)_3]^-[K^+(18\text{-crown-}6)]$ species produced by the chemical reduction of **1** using KC_8 (1905 and 1805 cm^{-1}). It is interesting, though, that these stretches are shifted 40 cm^{-1} lower in energy when compared to the equivalent stretches for $[Re(bipy\text{-}t\text{Bu})(CO)_3]^-$ reported previously.[17] Bond alternation in the bipyridine ring,[28] along with ADF calculations, indicate that significant electron density still resides on the bipyridine ring for complex **3**, but the very low energy CO stretching frequencies indicate that M-CO back bonding has been significantly increased as compared to the analogous Re complex. It is also noted that there is significant overlap between species in this IR-SEC due to the small separation in reduction potentials.

IR-SEC studies of complex **1** in CO_2-saturated acetonitrile are, admittedly, somewhat convoluted. Reduction of the complex at a potential at (or negative of) the second reduction potential leads to a spectrum with a large mixture of stretches indicative of all three species seen in the IR-SEC under N_2. Interestingly, though, two new peaks arise at 1687 and 1653 cm^{-1} as the potential is held negative of the second reduction. The new stretches indicate that, in this dry acetonitrile solution, the Mn anion binds CO_2 and is unable to turnover, stopping at the Mn-CO_2 adduct.

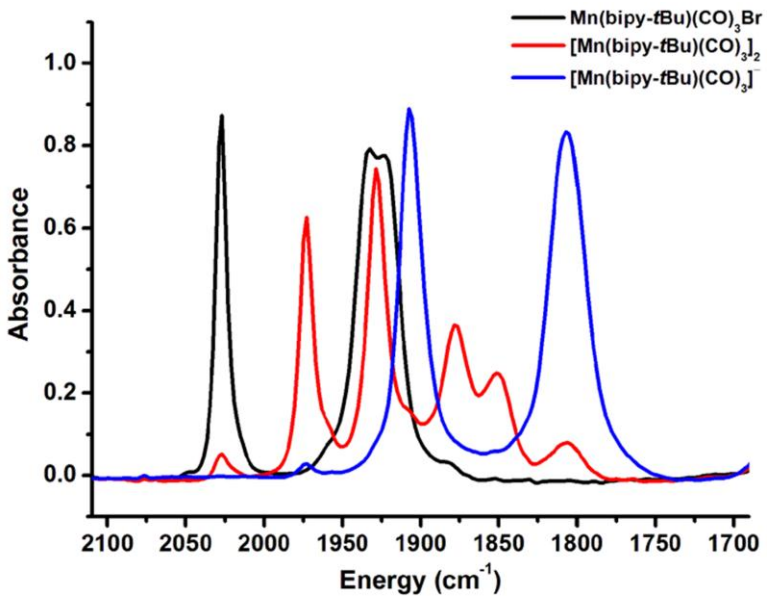

Figure 5-9. Three species are observed in the IR-SEC of complex **1** under an atmosphere of N_2. The rest species (black) has three characteristic ν(CO) stretches at 2028, 1933 and 1923 cm^{-1}. The singly reduced species (red) forms dimer rapidly and completely upon reduction and has ν(CO) stretches at 1973, 1928, 1878 and 1850 cm^{-1}. Finally, the doubly reduced species (blue) has only two ν(CO) stretches at 1907 and 1807 cm^{-1}, similar in shape to those of the closely related [Re(bipy-*t*Bu)$(CO)_3]^-$, but red shifted 40 cm^{-1}.

The same two ν(CO) stretches are observed under $^{13}CO_2$, but are shifted 40 cm^{-1} as is expected based on the harmonic oscillator model.

5.3 Conclusions and future work

We have described an earth-abundant metal complex, Mn(bipy-*t*Bu)$(CO)_3$Br (**1**), which acts as a robust, selective and efficient catalyst for the reduction of CO_2 to CO. The addition of Brönsted acid is necessary for catalyst turnover in the Mn system, unlike in the analogous Re system. This difference may be due to the anodic shift of 260 mV for the second reduction of **1** compared to Re(bipy-*t*Bu)$(CO)_3$Cl. The decrease in potential may act to decrease the basicity of the bound CO_2, rendering it ineffective at extracting protons from solvent or electrolyte to turn over. Three

different weak acids were used (water, methanol and trifluoroethanol) and catalytic current increased in cyclic voltammograms as the acid strength is increased. We were able to characterize both complex **1** and the active catalyst, $[Mn(bipy\text{-}tBu)(CO)_3]^-$ (**3**), by X-ray crystallography. The crystal structure of **3** is nearly identical to that of $[Re(bipy\text{-}tBu)(CO)_3]^-$ in geometry as well as in the DFT-calculated electronic structure. The exception to this similarity lies in the 40 cm^{-1} shift to lower energy for both bands in the IR of **3**. Infrared spectroelectrochemistry of complex **1** under nitrogen showed three distinct species. The first is the parent complex at rest, the second is Mn-Mn dimer formed by the first reduction and the immediate loss of bromide, and the third is the anionic species that serves as the active catalyst for CO_2 reduction. The same experiment under CO_2 yields a mixture of species upon second reduction with two new peaks appearing in the region expected for a metal-bound CO_2.

This class of carbon dioxide reduction electrocatalyst is exciting moving forward not only because of its ability to reduce CO_2 to CO at lower overpotentials than its Re counterpart, but also because of its earth-abundance. Further experiments are currently being undertaken in our lab to attach these catalysts to surfaces in hopes of maintaining catalytic activity while increasing catalyst longevity.

5.4 Experimental

General Experimental Procedures. NMR spectra were recorded on a Jeol 500 MHz spectrometer at 298 K and data was manipulated using Jeol Delta software. ^1H

chemical shifts are reported relative to solvent residual peaks. Infrared spectra were collected on a Thermo Scientific Nicolet 6700. Microanalyses were performed by Midwest Microlab, LLC (Indianapolis, IN) for C, H, and N.

Syntheses. Manipulations were performed under an atmosphere of argon in the dark. Solvents were sparged with argon, dried on a custom dry solvent system over alumina columns and stored over sieves before use. Potassium graphite (KC8) was prepared by literature methods and stored at –30 °C in the dry box.[29] Tetrabutylammonium hexafluorophosphate (TBAH, Aldrich, 98%) was twice recrystallized from methanol and dried under vacuum at 90 °C overnight before use. 18-crown-6 was recrystallized from acetonitrile and dried under vacuum at 90 °C overnight before use. Other reagents were used as received from the following: $Mn(CO)_5Br$ (Strem Chemical, 98%), 4,4'-di-*tert*-butyl-2,2'-bipyridine (Aldrich) and silver trifluoromethanesulfonate (AgOTf, Aldrich, 98%).

Synthesis of Mn(4,4'-di-*tert*-butyl-2,2'-bipyridine)$(CO)_3$Br. $Mn(CO)_5Br$ (500 mg, 1.82 mmol) was added to an argon-sparged Schlenk flask with 50 ml Et_2O. 4,4'-di-*tert*-butyl-2,2'-bipyridine (494 mg, 1.84 mmol) was added to the mixture and the reaction was brought to reflux. The mixture quickly turned from colorless to orange after reflux began and product began crashing out of solution after 30-40 minutes. The reaction mixture was removed from heat after one hour and submerged in a –80 °C acetone/dry ice bath. After 30 minutes in the cold bath, the reaction mixture was

removed and the yellow solid was filtered and dried under vacuum at 90 °C overnight. The yield of Mn(bipy-*t*Bu)$(CO)_3$Br was 601 mg (67%). ^{1}H NMR ($CDCl_3$): δ 1.43 (br, 18 H, *t*Bu), δ 7.50 (br, 2 H, 5 and 5' H's), δ 8.03 (br, 2 H, 6 and 6' H's), δ 9.13 (br, 2 H, 3 and 3' H's). IR (CH_3CN) ν(CO): 2028 cm^{-1}, 1933 cm^{-1}, 1923 cm^{-1}. Anal. Calcd for **1**, $C_{21}H_{24}BrMnN_2O_3$: C, 51.76; H, 4.96; N, 5.75. Found: C, 51.80; H, 4.95; N, 5.69.

Synthesis of [Mn(4,4'-di-*tert*-butyl-2,2'-bipyridine)$(CO)_3$(MeCN)](OTf). Complex **1** (400 mg, 0.82 mmol) was mixed with silver trifluoromethanesulfonate (AgOTf, 290 mg, 1.13 mmol) in a 50 ml Schlenk flask with 35 ml acetonitrile (MeCN) in the glove box. The reaction flask was brought out of the box, covered with foil (to avoid exposure to light), and heated to reflux overnight. The reaction mixture was orange during reflux and had a black/brown solid at the bottom (most likely AgBr). After 18 hours of reflux the heat was removed and the solid was filtered from the orange solution. Solvent was removed by rotary evaporation, yielding a yellow/orange solid. The product was purified by running through a neutral alumina plug in MeCN to eliminate manganese and silver impurities yielding pure product. The final yield of pure product was 340 mg (69 % yield). ^{1}H NMR ($CDCl_3$): δ 1.45 (br, 18 H, *t*Bu), δ 2.36 (br, 3 H, bound MeCN), δ 7.58 (br, 2 H, bipy), δ 8.03 (br, 2 H, bipy), δ 9.13 (br, 2 H, bipy). IR (CH_3CN) ν(CO): 2047 cm^{-1}, 1958 cm^{-1} (br). Anal. Calcd for **1**, $C_{24}H_{27}F_3MnN_3O_6S$: C, 48.24; H, 4.55; N, 7.03. Found: C, 48.77; H, 4.60; N, 6.77.

Electrochemistry. Electrochemical experiments were performed using a BAS Epsilon potentiostat. A two compartment cell was used for all cyclic voltammetry experiments with a glassy carbon electrode (1 mm in diameter from BASi), a Pt wire counter electrode, and an Ag/AgCl reference electrode separated from the solution by a Vycor tip. Fc/Fc^+ was added as an internal reference. All electrochemical experiments were performed with 0.1 M tetrabutylammonium hexafluorophosphate (TBAH) as the supporting electrolyte. All solutions were purged with argon or CO_2 before CVs were taken. Mn complex concentrations ranged from 0.1–5.0 mM and experiments with CO_2 were performed at gas saturation (~0.25 M) in acetonitrile.

Bulk electrolysis. Bulk electrolysis experiments were carried out in a two compartment cell designed in our laboratory and described below. The setup included a 3 mm glassy carbon working electrode, a platinum wire counter electrode, and an Ag/AgCl reference electrode separated from the solution by a Vycor tip. A BAS Epsilon potentiostat was used to apply potential and record current. The bulk reductions were carried out in a CH_3CN with various amounts of added Brönsted acids and 0.1 M TBAH. The bulk electrolysis solution was purged with CO_2 for 10 minutes prior to electrolysis. Gas analysis for bulk electrolysis experiments were performed using one ml sample injection volume on a Hewlett Packard 7890A Series gas chromatograph with two molsieve columns (30 m x 0.53 mm ID x 25 μm film). The one ml injection was split to two columns, one with N_2 as the carrier gas and one with He carrier gas, in order to quantify both CO and H_2 simultaneously in each run.

Infrared Spectroelectrochemistry (IR-SEC). The design of the IR spectroelectrochemical cell used for the manganese catalyst studies has been reported previously by our group.[30] IR spectral changes accompanying thin-layer bulk electrolyses were measured using a flow-through spectroelectrochemical cell. All spectroelectrochemical experiments were carried out in a 0.1 M TBAH solution using acetonitrile and all solutions were prepared under an atmosphere of dry nitrogen in a glove box. Blank acetonitrile solutions with 0.1 M TBAH were used for the FTIR solvent subtractions. A Pine Instrument Company Model AFCBP1 bipotentiostat was used to affect and monitor thin layer bulk electrolysis. The IR spectra were acquired using a Bruker Equinox 55 spectrometer. For the CO_2 experiments, CO_2 was bubbled through the catalyst solution for 10 minutes prior to injection into the SEC cell.

X-ray crystallographic studies. The single crystal X-ray diffraction studies were carried out on a Bruker Kappa APEX-II CCD diffractometer equipped with Mo Kα radiation (λ = 0.71073 Å) or a Bruker Kappa APEX CCD diffractometer equipped with Cu Kα radiation (λ = 1.54184 Å). The crystals were mounted on a Cryoloop with Paratone oil and data were collected under a nitrogen gas stream at 100(2) K using ω and ϕ scans. Data was integrated using the Bruker SAINT software program and scaled using the SADABS software program. Solution by direct methods (SHELXS) produced a complete phasing model consistent with the proposed structure. All non-hydrogen atoms were refined anisotropically by full-matrix least-squares (SHELXL-

97).[31] All hydrogen atoms were placed using a riding model. Their positions were constrained relative to their parent atom using the appropriate HFIX command in SHELXL-97. Crystallographic data are summarized in Table 5-1 in the appendix.

Note: The material in this chapter is unpublished work and was performed in collaboration with Eric E. Benson and Matthew D. Sampson.

5.5 References

1. Ibrahim H, Ilinca A, Perron J (2008) Energy storage systems—Characteristics and comparisons. *Renew. Sust. Energ. Rev.* 12(5):1221-1250.

2. International Panel on Climate Change (2005) *Carbon Dioxide Capture and Storage, Summary for Policy Makers*, Working Group III.

3. Zeman F (2007) Energy and Material Balance of CO2 Capture from Ambient Air. *Environ. Sci. Technol.* 41(21):7558-7563.

4. Stolaroff JK, Keith DW, Lowry GV (2008) Carbon Dioxide Capture from Atmospheric Air Using Sodium Hydroxide Spray. *Environ. Sci. Technol.* 42(8):2728-2735.

5. Yu KMK, Curcic I, Gabriel J, Tsang SCE (2008) Recent Advances in CO_2 Capture and Utilization. *ChemSusChem* 1(11):893-899.

6. Bhown AS, Freeman BC (2011) Analysis and Status of Post-Combustion Carbon Dioxide Capture Technologies. *Environ. Sci. Technol.* 45(20):8624-8632.

7. Wang T, Lackner KS, Wright A (2011) Moisture Swing Sorbent for Carbon Dioxide Capture from Ambient Air. *Environ. Sci. Technol.* 45(15):6670-6675.

8. Bernatis PR, Miedaner A, Haltiwanger RC, DuBois DL (1994) Exclusion of Six-Coordinate Intermediates in the Electrochemical Reduction of CO_2 Catalyzed by [Pd(triphosphine)(CH_3CN)]$(BF_4)_2$ Complexes. *Organometallics* 13(12):4835-4843.

9. DuBois DL, Miedaner A, Haltiwanger RC (1991) Electrochemical reduction of carbon dioxide catalyzed by [Pd(triphosphine)(solvent)]$(BF_4)_2$ complexes: synthetic and mechanistic studies. *J. Am. Chem. Soc.* 113(23):8753-8764.

10. Raebiger JW, *et al.* (2006) Electrochemical Reduction of CO_2 to CO Catalyzed by a Bimetallic Palladium Complex. *Organometallics* 25(14):3345-3351.

11. Steffey BD, Curtis CJ, DuBois DL (1995) Electrochemical Reduction of CO_2 Catalyzed by a Dinuclear Palladium Complex Containing a Bridging Hexaphosphine Ligand: Evidence for Cooperativity. *Organometallics* 14(10):4937-4943.

12. Steffey BD, *et al.* (1994) Synthesis and Characterization of Palladium Complexes Containing Tridentate Ligands with PXP (X = C, N, O, S, As) Donor Sets and Their Evaluation as Electrochemical CO_2 Reduction Catalysts. *Organometallics* 13(12):4844-4855.

13. Tanaka K, Ooyama D (2002) Multi-electron reduction of CO_2 via Ru-CO_2, -C(O)OH, -CO, -CHO, and -CH_2OH species. *Coord. Chem. Rev.* 226(1-2):211-218.

14. Slater S, Wagenknecht JH (1984) Electrochemical reduction of carbon dioxide catalyzed by Rh(diphos)$_2$Cl. *J. Am. Chem. Soc.* 106(18):5367-5368.

15. Hawecker J, Lehn JM, Ziessel R (1984) Electrocatalytic reduction of carbon dioxide mediated by Re(bipy)(CO)$_3$Cl (bipy = 2,2'-bipyridine). *J. Chem. Soc., Chem. Commun.* (6):328-330.

16. Kumar B, Smieja JM, Kubiak CP (2010) Photoreduction of CO_2 on p-type Silicon Using Re(bipy-*t*Bu)(CO)$_3$Cl: Photovoltages Exceeding 600 mV for the Selective Reduction of CO_2 to CO. *J Phys. Chem. C* 114(33):14220-14223.

17. Smieja JM, Kubiak CP (2010) Re(bipy-*t*Bu)(CO)$_3$Cl−improved Catalytic Activity for Reduction of Carbon Dioxide: IR-Spectroelectrochemical and Mechanistic Studies. *Inorg. Chem.* 49(20):9283-9289.

18. Sullivan BP, Bolinger CM, Conrad D, Vining WJ, Meyer TJ (1985) One- and two-electron pathways in the electrocatalytic reduction of CO_2 by *fac*-Re(bpy)(CO)$_3$Cl (bpy = 2,2'-bipyridine). *J. Chem. Soc., Chem. Commun.* (20):1414-1416.

19. Kumar B, Smieja JM, Sasayama AF, Kubiak CP (2012) Tunable, light-assisted co-generation of CO and H_2 from CO_2 and H_2O by Re(bipy-*t*Bu)(CO)$_3$Cl and p-Si in non-aqueous medium. *Chem. Commun.* 48(2):272-274.

20. Smieja JM, *et al.* (2012) Artificial photosynthesis of CO: Kinetic and structural studies, origins of selectivity, and importance of interfacial charge transfer. *PNAS* In Press.

21. *CRC Handbook of Chemistry and Physics* (2011-2012) W.M. Haynes (Ed.) (CRC Press, Boca Raton, FL) p 14.18.

22. Bourrez M, Molton F, Chardon-Noblat S, Deronzier A (2011) [Mn(bipyridyl)(CO)$_3$Br]: An Abundant Metal Carbonyl Complex as Efficient Electrocatalyst for CO_2 Reduction. *Angew. Chem. Int. Ed.* 50(42):9903-9906.

23. Staal LH, Oskam A, Vrieze K (1979) The syntheses and coordination properties of $M(CO)_3X(DAB)$ (M = Mn, Re; X = Cl, Br, I; DAB = 1,4-diazabutadiene). *J. Organomet. Chem.* 170(2):235-245.

24. Wang J (2006) *Analytical Electrochemistry* (John Wiley & Sons, Inc., Hoboken, New Jersey) Third Ed.

25. Addison AW, Rao TN, Reedijk J, van Rijn J, Verschoor GC (1984) Synthesis, structure, and spectroscopic properties of copper(II) compounds containing nitrogen-sulphur donor ligands; the crystal and molecular structure of aqua[1,7-bis(N-methylbenzimidazol-2[prime or minute]-yl)-2,6-dithiaheptane]copper(II) perchlorate. *J. Chem. Soc., Dalton Trans.* (7):1349-1356.

26. Johnson FPA, George MW, Hartl F, Turner JJ (1996) Electrocatalytic Reduction of CO_2 Using the Complexes $[Re(bpy)(CO)_3L]n$ (n = +1, L = $P(OEt)_3$, CH_3CN; n = 0, L = Cl^-, OTf^-; bpy = 2,2‘-Bipyridine; OTf^- = CF_3SO_3) as Catalyst Precursors: Infrared Spectroelectrochemical Investigation. *Organometallics* 15(15):3374-3387.

27. Hartl F, *et al.* (2003) Electronic Properties of 4,4‘,5,5‘-Tetramethyl-2,2‘-biphosphinine (tmbp) in the Redox Series *fac*-$[Mn(Br)(CO)_3(tmbp)]$, $[Mn(CO)_3(tmbp)]_2$, and $[Mn(CO)_3(tmbp)]^-$: Crystallographic, Spectroelectrochemical, and DFT Computational Study. *Inorg. Chem.* 42(14):4442-4455.

28. Gore-Randall E, Irwin M, Denning MS, Goicoechea JM (2009) Synthesis and Characterization of Alkali-Metal Salts of 2,2′- and 2,4′-Bipyridyl Radicals and Dianions. *Inorg. Chem.* 48(17):8304-8316.

29. Schwindt MA, Lejon T, Hegedus LS (1990) Improved synthesis of (aminocarbene)chromium(0) complexes with use of C_8K-generated $[Cr(CO)_5]^{2-}$. Multivariant optimization of an organometallic reaction. *Organometallics* 9(10):2814-2819.

30. Zavarine IS, Kubiak CP (2001) A versatile variable temperature thin layer reflectance spectroelectrochemical cell. *J. Electroanal. Chem.* 495(2):106-109.

31. Sheldrick G (2008) A short history of SHELX. *Acta Crystallogr. Sect. A* 64(1):112-122.

5.6 Appendix

Table 5-1. Crystal data and structure refinement for Mn(bipy-*t*Bu)$(CO)_3$Br.

Identification code	eb_111026mo_0m	
Empirical formula	C21 H24 Br Mn N2 O3	
Formula weight	487.27	
Temperature	100(2) K	
Wavelength	0.71073 Å	
Crystal system	Monoclinic	
Space group	P2(1)/n	
Unit cell dimensions	a = 13.5528(5) Å	α= 90°.
	b = 17.1546(6) Å	β= 96.8790(10)°.
	c = 19.1899(6) Å	γ = 90°.
Volume	4429.4(3) $Å^3$	
Z	8	
Density (calculated)	1.461 Mg/m^3	
Absorption coefficient	2.423 mm^{-1}	
F(000)	1984	
Crystal size	0.10 x 0.05 x 0.05 mm^3	
Theta range for data collection	2.11 to 31.78°.	
Index ranges	-19<=h<=19, -25<=k<=23, -22<=l<=28	
Reflections collected	45311	
Independent reflections	13529 [R(int) = 0.0384]	
Completeness to theta = 25.00°	99.9 %	
Absorption correction	Semi-empirical from equivalents	
Max. and min. transmission	0.8885 and 0.7937	
Refinement method	Full-matrix least-squares on F^2	
Data / restraints / parameters	13529 / 0 / 517	
Goodness-of-fit on F^2	1.079	
Final R indices [I>2sigma(I)]	R1 = 0.0407, wR2 = 0.1031	
R indices (all data)	R1 = 0.0617, wR2 = 0.1103	
Largest diff. peak and hole	0.866 and -0.716 e.$Å^{-3}$	

Table 5-2. Bond lengths [Å] and angles [°] for Mn(bipy-*t*Bu)$(CO)_3$Br.

Br(1)-Mn(1)	2.5101(5)	C(4)-C(5)	1.386(3)
Br(2)-Mn(2)	2.5234(5)	C(4)-H(4)	0.9500
Mn(1)-C(3)	1.806(3)	C(5)-C(6)	1.397(4)
Mn(1)-C(2)	1.813(3)	C(5)-H(5)	0.9500
Mn(1)-C(1)	1.848(3)	C(6)-C(7)	1.394(3)
Mn(1)-N(2)	2.040(2)	C(6)-C(14)	1.531(3)
Mn(1)-N(1)	2.045(2)	C(7)-C(8)	1.397(3)
Mn(2)-C(23)	1.810(3)	C(7)-H(7)	0.9500
Mn(2)-C(24)	1.815(3)	C(8)-C(9)	1.480(3)
Mn(2)-C(22)	1.848(3)	C(9)-C(10)	1.388(3)
Mn(2)-N(4)	2.038(2)	C(10)-C(11)	1.394(3)
Mn(2)-N(3)	2.046(2)	C(10)-H(10)	0.9500
O(1)-C(1)	1.091(3)	C(11)-C(12)	1.395(3)
O(2)-C(2)	1.144(3)	C(11)-C(18)	1.526(3)
O(3)-C(3)	1.141(3)	C(12)-C(13)	1.378(4)
O(4)-C(22)	1.082(3)	C(12)-H(12)	0.9500
O(5)-C(23)	1.147(3)	C(13)-H(13)	0.9500
O(6)-C(24)	1.145(3)	C(14)-C(17)	1.530(4)
N(1)-C(4)	1.344(3)	C(14)-C(16)	1.534(4)
N(1)-C(8)	1.349(3)	C(14)-C(15)	1.536(4)
N(2)-C(13)	1.343(3)	C(15)-H(15A)	0.9800
N(2)-C(9)	1.357(3)	C(15)-H(15B)	0.9800
N(3)-C(25)	1.344(3)	C(15)-H(15C)	0.9800
N(3)-C(29)	1.351(3)	C(16)-H(16A)	0.9800
N(4)-C(34)	1.342(3)	C(16)-H(16B)	0.9800
N(4)-C(30)	1.349(3)	C(16)-H(16C)	0.9800

Table 5-2 (Cont.)

C(17)-H(17A)	0.9800	C(32)-C(33)	1.397(3)
C(17)-H(17B)	0.9800	C(32)-C(39)	1.520(3)
C(17)-H(17C)	0.9800	C(33)-C(34)	1.381(3)
C(18)-C(19)	1.533(4)	C(33)-H(33)	0.9500
C(18)-C(21)	1.536(4)	C(34)-H(34)	0.9500
C(18)-C(20)	1.536(4)	C(35)-C(37)	1.524(4)
C(19)-H(19A)	0.9800	C(35)-C(38)	1.526(4)
C(19)-H(19B)	0.9800	C(35)-C(36)	1.545(4)
C(19)-H(19C)	0.9800	C(36)-H(36A)	0.9800
C(20)-H(20A)	0.9800	C(36)-H(36B)	0.9800
C(20)-H(20B)	0.9800	C(36)-H(36C)	0.9800
C(20)-H(20C)	0.9800	C(37)-H(37A)	0.9800
C(21)-H(21A)	0.9800	C(37)-H(37B)	0.9800
C(21)-H(21B)	0.9800	C(37)-H(37C)	0.9800
C(21)-H(21C)	0.9800	C(38)-H(38A)	0.9800
C(25)-C(26)	1.386(3)	C(38)-H(38B)	0.9800
C(25)-H(25)	0.9500	C(38)-H(38C)	0.9800
C(26)-C(27)	1.397(3)	C(39)-C(42)	1.537(4)
C(26)-H(26)	0.9500	C(39)-C(40)	1.538(4)
C(27)-C(28)	1.397(3)	C(39)-C(41)	1.539(4)
C(27)-C(35)	1.531(3)	C(40)-H(40A)	0.9800
C(28)-C(29)	1.398(3)	C(40)-H(40B)	0.9800
C(28)-H(28)	0.9500	C(40)-H(40C)	0.9800
C(29)-C(30)	1.477(3)	C(41)-H(41A)	0.9800
C(30)-C(31)	1.392(3)	C(41)-H(41B)	0.9800
C(31)-C(32)	1.399(3)	C(41)-H(41C)	0.9800
C(31)-H(31)	0.9500	C(42)-H(42A)	0.9800

Table 5-2 (Cont.)

C(42)-H(42B)	0.9800	N(4)-Mn(2)-N(3)	78.48(8)
C(42)-H(42C)	0.9800	C(23)-Mn(2)-Br(2)	91.66(11)
		C(24)-Mn(2)-Br(2)	85.01(9)
C(3)-Mn(1)-C(2)	87.44(12)	C(22)-Mn(2)-Br(2)	177.65(7)
C(3)-Mn(1)-C(1)	90.02(11)	N(4)-Mn(2)-Br(2)	89.14(6)
C(2)-Mn(1)-C(1)	90.84(11)	N(3)-Mn(2)-Br(2)	85.23(6)
C(3)-Mn(1)-N(2)	96.98(10)	C(4)-N(1)-C(8)	117.7(2)
C(2)-Mn(1)-N(2)	175.37(10)	C(4)-N(1)-Mn(1)	125.56(17)
C(1)-Mn(1)-N(2)	90.54(9)	C(8)-N(1)-Mn(1)	116.65(16)
C(3)-Mn(1)-N(1)	171.40(10)	C(13)-N(2)-C(9)	117.4(2)
C(2)-Mn(1)-N(1)	97.01(10)	C(13)-N(2)-Mn(1)	125.70(17)
C(1)-Mn(1)-N(1)	97.24(9)	C(9)-N(2)-Mn(1)	116.76(16)
N(2)-Mn(1)-N(1)	78.42(8)	C(25)-N(3)-C(29)	117.3(2)
C(3)-Mn(1)-Br(1)	85.66(9)	C(25)-N(3)-Mn(2)	125.80(17)
C(2)-Mn(1)-Br(1)	88.90(9)	C(29)-N(3)-Mn(2)	116.01(16)
C(1)-Mn(1)-Br(1)	175.68(7)	C(34)-N(4)-C(30)	117.6(2)
N(2)-Mn(1)-Br(1)	90.06(6)	C(34)-N(4)-Mn(2)	125.71(17)
N(1)-Mn(1)-Br(1)	87.07(6)	C(30)-N(4)-Mn(2)	116.70(16)
C(23)-Mn(2)-C(24)	87.04(12)	O(1)-C(1)-Mn(1)	175.7(2)
C(23)-Mn(2)-C(22)	86.32(13)	O(2)-C(2)-Mn(1)	177.3(2)
C(24)-Mn(2)-C(22)	93.69(11)	O(3)-C(3)-Mn(1)	177.5(2)
C(23)-Mn(2)-N(4)	177.60(11)	N(1)-C(4)-C(5)	123.1(2)
C(24)-Mn(2)-N(4)	95.28(10)	N(1)-C(4)-H(4)	118.4
C(22)-Mn(2)-N(4)	92.94(9)	C(5)-C(4)-H(4)	118.4
C(23)-Mn(2)-N(3)	99.33(10)	C(4)-C(5)-C(6)	120.2(2)
C(24)-Mn(2)-N(3)	168.49(11)	C(4)-C(5)-H(5)	119.9
C(22)-Mn(2)-N(3)	96.27(9)	C(6)-C(5)-H(5)	119.9

Table 5-2 (Cont.)

C(7)-C(6)-C(5)	116.4(2)	C(17)-C(14)-C(15)	109.3(2)
C(7)-C(6)-C(14)	123.5(2)	C(6)-C(14)-C(15)	108.8(2)
C(5)-C(6)-C(14)	120.1(2)	C(16)-C(14)-C(15)	109.1(2)
C(6)-C(7)-C(8)	120.6(2)	C(14)-C(15)-H(15A)	109.5
C(6)-C(7)-H(7)	119.7	C(14)-C(15)-H(15B)	109.5
C(8)-C(7)-H(7)	119.7	H(15A)-C(15)-H(15B)	109.5
N(1)-C(8)-C(7)	122.0(2)	C(14)-C(15)-H(15C)	109.5
N(1)-C(8)-C(9)	114.3(2)	H(15A)-C(15)-H(15C)	109.5
C(7)-C(8)-C(9)	123.7(2)	H(15B)-C(15)-H(15C)	109.5
N(2)-C(9)-C(10)	122.1(2)	C(14)-C(16)-H(16A)	109.5
N(2)-C(9)-C(8)	113.7(2)	C(14)-C(16)-H(16B)	109.5
C(10)-C(9)-C(8)	124.2(2)	H(16A)-C(16)-H(16B)	109.5
C(9)-C(10)-C(11)	120.6(2)	C(14)-C(16)-H(16C)	109.5
C(9)-C(10)-H(10)	119.7	H(16A)-C(16)-H(16C)	109.5
C(11)-C(10)-H(10)	119.7	H(16B)-C(16)-H(16C)	109.5
C(10)-C(11)-C(12)	116.4(2)	C(14)-C(17)-H(17A)	109.5
C(10)-C(11)-C(18)	123.7(2)	C(14)-C(17)-H(17B)	109.5
C(12)-C(11)-C(18)	119.9(2)	H(17A)-C(17)-H(17B)	109.5
C(13)-C(12)-C(11)	120.3(2)	C(14)-C(17)-H(17C)	109.5
C(13)-C(12)-H(12)	119.9	H(17A)-C(17)-H(17C)	109.5
C(11)-C(12)-H(12)	119.9	H(17B)-C(17)-H(17C)	109.5
N(2)-C(13)-C(12)	123.2(2)	C(11)-C(18)-C(19)	111.8(2)
N(2)-C(13)-H(13)	118.4	C(11)-C(18)-C(21)	109.5(2)
C(12)-C(13)-H(13)	118.4	C(19)-C(18)-C(21)	109.0(2)
C(17)-C(14)-C(6)	112.0(2)	C(11)-C(18)-C(20)	108.7(2)
C(17)-C(14)-C(16)	108.8(2)	C(19)-C(18)-C(20)	108.6(2)
C(6)-C(14)-C(16)	108.8(2)	C(21)-C(18)-C(20)	109.2(2)

Table 5-2 (Cont.)

C(18)-C(19)-H(19A)	109.5	C(26)-C(27)-C(28)	116.3(2)
C(18)-C(19)-H(19B)	109.5	C(26)-C(27)-C(35)	120.9(2)
H(19A)-C(19)-H(19B)	109.5	C(28)-C(27)-C(35)	122.8(2)
C(18)-C(19)-H(19C)	109.5	C(27)-C(28)-C(29)	120.3(2)
H(19A)-C(19)-H(19C)	109.5	C(27)-C(28)-H(28)	119.8
H(19B)-C(19)-H(19C)	109.5	C(29)-C(28)-H(28)	119.8
C(18)-C(20)-H(20A)	109.5	N(3)-C(29)-C(28)	122.5(2)
C(18)-C(20)-H(20B)	109.5	N(3)-C(29)-C(30)	114.2(2)
H(20A)-C(20)-H(20B)	109.5	C(28)-C(29)-C(30)	123.3(2)
C(18)-C(20)-H(20C)	109.5	N(4)-C(30)-C(31)	122.1(2)
H(20A)-C(20)-H(20C)	109.5	N(4)-C(30)-C(29)	114.0(2)
H(20B)-C(20)-H(20C)	109.5	C(31)-C(30)-C(29)	123.9(2)
C(18)-C(21)-H(21A)	109.5	C(30)-C(31)-C(32)	120.7(2)
C(18)-C(21)-H(21B)	109.5	C(30)-C(31)-H(31)	119.7
H(21A)-C(21)-H(21B)	109.5	C(32)-C(31)-H(31)	119.7
C(18)-C(21)-H(21C)	109.5	C(33)-C(32)-C(31)	116.0(2)
H(21A)-C(21)-H(21C)	109.5	C(33)-C(32)-C(39)	120.3(2)
H(21B)-C(21)-H(21C)	109.5	C(31)-C(32)-C(39)	123.7(2)
O(4)-C(22)-Mn(2)	176.2(2)	C(34)-C(33)-C(32)	120.4(2)
O(5)-C(23)-Mn(2)	173.0(3)	C(34)-C(33)-H(33)	119.8
O(6)-C(24)-Mn(2)	176.9(3)	C(32)-C(33)-H(33)	119.8
N(3)-C(25)-C(26)	123.1(2)	N(4)-C(34)-C(33)	123.2(2)
N(3)-C(25)-H(25)	118.4	N(4)-C(34)-H(34)	118.4
C(26)-C(25)-H(25)	118.4	C(33)-C(34)-H(34)	118.4
C(25)-C(26)-C(27)	120.4(2)	C(37)-C(35)-C(38)	109.7(3)
C(25)-C(26)-H(26)	119.8	C(37)-C(35)-C(27)	112.0(2)
C(27)-C(26)-H(26)	119.8	C(38)-C(35)-C(27)	108.6(2)

Table 5-2 (Cont.)

C(37)-C(35)-C(36)	108.1(2)	C(42)-C(39)-C(40)	108.6(2)
C(38)-C(35)-C(36)	109.0(2)	C(32)-C(39)-C(41)	108.1(2)
C(27)-C(35)-C(36)	109.5(2)	C(42)-C(39)-C(41)	108.5(2)
C(35)-C(36)-H(36A)	109.5	C(40)-C(39)-C(41)	109.5(2)
C(35)-C(36)-H(36B)	109.5	C(39)-C(40)-H(40A)	109.5
H(36A)-C(36)-H(36B)	109.5	C(39)-C(40)-H(40B)	109.5
C(35)-C(36)-H(36C)	109.5	H(40A)-C(40)-H(40B)	109.5
H(36A)-C(36)-H(36C)	109.5	C(39)-C(40)-H(40C)	109.5
H(36B)-C(36)-H(36C)	109.5	H(40A)-C(40)-H(40C)	109.5
C(35)-C(37)-H(37A)	109.5	H(40B)-C(40)-H(40C)	109.5
C(35)-C(37)-H(37B)	109.5	C(39)-C(41)-H(41A)	109.5
H(37A)-C(37)-H(37B)	109.5	C(39)-C(41)-H(41B)	109.5
C(35)-C(37)-H(37C)	109.5	H(41A)-C(41)-H(41B)	109.5
H(37A)-C(37)-H(37C)	109.5	C(39)-C(41)-H(41C)	109.5
H(37B)-C(37)-H(37C)	109.5	H(41A)-C(41)-H(41C)	109.5
C(35)-C(38)-H(38A)	109.5	H(41B)-C(41)-H(41C)	109.5
C(35)-C(38)-H(38B)	109.5	C(39)-C(42)-H(42A)	109.5
H(38A)-C(38)-H(38B)	109.5	C(39)-C(42)-H(42B)	109.5
C(35)-C(38)-H(38C)	109.5	H(42A)-C(42)-H(42B)	109.5
H(38A)-C(38)-H(38C)	109.5	C(39)-C(42)-H(42C)	109.5
H(38B)-C(38)-H(38C)	109.5	H(42A)-C(42)-H(42C)	109.5
C(32)-C(39)-C(42)	110.7(2)	H(42B)-C(42)-H(42C)	109.5
C(32)-C(39)-C(40)	111.4(2)		

Table 5-3. Crystal data and structure refinement for [Mn(bipy-*t*Bu)$(CO)_3$][K(18-crown-6)].

Identification code	eb_111019_0m	
Empirical formula	C74 H112 K2 Mn2 N4 O20	
Formula weight	1565.76	
Temperature	100(2) K	
Wavelength	1.54178 Å	
Crystal system	Monoclinic	
Space group	P2(1)/n	
Unit cell dimensions	a = 18.2559(4) Å	α = 90°.
	b = 18.4759(4) Å	β = 98.5560(10)°.
	c = 24.2973(5) Å	γ = 90°.
Volume	8104.1(3) $Å^3$	
Z	4	
Density (calculated)	1.283 Mg/m^3	
Absorption coefficient	4.023 mm^{-1}	
F(000)	3328	
Crystal size	0.10 x 0.10 x 0.01 mm^3	
Theta range for data collection	2.83 to 50.00°.	
Index ranges	-13<=h<=18, -18<=k<=18, -24<=l<=24	
Reflections collected	28572	
Independent reflections	8004 [R(int) = 0.0488]	
Completeness to theta = 50.00°	96.1 %	
Absorption correction	Semi-empirical from equivalents	
Max. and min. transmission	0.9609 and 0.6891	
Refinement method	Full-matrix least-squares on F^2	
Data / restraints / parameters	8004 / 0 / 957	
Goodness-of-fit on F^2	1.026	
Final R indices [I>2sigma(I)]	R1 = 0.0733, wR2 = 0.1941	
R indices (all data)	R1 = 0.1060, wR2 = 0.2255	
Largest diff. peak and hole	1.401 and -0.301 $e.Å^{-3}$	

Table 5-4. Bond lengths [Å] and angles [°] for [Mn(bipy-*t*Bu)(CO)$_3$][K(18-crown-6)].

Mn(1)-C(3A)	1.66(3)	K(2)-O(14)	2.820(5)
Mn(1)-C(1)	1.746(8)	K(2)-O(17)	2.843(5)
Mn(1)-C(2A)	1.796(13)	K(2)-O(5)	2.846(6)
Mn(1)-C(2B)	1.85(3)	K(2)-O(19)	2.871(5)
Mn(1)-N(2)	1.970(6)	O(1)-C(1)	1.203(9)
Mn(1)-C(3B)	1.98(6)	O(2A)-C(2A)	1.168(13)
Mn(1)-N(1)	1.987(6)	O(2B)-C(2B)	1.16(3)
Mn(2)-C(24)	1.765(9)	O(3A)-C(3A)	1.22(3)
Mn(2)-C(22)	1.773(9)	O(3B)-C(3B)	1.21(7)
Mn(2)-C(23)	1.785(8)	O(4)-C(22)	1.168(9)
Mn(2)-N(3)	1.980(5)	O(5)-C(23)	1.183(9)
Mn(2)-N(4)	1.992(5)	O(6)-C(24)	1.188(10)
K(1)-O(13)	2.698(6)	O(7)-C(44)	1.412(8)
K(1)-O(8)	2.742(5)	O(7)-C(45)	1.427(8)
K(1)-O(11)	2.785(5)	O(8)-C(47)	1.417(8)
K(1)-O(9)	2.791(5)	O(8)-C(46)	1.426(8)
K(1)-O(12)	2.814(5)	O(9)-C(49)	1.411(8)
K(1)-O(7)	2.836(5)	O(9)-C(48)	1.437(8)
K(1)-O(10)	2.895(5)	O(10)-C(51)	1.425(8)
K(1)-O(2A)	3.012(9)	O(10)-C(50)	1.426(8)
K(1)-C(55A)	3.52(6)	O(11)-C(53)	1.416(8)
K(1)-C(55B)	3.53(2)	O(11)-C(52)	1.441(9)
K(2)-O(20)	2.709(6)	O(12)-C(43)	1.399(8)
K(2)-O(15)	2.739(5)	O(12)-C(54)	1.429(8)
K(2)-O(18)	2.798(5)	O(13)-C(55B)	1.31(2)
K(2)-O(16)	2.817(5)	O(13)-C(58B)	1.380(14)

Table 5-4 (Cont.)

O(13)-C(55A)	1.40(6)	C(5)-C(6)	1.405(10)
O(13)-C(58A)	1.65(5)	C(5)-H(5)	0.9500
O(14)-C(60)	1.413(8)	C(6)-C(7)	1.360(10)
O(14)-C(61)	1.432(8)	C(6)-C(14)	1.526(10)
O(15)-C(63)	1.420(8)	C(7)-C(8)	1.413(9)
O(15)-C(62)	1.421(9)	C(7)-H(7)	0.9500
O(16)-C(64)	1.424(8)	C(8)-C(9)	1.414(9)
O(16)-C(65)	1.433(8)	C(9)-C(10)	1.427(10)
O(17)-C(67)	1.426(8)	C(10)-C(11)	1.346(10)
O(17)-C(66)	1.433(8)	C(10)-H(10)	0.9500
O(18)-C(69)	1.405(8)	C(11)-C(12)	1.443(10)
O(18)-C(68)	1.428(8)	C(11)-C(18)	1.519(10)
O(19)-C(59)	1.408(8)	C(12)-C(13)	1.367(10)
O(19)-C(70)	1.417(8)	C(12)-H(12)	0.9500
O(20)-C(71)	1.369(11)	C(13)-H(13)	0.9500
O(20)-C(74A)	1.438(13)	C(14)-C(15)	1.515(10)
O(20)-C(74B)	1.62(4)	C(14)-C(17)	1.536(11)
N(1)-C(4)	1.350(9)	C(14)-C(16)	1.544(10)
N(1)-C(8)	1.372(9)	C(15)-H(15A)	0.9800
N(2)-C(13)	1.366(9)	C(15)-H(15B)	0.9800
N(2)-C(9)	1.389(8)	C(15)-H(15C)	0.9800
N(3)-C(25)	1.376(9)	C(16)-H(16A)	0.9800
N(3)-C(29)	1.395(9)	C(16)-H(16B)	0.9800
N(4)-C(34)	1.360(8)	C(16)-H(16C)	0.9800
N(4)-C(30)	1.385(9)	C(17)-H(17A)	0.9800
C(4)-C(5)	1.350(10)	C(17)-H(17B)	0.9800
C(4)-H(4)	0.9500	C(17)-H(17C)	0.9800

Table 5-4 (Cont.)

C(18)-C(21)	1.529(10)	C(33)-H(33)	0.9500
C(18)-C(19)	1.530(12)	C(34)-H(34)	0.9500
C(18)-C(20)	1.548(12)	C(35)-C(38)	1.518(11)
C(19)-H(19A)	0.9800	C(35)-C(36)	1.519(10)
C(19)-H(19B)	0.9800	C(35)-C(37)	1.527(10)
C(19)-H(19C)	0.9800	C(36)-H(36A)	0.9800
C(20)-H(20A)	0.9800	C(36)-H(36B)	0.9800
C(20)-H(20B)	0.9800	C(36)-H(36C)	0.9800
C(20)-H(20C)	0.9800	C(37)-H(37A)	0.9800
C(21)-H(21A)	0.9800	C(37)-H(37B)	0.9800
C(21)-H(21B)	0.9800	C(37)-H(37C)	0.9800
C(21)-H(21C)	0.9800	C(38)-H(38A)	0.9800
C(25)-C(26)	1.351(10)	C(38)-H(38B)	0.9800
C(25)-H(25)	0.9500	C(38)-H(38C)	0.9800
C(26)-C(27)	1.437(10)	C(39)-C(40)	1.512(11)
C(26)-H(26)	0.9500	C(39)-C(41)	1.542(10)
C(27)-C(28)	1.361(9)	C(39)-C(42)	1.552(10)
C(27)-C(35)	1.514(10)	C(40)-H(40A)	0.9800
C(28)-C(29)	1.403(10)	C(40)-H(40B)	0.9800
C(28)-H(28)	0.9500	C(40)-H(40C)	0.9800
C(29)-C(30)	1.406(10)	C(41)-H(41A)	0.9800
C(30)-C(31)	1.430(10)	C(41)-H(41B)	0.9800
C(31)-C(32)	1.363(10)	C(41)-H(41C)	0.9800
C(31)-H(31)	0.9500	C(42)-H(42A)	0.9800
C(32)-C(33)	1.428(10)	C(42)-H(42B)	0.9800
C(32)-C(39)	1.507(10)	C(42)-H(42C)	0.9800
C(33)-C(34)	1.349(10)	C(43)-C(44)	1.493(10)

Table 5-4 (Cont.)

C(43)-H(43A)	0.9900	C(54)-H(54A)	0.9900
C(43)-H(43B)	0.9900	C(54)-H(54B)	0.9900
C(44)-H(44A)	0.9900	C(55A)-C(56A)	1.81(7)
C(44)-H(44B)	0.9900	C(55A)-H(55A)	0.9900
C(45)-C(46)	1.482(10)	C(55A)-H(55B)	0.9900
C(45)-H(45A)	0.9900	C(55B)-C(56B)	1.51(2)
C(45)-H(45B)	0.9900	C(55B)-C(58A)	1.96(5)
C(46)-H(46A)	0.9900	C(55B)-H(55C)	0.9900
C(46)-H(46B)	0.9900	C(55B)-H(55D)	0.9900
C(47)-C(48)	1.509(9)	C(56A)-C(57)	1.21(5)
C(47)-H(47A)	0.9900	C(56A)-H(56A)	0.9900
C(47)-H(47B)	0.9900	C(56A)-H(56B)	0.9900
C(48)-H(48A)	0.9900	C(56B)-C(57)	1.546(17)
C(48)-H(48B)	0.9900	C(56B)-C(58A)	2.00(5)
C(49)-C(50)	1.507(9)	C(56B)-H(56C)	0.9900
C(49)-H(49A)	0.9900	C(56B)-H(56D)	0.9900
C(49)-H(49B)	0.9900	C(57)-C(58B)	1.402(16)
C(50)-H(50A)	0.9900	C(57)-C(58A)	1.43(5)
C(50)-H(50B)	0.9900	C(57)-H(57C)	0.9900
C(51)-C(52)	1.504(10)	C(57)-H(57D)	0.9900
C(51)-H(51A)	0.9900	C(57)-H(57A)	0.9900
C(51)-H(51B)	0.9900	C(57)-H(57B)	0.9900
C(52)-H(52A)	0.9900	C(58A)-H(58A)	0.9900
C(52)-H(52B)	0.9900	C(58A)-H(58B)	0.9900
C(53)-C(54)	1.495(10)	C(58B)-H(58C)	0.9900
C(53)-H(53A)	0.9900	C(58B)-H(58D)	0.9900
C(53)-H(53B)	0.9900	C(59)-C(60)	1.486(10)

Table 5-4 (Cont.)

C(59)-H(59A)	0.9900	C(70)-H(70A)	0.9900
C(59)-H(59B)	0.9900	C(70)-H(70B)	0.9900
C(60)-H(60A)	0.9900	C(71)-C(72)	1.438(13)
C(60)-H(60B)	0.9900	C(71)-H(71A)	0.9900
C(61)-C(62)	1.489(10)	C(71)-H(71B)	0.9900
C(61)-H(61A)	0.9900	C(72)-C(73A)	1.446(14)
C(61)-H(61B)	0.9900	C(72)-C(73B)	1.52(3)
C(62)-H(62A)	0.9900	C(72)-H(72C)	0.9900
C(62)-H(62B)	0.9900	C(72)-H(72D)	0.9900
C(63)-C(64)	1.486(10)	C(72)-H(72A)	0.9900
C(63)-H(63A)	0.9900	C(72)-H(72B)	0.9900
C(63)-H(63B)	0.9900	C(73A)-C(74A)	1.529(16)
C(64)-H(64A)	0.9900	C(73A)-H(73A)	0.9900
C(64)-H(64B)	0.9900	C(73A)-H(73B)	0.9900
C(65)-C(66)	1.498(9)	C(73B)-C(74B)	1.56(4)
C(65)-H(65A)	0.9900	C(73B)-H(73C)	0.9900
C(65)-H(65B)	0.9900	C(73B)-H(73D)	0.9900
C(66)-H(66A)	0.9900	C(74A)-H(74A)	0.9900
C(66)-H(66B)	0.9900	C(74A)-H(74B)	0.9900
C(67)-C(68)	1.500(10)	C(74B)-H(74C)	0.9900
C(67)-H(67A)	0.9900	C(74B)-H(74D)	0.9900
C(67)-H(67B)	0.9900		
C(68)-H(68A)	0.9900	C(3A)-Mn(1)-C(1)	86.0(8)
C(68)-H(68B)	0.9900	C(3A)-Mn(1)-C(2A)	104.2(15)
C(69)-C(70)	1.493(10)	C(1)-Mn(1)-C(2A)	89.2(5)
C(69)-H(69A)	0.9900	C(3A)-Mn(1)-C(2B)	66.8(18)
C(69)-H(69B)	0.9900	C(1)-Mn(1)-C(2B)	95.0(9)

Table 5-4 (Cont.)

C(2A)-Mn(1)-C(2B)	38.4(10)	O(13)-K(1)-O(11)	80.81(17)
C(3A)-Mn(1)-N(2)	143.3(14)	O(8)-K(1)-O(11)	168.43(15)
C(1)-Mn(1)-N(2)	94.9(3)	O(13)-K(1)-O(9)	76.61(17)
C(2A)-Mn(1)-N(2)	112.5(6)	O(8)-K(1)-O(9)	60.57(13)
C(2B)-Mn(1)-N(2)	149.0(12)	O(11)-K(1)-O(9)	118.50(15)
C(3A)-Mn(1)-C(3B)	17.5(16)	O(13)-K(1)-O(12)	97.13(18)
C(1)-Mn(1)-C(3B)	88.3(17)	O(8)-K(1)-O(12)	120.13(14)
C(2A)-Mn(1)-C(3B)	122(2)	O(11)-K(1)-O(12)	59.38(14)
C(2B)-Mn(1)-C(3B)	84(2)	O(9)-K(1)-O(12)	173.73(15)
N(2)-Mn(1)-C(3B)	125.8(19)	O(13)-K(1)-O(7)	86.3(2)
C(3A)-Mn(1)-N(1)	95.5(8)	O(8)-K(1)-O(7)	60.09(13)
C(1)-Mn(1)-N(1)	171.3(3)	O(11)-K(1)-O(7)	116.16(15)
C(2A)-Mn(1)-N(1)	98.7(5)	O(9)-K(1)-O(7)	118.42(14)
C(2B)-Mn(1)-N(1)	93.5(9)	O(12)-K(1)-O(7)	60.80(14)
N(2)-Mn(1)-N(1)	78.8(2)	O(13)-K(1)-O(10)	81.30(19)
C(3B)-Mn(1)-N(1)	90.7(16)	O(8)-K(1)-O(10)	120.87(14)
C(24)-Mn(2)-C(22)	91.3(4)	O(11)-K(1)-O(10)	60.10(13)
C(24)-Mn(2)-C(23)	88.9(4)	O(9)-K(1)-O(10)	60.36(13)
C(22)-Mn(2)-C(23)	97.2(4)	O(12)-K(1)-O(10)	118.86(14)
C(24)-Mn(2)-N(3)	93.0(3)	O(7)-K(1)-O(10)	167.48(15)
C(22)-Mn(2)-N(3)	139.7(3)	O(13)-K(1)-O(2A)	160.5(2)
C(23)-Mn(2)-N(3)	122.9(3)	O(8)-K(1)-O(2A)	75.80(18)
C(24)-Mn(2)-N(4)	171.7(3)	O(11)-K(1)-O(2A)	114.73(18)
C(22)-Mn(2)-N(4)	95.8(3)	O(9)-K(1)-O(2A)	103.7(2)
C(23)-Mn(2)-N(4)	94.6(3)	O(12)-K(1)-O(2A)	82.3(2)
N(3)-Mn(2)-N(4)	78.8(2)	O(7)-K(1)-O(2A)	76.4(2)
O(13)-K(1)-O(8)	87.91(17)	O(10)-K(1)-O(2A)	116.2(2)

Table 5-4 (Cont.)

O(13)-K(1)-C(55A)	21.3(11)	O(20)-K(2)-O(17)	81.12(19)
O(8)-K(1)-C(55A)	90.1(9)	O(15)-K(2)-O(17)	121.27(14)
O(11)-K(1)-C(55A)	78.4(9)	O(18)-K(2)-O(17)	61.04(13)
O(9)-K(1)-C(55A)	96.1(10)	O(16)-K(2)-O(17)	61.40(13)
O(12)-K(1)-C(55A)	77.7(10)	O(14)-K(2)-O(17)	167.49(14)
O(7)-K(1)-C(55A)	69.2(11)	O(20)-K(2)-O(5)	158.20(18)
O(10)-K(1)-C(55A)	98.3(11)	O(15)-K(2)-O(5)	78.54(15)
O(2A)-K(1)-C(55A)	145.4(12)	O(18)-K(2)-O(5)	115.49(15)
O(13)-K(1)-C(55B)	19.0(3)	O(16)-K(2)-O(5)	82.90(16)
O(8)-K(1)-C(55B)	98.6(3)	O(14)-K(2)-O(5)	99.74(16)
O(11)-K(1)-C(55B)	69.8(3)	O(17)-K(2)-O(5)	92.69(16)
O(9)-K(1)-C(55B)	95.6(3)	O(20)-K(2)-O(19)	97.22(16)
O(12)-K(1)-C(55B)	78.2(3)	O(15)-K(2)-O(19)	119.96(15)
O(7)-K(1)-C(55B)	78.4(4)	O(18)-K(2)-O(19)	58.30(13)
O(10)-K(1)-C(55B)	89.3(4)	O(16)-K(2)-O(19)	172.98(14)
O(2A)-K(1)-C(55B)	153.4(4)	O(14)-K(2)-O(19)	59.84(14)
C(55A)-K(1)-C(55B)	10.1(12)	O(17)-K(2)-O(19)	118.51(14)
O(20)-K(2)-O(15)	86.82(18)	O(5)-K(2)-O(19)	104.05(16)
O(20)-K(2)-O(18)	79.81(17)	C(2A)-O(2A)-K(1)	127.6(10)
O(15)-K(2)-O(18)	165.96(15)	C(23)-O(5)-K(2)	122.9(5)
O(20)-K(2)-O(16)	75.77(16)	C(44)-O(7)-C(45)	112.4(5)
O(15)-K(2)-O(16)	59.90(14)	C(44)-O(7)-K(1)	109.6(4)
O(18)-K(2)-O(16)	119.87(14)	C(45)-O(7)-K(1)	113.4(4)
O(20)-K(2)-O(14)	86.76(19)	C(47)-O(8)-C(46)	112.7(5)
O(15)-K(2)-O(14)	60.66(14)	C(47)-O(8)-K(1)	118.3(4)
O(18)-K(2)-O(14)	113.83(14)	C(46)-O(8)-K(1)	117.2(4)
O(16)-K(2)-O(14)	118.51(15)	C(49)-O(9)-C(48)	113.2(5)

Table 5-4 (Cont.)

C(49)-O(9)-K(1)	113.4(4)	C(64)-O(16)-C(65)	113.4(5)
C(48)-O(9)-K(1)	109.6(4)	C(64)-O(16)-K(2)	109.1(4)
C(51)-O(10)-C(50)	111.7(5)	C(65)-O(16)-K(2)	109.5(4)
C(51)-O(10)-K(1)	110.4(4)	C(67)-O(17)-C(66)	111.9(5)
C(50)-O(10)-K(1)	110.4(4)	C(67)-O(17)-K(2)	110.1(4)
C(53)-O(11)-C(52)	112.4(5)	C(66)-O(17)-K(2)	111.3(4)
C(53)-O(11)-K(1)	117.3(4)	C(69)-O(18)-C(68)	113.1(5)
C(52)-O(11)-K(1)	116.8(4)	C(69)-O(18)-K(2)	119.2(4)
C(43)-O(12)-C(54)	112.0(5)	C(68)-O(18)-K(2)	114.5(4)
C(43)-O(12)-K(1)	114.8(4)	C(59)-O(19)-C(70)	112.9(5)
C(54)-O(12)-K(1)	116.3(4)	C(59)-O(19)-K(2)	114.9(4)
C(55B)-O(13)-C(58B)	110.7(11)	C(70)-O(19)-K(2)	116.3(4)
C(55B)-O(13)-C(55A)	26(3)	C(71)-O(20)-C(74A)	107.3(8)
C(58B)-O(13)-C(55A)	99(2)	C(71)-O(20)-C(74B)	86.8(16)
C(55B)-O(13)-C(58A)	82.1(18)	C(74A)-O(20)-C(74B)	48.0(13)
C(58B)-O(13)-C(58A)	44.0(16)	C(71)-O(20)-K(2)	126.7(6)
C(55A)-O(13)-C(58A)	61(3)	C(74A)-O(20)-K(2)	121.5(6)
C(55B)-O(13)-K(1)	118.9(10)	C(74B)-O(20)-K(2)	109.5(10)
C(58B)-O(13)-K(1)	124.2(7)	C(4)-N(1)-C(8)	116.1(6)
C(55A)-O(13)-K(1)	114(3)	C(4)-N(1)-Mn(1)	126.6(5)
C(58A)-O(13)-K(1)	119.7(17)	C(8)-N(1)-Mn(1)	117.1(5)
C(60)-O(14)-C(61)	111.6(5)	C(13)-N(2)-C(9)	115.3(6)
C(60)-O(14)-K(2)	110.8(4)	C(13)-N(2)-Mn(1)	127.5(5)
C(61)-O(14)-K(2)	112.8(4)	C(9)-N(2)-Mn(1)	117.1(4)
C(63)-O(15)-C(62)	113.4(6)	C(25)-N(3)-C(29)	114.7(6)
C(63)-O(15)-K(2)	119.5(4)	C(25)-N(3)-Mn(2)	127.6(5)
C(62)-O(15)-K(2)	116.5(4)	C(29)-N(3)-Mn(2)	117.4(5)

Table 5-4 (Cont.)

C(34)-N(4)-C(30)	117.3(6)	C(11)-C(10)-H(10)	118.6
C(34)-N(4)-Mn(2)	126.4(5)	C(9)-C(10)-H(10)	118.6
C(30)-N(4)-Mn(2)	116.2(5)	C(10)-C(11)-C(12)	115.6(7)
O(1)-C(1)-Mn(1)	178.2(8)	C(10)-C(11)-C(18)	125.1(7)
O(2A)-C(2A)-Mn(1)	178.6(11)	C(12)-C(11)-C(18)	119.3(7)
O(2B)-C(2B)-Mn(1)	173(3)	C(13)-C(12)-C(11)	120.2(7)
O(3A)-C(3A)-Mn(1)	175(2)	C(13)-C(12)-H(12)	119.9
O(3B)-C(3B)-Mn(1)	173(5)	C(11)-C(12)-H(12)	119.9
C(5)-C(4)-N(1)	125.2(7)	N(2)-C(13)-C(12)	124.9(7)
C(5)-C(4)-H(4)	117.4	N(2)-C(13)-H(13)	117.6
N(1)-C(4)-H(4)	117.4	C(12)-C(13)-H(13)	117.6
C(4)-C(5)-C(6)	120.3(7)	C(15)-C(14)-C(6)	110.1(6)
C(4)-C(5)-H(5)	119.8	C(15)-C(14)-C(17)	108.6(7)
C(6)-C(5)-H(5)	119.8	C(6)-C(14)-C(17)	112.5(7)
C(7)-C(6)-C(5)	115.3(6)	C(15)-C(14)-C(16)	108.6(7)
C(7)-C(6)-C(14)	124.5(7)	C(6)-C(14)-C(16)	109.8(6)
C(5)-C(6)-C(14)	120.1(7)	C(17)-C(14)-C(16)	107.1(6)
C(6)-C(7)-C(8)	123.2(7)	C(14)-C(15)-H(15A)	109.5
C(6)-C(7)-H(7)	118.4	C(14)-C(15)-H(15B)	109.5
C(8)-C(7)-H(7)	118.4	H(15A)-C(15)-H(15B)	109.5
N(1)-C(8)-C(7)	119.8(6)	C(14)-C(15)-H(15C)	109.5
N(1)-C(8)-C(9)	113.6(6)	H(15A)-C(15)-H(15C)	109.5
C(7)-C(8)-C(9)	126.5(7)	H(15B)-C(15)-H(15C)	109.5
N(2)-C(9)-C(8)	113.3(6)	C(14)-C(16)-H(16A)	109.5
N(2)-C(9)-C(10)	121.1(6)	C(14)-C(16)-H(16B)	109.5
C(8)-C(9)-C(10)	125.6(6)	H(16A)-C(16)-H(16B)	109.5
C(11)-C(10)-C(9)	122.9(7)	C(14)-C(16)-H(16C)	109.5

Table 5-4 (Cont.)

H(16A)-C(16)-H(16C)	109.5	C(18)-C(21)-H(21B)	109.5
H(16B)-C(16)-H(16C)	109.5	H(21A)-C(21)-H(21B)	109.5
C(14)-C(17)-H(17A)	109.5	C(18)-C(21)-H(21C)	109.5
C(14)-C(17)-H(17B)	109.5	H(21A)-C(21)-H(21C)	109.5
H(17A)-C(17)-H(17B)	109.5	H(21B)-C(21)-H(21C)	109.5
C(14)-C(17)-H(17C)	109.5	O(4)-C(22)-Mn(2)	179.0(8)
H(17A)-C(17)-H(17C)	109.5	O(5)-C(23)-Mn(2)	179.2(7)
H(17B)-C(17)-H(17C)	109.5	O(6)-C(24)-Mn(2)	178.6(9)
C(11)-C(18)-C(21)	109.9(6)	C(26)-C(25)-N(3)	124.8(7)
C(11)-C(18)-C(19)	111.9(7)	C(26)-C(25)-H(25)	117.6
C(21)-C(18)-C(19)	107.8(7)	N(3)-C(25)-H(25)	117.6
C(11)-C(18)-C(20)	109.6(7)	C(25)-C(26)-C(27)	121.2(7)
C(21)-C(18)-C(20)	107.9(7)	C(25)-C(26)-H(26)	119.4
C(19)-C(18)-C(20)	109.6(8)	C(27)-C(26)-H(26)	119.4
C(18)-C(19)-H(19A)	109.5	C(28)-C(27)-C(26)	114.4(6)
C(18)-C(19)-H(19B)	109.5	C(28)-C(27)-C(35)	126.1(7)
H(19A)-C(19)-H(19B)	109.5	C(26)-C(27)-C(35)	119.5(7)
C(18)-C(19)-H(19C)	109.5	C(27)-C(28)-C(29)	123.6(7)
H(19A)-C(19)-H(19C)	109.5	C(27)-C(28)-H(28)	118.2
H(19B)-C(19)-H(19C)	109.5	C(29)-C(28)-H(28)	118.2
C(18)-C(20)-H(20A)	109.5	N(3)-C(29)-C(28)	121.3(7)
C(18)-C(20)-H(20B)	109.5	N(3)-C(29)-C(30)	112.5(6)
H(20A)-C(20)-H(20B)	109.5	C(28)-C(29)-C(30)	126.1(7)
C(18)-C(20)-H(20C)	109.5	N(4)-C(30)-C(29)	114.8(6)
H(20A)-C(20)-H(20C)	109.5	N(4)-C(30)-C(31)	119.5(6)
H(20B)-C(20)-H(20C)	109.5	C(29)-C(30)-C(31)	125.7(7)
C(18)-C(21)-H(21A)	109.5	C(32)-C(31)-C(30)	122.5(7)

Table 5-4 (Cont.)

C(32)-C(31)-H(31)	118.8	H(37A)-C(37)-H(37C)	109.5
C(30)-C(31)-H(31)	118.8	H(37B)-C(37)-H(37C)	109.5
C(31)-C(32)-C(33)	115.8(7)	C(35)-C(38)-H(38A)	109.5
C(31)-C(32)-C(39)	124.0(7)	C(35)-C(38)-H(38B)	109.5
C(33)-C(32)-C(39)	120.2(7)	H(38A)-C(38)-H(38B)	109.5
C(34)-C(33)-C(32)	120.8(7)	C(35)-C(38)-H(38C)	109.5
C(34)-C(33)-H(33)	119.6	H(38A)-C(38)-H(38C)	109.5
C(32)-C(33)-H(33)	119.6	H(38B)-C(38)-H(38C)	109.5
C(33)-C(34)-N(4)	124.1(7)	C(32)-C(39)-C(40)	112.6(7)
C(33)-C(34)-H(34)	118.0	C(32)-C(39)-C(41)	110.3(6)
N(4)-C(34)-H(34)	118.0	C(40)-C(39)-C(41)	107.5(6)
C(27)-C(35)-C(38)	111.3(6)	C(32)-C(39)-C(42)	109.4(6)
C(27)-C(35)-C(36)	110.3(6)	C(40)-C(39)-C(42)	109.2(7)
C(38)-C(35)-C(36)	108.3(7)	C(41)-C(39)-C(42)	107.7(7)
C(27)-C(35)-C(37)	110.0(6)	C(39)-C(40)-H(40A)	109.5
C(38)-C(35)-C(37)	107.4(7)	C(39)-C(40)-H(40B)	109.5
C(36)-C(35)-C(37)	109.6(7)	H(40A)-C(40)-H(40B)	109.5
C(35)-C(36)-H(36A)	109.5	C(39)-C(40)-H(40C)	109.5
C(35)-C(36)-H(36B)	109.5	H(40A)-C(40)-H(40C)	109.5
H(36A)-C(36)-H(36B)	109.5	H(40B)-C(40)-H(40C)	109.5
C(35)-C(36)-H(36C)	109.5	C(39)-C(41)-H(41A)	109.5
H(36A)-C(36)-H(36C)	109.5	C(39)-C(41)-H(41B)	109.5
H(36B)-C(36)-H(36C)	109.5	H(41A)-C(41)-H(41B)	109.5
C(35)-C(37)-H(37A)	109.5	C(39)-C(41)-H(41C)	109.5
C(35)-C(37)-H(37B)	109.5	H(41A)-C(41)-H(41C)	109.5
H(37A)-C(37)-H(37B)	109.5	H(41B)-C(41)-H(41C)	109.5
C(35)-C(37)-H(37C)	109.5	C(39)-C(42)-H(42A)	109.5

Table 5-4 (Cont.)

C(39)-C(42)-H(42B)	109.5	C(45)-C(46)-H(46B)	109.9
H(42A)-C(42)-H(42B)	109.5	H(46A)-C(46)-H(46B)	108.3
C(39)-C(42)-H(42C)	109.5	O(8)-C(47)-C(48)	107.7(6)
H(42A)-C(42)-H(42C)	109.5	O(8)-C(47)-H(47A)	110.2
H(42B)-C(42)-H(42C)	109.5	C(48)-C(47)-H(47A)	110.2
O(12)-C(43)-C(44)	110.5(6)	O(8)-C(47)-H(47B)	110.2
O(12)-C(43)-H(43A)	109.5	C(48)-C(47)-H(47B)	110.2
C(44)-C(43)-H(43A)	109.5	H(47A)-C(47)-H(47B)	108.5
O(12)-C(43)-H(43B)	109.5	O(9)-C(48)-C(47)	107.0(5)
C(44)-C(43)-H(43B)	109.5	O(9)-C(48)-H(48A)	110.3
H(43A)-C(43)-H(43B)	108.1	C(47)-C(48)-H(48A)	110.3
O(7)-C(44)-C(43)	108.9(6)	O(9)-C(48)-H(48B)	110.3
O(7)-C(44)-H(44A)	109.9	C(47)-C(48)-H(48B)	110.3
C(43)-C(44)-H(44A)	109.9	H(48A)-C(48)-H(48B)	108.6
O(7)-C(44)-H(44B)	109.9	O(9)-C(49)-C(50)	107.3(5)
C(43)-C(44)-H(44B)	109.9	O(9)-C(49)-H(49A)	110.3
H(44A)-C(44)-H(44B)	108.3	C(50)-C(49)-H(49A)	110.3
O(7)-C(45)-C(46)	108.7(6)	O(9)-C(49)-H(49B)	110.3
O(7)-C(45)-H(45A)	109.9	C(50)-C(49)-H(49B)	110.3
C(46)-C(45)-H(45A)	109.9	H(49A)-C(49)-H(49B)	108.5
O(7)-C(45)-H(45B)	109.9	O(10)-C(50)-C(49)	107.5(6)
C(46)-C(45)-H(45B)	109.9	O(10)-C(50)-H(50A)	110.2
H(45A)-C(45)-H(45B)	108.3	C(49)-C(50)-H(50A)	110.2
O(8)-C(46)-C(45)	108.7(6)	O(10)-C(50)-H(50B)	110.2
O(8)-C(46)-H(46A)	109.9	C(49)-C(50)-H(50B)	110.2
C(45)-C(46)-H(46A)	109.9	H(50A)-C(50)-H(50B)	108.5
O(8)-C(46)-H(46B)	109.9	O(10)-C(51)-C(52)	108.3(6)

Table 5-4 (Cont.)

O(10)-C(51)-H(51A)	110.0	C(56A)-C(55A)-H(55A)	110.4
C(52)-C(51)-H(51A)	110.0	K(1)-C(55A)-H(55A)	72.6
O(10)-C(51)-H(51B)	110.0	O(13)-C(55A)-H(55B)	110.4
C(52)-C(51)-H(51B)	110.0	C(56A)-C(55A)-H(55B)	110.4
H(51A)-C(51)-H(51B)	108.4	K(1)-C(55A)-H(55B)	102.7
O(11)-C(52)-C(51)	107.9(6)	H(55A)-C(55A)-H(55B)	108.6
O(11)-C(52)-H(52A)	110.1	O(13)-C(55B)-C(56B)	108.0(14)
C(51)-C(52)-H(52A)	110.1	O(13)-C(55B)-C(58A)	56.4(15)
O(11)-C(52)-H(52B)	110.1	C(56B)-C(55B)-C(58A)	68.8(15)
C(51)-C(52)-H(52B)	110.1	O(13)-C(55B)-K(1)	42.0(8)
H(52A)-C(52)-H(52B)	108.4	C(56B)-C(55B)-K(1)	148.3(11)
O(11)-C(53)-C(54)	107.9(6)	C(58A)-C(55B)-K(1)	82.2(14)
O(11)-C(53)-H(53A)	110.1	O(13)-C(55B)-H(55C)	110.1
C(54)-C(53)-H(53A)	110.1	C(56B)-C(55B)-H(55C)	110.1
O(11)-C(53)-H(53B)	110.1	C(58A)-C(55B)-H(55C)	87.4
C(54)-C(53)-H(53B)	110.1	K(1)-C(55B)-H(55C)	80.1
H(53A)-C(53)-H(53B)	108.4	O(13)-C(55B)-H(55D)	110.1
O(12)-C(54)-C(53)	109.6(6)	C(56B)-C(55B)-H(55D)	110.1
O(12)-C(54)-H(54A)	109.7	C(58A)-C(55B)-H(55D)	162.8
C(53)-C(54)-H(54A)	109.7	K(1)-C(55B)-H(55D)	93.7
O(12)-C(54)-H(54B)	109.7	H(55C)-C(55B)-H(55D)	108.4
C(53)-C(54)-H(54B)	109.7	C(57)-C(56A)-C(55A)	95(3)
H(54A)-C(54)-H(54B)	108.2	C(57)-C(56A)-H(56A)	112.7
O(13)-C(55A)-C(56A)	106(4)	C(55A)-C(56A)-H(56A)	112.7
O(13)-C(55A)-K(1)	44(2)	C(57)-C(56A)-H(56B)	112.7
C(56A)-C(55A)-K(1)	143(3)	C(55A)-C(56A)-H(56B)	112.7
O(13)-C(55A)-H(55A)	110.4	H(56A)-C(56A)-H(56B)	110.2

Table 5-4 (Cont.)

C(55B)-C(56B)-C(57)	103.7(11)	C(58A)-C(57)-H(57A)	101.6
C(55B)-C(56B)-C(58A)	66.4(14)	C(56B)-C(57)-H(57A)	143.9
C(57)-C(56B)-C(58A)	45.4(13)	H(57C)-C(57)-H(57A)	95.4
C(55B)-C(56B)-H(56C)	111.0	H(57D)-C(57)-H(57A)	30.7
C(57)-C(56B)-H(56C)	111.0	C(56A)-C(57)-H(57B)	108.3
C(58A)-C(56B)-H(56C)	100.7	C(58B)-C(57)-H(57B)	108.3
C(55B)-C(56B)-H(56D)	111.0	C(58A)-C(57)-H(57B)	148.1
C(57)-C(56B)-H(56D)	111.0	C(56B)-C(57)-H(57B)	80.1
C(58A)-C(56B)-H(56D)	148.2	H(57C)-C(57)-H(57B)	50.3
H(56C)-C(56B)-H(56D)	109.0	H(57D)-C(57)-H(57B)	97.3
C(56A)-C(57)-C(58B)	116(2)	H(57A)-C(57)-H(57B)	107.4
C(56A)-C(57)-C(58A)	74(3)	C(57)-C(58A)-O(13)	98(3)
C(58B)-C(57)-C(58A)	48.4(19)	C(57)-C(58A)-C(55B)	89(3)
C(56A)-C(57)-C(56B)	39(3)	O(13)-C(58A)-C(55B)	41.5(12)
C(58B)-C(57)-C(56B)	102.2(10)	C(57)-C(58A)-C(56B)	50.3(16)
C(58A)-C(57)-C(56B)	84(2)	O(13)-C(58A)-C(56B)	77(2)
C(56A)-C(57)-H(57C)	152.9	C(55B)-C(58A)-C(56B)	44.8(13)
C(58B)-C(57)-H(57C)	66.2	C(57)-C(58A)-H(58A)	112.2
C(58A)-C(57)-H(57C)	114.6	O(13)-C(58A)-H(58A)	112.2
C(56B)-C(57)-H(57C)	114.6	C(55B)-C(58A)-H(58A)	78.7
C(56A)-C(57)-H(57D)	84.9	C(56B)-C(58A)-H(58A)	78.6
C(58B)-C(57)-H(57D)	138.2	C(57)-C(58A)-H(58B)	112.2
C(58A)-C(57)-H(57D)	114.6	O(13)-C(58A)-H(58B)	112.2
C(56B)-C(57)-H(57D)	114.6	C(55B)-C(58A)-H(58B)	150.4
H(57C)-C(57)-H(57D)	111.7	C(56B)-C(58A)-H(58B)	162.2
C(56A)-C(57)-H(57A)	108.3	H(58A)-C(58A)-H(58B)	109.8
C(58B)-C(57)-H(57A)	108.3	O(13)-C(58B)-C(57)	113.3(11)

Table 5-4 (Cont.)

O(13)-C(58B)-H(58C)	108.9	C(61)-C(62)-H(62B)	110.0
C(57)-C(58B)-H(58C)	108.9	H(62A)-C(62)-H(62B)	108.4
O(13)-C(58B)-H(58D)	108.9	O(15)-C(63)-C(64)	107.9(6)
C(57)-C(58B)-H(58D)	108.9	O(15)-C(63)-H(63A)	110.1
H(58C)-C(58B)-H(58D)	107.7	C(64)-C(63)-H(63A)	110.1
O(19)-C(59)-C(60)	110.6(6)	O(15)-C(63)-H(63B)	110.1
O(19)-C(59)-H(59A)	109.5	C(64)-C(63)-H(63B)	110.1
C(60)-C(59)-H(59A)	109.5	H(63A)-C(63)-H(63B)	108.4
O(19)-C(59)-H(59B)	109.5	O(16)-C(64)-C(63)	108.3(6)
C(60)-C(59)-H(59B)	109.5	O(16)-C(64)-H(64A)	110.0
H(59A)-C(59)-H(59B)	108.1	C(63)-C(64)-H(64A)	110.0
O(14)-C(60)-C(59)	109.0(6)	O(16)-C(64)-H(64B)	110.0
O(14)-C(60)-H(60A)	109.9	C(63)-C(64)-H(64B)	110.0
C(59)-C(60)-H(60A)	109.9	H(64A)-C(64)-H(64B)	108.4
O(14)-C(60)-H(60B)	109.9	O(16)-C(65)-C(66)	107.0(6)
C(59)-C(60)-H(60B)	109.9	O(16)-C(65)-H(65A)	110.3
H(60A)-C(60)-H(60B)	108.3	C(66)-C(65)-H(65A)	110.3
O(14)-C(61)-C(62)	108.9(6)	O(16)-C(65)-H(65B)	110.3
O(14)-C(61)-H(61A)	109.9	C(66)-C(65)-H(65B)	110.3
C(62)-C(61)-H(61A)	109.9	H(65A)-C(65)-H(65B)	108.6
O(14)-C(61)-H(61B)	109.9	O(17)-C(66)-C(65)	108.0(5)
C(62)-C(61)-H(61B)	109.9	O(17)-C(66)-H(66A)	110.1
H(61A)-C(61)-H(61B)	108.3	C(65)-C(66)-H(66A)	110.1
O(15)-C(62)-C(61)	108.3(6)	O(17)-C(66)-H(66B)	110.1
O(15)-C(62)-H(62A)	110.0	C(65)-C(66)-H(66B)	110.1
C(61)-C(62)-H(62A)	110.0	H(66A)-C(66)-H(66B)	108.4
O(15)-C(62)-H(62B)	110.0	O(17)-C(67)-C(68)	108.2(6)

Table 5-4 (Cont.)

O(17)-C(67)-H(67A)	110.1	C(72)-C(71)-H(71B)	109.3
C(68)-C(67)-H(67A)	110.1	H(71A)-C(71)-H(71B)	107.9
O(17)-C(67)-H(67B)	110.1	C(71)-C(72)-C(73A)	106.0(9)
C(68)-C(67)-H(67B)	110.1	C(71)-C(72)-C(73B)	89.9(13)
H(67A)-C(67)-H(67B)	108.4	C(73A)-C(72)-C(73B)	56.7(15)
O(18)-C(68)-C(67)	108.9(6)	C(71)-C(72)-H(72C)	110.5
O(18)-C(68)-H(68A)	109.9	C(73A)-C(72)-H(72C)	110.5
C(67)-C(68)-H(68A)	109.9	C(73B)-C(72)-H(72C)	159.0
O(18)-C(68)-H(68B)	109.9	C(71)-C(72)-H(72D)	110.5
C(67)-C(68)-H(68B)	109.9	C(73A)-C(72)-H(72D)	110.5
H(68A)-C(68)-H(68B)	108.3	C(73B)-C(72)-H(72D)	66.4
O(18)-C(69)-C(70)	108.6(6)	H(72C)-C(72)-H(72D)	108.7
O(18)-C(69)-H(69A)	110.0	C(71)-C(72)-H(72A)	113.7
C(70)-C(69)-H(69A)	110.0	C(73A)-C(72)-H(72A)	57.3
O(18)-C(69)-H(69B)	110.0	C(73B)-C(72)-H(72A)	113.7
C(70)-C(69)-H(69B)	110.0	H(72C)-C(72)-H(72A)	54.4
H(69A)-C(69)-H(69B)	108.4	H(72D)-C(72)-H(72A)	135.8
O(19)-C(70)-C(69)	110.0(6)	C(71)-C(72)-H(72B)	113.7
O(19)-C(70)-H(70A)	109.7	C(73A)-C(72)-H(72B)	139.4
C(69)-C(70)-H(70A)	109.7	C(73B)-C(72)-H(72B)	113.7
O(19)-C(70)-H(70B)	109.7	H(72C)-C(72)-H(72B)	63.5
C(69)-C(70)-H(70B)	109.7	H(72D)-C(72)-H(72B)	47.4
H(70A)-C(70)-H(70B)	108.2	H(72A)-C(72)-H(72B)	110.9
O(20)-C(71)-C(72)	111.8(9)	C(72)-C(73A)-C(74A)	105.5(9)
O(20)-C(71)-H(71A)	109.3	C(72)-C(73A)-H(73A)	110.6
C(72)-C(71)-H(71A)	109.3	C(74A)-C(73A)-H(73A)	110.6
O(20)-C(71)-H(71B)	109.3	C(72)-C(73A)-H(73B)	110.6

Table 5-4 (Cont.)

C(74A)-C(73A)-H(73B)	110.6	O(20)-C(74A)-H(74B)	110.4
H(73A)-C(73A)-H(73B)	108.8	C(73A)-C(74A)-H(74B)	110.4
C(72)-C(73B)-C(74B)	101(2)	H(74A)-C(74A)-H(74B)	108.6
C(72)-C(73B)-H(73C)	111.5	C(73B)-C(74B)-O(20)	106.1(19)
C(74B)-C(73B)-H(73C)	111.5	C(73B)-C(74B)-H(74C)	110.5
C(72)-C(73B)-H(73D)	111.5	O(20)-C(74B)-H(74C)	110.5
C(74B)-C(73B)-H(73D)	111.5	C(73B)-C(74B)-H(74D)	110.5
H(73C)-C(73B)-H(73D)	109.3	O(20)-C(74B)-H(74D)	110.5
O(20)-C(74A)-C(73A)	106.4(9)	H(74C)-C(74B)-H(74D)	108.7
O(20)-C(74A)-H(74A)	110.4		
C(73A)-C(74A)-H(74A)	110.4		

Chapter 6

Heterogenization of CO_2 reduction electrocatalysts.

6.1 Introduction

There is widespread agreement amongst chemists and engineers that a potential catalyst for the large-scale electrochemical reduction of CO_2 to value-added products will be heterogeneous in nature. This "requirement" can, of course, take many forms. The first type of heterogeneous catalyst is the typical metal or metal oxide. Examples of these include copper electrodes, surfaces decorated with platinum nanoparticles, films of ruthenium oxide and many others. These types of catalysts have the advantage of long-term stability and ease of synthesis, but suffer from a lack of mechanistic understanding (in many cases) and low selectivity for desired products.[1]

A second type heterogenization is the covalent bonding of discrete molecules to a surface. This method has the advantage of being able to develop a homogeneous catalyst first, optimizing it and later anchoring it to a surface. Optimization includes improving selectivity, increasing efficiency, lowering overpotential, and increasing rates to acceptable levels. In addition, homogeneous catalysis lends itself to mechanistic studies that are well-developed and understood by a wide swath of the scientific community. The heterogenization of this type of catalyst is an exciting opportunity for research going forward. Although not small molecules, heterogenization of homogeneous systems has been accomplished by the adsorption of enzymes to electrode surfaces.[2, 3]

We have explored three different heterogenization methods for the Re(η^2-L)$(CO)_3$Cl catalysts studied in our laboratory (η^2-L = 4,4'-disubstituted-2,2'-bipyridine *or* phenanthroline derivatives). The three methods include intercalation into edge plane graphite and attachment through covalent bonds to both gold and p-type silicon (p-Si). In each case, the goal is to take a well understood catalyst and anchor it to the surface to increase stability and enhance heterogeneous charge transfer from the electrode surface to the active site.

6.2 Intercalation

One very common form of intercalation is the inclusion of guest molecules in a graphite lattice.[4] This form of intercalation compound includes KC_8, a very useful compound for performing strong chemical reductions. Another common intercalation

strategy is the interaction of molecules with DNA helices.[5] In this effort, we used a less widely known method of intercalation that almost serves as a hybrid of the two methods. Here we constructed a metal complex with a large aromatic ligand identical to the ligands used in many DNA intercalation studies, but aimed to combine it with edge-plane graphite and exploit π interactions.

A suitable phenanthroline derivate for intercalation into edge-plane graphite had been reported previously.[6] The ligand, benzo[i]dipyrido[3,2-a:2',3'-c]phenazine (dppn), is readily synthesized by the reflux of 1,10-phenanthroline-5,6-dione and diaminonaphthalene in ethanol. After isolating the ligand, we were able to synthesize

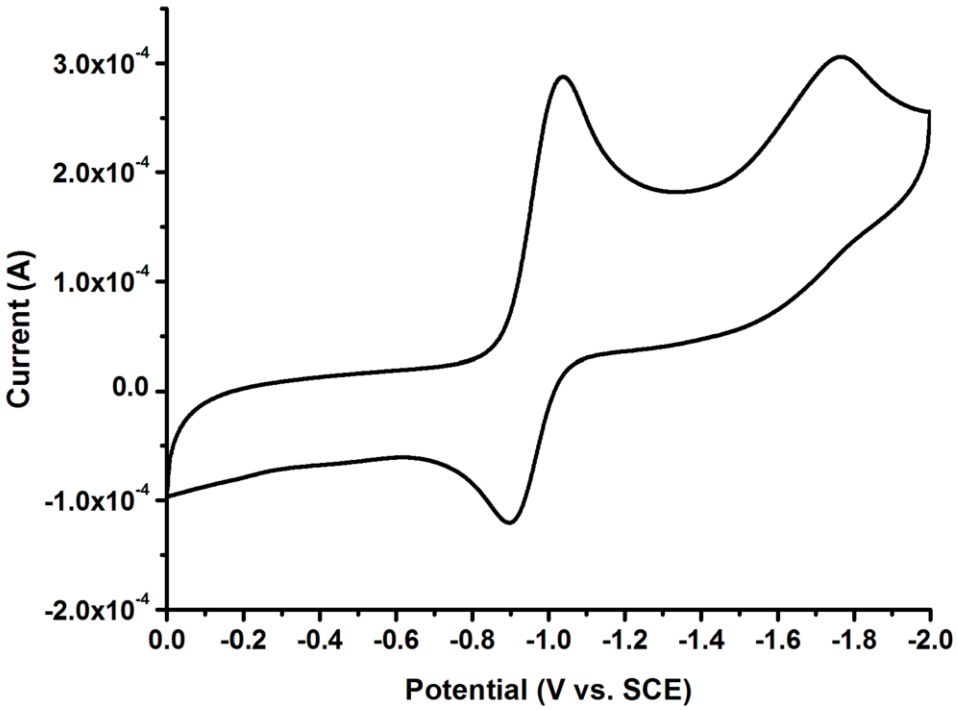

Figure 6-1. Cyclic voltammogram of 0.5 mM $Re(dppn)(CO)_3Cl$ at a glassy carbon electrode in acetonitrile. The two reductions are typical of this type of Re complex. Electrochemical conditions are as follows: GC working electrode, Pt wire counter electrode, Ag wire pseudo-reference electrode, Fc added as an internal reference, 0.1 M TBAH as supporting electrolyte.

the Re complex by the reflux of dppn with $Re(CO)_5Cl$ in toluene. The complex, $Re(dppn)(CO)_3Cl$, was studied by cyclic voltammetry at a glassy carbon electrode before intercalation was attempted. The complex has two reductions. The first is quasi-reversible and has an $E_{1/2}$ of –960 mV (vs. SCE). The second reduction is irreversible and has a peak value of –1540 mV (vs. SCE) (Figure 6-1).

After the initial cyclic voltammetric studies, the glassy carbon electrode was replaced by an edge-plane pyrolytic graphite (PGEE) electrode and the cyclic voltammograms were cycled several times. This cycling served to bring the Re complex in close proximity to the PGEE electrode by diffusion and caused intercalation (schematic in Figure 6-2). After cycling, the PGEE electrode was removed from the solution of $Re(dppn)(CO)_3Cl$, rinsed copiously and placed in a blank solution to see if intercalation had occurred. The continued appearance of peaks in the cyclic voltammogram was an indication of intercalation. Another indication of intercalation is that the splitting between the peaks of a reversible couple diminishes.

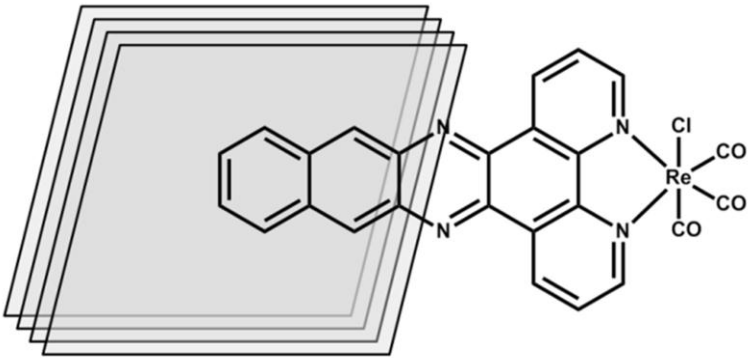

Figure 6-2. Schematic of dppn ligand intercalation into an edge-plane pyrolytic graphite (PGEE) electrode.

Ideal Nernstian behavior for a surface-confined species manifests itself as symmetric cyclic voltammetric peaks (E_p = 0 mV), and a peak half-width of 90.6/*n* mV.[7] Lastly, the current scaled linearly with an increase in scan rate, indicating (based on E6-1) that the species is surface attached.[7]

$$i_p = \frac{n^2 F^2 \Gamma A v}{4RT} \qquad \textbf{E6-1}$$

In equation 6-1, i_p is the peak current, n is the number of electrons, F is Faraday's constant, Γ is the surface coverage, A is the electrode area, v is the scan rate, R is the ideal gas constant, and T is the temperature. For the Re(dppn)$(CO)_3$Cl species

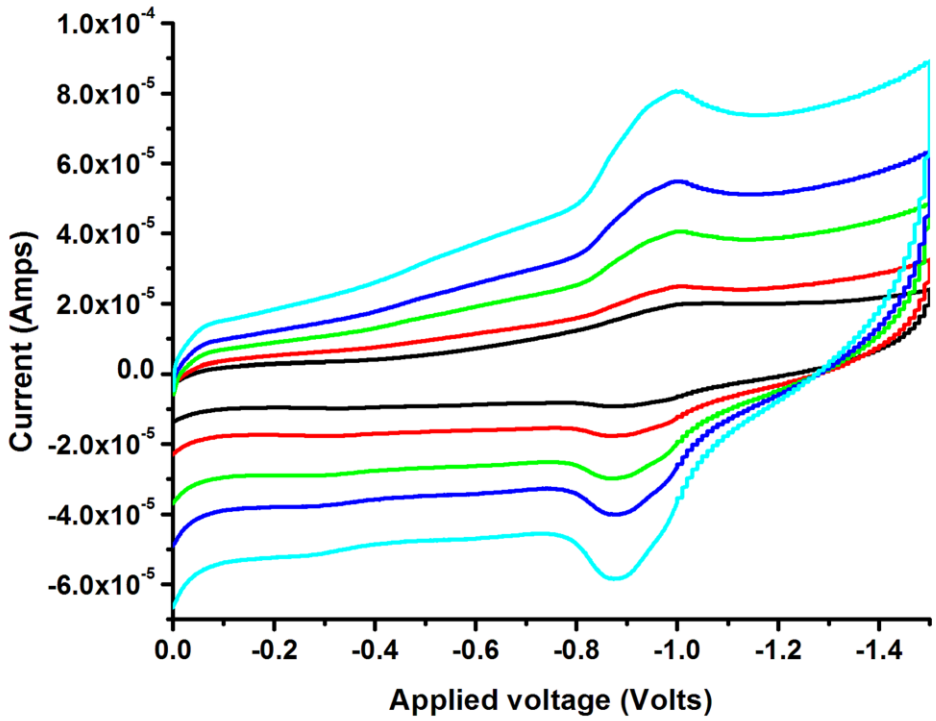

Figure 6-3. Re(dppn)$(CO)_3$Cl at a PGEE electrode (intercalated). Scan rate increased from 50 mV/s to 500 mV/s with only the first reduction of the complex shown. Electrochemical conditions: PGEE working electrode, Pt wire counter electrode, Ag wire pseudo-reference electrode, acetonitrile with 0.1 M TBAH as supporting electrolyte.

intercalated in a PGEE electrode the reduction and re-oxidation peaks for the first reduction are separated by nearly 80 mV and have a peak half width greater than 90.6 mV. This indicates that the first reduction is not completely reversible, an assumption we had made prior to these studies based on the chemical step of halide loss that occurs after the first reduction. The reduction peak current does, however, scale linearly with scan rate as can be seen in Figures 6-3 and 6-4, indicating that the Re complex is, in fact, intercalated.

Catalytic studies with this intercalated system proved unsuccessful. One main goal of intercalation was to make water a viable solvent option by eliminating the

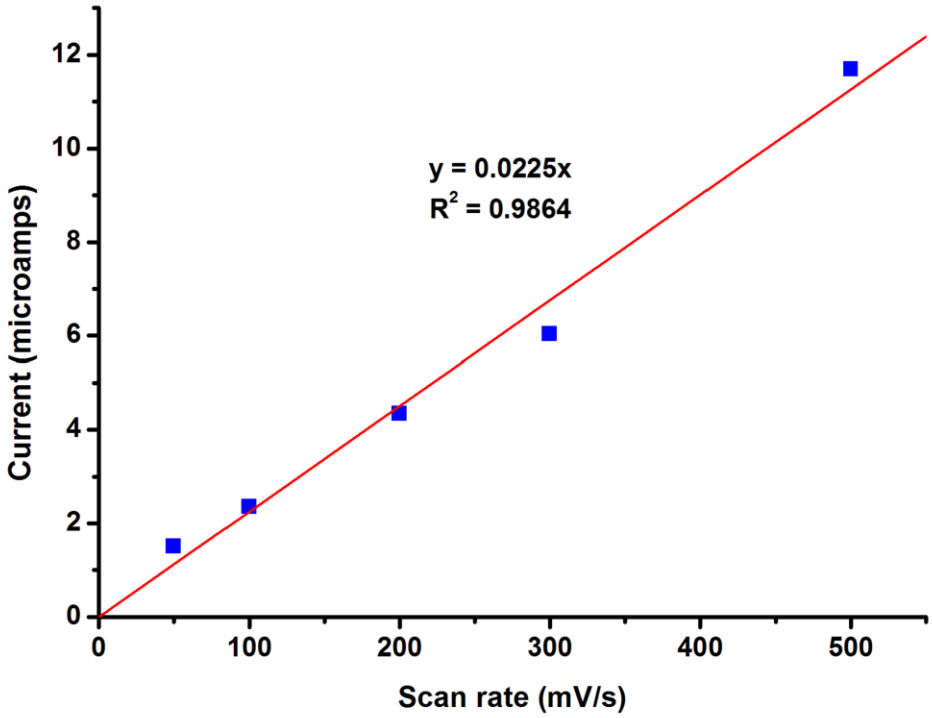

Figure 6-4. Scan rate *versus* current for the intercalated Re(dppn)$(CO)_3$Cl complex at a PGEE electrode. The linear relationship between scan rate and current is indicative of a surface-attached species.

requirement of catalyst solubility. Attempting to obtain this goal, the PGEE electrode with Re(dppn)$(CO)_3$Cl intercalated was placed in an aqueous KOH solution saturated with CO_2 and scans were run to determine catalytic activity. Aqueous KOH was used as the solvent media because it allows for the most negative solvent window before proton reduction to H_2 begins. No increase in current was seen with CO_2 saturation in those studies and, in fact, the second reduction of the Re complex was not seen in those scans.

Catalytic studies in blank acetonitrile (MeCN) solutions were also attempted. In those solutions, we were able to see both reductions of the intercalated Re complex, but no catalysis occurred when the MeCN solution was saturated with CO_2. Possible reasons for the lack of catalysis are insufficiently negative reduction potentials, lack of freedom for geometric rearrangement of the molecule in the reduced state, or insufficient access of the CO_2 to the active site because of molecular packing effects. These are issues that could be addressed with further experimentation and are discussed below in the conclusions.

6.3 Covalent bonds to gold

Another well-known surface attachment strategy is the covalent binding of a thiol to a gold surface. This method has been employed for countless applications and has been used previously in our laboratory.[8] In an effort to attach a Re(bipy)$(CO)_3$X catalyst to a planar gold surface we employed a four step synthesis to make Re(bipy-SH)$(CO)_3$Cl (where bipy-SH = 4-methyl-4'-(butane-1-thiol)-2,2'-bipyrdine) (Figure

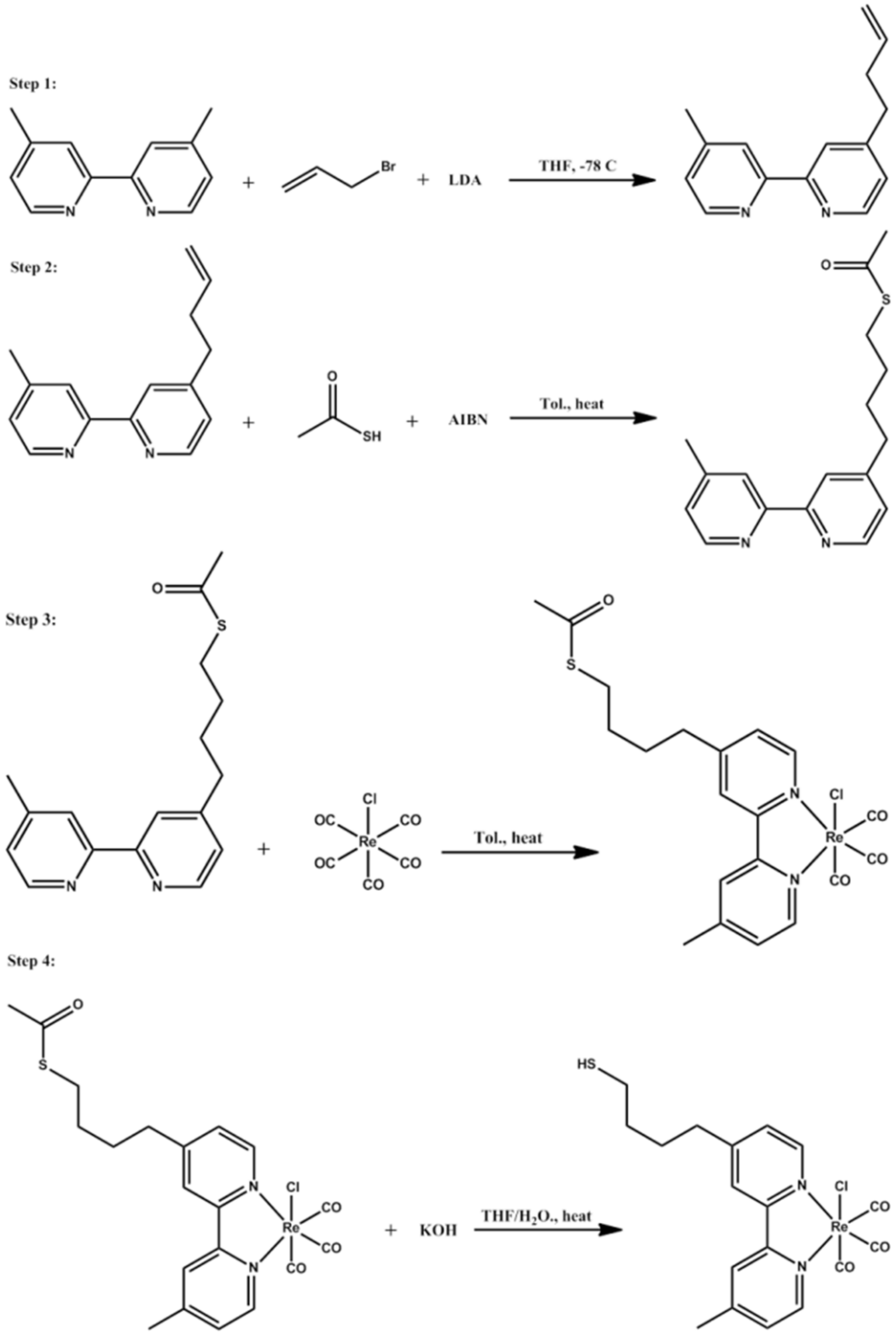

Figure 6-5. Scheme for the synthesis of Re(bipy-SH)$(CO)_3$Cl for covalent attachment to a gold surface.

6-5). The synthesis of both the ligand and the Re complex are described in detail in the Experimental section.

Once the Re(bipy-SH)$(CO)_3$Cl complex was synthesized, a self-assembled monolayer (SAM) was formed by allowing a gold slide to rest in a 10 mM solution of the Re complex in methylene chloride (CH_2Cl_2) for 48 hours. After that time the surface was rinsed copiously with organic solvents and polarization modulation infrared reflection absorption spectroscopy (PM-IRRAS) was performed to characterize the surface of the Au slide. The PM-IRRAS showed two ν(CO) stretching frequencies at 2031 cm^{-1} and 1927 cm^{-1} (broad) (Figure 6-6). The broad absorption at 1927 cm^{-1} is most likely the overlap of the two lower energy stretches referenced

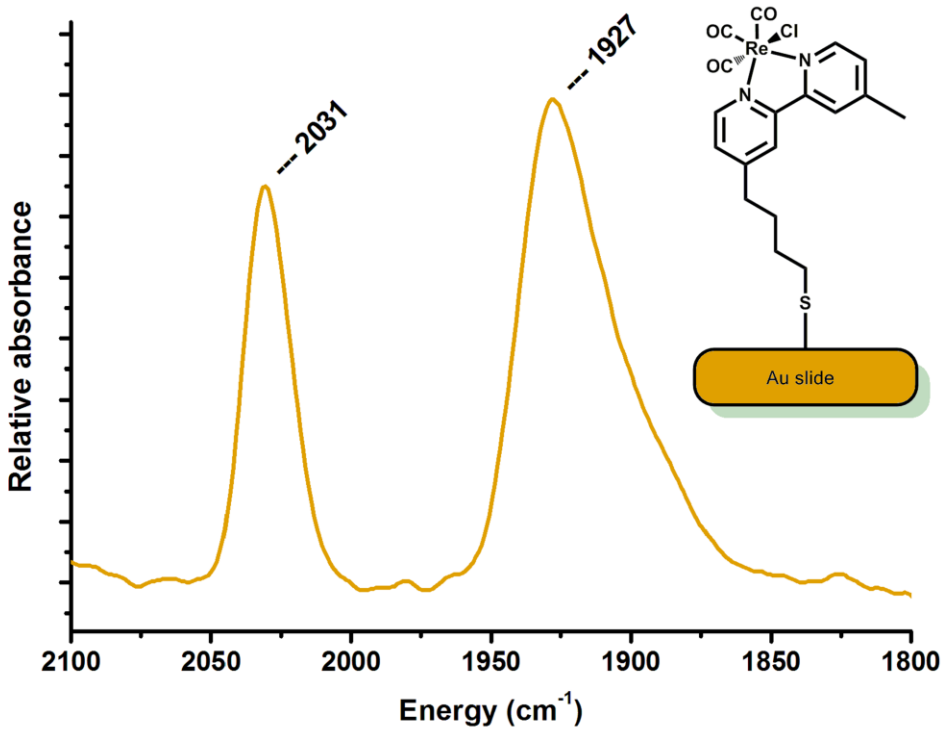

Figure 6-6. PM-IRRAS of a SAM of Re(bipy-SH)$(CO)_3$Cl on a gold slide.

throughout this dissertation.

Electrochemical experiments were attempted using the Au slides with Re(bipy-SH)$(CO)_3$Cl SAMs, but several difficulties were encountered. The first of these is that the monolayer coverage of Re complexes seemed to be inhibiting electrolyte penetration in the initial studies. In order to combat this problem, the electrolyte was changed from tetrabutylammonium hexafluorophosphate (TBAH) to tetramethylammonium hexafluorophosphate (TMAH) in order to decrease size and

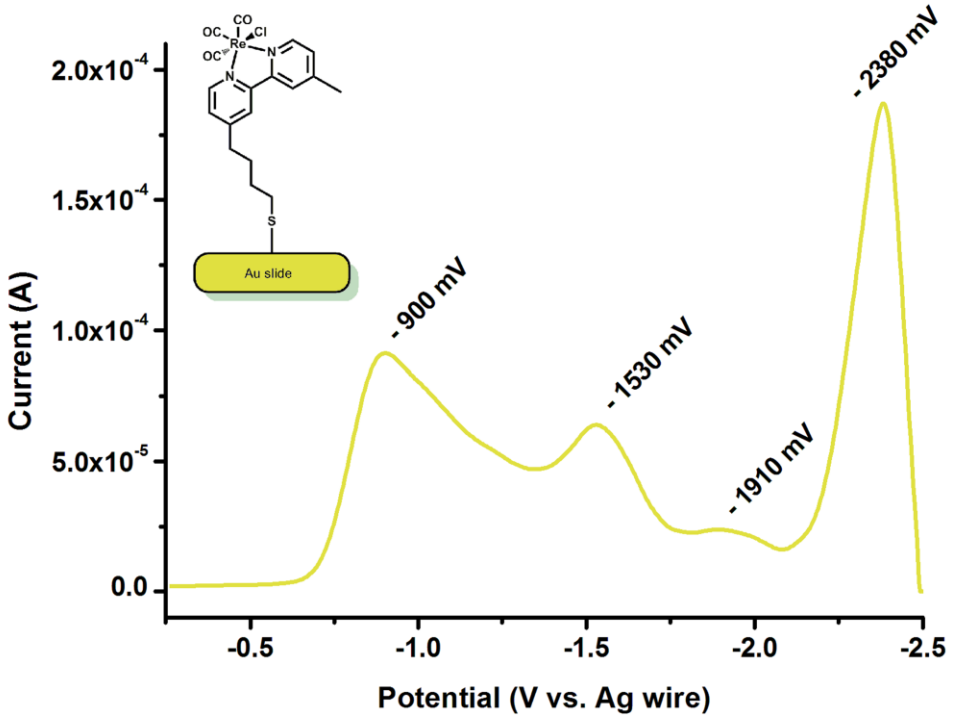

Figure 6-7. Differential Pulse Voltammogram of Re(bipy-SH)$(CO)_3$Cl on a gold electrode. The first feature at –900 mV is O_2 and diminishes with argon-sparging, the second feature at –1530 mV is the first reduction of the complex, the small feature at –1910 mV is the second reduction of the complex, and the last feature at –2530 mV appears to be the production of H_2 by the gold surface. The second reduction feature (–1910 mV) is very small, presumably because the Au–S bond is not stable at these negative potentials and the Re complex is released from the surface.

minimize resistance in the cell. This method seemed to work and electrochemistry improved.

The second problem that was encountered was the low stability of Au–S bonds to reductive chemistry. At the very negative potentials needed to reduce the Re complex a second time, the Au–S bond is not stable and complex begins to come off the surface. We were able to obtain one differential pulse voltammogram (DPV) that may show both reductions, but the second of the two is much smaller, possibly indicating release of the complex from the surface (Figure 6-7). In the end, we were not able to see either reduction cleanly and were not able to further characterize the complex by electrochemical methods.

6.4 Covalent bonds to p-Si

One major goal of the energy-related research in our laboratory has been the photoelectrochemical reduction of CO_2 to value-added products at semiconductor electrodes.[9, 10] Through the use of semiconductor electrodes, coupled with irradiation by light in the visible spectrum, we are able to realize a photovoltage and reduce substrates with less overpotential. Practically, this photovoltage leads to a decrease in the energy needed from wall source electricity. Several studies in our laboratory have concluded that this type of electrochemical reduction is possible using a p-Si surface that is hydrogen-terminated or modified with hexyl or ethyl phenyl groups, and a homogeneous catalyst. Through these studies it was also evident that p-Si surfaces modified with hexyl or ethyl phenyl groups are more robust than those that are

hydrogen terminated. For these reasons, Dr. Bhupendra Kumar and I attempted to attach rhenium CO_2 reduction catalysts to p-Si surfaces in an effort to make the overall system more robust and efficient.

The Lewis acid method for silicon surface modification was used. This method requires a terminal alkene at the point of contact to the surface. Towards this end, we employed a two-step ligand synthesis starting from 4,4'-dimethyl-2,2'-bipyridine that is described in detail in the Experimental section. The synthesis yielded what I will refer to as bipy-R (where bipy-R = 4-methyl-4'(dodec-11-en-1-yl)-2,2'-bipyridine) (Figure 6-8), a ligand suitable for attachment to a p-Si surface. In the Lewis acid method for covalently linking alkenes to p-Si, ethyl aluminum dichloride ($EtAlCl_2$) is mixed with the alkene and exposed to the hydrogen-terminated silicon surface for some time at room temperature.[11] After ligand attachment, the bipyridine-modified p-Si surface was exposed to $Re(CO)_5Cl$ in toluene at elevated temperatures for 24 hours to yield the Re complex covalently attached to p-Si. The surface-attached Re complex

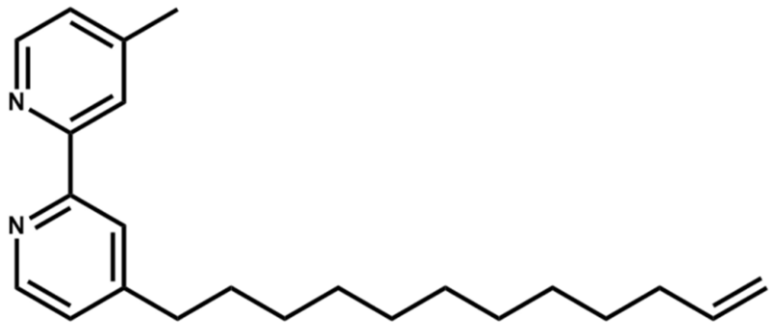

Figure 6-8. Chemical structure of 4-methyl-4'-(dodec-11-en-1-yl)-2,2'-bipyridine for covalent attachment to a p-Si surface.

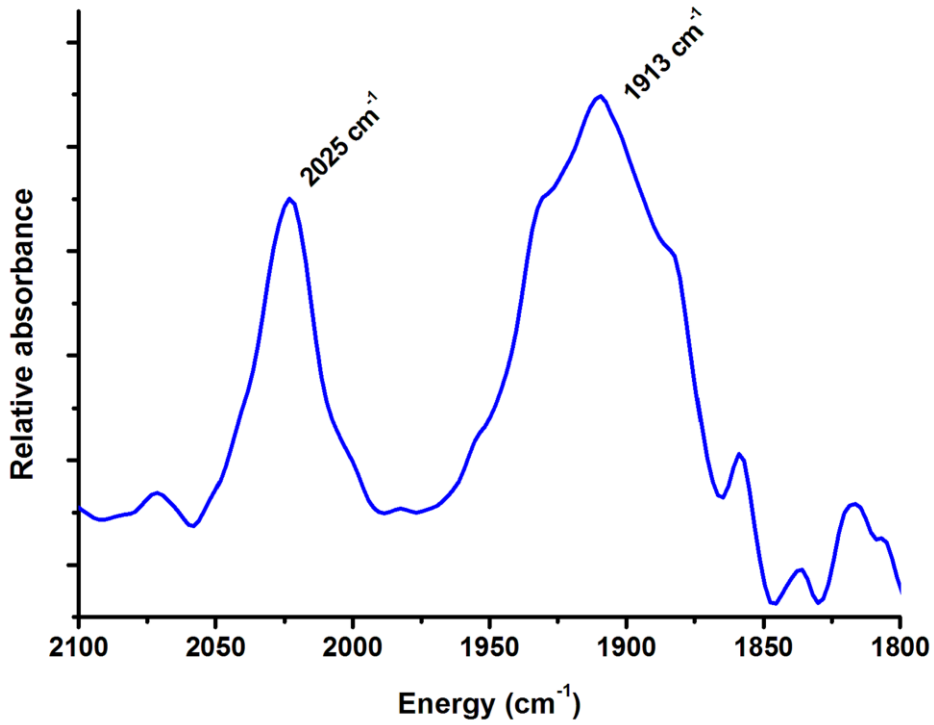

Figure 6-9. IR of Re(bipy-R)$(CO)_3$Cl on a p-Si surface. The two lower energy ν(CO) stretching frequencies are overlapped and broad.

was characterized by both grazing angle transmittance IR and XPS.[12] The IR, shown in Figure 6-9, clearly shows two ν(CO) stretching frequencies where the lower energy band is broad and represents an overlap of two bands.

Electrochemical experiments with these samples showed no reduction peaks. The possible reasons we propose for this problem are: 1) oxidation of the surface during one or more of the modification steps that results in an excess of defects, preventing clean electrochemistry and/or 2.) close packing of the Re complexes on the surface that limits the electrons that are transferred from the surface to the

electrochemically active center. There are possibilities to improve this system that I will discuss in the next section.

6.5 Conclusions and future experiments

Three heterogenization methods were performed to anchor $Re(\eta^2\text{-}L)(CO)_3Cl$ catalysts to electrode surfaces with the goal of improving catalyst stability and heterogeneous charge transfer properties. The first method, intercalation, was achieved using $Re(dppn)(CO)_3Cl$ and edge-plane pyrolytic graphite (PGEE) electrodes. Electrochemical properties of the surface were probed, but no catalysis was seen in

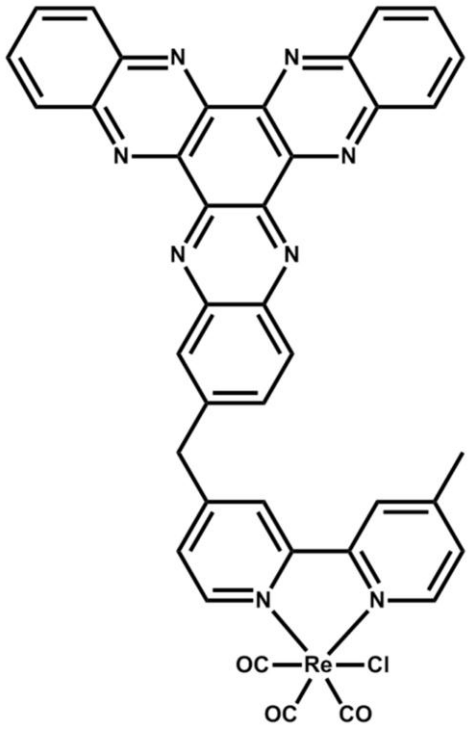

Figure 6-10. Possible ligand for the intercalation of electrocatalysts into PGEE electrodes.

this system. One possible reason for the lack of catalysis is the decreased reduction potential of the system when compared to working catalysts like Re(bipy)$(CO)_3$Cl or those complexes with bipyridines modified in the 4,4' positions by alkyl groups. This decrease in potential is caused by the electron withdrawing nature of the aromatic backbone in the dppn ligand. One possible solution to this problem would be a different ligand, such as the one shown in Figure 6-10. In that ligand, the aromatic intercalating backbone is separated from the bipyridine moiety by a methylene bridge, a feature that should make the ligand behave electronically more like a 4,4'-dialkyl-2,2'-bipyridine.

Covalent attachment to gold was also accomplished through the synthesis of a new thiol-bipyridine ligand. That product also proved unsuccessful for the electrochemical reduction of CO_2 due to a lack of stability of Au–S bonds at the very negative potentials needed to reach the second reduction of the complex. This heterogenization method has the potential to succeed only at much lower potentials with catalysts that can carry appreciable current densities closer to the thermodynamic potential for the multi-electron reductions of CO_2 to value-added products.

The third heterogenization method, covalent attachment of CO_2 electrocatalysts to p-Si, was also achieved. A new bipyridine derivative with a terminal alkene was synthesized and attached to p-Si by the Lewis acid method. That ligand was then metallated to make the Re complex. Electrochemistry of these samples proved unsuccessful for various reasons. This method, however, is one that should be explored further. One way to improve the surface kinetics of these samples

is to make a mixed monolayer of the bipy-alkene with ethyl phenyl groups. A previous report from our laboratory showed that the ethyl phenyl surface possesses very good heterogeneous charge transfer properties to the solution.[13] That property, combined with the "diluting" nature of the mixed monolayer, may result in better electrochemistry and the opportunity to reduce CO_2 to CO with a heterogenized molecular catalyst.

6.6 Experimental

General considerations. ^{1}H NMR spectra were collected on a Jeol 500 MHz NMR spectrometer and data was manipulated using the Jeol Delta Software package. Infrared spectra were collected on a Bruker Equinox 55 spectrometer. Electrochemistry was performed with a Bas Epsilon potentiostat. All chemicals were used as received from the manufacturer with the exception of the tetrabutyl- and tetramethyl-ammonium hexafluorophosphate that were both twice recrystallized from methanol before use, and the solvents that were sparged with argon and purified over alumina columns on a custom-dry solvent system.

Synthesis of benzo[i]dipyrido[3,2-a:2',3'-c]phenazine (dppn). 1,10-phenanthroline-5,6-dione (500 mg, 2.37 mmol) was added to a round bottom flask with 100 mL of reagent grade EtOH that had been sparged with argon for 15 minutes. The solution was stirred and heated until all solid was dissolved. To that solution, diaminophenanthroline (375 mg, 2.37 mmol) was added and a reflux condenser was

attached with a flow of argon. The reaction mixture started to turn orange almost immediately upon mixing and solid began to crash out. The reaction mixture was allowed to reflux for 18 hours. Upon cooling to room temperature, followed by cooling to –30 °C in the freezer, solid had crashed out. The solid was filtered and dried overnight under vacuum at 60 °C. The dried product was an orange crystalline solid (505 mg, 64% yield). Es^+-MS Calc: 333.11 (100%), Found: 333.45 (100%). ^1H NMR (400 MHz, ppm, CD_2Cl_2) 9.47 (d, 2H), 9.05 (d, 2H), 8.80 (d, 2H), 8.07 (d, 2H), 7.71 (d, 2H), 7.43 (d, 2H).

Synthesis of $Re(dppn)(CO)_3Cl$. $Re(CO)_5Cl$ (162 mg, 0.45 mmol) and dppn (148 mg, 0.45 mmol) were added to a Schlenk flask containing 60 mL of toluene that had been sparged with argon for 15 minutes. The reaction mixture was refluxed for 2 hours. Once reflux was achieved the solution quickly turned deep orange. The solution was then cooled to room temperature and became cloudy. After sitting overnight at –30 °C the product had crashed out of solution and was filtered. The yellow/orange product was dried under vacuum overnight at 60 °C. During solubility tests it was observed that the complex is sparingly soluble in organic solvents including MeCN, THF and DMSO. IR (KBr pellet) ν(CO): 2020 cm^{-1}, 1914 cm^{-1}, 1897 cm^{-1}. ^1H NMR (300 MHz, ppm, DMSO-d_6, peaks difficult to resolve due to low solubility) 9.81 (m, 2H), 9.52 (dd, 2H), 9.21 (d, 2H), 8.40 (m, 2H), 8.25 (m, 2H), 7.75 (m, 2H).

Synthesis of 4-(but-3-en-1-yl)-4'-methyl-2,2'-bipyridine. 4,4'-dimethyl-2,2'-bipyridine (1.66 g, 9.0 mmol) was dissolved in 100 mL dry THF and cooled to –78 °C. Lithium diisopropyl amide (LDA, 1.8 M in heptane/THF/ethyl benzene, 5.0 mL, 9.0 mmol) was added dropwise over a period of *ca.* 10 minutes. The reaction mixture turned dark brown upon addition and was stirred for 30 minutes while warming to 0 °C. After 30 minutes, the reaction mixture was cooled back to –78 °C and allyl bromide (1.5 mL, 17.3 mmol) was added *via* syringe and the reaction mixture was stirred overnight while slowly warming to room temperature. DI-H_2O (5 mL) was added to quench the remaining LDA and the other solvents were removed by rotary evaporation. The product was extracted from the aqueous layer with three portions of Et_2O (50 mL each). The combined organic phase was dried with $MgSO_4$ and the Et_2O was removed under vacuum. The product was dissolved in 10 mL of pentane and filtered through a plug of celite to remove educt. Pentane was removed by rotary evaporation to yield a brown oil (1.66 g, 82% yield). ^{1}H NMR (500 MHz, ppm, $CDCl_3$) 2.35 (s, 3H), 2.39 (t, 2H), 2.72 (t, 2H), 4.93 (d, 1H), 4.99 (d, 1H), 5.77 (m, 1H), 7.05 (t, 2H), 8.18 (d, 2H), 8.48 (dd, 2H).

Synthesis of S-(4-(4'-methyl-[2,2'-bipyridin]-4-yl)butyl) ethanethioate [bipy-SCOCH$_3$]. A solution of 4-(but-3-en-1-yl)-4'-methyl-2,2'-bipyridine (1.02 g, 4.45 mmol) and thioacetic acid (2.0 mL, 28.4 mmol) in 50 mL chloroform was refluxed with stirring overnight in the presence of a small amount (spatula tip) of AIBN. The next day the reaction mixture was irradiated with UV light for four hours. The solution

was removed from irradiation and the solvent was removed by rotary evaporation resulting in an orange liquid. The product was purified by recrystallization from a solution of CH_2Cl_2 with hexanes, followed by being filtered through a plug of celite in CH_2Cl_2. The final product was a yellow solid (400 mg, 29%). ^{1}H NMR (500 MHz, ppm, Acetone-d_6) 1.65 (quint., 2H), 1.78 (quint., 2H), 2.29 (s, 3H), 2.44 (s, 3H), 2.76 (t, 2H), 2.93 (t, 2H), 7.25 (dd, 2H), 8.31 (d, 2H), 8.52 (dd, 2H).

Synthesis of Re(bipy-SCOCH$_3$)(CO)$_3$Cl. Bipy-SCOCH$_3$ (200 mg, 0.66 mmol) and Re(CO)$_5$Cl (250 mg, 0.69 mmol) were added to a round bottom flask containing 30 mL of toluene. The reaction mixture was refluxed for two hours. With heating the solution turned yellow. After two hours of reflux, the heat was removed and the reaction mixture was allowed to cool to room temperature. Toluene was removed by rotary evaporation and the resulting oil was dissolved in a minimal amount of acetone. Hexane was added dropwise to crash the product out of solution. The solid was filtered and weighed (150 mg, 40% yield). IR (CH_3CN) ν(CO): 2024 cm^{-1}, 1916 cm^{-1}, 1899 cm^{-1}. ^{1}H NMR (500 MHz, ppm, Acetone-d_6) 1.67 (quint., 2H), 1.86 (quint., 2H), 2.31 (s, 3H), 2.61 (s, 3H), 2.83 (t, 2H), 2.94 (t, 2H), 7.62 (dd, 2H), 8.58 (d, 2H), 8.92 (dd, 2H).

Synthesis of Re(4-methyl-4'-(butane-1-thiol)-2,2'-bipyrdine)(CO)$_3$Cl. Re(bipy-SCOCH$_3$)(CO)$_3$Cl (500 mg, 0.82 mmol) and an excess of powdered KOH (400 mg, 7.13 mmol) was stirred in 50 mL THF and 10 mL H_2O overnight with reflux. After

reflux, the THF was removed by rotary evaporation, leaving the water and a brown, oily product. The aqueous phase was extracted four times with $CHCl_3$ (25 mL each) and the combined organic phases were dried with $MgSO_4$. The solvent was then removed under vacuum, leaving a brown oil as the product. Column chromatography was performed (silica, $CHCl_3$/hexane/MeOH 7:3:1) and four different fractions were obtained. The last of the four fractions contained pure product as an orange oil. The oil was dissolved in acetone and crashed out as a solid with hexane. The solid was obtained by filtration (280 mg, 60% yield). ^{1}H NMR (500 MHz, ppm, Acetone-d_6) 1.74 (quint., 2H), 1.85 (quint., 2H), 2.57 (s, 3H), 2.73 (t, 2H), 2.89 (t, 2H), 7.61 (dd, 2H), 8.54 (d, 2H), 8.91 (dd, 2H). IR (CH_3CN) ν(CO): 2024 cm^{-1}, 1916 cm^{-1}, 1899 cm^{-1}.

Synthesis of 4-methyl-4'(dodec-11-en-1-yl)-2,2'-bipyridine. 4,4'-dimethyl-2,2'-bipyridine (500 mg, 2.71 mmol) was dissolved in 80 mL of THF from the dry solvent system. To that solution, LDA (1.8 M in heptane/THF/ethyl benzene, 1.66 mL, 2.98 mmol) was added dropwise at –78 °C. The reaction mixture turned dark red/brown upon addition of LDA. The mixture was allowed to warm to 0 °C for 10 minutes before being cooled back down to –78 °C. After re-cooling, 1-bromo undecene (640 mg, 2.74 mmol) was added dropwise to the reaction mixture and left to stir overnight while slowly warming to room temperature. After that period of time, the reaction mixture had changed color to mostly clear, with a hint of green. The reaction was quenched with 20 mL of DI-H_2O and THF was removed by rotary evaporation,

leaving a cloudy H_2O solution. The aqueous layer was extracted three times with 200 mL of Et_2O and the combined organic layers were dried with Na_2SO_4 before being evaporated to dryness. What remained was oil that was put under vacuum in the dark for 48 hours. The oily product was dissolved in pentane, leaving a small amount of white powder undissolved that was later identified as dimethyl bipyridine starting material. The pentane was removed under vacuum, leaving an off-white powder in 70% yield (638 mg). ^{1}H NMR (500 MHz, ppm, $CDCl_3$) 1.30 (m, 14H), 1.67 (quintet, 2H), 2.01 (quartet, 2H), 2.42 (s, 3H), 2.67 (t, 2H), 4.90 (m, 1H), 4.97 (m, 1H), 5.78 (m, 1 H), 7.13 (d, 2H), 8.25 (d, 2H), 8.53 (dd, 2H).

Surface modification of p-Si with 4-methyl-4'(dodec-11-en-1-yl)-2,2'-bipyridine. This work was performed by Dr. Bhupendra Kumar and is published in detail in his recently published dissertation.[12]

Metallation of surface-bound 4-methyl-4'(dodec-11-en-1-yl)-2,2'-bipyridine. A schematic for the set-up used in this synthesis can be found in Figure 6-11. Under an atmosphere of argon, p-Si wafers that had been modified with 4-methyl-4'(dodec-11-en-1-yl)-2,2'-bipyridine were submerged in toluene in small (7.5 mL) scintillation vials that allowed them to stand on edge with the modified face exposed to solution. Those vials were placed in a flask that also contained toluene and an excess of $Re(CO)_5Cl$ was added. A reflux condenser was affixed to the top of that flask and heat was applied to reflux for a period of 16 hours. After reflux, heat was removed from the

reaction mixture and the solution was allowed to cool to room temperature. The Si wafers were removed from solution and rinsed copiously with toluene, acetonitrile, THF and acetone. Those samples were analyzed by XPS in the Lewis laboratory at CalTech and were positive for both nitrogen (in the bipyridine ring) and Re. We also performed grazing angle transmittance IR and found two ν(CO) stretches at 2025 and 1913 cm^{-1}.

Note: The material in this chapter is unpublished work and much of it was performed in collaboration with Mr. Timo Schotzko and Dr. Bhupendra Kumar.

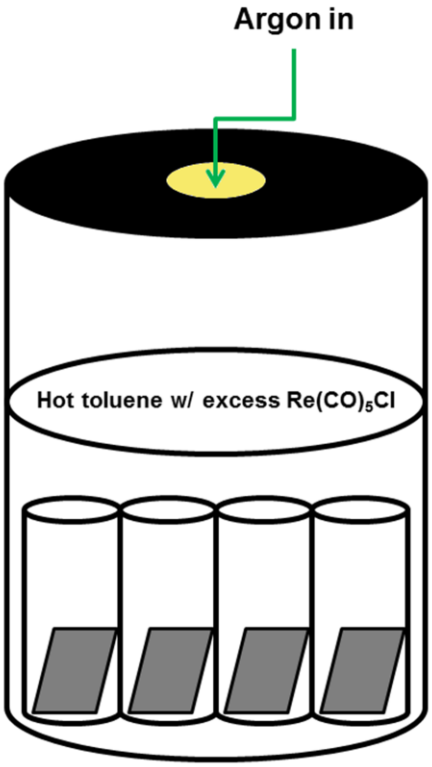

Figure 6-11. Set-up for the metalation of bipyridine ligands covalently attached to p-Si. A reflux condenser is attached in the "Argon in" hole and the reaction flask is heated by sand bath. The p-Si 1 cm^2 p-Si wafers are propped inside 7.5 mL scintillation vials to assure constant exposure of the modified surface with the bulk solution.

6.7 References

1. Hori Y, Wakebe H, Tsukamoto T, Koga O (1994) Electrocatalytic process of CO selectivity in electrochemical reduction of CO_2 at metal electrodes in aqueous media. *Electrochim. Acta* 39(11–12):1833-1839.

2. Reda T, Plugge CM, Abram NJ, Hirst J (2008) Reversible interconversion of carbon dioxide and formate by an electroactive enzyme. *PNAS* 105(31):10654-10658.

3. Armstrong FA, Hirst J (2011) Reversibility and efficiency in electrocatalytic energy conversion and lessons from enzymes. *PNAS* 108(34):14049-14054.

4. Dresselhaus MS, Dresselhaus G (2002) Intercalation compounds of graphite. *Adv. Phys.* 51(1):1-186.

5. Long EC, Barton JK (1990) On demonstrating DNA intercalation. *Acc. Chem. Res.* 23(9):271-273.

6. Tao J-Q, Yu Z, Shao T, Wang T-W, You X-Z (2003) Syntheses and magnetic properties of 1',8'-diazaanthraceno-[a,5,6]-1,10-phenanthroline and its Fe(II) complex. *Yingyong Huaxue* 20(11):1102-1104.

7. Wang J (2006) *Analytical Electrochemistry* (John Wiley & Sons, Inc., Hoboken, New Jersey) Third Ed.

8. Goeltz JC, Kubiak CP (2008) Mixed Valence Self-Assembled Monolayers: Electrostatic Polarizabilities of the Mixed Valence States. *J. Phys. Chem. C* 112(22):8114-8116.

9. Kumar B, Smieja JM, Kubiak CP (2010) Photoreduction of CO_2 on p-type Silicon Using Re(bipy-*t*Bu)$(CO)_3$Cl: Photovoltages Exceeding 600 mV for the Selective Reduction of CO_2 to CO. *J Phys. Chem. C* 114(33):14220-14223.

10. Kumar B, Smieja JM, Sasayama AF, Kubiak CP (2012) Tunable, light-assisted co-generation of CO and H_2 from CO_2 and H_2O by Re(bipy-*t*Bu)$(CO)_3$Cl and p-Si in non-aqueous medium. *Chem. Commun.* 48(2):272-274.

11. Buriak JM*, et al.* (1999) Lewis Acid Mediated Hydrosilylation on Porous Silicon Surfaces. *J. Am. Chem. Soc.* 121(49):11491-11502.

12. Kumar B (2012) Solar fuels: Integration of molecular catalysts with p-type semiconductor photocathode. Ph.D. (University of California, San Diego, La Jolla, CA).

13. Smieja JM*, et al.* (2012) Artificial photosynthesis of CO: Kinetic and structural studies, origins of selectivity, and importance of interfacial charge transfer. *PNAS* In Press.